SCUOLA DI DOTTORATO
UNIVERSITÀ DEGLI STUDI DI MILANO-BICOCCA

Department of
Earth and Environmental Sciences

PhD program in Chemical, Geological and Environmental Sciences
Cycle XXX

Curriculum in Environmental Sciences

POTENTIALLY TOXIC COMPOUNDS FOR HUMAN HEALTH IN THE GASEOUS AND PARTICULATE PHASE OF THE ATMOSPHERE: FROM THE EFFECT OF LOW EMISSION ZONES TO REMOTE SITES

Cristiana Rizzi

ID 704156

Tutor: Prof. Ezio Bolzacchini

Coordinator: Prof.ssa Maria Luce Frezzotti

ACADEMIC YEAR 2016-2017

ABSTRACT

Air quality is a serious problem for the effects on population health[1]. Despite the emissions of some pollutants decreased over the past twenty years in Europe and Italy, atmospheric pollution continues to be an emergency for the high levels of some pollutants in the atmosphere and for the consequent exposure of the population to them. The emergency concerns, particularly, large urban areas characterized by high population density, anthropization and industrialization, which result in greater emissions and higher exposure of the population to atmospheric pollutants. An example of critical area is the Po valley (northern Italy), where the morphological and meteorological conditions, together with the high urbanization and industrialization, determine frequent high air pollution situations.

This study is focused on the atmospheric concentration and behavior of specific organic compounds in the Lombardy Region, a critical area for atmospheric pollution, and in the North Sea. The attention will be focused on compounds that are potentially toxic for human health (such as Polycyclic Aromatic Hydrocarbons) and that can give information on their emission source (such as alkanes). The correct identification of the anthropogenic pollutant sources would allow to design suitable abatement strategies to improve air quality.

Samples of atmospheric particulate and gaseous phases collected in Milan were analyzed to study the atmospheric gas/particle partitioning of semi-volatile Polycyclic Aromatic Hydrocarbons (PAHs) and n-alkanes in different seasons. Since one of the most important source of the particulate matter in Lombardy Region during all the year is vehicle exhausts, a comparison between the concentrations and the chemical composition of particulate matter collected in Milan, at two sites with different traffic loads, was performed for the purpose of evaluating the effect of the Low Emission Zone.

In addition to car exhausts, emissions related to airport activities aroused great interest in recent years since civil aviation is one of the fastest-growing sectors of the global economy. In the Lombardy region is located the international airport of Milan-Malpensa that represents the main airport of northern Italy and the second Italian airport for passenger traffic after that of Rome-Fiumicino. A sample campaign was performed inside the airport, in order to study the contribution of airport activities to the emissions of the main atmospheric pollutants and to assess the impact of these activities on the surrounding area.

Air pollution, however, is a problem not only for urban sites; pollutants can, in fact, be transported over long distances and thus contribute to the air pollution of remote sites. The study of atmospheric pollutants in remote sites can provide information on the extension of human and natural emissions into ecosystems far from the emission sources. The atmospheric gas/particle partitioning of semi-volatile PAHs and n-alkanes in samples collected during a campaign in the North Sea, thus coming from environments with very different characteristics from an urban site (degree of anthropization, source types, climatic conditions and different temperatures) was performed to assess how these parameters affect the phase partitioning of the considered chemical species. The experimental data were used for the implementation of phase partitioning models, which have so far been applied almost exclusively to aromatic polycyclic hydrocarbons, while very few works concern other classes of compounds such as n-alkanes.

Finally, since PAHs are of particular concern because of their mutagenic and carcinogenic properties, the carcinogenic potency of the emitted PAHs and the lifetime lung cancer risk of PAH exposure by inhalation in people living in urban and near remote sites, was assessed.

Contents

List of Abbreviations

ACT = acenaphtene
ACTY = acenaphtylene
ALKs = alkanes
AU = autumn
BaA = benzo(a)anthracene
BaP= benzo(a)pyrene
BbF = benzo(b)fluoranthene
BC = black carbon
BeP = benzo(e)pyrene
BkF= benzo(k)fluoranthene
BTEX = benzene, toluene, ethylbenzene, xylene
C18 = octadecane
C19 = nonadecane
C20 = eicosane
C21 = henicosane
C22 = docosane
C2 = dotriacontane
C23 = tricosane
C24 = tetracosane
C25 = pentacosane
C26 = hexacosane
C27 = heptacosane
C28 = octacosane
C29 = nonacosane
C30 = triacontane
C31 = hentriacontane
CHR = chrisene
CPcdP = cyclopenta(c,d)pyrene
DBahA = dibenzo(a,h)anthracene
DBghiP = dibenzo(g,h,i)perylene
DL = detection limit
DMSO = dimethyl sulfoxide
EC = elemental carbon
FLN = fluorine
FLNT = fluoranthene
I123cdP = indeno (1,2,3 c,d)pyrene
LEZ = low emission zones
LRT = long range transport
NAPH = naphtalene
OC = organic carbon
OCT = octanol
OM = organic matter
OP = organic polymers
OSWSOM = organic soluble water soluble organic matter
PAHs = polycyclic aromatic hydrocarbons
PM = particulate matter
POPs = persistent organic pollutants
ppLFER = poly-parameter linear free energy relationships
PTFE = poly-tetra-fluoro-ethylene
PYR = pyrene
SOC = semi-volatile organic compound
SpLFER = single-parameter linear free energy relationships
SU = summer
TSP = total suspended particles
UR = Inhalation unit risk of exposure
VOC = volatile organic compounds
WI = winter
WSOM = water soluble organic matter

CHAPTER 1. INTRODUCTION

1.1 ATMOSPHERIC AEROSOL

Among the pollutants, atmospheric particulate matter (PM) has been of great importance for years, mainly because of the health effects on the exposed population. Particulate Matter (PM) is a heterogeneous mixture of particles of different size (from very few nm up to over 100 um) and chemical composition that are suspended in the atmosphere [2,3]

1.1.1 SIZE

Particles size is an important parameter for describing their behavior in the atmosphere. Conventionally, the atmospheric particles are subdivided into a coarse fraction (d>1μm), a fine fraction (d between 1 and 0.1 μm) and an ultrafine fraction (d<0.1 μm).

Fine and coarse particles have different origins, chemical composition and optical properties, they undergo different transformations and removal mechanisms and differ in the way they are deposited in the respiratory tract. For this reason, particle size is an important characteristic for the classification of particles.

Particles can be divided in 4 modes. The *nucleation mode* includes particles with diameter <10 nm formed by nucleation processes and condensation of gaseous species. The *Aiken nuclei mode* includes particles with a diameter between 10 and 100 nm. The largest number of particles is included in this dimensional range but, because of their small size, they rarely constitute an important part of the total mass of particulate. Particles in the *accumulation mode* (diameter between 100 and 250 nm) are mainly formed by coagulation of smaller particles or by condensation of volatile compounds on pre-existing particles, favoring an increase in size. Particles in this range stay longer in the atmosphere due to inefficient removal mechanisms, causing their accumulation. Finally, the *coarse mode* (> 2.5 μm) originated mainly by mechanical or erosion processes, sea spray, desert aerosols or other natural sources. Because of their mass, they tend to settle out of the atmosphere in a short time [4,5].

Since the size of particles determines their ability to enter the human respiratory system causing effects on health, particles can also be divided in: *inhalable particles*, which penetrate but are removed at the upper airway level of the respiratory system;

thoracic particles which reach lungs and accumulate in bronchi or bronchioles and *respirable particles* which penetrate alveoli and hence the circulatory system [6,7].

PM can also be classified as PM10 and PM2.5 on the basis of certain geometric parameters related to measurement instruments and parameters for sampling flows[6]. This method is widely used for the definition of air quality standards and legislature. PM 10 was chosen to take into account particles able to penetrate the respiratory tract while PM2.5 was chosen to represent the fine fraction (respirable fraction) that could penetrate deeper into the respiratory tract (Fig 1.1)

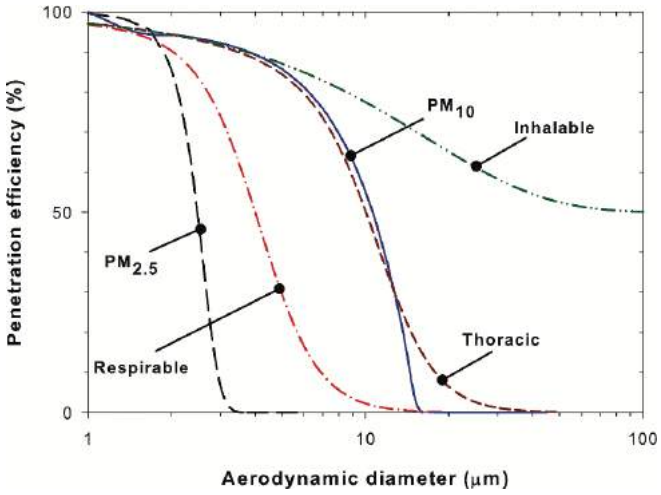

Figure 1.1 PM 2.5, PM10, Inhalable, thoracic and respirable particulate matter sampling conventions promulgated by US-EPA and the ACGIH (7)

1.1.2 SOURCES AND CHEMICAL COMPOSITION

When speaking about PM pollution, an important parameter beside the PM size and the mass concentration, is the chemical composition of particles, since a relation between physical-chemical properties of PM and biological effects induced by particles has been demonstrated [8].

The chemical composition of PM is influenced both by sources and atmospheric processes and can vary significantly in time and space. A great number of sources both natural (soil erosion, dust resuspension, volcanoes, sea spray, forest fire, biological activity etc.) and anthropic (engine combustion and vehicle brakes and tires wear, domestic heating, biomass burning, industrial processes, energy production etc.) contribute to the generation of aerosol particles.

The ratio between natural and anthropic sources is very different depending on the sites. In urban areas, road traffic and domestic heating are the main sources of atmospheric particulate emissions[9]. While road-related emissions tend to be constant throughout the year, the heating source is only active in winter; in summer, instead, photochemical reactions become important.

When directly emitted from these sources, the particles are defined primary; on the contrary, secondary aerosol originates in the atmosphere through chemical reactions that occur between primary compounds or through processes such as condensation of gaseous molecules, nucleation and coagulation.

PM particles are characterized by a carbon core to which organic and inorganic compounds and biological elements are adsorbed [10].

The inorganic fraction represents an important part of the PM mass and is subdivided into a water-soluble fraction and insoluble components. The first includes inorganic ions such as sulfates, nitrates and ammonium, secondary compounds formed in the atmosphere from gaseous precursors (NH_3, NO_X, SO_2) that undergo gas-particle conversion processes through radical oxidative reactions in the atmosphere. Thanks to these reactions, nitrogen oxides are oxidized and transformed into nitric acid while sulfur oxides in sulfuric acid. Subsequent neutralization reactions (with ammonia) lead to the formation of ammonium nitrate or sulfate.

They constitute the preponderant percentage of PM (40% of the mass of PM2.5[11]). The levels of these ions vary depending on the season: nitrates are more abundant in winter when low temperatures ensure that ammonium nitrate remains in the condensed phase by limiting its volatilization[12], while sulfates are higher in summer due to weather conditions, characterized by high temperature and humidity and strong solar radiation that allow the transformation of SO_2 into gaseous sulfate.

Other inorganic ions derive from marine spray or crustal components (Na^+, Cl^-, SO_4^{2-} Mg^{2+}, Ca^{2+} F^- and K^+)[2].

The insoluble fraction derives from road dust or mineral dust and includes trace elements and metals (Al, Si, Ca, Mg, Fe, Ti, Sc, Na, K, Cu, Pb, V, etc.)[13] mainly present in the coarse fraction of PM.

The carbonaceous fraction, which contributes largely to the total mass of PM, is composed of organic and elemental carbon. Elemental carbon (EC) can represents 20-30% of the mass of aerosol [3]. It has a graphite-like structure and is emitted directly into the atmosphere by combustion processes. In urban environments one of the main

sources of this pollutant is represented by diesel emissions; for this reason it is often used as a marker for urban pollution. It is also capable of causing blackening of surfaces and deterioration of stone materials.

Elemental carbon is often called soot to emphasize its origin from incomplete combustion; soot consists almost purely of carbon, with minor amounts of bound heteroelements, especially hydrogen and oxygen.

EC is often also referred to as BC, if determined by means of optical absorption techniques, due to light absorbing properties [14]. Thus, while EC refers mainly to the thermal stability of the compound, Black Carbon refers to its optical properties. In addition to strong light absorption in the visible field, BC is refractory and insoluble in water and other organic solvents. The presence of BC plays an important role in radiative forcing as it is able to absorb solar radiation.

Organic carbon (OC) is a complex mix that contains a large amount of organic substances belonging to different classes such as aliphatic and aromatic hydrocarbons (PAHs), carboxylic acids, amines, alcohols, amino acids, levoglucosan, cellulose. OC may have primary or secondary origin: the primary fraction originates during combustion processes (fossil-fuels, biomass burning industrial activities) and through biogenic emissions. Primary biogenic organic components such as pollen, plant debris, spores, viruses and bacteria represent a consistent portion of the overall organic fraction of atmospheric aerosols (up to 25% of the global aerosol mass) [15].

Many organic species in aerosols are present in the atmospheric aerosol in very small amounts, but they can be of great interest because of their negative health effect.

SOURCE MARKERS: PAHs AND ALKANES

PAHs. Despite they account for less than 0.1% of the total mass of PM, polycyclic aromatic hydrocarbons represent an important class of compounds in the OC fraction due to their high toxic potential [16,17]. They are mainly present in the fine fraction and are about ten times more concentrated in the winter PM [18]. They are structurally characterized by the presence of two or more aromatic rings and they are generally divided into lighter PAHs (2-3 aromatic rings) and heavy PAHs (4-6 rings). For low molecular weight polycyclic aromatic hydrocarbons, the gaseous state is predominant. They tend to degrade through a sequence of radical reactions leading to the formation of more toxic or persistent secondary pollutants. The main reaction for these compounds is the one with the hydroxide radical (OH), but the reactions with the nitrate radical, which occur mostly at night, and with ozone, which occur mainly by day,

may have an important role, leading to the formation of nitro- and oxy-PAHs [19].

Conversely, PAHs with more than four benzene rings do not stay in the atmosphere long as gaseous molecules: because of their low vapor pressure, they tend to condense and absorb to particles quickly [20].

PAHs are primarily emitted by incomplete combustion processes. Then, one of the strongest PAH source is vehicle exhausts, but in general they are emitted by all the processes that use combustion of coal, oil, natural gas, wood etc. [21,22,23,24]. PAHs can be used as source markers, since they can give information about the sources from which they were generated.

Among trace compounds, PAHs are probably the most dangerous class for human health. Some of them, indeed, are known to be carcinogenic, mutagenic and teratogenic [25,26]. Once entered in the human body, PAHs spread rapidly because of their liposolubility, which makes them able to cross the cell membranes, penetrate and settle into adipose tissues.

Photochemical reactions requiring long times and deposition mechanisms that are not always effective, allow PAHs to be transported over long distances and reach locations far from the source of production. Generally, these molecules tend to volatilize in tropical regions due to high temperatures, and to condense in cold regions where they accumulate.

Knowledge of the chemical-physical properties and the environmental fate of PAHs has improved considerably in recent years. Some aspects, however, need some clarification; one of these is the Long-Range Transport (LRT) associated with the particles [27]. The reactivity of PAHs related to aerosol particles is, in fact, still not well known and involves rather complex mechanisms, influenced by a large number of factors.

Alkanes. The n-alkanes are a minor group of not-polar and relatively stable compounds of PM. At ambient temperature and pressure, lighter alkanes (up to 4 carbon atoms) are gaseous or partition between the gaseous and particulate phases, while those having 5 to 16 carbon atoms are liquid. Gaseous alkanes can react with hydroxyl and nitrate radical to form products (aldehydes, ketones and monocarboxylic acids) that are thermally very unstable and consequently decay quickly.

The n-alkanes originate from both anthropogenic and natural sources. Anthropogenic n-alkanes are emitted mainly by vehicles (incomplete fuel combustion, tyre abrasion, brake lining dust, road dust, lubricant oil etc.) [29] and biomass burning. Natural

particulate n-alkanes are originated mainly by plant debris [30] and in part by suspension of pollens, microbial degradation and insects. [28,29, 30, 31.]

The importance of alkane characterization in atmospheric particulate samples is mainly related to the ability to distinguish the different contribution of sources; in fact, the n-alkane are defined "source-specific" [21,32, 33].

A widely used parameter to assess the natural or anthropogenic origin of these compounds is the Carbon Preference Index (CPI) which considers the carbon distribution number of the homologues series [34]:

$$CPI = 0.5 * [(\Sigma_{2m+1}C_m / \Sigma_{2m} C_m) + (\Sigma_{2m+1}C_m / \Sigma_{2m+2} C_m)]$$

In general, it has been assessed that no preference for odd or even carbon numbers is typical of vehicular source, while an odd preference suggests a natural origin [35].

1.1.3 PM HEALTH EFFECTS

Several epidemiological studies have highlighted that exposure to PM may have important health effects, so much so that it has been classified as a carcinogenic compound for humans (Group 1) by the International Agency for Research on Cancer (IARC) [36]. Approximately 90% of the inhaled particles are removed at the upper respiratory tract airways by clearance processes, defense mechanisms that involve the removal of particles by the ciliary cells and the production of mucus. However, in case of chronic exposure or high concentrations, the particles can overcome this barrier.

Concentrations of PM in the atmosphere has been directly related to an increase in the incidence of acute and chronic pathologies of the respiratory system (asthma, bronchitis, allergies), and cardiovascular disease as well as an increase in the risk of lung cancer [37].

Particulate matter from combustion sources was associated with increased mortality[38] in the population. Particles from vehicle exhaust were more strongly associated with deaths due to ischemic heart disease; in contrast, the coal-derived particles were more strongly associated with respiratory death.

The importance of particle size has been evaluated and positive relations both with PM10 and PM2.5 were found [39,40]. Experimental and epidemiological studies suggest that the coarse fraction may have higher pro-inflammatory potential [41] and may be responsible for respiratory disease while fine PM has been linked with an increase of risk of cardiovascular mortality and lung cancer. Ultrafine particles < 0.1 µm (UFPs) are important because they have order of magnitudes higher particle number

concentration and surface area, and larger concentrations of adsorbed or condensed toxic air pollutants (oxidant gases, organic compounds, transition metals). Many of these toxic air pollutants have been identified as having pro-inflammatory effect. Results from several recent studies, mostly in urban areas, showed that a large portion of urban UFPs consists of primary combustion products from mobile source emissions (particularly diesel exhaust) and includes organic compounds, EC, and metals[42]. Trace metals can influence the toxicity of airborne particulate matter. Such evidence derives from toxicological rather than epidemiological studies and depends mechanistically on the idea that metals are redox-active and can, therefore, induce or catalyze chemical change, leading to the production of free radicals such as hydroxyl radical which have a known ability to cause tissue inflammation. Even sulfates have long been implicated as the major toxicological component in fine particulates and have been shown to be associated with respiratory disease and mortality [42]. When nitrate and sulfate are formed in the atmosphere from oxidation of nitrogen dioxide and sulfur dioxide, respectively, they are formed as their strong acids, nitric acid and sulfuric acid. In the case of sulfuric acid, the acid is not-volatile, and once formed, is immediately incorporated into airborne particles which are only subsequently neutralized by atmospheric ammonia. Thus, in environments with low airborne ammonia concentrations, airborne particles may have an appreciable strong acid content [43].

Organic components of PM such as PAHs, have been shown to induce the expression of cytokines and chemokines in respiratory epithelium. This effect may be due to the action of metals, PAHs and related compounds that lead to the production of cytotoxic ROSs, which induce oxidant injury and inflammatory responses [43]. Some PAHs are well known as carcinogens, mutagens, and teratogens and therefore pose a serious threat to the health [16].

As molecular weight increases, the carcinogenicity of PAHs also increases. The most potent PAH carcinogens have been identified to include benzo[a]anthracene, benzo[a]pyrene, and dibenz[ah]anthracene.

Short-term exposure to PAHs has also been reported to cause impaired lung function in asthmatics and thrombotic effects in people affected by coronary heart disease. Mixtures of PAHs are also known to cause skin irritation and inflammation. Moreover, PAHs have the potential to interfere with hormone systems and they can exert harmful effects on reproduction and immune function [44]. PAHs can also metabolize and become reactive electrophilic intermediates that can form DNA adducts, which may induce mutations and ultimately tumors [44]. Reactive metabolites (e.g., epoxides and dihydrodiols) of some PAHs have become one of the major health concerns because of

their potential to bind to cellular proteins and DNA with toxic effects [45].

The International Agency for Research on Cancer (IARC) classified Benzo(a)pyrene (BaP) as carcinogenic to humans (group 1); other PAHs, such as dibenzo[*a*,*h*]anthracene, as probably carcinogenic to humans (group 2A) and other PAHs, such as naphthalene, benzo[*a*]anthracene, chrysene, benzo[*b*]fluoranthene, benzo[*j*]fluoranthene, and indeno[1,2,3-*cd*]pyrene as possibly carcinogenic to humans (group 2B).

The risk estimation for PAH exposures is complex for several reasons. To evaluate the human health risk associated with PAHs, the carcinogenic potency of each PAH can be calculated based on the "toxic equivalence factor" (TEF) approach. The application of TEF can be used to estimate the excess lifetime risk of lung cancer due to PAH exposures [45].

1.1.4 PM LEGISLATION

In order to avoid, prevent or reduce the adverse effects on human health and on the environment, the European Community established limits for the concentrations of various pollutants in the air. It is extremely important to limit at the source the emission of pollutants as well as to identify and implement the most effective emission reduction measures at local, national and European level. It is therefore appropriate to define target values for air quality.

Italian legislation with the Decree n. 155/2010, transposing the European Directive (2008/50/CEE), set the annual limit of PM10 at 40 μg m^{-3} and of PM2.5 at 25 μg m^{-3}. For PM10 was also set a daily limit at 50 μg m^{-3}, which should not be exceeded more than 35 days a year.

As for PAHs, BaP is the target of regulation and it is also taken as a marker compound. In European air, the target annual average concentration of BaP in the PM10 fraction is 1 ng m^{-3}.

1.2 URBAN AND REMOTE SITES

1.2.1 THE CITY OF MILAN

Northern Italy is a known hotspot for atmospheric pollution levels, and Milan, the biggest city of Northern Italy, is characterized by high PM levels which are often above limit and quality values indicated by the European Union (EU) air quality Directive 2008/50/EC for PM10 and PM2.5 mass concentrations [46].

Bad air quality in Milan is enhanced by sever meteorological condition, low mixing layer height and a high density of anthropogenic PM sources [47,48,49].

Even if the average annual concentrations of some pollutants (i.e SO_2 and benzene) show a downward trend, PM pollution is still an unsolved problem in the city of Milan and in the whole Po Valley. The situation gets worse in winter, when the inversion layer tends to remain low, limiting each vertical mixing, facilitating the formation of fog, mist and smog and concentrating the pollutants in the layer closer to the ground[49]. Conversely, during the warm season, higher average wind speed and a broader mixing layer improve the atmospheric dispersion of pollutants [9].

The contribution to concentration of pollutants in Milan comes from several primary emission sources.

In general, in urban areas, road traffic and domestic heating are the main sources of atmospheric particulate emissions[9]. Whereas the emissions related to road transport (vehicle emissions and road dust resuspension) tend to be constant throughout the year, the heating source is activated only in the winter.

From the Regional Emission database (INEMAR, 2014) it emerges that in the province of Milan transport on road and domestic heating show the major contribution of primary PM and NOx.

As far as PM is concerned, transport on road covers about 37% and 41% of primary PM 2.5 and PM10 while non-industrial combustion sector covers about 31% and 27% of PM2.5 and PM10 respectively.

The fine fraction represents a large part of the total PM: the ratio PM2.5/PM10 is around 80% in the last decade[49,50]. In general, Inorganic Ions accounts for about the 40% of the total mass of PM in Milan and in particular NH_4^+, NO_3^-, SO_4^{2} represent more than 95% of the total inorganic ions. Organic Matter (OM) explains 30-40% of the total PM2.5 mass, while Elemental Carbon (EC) explains the 10-15%.

Considering NO_X emissions, the annual contribution of the transport on road and residential sectors amount to about 68% and 12% respectively. Other emission sources (industrial processes, agriculture, wastes management etc.) are less relevant.

With regard to VOC, the main source of emission is represented by the use of solvents which amount to about 59%, while road transport represents the second source, accounting for 12% of the total emissions.

Since anthropogenic sources are able to emit larger quantities of particles containing toxicologically relevant substances for the health and the environment, such as PAHs,

many European cities have attempted to reduce pollution caused by traffic by adopting traffic limitation measures. Among them, the city of Milan, starting from January 2012, established a system of paid access to the central area of the city, called AREA C.

Other examples of LEZ can be found in many Italian and European cities. More than 70 cities in 8 European countries (including Germany, Sweden, the United Kingdom, Denmark and the Netherlands) adopted or are about to introduce limitations on vehicle access to the central areas of the city in order to improve air quality. Depending on local conditions, access to the LEZ is prohibited or subject to payment. Most restricted traffic areas regulate access only to vans and trucks, but some, including those in Germany and Italy, also affect passenger cars.

Several studies evaluated the effectiveness of low emission zones in reducing PM concentrations by comparing the concentrations within LEZ with data collected before the introduction of the measure. In Milan, Invernizzi et al [51], after a 3-day sampling performed simultaneously within and outside the LEZ, found a 47% reduction in the contribution of black carbon to PM10 within the LEZ, but no reductions in PM10 concentrations were found. On the contrary, In London, over the last ten years, an average annual reduction of PM10 emissions of 2.5-3% was recorded within the LEZ, while the reduction was only 1% at external sites[52]. Panteliadis et al.[53] reported a 4.9% and 5.9% reduction in NO_2 and NO_X concentration respectively and a 5.8% reduction for PM10 after the introduction of the low emission zones in Amsterdam. From these studies, it can be noted that the variation in the PM concentrations is influenced by many factors and that a reduction in the PM concentration due to the introduction of LEZ, may depend on the sampling site. However, information regarding the variation of concentrations of compounds present in the PM is still very inadequate and is limited to measurement on black carbon obtained from measure campaigns carried out over a very limited period of time.

1.2.2 AIRPORT CONTRIBUTION TO AIR POLLUTION

Airports are sources of concentrated emissions, highly variable over time, whose influence on air quality and, consequently, on health is still being studied. An airport is a complex system that can potentially have a significant impact on the surrounding environment. In particular, the presence of an airport is mainly associated with an increase in environmental noise, whose impact on the health of the population living in the surrounding areas has been the subject of numerous epidemiological studies.

Exposure to noise can, in fact, have consequences on health, causing hearing damage, increase in blood pressure and cardiovascular disorders [54,55,56,57,58]. Other effects such

as immune system dysfunction [59], psychic alterations, worsening of sleep quality and decrease of cognitive performance have been observed in subjects exposed to airport noise.

Airport activities can lead to the release of pollutants into the atmosphere, mainly caused by fossil fuels combustion. Exhaust emissions represent the main sources of pollutants but there can be differences depending on the phase of movement and the relative engine speed.

Aircraft emissions must comply with the limits established by the International Civil Aviation Organization (ICAO). To obtain a good estimate of aircraft emissions, reference may be made to the Landing and Take-Off cycles (LTO), which includes all the aircraft operations (in flight and ground phases) made below the 3000 ft limit (about 1000 m) corresponding to the height of the mixing layer [60]. It consists of in-flight phases (approach, take-off and climb out) and those on the ground, such as the transfer from the aircraft stands to the runway and vice versa (taxi/ground idle).

Other sources of emission in the airports are the exhaust of auxiliary vehicles generally powered by diesel [61] used for aircraft maintenance and for personnel and passengers' transportation.

The emitted pollutants are similar to the vehicles exhaust: carbon dioxide (CO_2), carbon monoxide (CO), nitrogen oxides (NO_x), sulfur oxides (SO_2), volatile and semi-volatile organic compounds (VOC), and particulate matter (PM). Aircrafts emit ultra-fine particles (<0.1 μm) both immediately to the exhaust and as a result of the rapid condensation and coagulation of gases [62]. Emissions are characterized by a wide variability in particular depending on the engine speed, the duration of the most critical phases for each flight and the environmental conditions (temperature, pressure and relative humidity) [62].

The contribution of airports to air pollution is therefore not-negligible and highly spatially variable but in many cases, it is not dominant compared to other concomitant pollution sources [63]. Levels of pollutants measured near the airports are often not significantly higher than those found in other areas affected by vehicular traffic emissions. A study at Rome-Ciampino airport has highlighted that the contribution of the airport to air pollution is low if compared to the main source in the area, namely vehicular traffic [63].

However, high temporal resolution measures allowed to detect high aerosol levels attributable to the take-off (number of particles and soot concentration) and landing

phases (coarse fraction) that could contribute to the exposure of the population around the airport.

It has also been noted that regarding NO_X emission, the primary component is NO_2 in the minimum engine thrust phase, while at full throttle, NO_X is emitted primarily as NO[64]. Conversion of NO to NO_2 occurs quickly and does not involve ozone chemistry. The consequence is that overall, during a complete LTO cycle, according to the ICAO standards, 50% of NO_X emissions emitted within the first 150 m of the ground floor is composed of NO_2 [65].

NO_X AND O_3

NO_X. Nitrogen oxides (NO_X) are primary gaseous pollutants and they are very important in polluted atmospheres. They are emitted by high temperature combustion reactions, they can persist in the atmosphere and be transported from the emitting source over long distances.

Nitrogen monoxide (NO) and nitrogen dioxide (NO_2) are emitted by anthropic sources (in particular from combustion processes) or, to a lesser extent, by natural sources (e.g. from soil). NO_2 is mainly emitted by traffic, especially from Diesel engines, and from power plants. It is a strong oxidant and irritant and it is responsible for respiratory diseases. To protect human health, the Italian legislation (D.Lgs 155/2010), following the guidelines of the World Health Organization, sets a limit value for NO_2 of 200 μg m^{-3} not to be exceeded more than 18 times a year and an annual limit of 40 μg m^{-3}.

Despite it is an actual pollutant, no limits have set for NO because of its low half-life in the atmosphere.

NO_X reactivity plays an important role in the chemistry of the atmosphere as it leads to the formation of various chemical compounds including the nitric anhydride and nitrate radical from which nitric acid, which is responsible for the acidification of the rain, can be produced.

The photolytic cycle of NO_2 is the series of atmospheric reactions that explain the link between NO_X and ozone: NO_2 absorbs the radiation that enter the troposphere (<430 nm) causing the photo-dissociation of NO_2 with ozone production ($NO_2 + hv \rightarrow NO + O(^3P)$; $O(^3P) + O_2 \rightarrow O_3$) which reacts with NO to form again NO_2 ($NO + O_3 \rightarrow NO_2 + O_2$)

This leads to a condition known as "photo-stationary equilibrium", a dynamic balance between ozone production / destruction.

Nevertheless, the presence of hydrocarbons and other volatile organic compounds determines the opening of the cycle, through competitive reactions that convert NO to NO_2 without consuming ozone. This process breaks the photo-stationary equilibrium causing an accumulation of O_3 in the troposphere; this is associated with photochemical smog.

O_3. Ozone is present throughout the atmosphere but with a strongly uneven distribution that sees about 90% of the total O_3 in the stratosphere and 10% in the troposphere. It is a secondary gaseous pollutant: it is generated through photochemical reactions from its precursors. The stratospheric ozone absorbs low wavelength radiation in the UV range (200 - 300 nm) thus eliminating part of that solar radiation which can have harmful effects on human health, microorganisms and plants.

Ozone regulates oxidation processes in the troposphere through the formation of the hydroxide radical (OH), which controls the life time of many gases in the atmosphere; OH is formed by the photo dissociation of O_3 in the presence of water vapor.

Tropospheric ozone is formed locally in the atmosphere in the presence of nitrogen oxides, often emitted in polluted urban areas simultaneously with hydrocarbons (RH) and carbon monoxide (CO), in particular by anthropogenic sources.

The presence and the distribution of tropospheric ozone, therefore, presents a high local variability due to its formation by means of photochemical reactivity and transport / distribution phenomena occurring in the atmosphere.

In polluted and densely populated areas, like the Po Valley, the significant emission of ozone precursors and the photochemical activity play a fundamental role.

The negative effects of tropospheric ozone on human health have long been known: the exposure to ozone concentrations have well-documented effect on respiratory function. The Italian legislation established target values to ensure the protection of human health of 120 $\mu g\ m^{-3}$ not to be exceeded more than 25 times per year as an average over three years.

In high-traffic areas the ozone concentrations are generally lower than in suburban sites because of depletion effect due to the reaction of O_3 with NO (NO represents 90% of NO_X primary emission in traffic sites). On the contrary, high concentrations of high O_3 are often recorded in suburban areas: here lower NO emissions do not allow an effective ozone removal. Moreover, NO_X that reach suburban areas are mainly NO_2 which results in a high ozone production.

In remote sites, such as Scandinavia, limited NO_X emissions and a lower incidence of solar radiation due to high latitudes, ensure that O_3 contribution becomes much less significant than polluted areas at lower latitudes. Here the role of air mass transport, such as those from Central and Southern Europe, and the deposition, are crucial to explaining the changes in ozone concentrations.

1.2.3 REMOTE SITES: ARCTIC AEROSOL

The Arctic air mass is a unique meteorological feature of the troposphere characterized by subzero temperatures much of the year, little precipitation, stable stratification that prevents strong vertical mixing and low levels of solar radiation especially during winter[67].

It is generally assumed that the high latitudes of both hemispheres are uncontaminated regions but in the 1970s the presence of contaminants of anthropic origin in the Arctic was discovered.

Soon after, high concentrations of several pollutants were revealed in and around the Arctic, particularly during winter. This unexpected result prompted the scientific community to study and speculate about the origins of airborne pollutants to the Arctic[68]. Once the anthropogenic origin of the haze became evident, it was debated whether the pollution aerosol was local, derived from human activities near the sampling sites, or was of regional significant, extending over the entire Arctic, and thus probably transported from large, mid-latitude source regions. It was finally discovered that Arctic pollution is to ascribe to very long-range atmospheric transport from mid-latitude source regions, and to the sparsity of precipitation in the Arctic which increases normal residence times by almost an order of magnitude[69].

The concentration of pollutants varies according to the season: during winter the low pressure on the Arctic Ocean and the high pressure on the continents favors the transport of pollutants to the high latitudes, while during the summer the high continental pressure disappears, the transportation from medium latitudes decreases and the degradation by photochemical reactions becomes important.

As a result of all the research efforts, the major aspects of Arctic air chemistry are now fairly well established. From December to April each year, the entire Arctic air mass, up to about 5 km altitude, is polluted by anthropogenic mid-latitudinal emissions from fossil fuel combustion, smelting and industrial processes. Northern Eurasia appears to be the main source of SO_4^{2-}, Pb, non-crustal V (emitted by combustion of residual oil in mid-latitudes) and of various other elements in the aerosol. in winter, the

concentrations of heavy metals and of SO_4^2 are about 10-40 times higher than in summer[70].

It was observed that samples of particulate matter were generally gray when collected in winter. This suggested the presence of elemental carbon and associated particulate organic matter, including compounds such as PAH during winter. Long-range transport of PAHs has been studied by many authors through both atmospheric measurements and numerical modelling. PAHs are often referred to as persistent organic pollutants (POPs) because of their resistance to degradation. However, they are reactive in the atmosphere, forming oxidized product. A further complexity in studying PAHs arises from their semi-volatility. They partition between the particle and gaseous phase and hence undergo chemical reactions in both phases. Most of the 3-4 rings PAHs are semi-volatile therefore they are subject to re-volatilization upon condensation on surfaces and to gas exchange with vegetation, soils and water surfaces; Long Range Transport of PAHs may be enhanced by re-evaporation [71].

Deposition trends of PAHs, have shown a dramatic increase in concentrations over the last 100 years that correlate well with the historical record of world petroleum production[72].

1.3 GAS-PARTICLE PARTITIONING OF SOC

A semi-volatile compound is a compound that partition between the gaseous and the particulate phase of the atmosphere at standard temperature (25°C) and pressure (1 atm)[73]. The distribution of a semi-volatile organic compound (SOC) between the gaseous and the particulate phase of the atmosphere is probably the most important parameter to describe its destiny, its stay in the atmosphere, its transport and its transformation. Indeed, the partitioning of SOCs is central to many process of environmental concern such as the formation of secondary organic PM and the role of organic aerosols in climate change[74].

Atmospheric transport and deposition of particles are important mechanisms that can influence the movement of contaminants from urban and industrial areas to distant regions[75]. In particular, the degradation and deposition of a SOC, which strongly depend on the presence of the compound in the gaseous or particulate phase, limit the Long Range Atmospheric Transport.

Photochemical reactions requiring long times and deposition mechanisms that are not always efficient, allow the SOC to be transported and to reach locations far from the

source of production. Generally, these molecules tend to volatilize in tropical regions due to high temperatures and recycle in cold regions where they accumulate.

Knowledge of the chemical-physical properties and the environmental fate of some SOC such as PAHs improved considerably in recent years. Some aspects, however, need some clarification; one of these is the LRT associated with the particles[28]. The reactivity of PAHs related to aerosol particles is, in fact, still not well known and involves rather complex mechanisms, influenced by a large number of factors.

Due to the importance of these mechanisms, efforts have been made in the last twenty years to clarify the relations governing the distribution of semi-volatile organic compounds in order to accurately predict their concentration in the atmosphere[73,76].

1.4 AIMS OF THE STUDY

The gas-particle partitioning of semi-volatile organic compound is of great interest for the understanding of the destiny of the pollutants in the atmosphere. The study of the concentrations of SOC compounds and their partitioning represent the subject of research of this thesis and they have been investigated in different environments, characterized by different sources, climatic conditions, temperatures and degree of anthropization.

Firstly, the concentrations of particulate matter were investigated at three different sites: the urban area of Milan, the airport of Milano- Malpensa and the Arctic region. These environments are very different, and they are characterized by different sources, climatic conditions, temperatures and degree of anthropization.

The chemical composition of the measured PM was subsequently studied, with particular reference to organic micro-pollutants such as PAHs and alkanes. PAHs are an important class of compounds because of their high toxic potential. For this reason, the carcinogenic potency of the emitted PAHs and the lifetime lung cancer risk of PAH exposure by inhalation in people living in urban and near remote sites, was assessed.

The distribution of semi-volatile compounds in samples collected during the different sampling campaigns thus coming from different environments was described with the aim of understating how different classes of SOCs partition between the particulate phase and the gaseous phase in the atmosphere.

The experimental data were used for the implementation of phase partitioning models, which have so far been applied almost exclusively to aromatic polycyclic hydrocarbons, while very few work concerns other classes of compounds such as n-alkanes. This is an

important aim because many factors such as the residence time in the atmosphere and the transport depend on this parameter. Furthermore, the implementation of a model that is valid for samples with different characteristics (eg. urban samples and samples from the Arctic Sea) will make it possible to predict the partitioning between the gaseous phase and the particular phase of the compounds, without having to perform experimental analyzes.

Before presenting the obtained results, Chapter 2 discusses the sampling campaigns, describing the sites, the instrumentation and techniques used for the extraction and the analysis. Results from the direct measurements regarding the concentrations and the chemical compositions of PM in Milan are presented and discussed in Chapter 3, where the gas-particle partitioning of PAH and alkanes is addressed as well. Chapter 4 describes the measurements conducted at the Milano-Malpensa airport and the obtained results with reference, above all, to the compounds regulated by law. Chapter 5 focuses on the semi-volatile organic compound measured in the Arctic Region, with an attempt to apply some of the best available models to evaluate the relative importance of adsorption on soot and absorption into the organic matter. The carcinogenic potency of the emitted PAHs and the lifetime lung cancer risk of PAH exposure by inhalation in people living in urban and near remote sites, is described in Chapter 6.

CHAPTER 2. MATERIALS AND METHODS

To determine the environmental concentrations of atmospheric particulate matter and to analyze its chemical composition, it is first necessary to collect samples and to analyze them in laboratory.

This chapter will describe the sampling campaigns carried on, the sampling sites, the instrumentation and the methods used to extract analytes from the support. It will follow a description of the analytical procedures used in the analysis of target compounds (PAHs and Alkanes) and a brief description of the methods used for other pollutants, in order to provide a general overview of the chemical composition of particulate matter and air quality in the sampling sites.

2.1 SAMPLING CAMPAIGNS

2.1.1 THE URBAN AREA OF MILAN

The first sampling campaign was carried out in the urban area of Milan. PM was sampled at 2 locations in Milan, with different traffic loads. The two sites are: a traffic site (TR), located within the Campus of the University of Milano Bicocca, about 10 m away from a crossroad (Viale Sarca-Viale Chiese; traffic flux = 33000 vehicles day^{-1}); a limited traffic site in the city centre within the low emission zone (LEZ) (Fig. 2.1). The LEZ site was located in the courtyard of the National Museum of Science and Technology "Leonardo da Vinci", at a distance of about 15 m away from the traffic road Via San Vittore, where the traffic flux is = 15000 vehicles day^{-1} (traffic data from AMAT Agenzia Mobilità Ambiente Territorio, www.amat.mi.it). LEZ in Milan (known as "Area C") restricts certain vehicles entering the historic city centre. The activation is during all weekdays from 7.30 am to 7.30 pm (Thursday from 7.30 am to 6.00 pm). During the activation time, the access to the LEZ is forbidden to Euro 0 gasoline, Euro 0, 1, 2, 3 diesel vehicles, vehicles with a length more than 7.5 m, and it is regulated by the payment of the congestion charge for other vehicles.

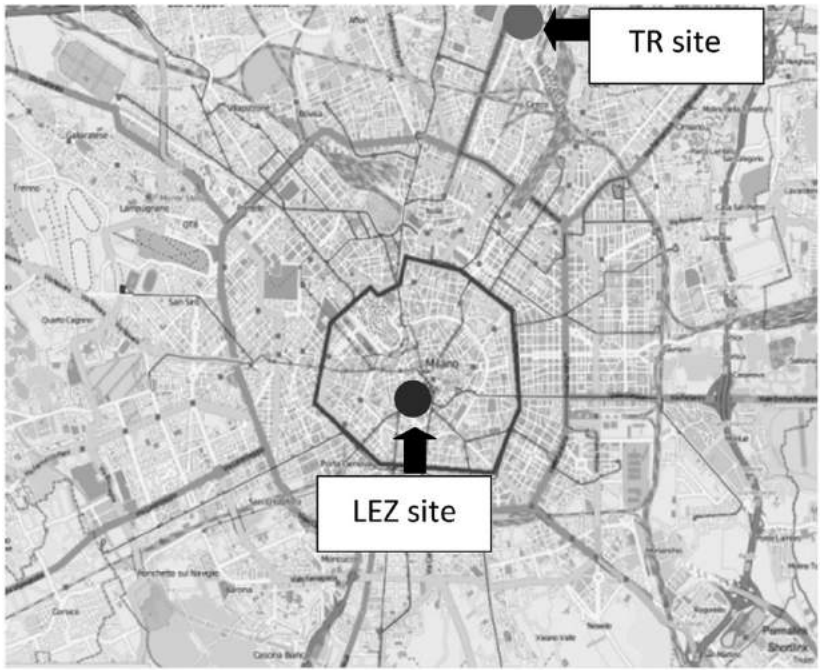

Figure 2.1 Map of the city of Milan, with the location of the two sampling sites: the traffic site (TR site) and the site within the low emission zone (LEZ site). The LEZ area is delimited by the dark map.

The sampling campaigns were conducted during 2013 in 3 seasonal periods at the TR site: 3rd -10th December / 16-24th January, 8-18th July, 2-15th October. During December/January and July daily samples (24 h) of PM were collected. In October, the sampling was simultaneously performed at both sites during working days from 8.00 am to 6.00 pm (daytime 10 h sampling), when traffic limitation inside the LEZ was implemented.

The particulate and the gaseous phase of the atmospheric compounds was collected simultaneously using two identical high-volume samplers (200-250 l min^{-1}, ECHO-PUF, TCR Tecora). The sampler was equipped with a filter and a PolyUrethane Foam (PUF) plug in serial so that the air passed through the filter on which the Total Suspended Particles (TSP) deposited and then through the PUF plug which adsorbs the gaseous phase (Fig.2.2)

The total suspended particles (TSP) were collected on quartz fibre filters (QFF; diameter 102 mm; Whatman, USA). Before sampling, the filters were baked at 600°C for 2 h to reduce the impurities. Before and after sampling, filters were equilibrated (48 h at 35% RH, ambient T) and weighed with a microbalance (0.1 mg precision, Gibertini) in order to measure ambient TSP concentration (unit: mg m^{-3}). The gaseous phase was collected on PUF Plugs (Ø 58 mm, length 125 mm; Supelco).

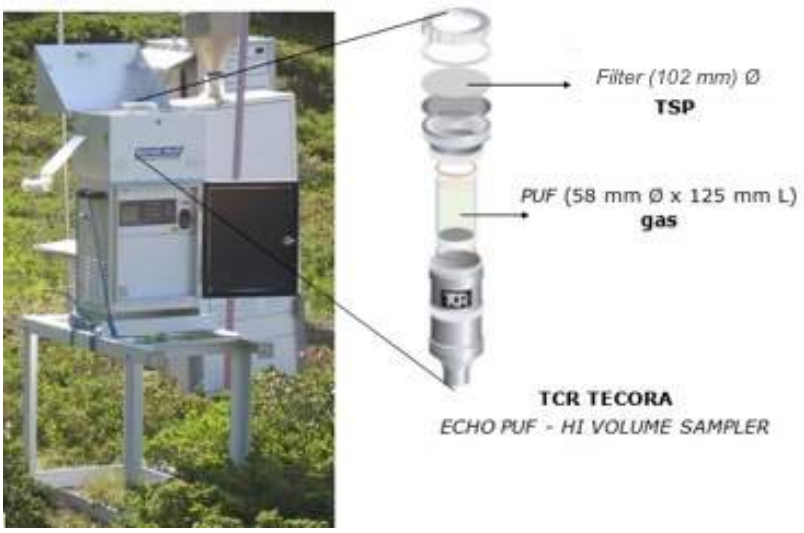

Figure 2.2 High Volume Echo PUF (TCR Tecora); scheme of the filter and PUF lodging.

All sampled filters were kept in the dark at 4°C to avoid photo-degradation and evaporation until the chemical analysis.

In order to guarantee the quality of the PM measurements and analysis, totally six blank field filters were used during these campaigns (2 in January, 2 in July and 2 in October).

Quartz filters were cut in punches to perform all the analyses. A spot of 4.5 cm Ø was cut from the filter to analyse PAHs and alkanes by gas chromatography coupled to mass spectrometry (GC-MS).

In addition to the GC-MS analysis, three punches more were used to perform the following chemical analysis: ion chromatography (IC, spot of 2.5 cm Ø), thermal optical transmission (TOT; rectangular spot of 1 1.5 cm^2) and inductively coupled plasma mass spectrometry (ICP-MS; spot of 2.5 cm Ø).

PM samples collected in January, July and October were analysed for PAHs and n-alkanes, EC/OC, inorganic ions, elements and trace organic compounds: carboxylic acids, alkylamines (the samples collected in December were analysed only for PAHs and Alkanes). The methods of chemical analysis will be described in Par. 2.3.

PUF plug were extracted to analysed PAHs and alkanes by gas chromatography coupled to mass spectrometry (GC-MS).

2.1.2 MILAN-MALPENSA AIRPORT

The experimental measures were conducted at the airport of Milano-Malpensa in two sites affected by different operating conditions, with sources that have different emissive patterns (Fig 2.3).

Site 1 is located between the two runways (45°37’13.49” N e 8°43’48.33” E), in an area that correspond to the early stages of “ground roll” both for landing operations, when the aircraft touches the ground and continues in its slowdown, and take-off operations when it reaches the maximum acceleration for the lift-off. Therefore Site 1 has been chosen because it is primarily influenced by aircraft emissions during take-off and landing.

Site 2 is located near located near the service pitch 511 of the Terminal 1 (N 45°37’37.35’’; E 8°42’56.37’’) in an area that serves medium and big-sized aircraft, with the movement of service vehicles for taxing operations. Thus, Site 2 is characterized by the emissions related to maintenance, refueling, loading and unloading of luggage and passengers.

The sampling was performed from 27/10/2016 to 10/01/2017 at Site 1 and from 10/01/2017 to 08/03/2017 at Site 2. The sampling campaigns were conducted in winter, in order to highlight the possible impacts of the airport during the most critical season from the point of view of air quality.

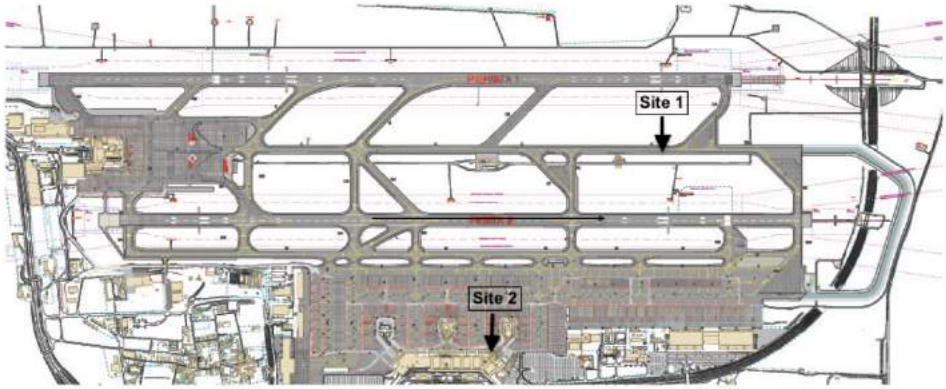

Figure 2.3 Planimetry of Milan-Malpensa Airport. Localization of the two sites within the airport.

Daily samples of Particulate Matter were collected using a Low Volume Hydra Dual Channel Air Samplers (gravimetric sampler, Fig. 2.4), equipped with a 10 µm and a 2.5

µm inlets to collect the particles with equivalent aerodynamic diameter below 10 µm (PM10) and 2.5 µm (PM2.5) µm, respectively. The sampler had two distinct independent channels that allow to collect simultaneously particles with different dimension on two different filtering membranes.

The sampler is equipped with a conditioning unit with thermostatic control at 20°C ± 4 °C to operate in an outdoor environment. The Dual Sampler can automatically manage 30 or more filtering membranes that are automatically loaded. At the end of each sampling cycle, the sampled filters are automatically transferred to the unloader.

The samplers operated at a flow rate of 2.3 m^3 h^{-1} and every sample was collected for 24 h (start at 0:00, stop at 24:00 of the same day). PTFE filters with PolyMethylPentene ring (Ø 47 mm; Pall Corporation) were used to collect the particles. Before and after the sampling, the filters were conditioned for 48 h at 20°C and 35% of relative humidity and weighed on an electronic balance (reading precision of 1 µg; Sartorius). After the sampling, the filters were weighed to determine the particulate mass concentration and then stored in the dark in a refrigerator until the chemical analysis to limit or prevent the volatilization losses or the reaction of the compounds.

Figure 2.4 Low volume Hydra Dual Channel Air Sampler (gravimetric sampler, FAI)

In order to guarantee the quality of the PM measurements and analysis, totally twelve blank field filters were used during these campaigns.

PTFE filters were used in punches to analyse PAHs and alkanes by gas chromatography coupled to mass spectrometry (GC-MS).

In addition to PM sampling and analysis, the numerical concentration and dimensional distribution of the particles were determined using an Optical Particle Counter (OPC) and a Condensation Particle Counter (CPC). The measures also involved other atmospheric pollutants that are important because of their potential effects on human health and on the environment, such as black carbon, nitrogen oxides, ozone and volatile organic compounds.

An OPC (Optical Particle Counter; 107 GRIMM; 1.2 l min^{-1}) was used for the determination of the numerical concentration of particles and their equivalent optical diameter (at 655 nm wavelength and 1.58 of calibration refractive index), classified in 31 dimensional classes from 0.25µm to 32µm. The instrument uses light-scattering technology for single-particle counts, whereby a semiconductor-laser serves as the light-source. The scattered signal from the particle passing through the laser beam is collected at approximately 90° by a mirror and transferred to a diode and later to a multi-channel size classifier. The sampled air is not heated to avoid losing semi-volatile particles before measurement. Above 65% relative humidity, a dehumidification system is activated. A separate humidity and temperature sensor controls at all time the parameters.

The instrument also carried out its own estimation of the mass concentrations of PM10, PM2.5 and PM1. Although these values are not obtained by a certified method (gravimetric method), they have the advantage of describing the time course of high resolution mass concentration.

A Condensation Particle Counter (Model 3775 TSI, flow 1.5 l min^{-1}) was used to determine the total number concentration of particles > 4 nm by means of a butanol condensation system. It provides highly accurate measurements over a wide concentration range from 0 to 10^7 particles cm^{-3}. In a supersaturated vapor, suspended particles act as nuclei for vapor condensation and may grow to form droplets. Particle laden air passes through a heated porous block or wick in contact with the working fluid, which is usually butanol, and becomes saturated. On exiting the saturator, the saturated air is cooled in the condenser, becoming supersaturated and causing particles above a certain size to grow into drops. These drops pass through the laser beam and are counted using a photometric light scattering technique (i.e. particle count is related to total scattered light during the integration period)

The coupled measure with CPC-OPC system allowed to determine the trend of three dimensional macro-ranges of suspended particles in the atmosphere: 4-250nm; 250-1000nm; >1000nm. N <250 includes the totality of nanoparticles, or ultrafine particles (d <100 nm), and a fraction of the accumulation mode (from 100 to 250 nm). Since the

number of ultrafine particles in the atmosphere greatly exceeds that of the accumulation mode in the Po Valley[49], N <250 mainly describes the behavior of ultrafine fraction and does not essentially contribute to the final mass concentration of atmospheric particulate matter due to the small size[2]. The complementary numerical concentration instead (N> 250) which is the sum of N250-1000 and N> 1000 includes most of the particles in the accumulation mode and the coarse fraction; both contribute to determine the final mass concentration of atmospheric particulate matter (due to its high dimensions)[2].

Black Carbon (BC) monitoring was conducted using a aethalometer (AE31, Magee Scientific Co. Berkeley CA, 7 wavelengths, 370 nm, 470 nm, 520 nm, 590 nm, 660 nm, 880 nm and 950 nm, and a flow of 4.9 l min^{-1}) which estimates in real-time the concentration of the optically absorbable carbonaceous fraction of atmospheric particulate matter. From an operational point of view, BC is defined as the fraction of the carbonaceous aerosol that absorbs light over a broad region of the visible spectrum and is measured by determining the attenuation of light transmitted through the sample when collected on a fibrous filter.

The air sample is drawn through an inlet port using an internal pump. The flow rate is monitored by an internal device and stabilized electronically. The sample is collected on a quartz fiber filter tape and the optical analysis is performed while the sample is collecting. The aethalometer uses an optical method based on the measurement of the attenuation of a beam of light transmitted through the sample when collected on a fibrous filter. This quantity is linearly proportional to the amount of BC in the filter deposit. The light penetrating the tape is detected by a photodiode placed underneath the filter. If black carbon is present on the filter, the amount of light detected by the diode will be less than that emitted. For accuracy, it is needed a reference beam measure that is a blank signal which is recorded by a second photodiode placed next to the first one, where Black Carbon is not collected.

The 'Optical Attenuation' ATN is defined as: $ATN= 100*\ln(I0 /I)$

Where I0 is the intensity of light transmitted through the original filter, or through a blank portion of the filter and I is the intensity of light transmitted through the portion of the filter on which the aerosol deposit is collected. The factor of 100 is for numerical convenience.

By adopting the nomenclature recommended by Petzold et al.[77] and other authors[2,78,79] the measured parameter can be defined as the equivalent Black Carbon (eBC). The eBC values were then estimated at 880 nm using the instrumental internal calibration

parameters (attenuation cross section of 16.6 m2 g-1). The use of the aethalometer allowed to separate the contribution of fossil fuel combustion (FF) and biomass (BB) to the total concentration of eBC.

DETERMINATION OF THE CONCENTRATIONS OF NO_X AND O_3. The measurement of NO_X was carried out using the AC32M analyzer (Environment SA) designed to monitor ambient NO and NO_2 concentrations. It operates on the principle that nitrogen oxide (NO) will emit light (chemiluminescence) in the presence of highly oxidizing ozone molecules. Chemilumiencence corresponds to an oxidation of NO molecules by ozone: $NO + O_3 \rightarrow NO_2^* + O_2$

The return to a fundamental electronic state of the excited NO_2* molecules is made by luminous radiation in a 600-1200 nm spectrum: $NO_2^* \rightarrow NO_2 + h\nu$

This energy can be lost by collision with molecules in the sample. By lowering the pressure in the reaction chamber, the probability of collision is reduced to obtain a better yield in terms of chemiluminescence.

The reaction chamber is separated from the detector by an optical filter, which selects only the radiation of wavelength greater than 610 nm. The radiation measure is performed by a photomultiplier. In order to be measured by chemiluminescence, NO_2 must be converted to NO according to the reaction:

$$2NO_2 \xrightarrow{Mo} 2NO + O_2$$

Sampling is performed by a pump placed at the end of the circuit. The measure is completed in 3 cycle steps:

- Reference cycle: the sample is driven into a pre-reaction chamber for mixing with ozone. The NO molecules contained in the gas are oxidized to give NO_2 before entering the reaction chamber.
- NO cycle: the sample is directly conducted into the measurement chamber where NO oxidation is performed by O_3. The signal measured by the photomultiplier is proportional to the number of NO molecules contained in the sample.
- NO_x cycle: the sample passes through the converter oven; then it is mixed with the ozone inside the reaction chamber. The signal measured by the photomultiplier is proportional to the number of NO and NO_2 molecules (from NO reduction) contained in the sample.

The ozone required for the chemiluminescence reaction is provided by an ozone generator discharge.

Ozone sampling was carried out using the O342M sampler (Environment SA), a continuous ozone analyzer, specific to detect concentrations ranging from 0 to 500 ppb, operating at any temperature between 10 and 35°C. The instrument is based on a photometric analysis of the ozone concentrations in a dynamic flow system. It considers the O_3 absorption capacity of electromagnetic radiation in the UV (200-300 nm). The ozone concentration is determined by measuring the amount of light radiation at 253.7 nm (the maximum ozone absorption coefficient) absorbed by the sample. The intensity of the light radiation passing through the measuring cell is perceived by the detector, returning the concentration of ozone in the sample:

$[O3]\ ppm = \frac{10^6}{\alpha l} ln \frac{i_0}{i}$ at p_0 (101.3 kPa) and t_0 (0°C)

where i_0 is UV energy detected through measurement cell when the sample does not contain ozone molecules and *i* is the UV energy measured on sample containing ozone to be measured.

Calculated ozone concentrations must be corrected for ozone losses that may occur in the UV photometer and for sample temperature and pressure. In order to compensate for the drifts in the UV lamp and to make the two measurements i_0 and *i* under the same conditions, a "UV reference" detector integrates the energy emitted by the UV lamp. Linear analog to digital converters convert reference and measurement signals from UV detectors into a series of frequency pulse train. Measurement values are averaged and compensated by reference values. Half of the cycle during which the sample passes through the ozone selective filter gives the values i_0. The next half of the cycle in which the sample passes directly into the measurement chamber gives the value *i.*

SAMPLING AND ANALYSIS OF VOCS, BTEX AND ALDEHYDES

VOC and BTEX sampling was performed by direct exposure to atmosphere of RADIELLO diffusion samplers exposed at regular intervals on a weekly basis. For VOC and BTEX, a stainless-steel mesh cartridge (3x8 μm), filled with 350 ± 10 mg of graphite charcoal (Carbograph 4) was used.

20 VOCs (1,1,1-trichloroethane, benzene, cyclohexane, trichloroethylene, n-heptane, 2-ethoxyethanol, toluene, n-octane, tetrachlorethylene, ethylbenzene, m / p-xylene, styrene, o-xylene, acetaldehyde, acrolein, benzaldehyde, butanal, hexane, formaldehyde, isopentanal, n-hexane, n-hexane, pentane, propane) were analyzed using GC Thermo Trace Ultra with ISQ / DSQ mass spectrometer detector and DANI Master TD heat desorber.

During the exposure phase, the cartridges were inserted into polypropylene macro-porous diffusers, connected to a support plate to ensure stability and resistance to meteorological factors. Knowing the exposure time (t), the sample mass (M) and the sampling rate (Q), it is possible to measure the environmental concentration: C = M / (t * Q)

2.1.3 THE NORTH SEA

The sampling campaign was performed during summer 2011 (20 June - 8 August) on board of the OCEANIA oceanographic ship (Polish Academy of Sciences). The campaign started in Tromsø (Norway) and finished in the Svalbard Islands (Norway), performing a two-months long cruise along the Arctic Ocean; longitudinal and latitudinal transects encompassed the Norwegian and Greenland Sea (Fig 2.5).

Figure 2.5 Route followed by the OCEANIA oceanogrphic ship during the sampling campaign.

A total of 24 samples of Total Suspended Particles (TSP) were collected. Air samples were taken by using a high-volume sampler (ECHO-PUF, TCR Tecora) designed to simultaneously collect the particulate and gaseous phases of the air (See paragraph 2.1.1). The collection of the TSP was performed on quartz fiber filters (QFFs, diameter 102 mm; Whatman, Springfield Mill, UK), whereas the gaseous compounds were captured by using a PolyUrethane Foam cartridge (PUF, diameter 60 mm, length 76 mm, ORBOTM 2000; Supelco, Sigma-Aldrich, St. Louis, MO, USA). The air sampler was installed at around 4 m above the upper deck of the ship (6-7 m above the sea level) and close to the bow (Fig 2.6). It was operated at 200 L min^{-1}, with an average sampling time of 48 h (average sampling volume = 566 m^3). The selected sampling flow rate

minimizes the sampling artifacts due to the sorption of gases on the filter and the volatilization of particle-bound compounds from the filter[80]. Air samples were collected continuously during the cruises, even if the ship was stopped at harbors.

Figure 2.6 Echopuf sampler on board of the oceanographic ship OCEANIA

Prior to sampling, the QFFs were baked at 600°C for 2 hours to reduce impurities and were then stored at room temperature wrapped in aluminum foils. After sampling, the samples were stored in aluminum foils at -20°C in the dark until analysis. Before and after sampling, the filters were equilibrated (48 h at 35% RH, room temperature) and weighted with a microbalance (1 µg precision, model M5P-000V001; Sartorius) in order to measure the mass of collected TSP. Together with the field filters, 6 blank field filters were collected.

TSP samples were divided into three different portions, each one dedicated to a different analysis: ionic chromatography (IC; ~ 1700 mm^2), gas chromatography coupled with mass spectrometry (GC–MS; ~ 3000 mm^2), carbon analyzer (150 mm^2). The portions were individually extracted and analyzed as described hereafter in order to determine Organic Carbon (OC) and Elemental Carbon (EC), water-soluble inorganic ions, and trace organic compounds, specifically alkylamines, mono- and dicarboxylic acids, polycyclic aromatic hydrocarbons (PAHs) and *n*-alkanes.

2.2 EXTRACTION OF PAHS AND ALKANES

To determine the concentration of n-alkanes and PAHs in the particulate and gaseous phases, the analytes were extracted from the matrix (filter or PUF) with a liquid solvent and then the extract was analyzed. This extraction procedure allowed the simultaneous determination of the n-alkanes and PAHs in the sample extracts.

2.2.1 PARTICULATE PHASE EXTRACTION

Before extraction, a known quantity of deuterated standards, used as internal standard, was added to each filter. The internal standard is a chemical species other than the compound of interest, which is added in a known quantity to the sample. During the extraction operations, a certain percentage of analytes is inevitably lost. By adding a known amount of deuterated standards to the samples, it is possible to determine the magnitude of these losses. The comparison between the internal standard signal after filter extraction and the internal standard signal as it stands, allows to calculate the percentage of analyte retrieved after extraction.

Filters were put into amber glass vials and extracted with 2 ml of dichloromethane (CH_2Cl_2; purity ≥ 99.9%, Sigma Aldrich) in an ultrasonic bath (Sonica®, Soltec) for 20 minutes. The extract was filtered with a PTFE syringe filter (cut 0.45 µm, Alltech) to remove any particles. The extraction solvent was evaporated under a gentle nitrogen (N_2; purity ≥ 99.9999%, Sapio) stream until dryness and dissolved in isooctane (C_8H_{18}; purity ≥ 99.5%, Panreac).

2.2.2 GASEOUS PHASE EXTRACTION

Before extraction, a known quantity of deuterated standards, used as internal standard, was added to each PUF. The samples were then extracted in a Soxhlet apparatus for 6 h (> 20 cycles) with 200 ml of dichloromethane (CH_2Cl_2; purity ≥ 99.9%, Sigma Aldrich). The extract was concentrated using a rotary evaporator (bath temperature ~ 40°C) until about 5 ml and then filtered through a PTFE syringe filter (cut 0.22 µm, Alltech) to remove any particles (e.g., foam particles). The solvent was evaporated under a gentle nitrogen (N_2; purity ≥ 99.9999%, Sapio) stream until dryness and dissolved in isooctane (C_8H_{18}; purity ≥ 99.5%, Panreac).

2.3 ANALYTICAL PROCEDURE

2.3.1 PAH AND N-ALKANES: INSTRUMENTAL ANALYSIS

The samples were analyzed by a Gas Chromatograph (GC) system coupled with a Mass Spectrometer (MS). The measurements were realized with a 6850 Agilent Technologies GC outfitted with an autosampler and a split/splitless injector.

A Zebron phase a ZB-XLB capillary column (length 60 m, i.d. 250 µm, film 0.25 µm; J&W Scientific) was used. The injected volume was 2 µl.

The quadrupole mass spectrometer (5973 Network Mass Selective Detector, Agilent Technologies) operated at 70 eV in the electron ionization (EI) mode. The mass spectra were recorded in the SIM (Single Ion Monitoring) mode.

PAHs. For the analysis of PAHs, the injector was kept at 280°C and operated in splitless mode. The oven temperature program started at 80°C, kept for 1 minute, then the temperature increased by 40°C/minute to 150°C. After that the temperature rises steadily at 5 °C/min until it reaches 300 °C, which is maintained for 24.25 minutes and is then further increased by 40 °C /min to 330°C. A single chromatographic run took 62 minutes (Tab. 2.1). The transfer line was kept at 310°C. As carrier gas helium (He; purity 99.999%, Sapio) was used with a variable flow of 1ml/min

Table 2.1 Oven temperature ramp for PAHs.

Start		80 °C	kept for 1 min
Ramp 1	40° C/min	until 150 °C	kept for 0 min
Ramp 2	5° C/min	until 300 °C	kept for 24.25 min
Ramp 3	40° C/min	until 330 °C	kept for 14.25 min
Post Run		80 °C	

The mass spectra were recorded in the SIM (Single Ion Monitoring) mode. This method allowed to determine and quantify the PAHs presented in Tab 2.2.

The 18 compounds determined by this procedure included the 16 PAHs specified by US-EPA (US-EPA Method 610) as priority pollutants because of their potentially toxic effect on human health. Other two PAHs (CPcdP and BeP) were added because of their important mutagenic effects [25,26].

Table 2.2 PAHs detected by the analytical method.

Name	Legend	Molecular Mass	Diagnostic Ion	n° of rings
Naphtalene	NAPH	128	128	2
Acenaphthylene	ACTY	152	152	3
Acenaphthene	ACT	154	154	3
Fluorene	FLN	166	166	3
Phenanthrene	PHE	178	178	3
Anthracene	ANT	178	178	3
Fluoranthene	FLNT	202	202	4
Pyrene	PYR	202	202	4
Benzo(a)Antracene	BaA	228	228	4
Ciclopenta(c,d)Pyrene	CPcdP	226	226	4
Chrysene	CHR	228	228	4
Benzo(b)Fluoranthene	BbF	252	252	5
Benzo(k)Fluoranthene	BkF	252	252	5
Benzo(e)Pyrene	BeP	252	252	5
Benzo(a)Pyrene	BaP	252	252	5
Dibenzo(a,h)Anthracene	DBahA	278	278	5
Indeno(1,2,3 c,d)Pyrene	I123cdP	276	276	6
Benzo(g,h,i)Perylene	DBghiP	276	276	6

Standards and Quantification. The PAHs mix standard was prepared using:

a. 1) a mix standard containing the 16 at 20 µg/ml (Supelco) to which 2 IPA (BeP, CPcdP) were added as single standard at 10 µg / ml
b. 2) a mix of 7 IPA deuterated at 200 µg / ml (Tab. 2.3)

All these standards were mixed together obtaining a mix of all the PAHs at the same concentration (1 µg ml^{-1}). The standard mix and their dilutions were analyzed and used for the identification and quantification of the analytes. The recovery rates of the samples were evaluated using deuterated internal standards.

Table 2.3 List of the deuterated PAHs used as internal standard

Name	Legend	Molecular Mass	Diagnostic Ion	n° of rings
Acenaphthene-d10	ACT-D	164	164	3
Phenanthrene-d10	PHE-D	188	188	3
Fluoranthene-d10	FLNT-D	212	212	4
Benzo(a)Antracene-d12	BaA-D	240	240	4
Benzo(a)Pyrene-d12	BaP-D	264	264	5
Dibenzo(a,h)Anthracene-d14	DBahA-D	292	292	5
Dibenzo(a,i)pyrene-d14	DBaiP-D	316	316	6

N-ALKANES. For the analysis of the alkanes, the injector was kept at 300°C and operated in splitless mode. The oven temperature program started at 60°C and increased by 6° per minute until it reached 300°C, kept for 20 minutes for a total time of 60 minutes for each run (Tab.2.4). The transfer line was kept at 305°C. As carrier gas helium (He; purity 99.999%, Sapio) was used with a constant flow of 1 ml/min.

Table 2.4 Oven temperature ramp for n-alkanes

Start		60 °C	kept for 1 min
Ramp 1	6° C/min	until 300 °C	kept for 20 min
Post Run		60 °C	

The mass spectra were recorded in the SIM (Single Ion Monitoring) mode, monitoring three m/z ratios (57, 71 and 85) for alkanes. A for the analysis of deuterated alkanes (C20-d, C24-d, C28-d) three more m/z ratios were monitored: 50, 66 and 82

This method allowed to determine and quantify the n-alkanes from octadecane to dotriacontante (Tab. 2.5).

Table 2.5 Alkanes detected by the analytical method

Name	Legend	Molecular Mass
Octadecane	n-c18	255
Nonadecane	n-c19	269
Eicosane	n-c20	283
Henicosane	n-c21	297
Docosane	n-c22	311
Tricosane	n-c23	325
Tetracosane	n-c24	339
Pentacosane	n-c25	353
Hexacosane	n-c26	367
Heptacosane	n-c27	381
Octacosane	n-c28	395
Nonacosane	n-c29	409
Triacontane	n-c30	423
Hentriacontane	n-c31	437
Dotriacontane	n-c32	451

Standards and Quantification. The n-alkane standard mix was prepared from single standards (from n-C18 to n-C32, Alltech) mixed together. The standard mix and their dilutions were analyzed and used for the identification and quantification of the analytes.

The n-alkane identification was obtained by comparison of the sample retention time against that of the standard. The recovery rates of the samples were evaluated using deuterated internal standards.

2.3.2 OTHER CHEMICAL ANALYSIS:

EC and OC were quantified by means of an EC/OC carbon analyzer (Sunset Laboratory Inc., USA) by thermal optical transmission, TOT, using the NIOSH 5040 protocol. Details on methods are given by Birch and Cary (1996) [81].

Inorganic ions (cations: Na^+, NH_4^+, K^+, Mg^{2+} and Ca^{2+}; anions: F^-, Cl^-, NO_3^-, SO_4^{2-}), carboxylic acids (C1-C5 mono and dicarboxylic acids) and alkylamines (metyil and ethil amines) were determined by extracting filters under sonication in ultrapure water (18.2 MU cm-1 Milli-Q water system, Millipore, Billerica, MA, USA). The extract was then filtered (0.45 mm pore size PTFE filter, Alltech USA) and analysed by IC (ICS-2000, Dionex) with a conductivity detector.

For the analysis of inorganic cations (Na^+, NH_4^+, K^+, Mg^{2+}, Ca^{2+}) as well as alkylamines (methylamine, dimethylamine, trimethylamine, ethylamine, diethylamine, triethylamine), an Ion Pac CG17 (4 x 50 mm) guard column and an Ion Pac CS17 (4 x 250 mm) analytical column were used, with a gradient elution of MethaneSulphonic Acid (MSA) from 3 to 40 mM at a constant flow rate of 1.0 mL/min, together with a CSRS 300 (4 mm) electrolytic suppressor. The column and detector cell temperatures were kept both at 50°C. For the analysis of inorganic anions (F^-, Cl^-, NO_3^-, SO_4^{2-}) as well as mono- and dicarboxylic acids (formiate, acetate, propionate, oxalate, malonate, succinate, glutarate), an Ion Pac AG11 (4 x 50 mm) guard column and an Ion Pac AS11 (4 x 250 mm) analytical column were used, with a gradient elution of KOH from 0.1 to 50 at a constant flow rate of 0.8 mL/min, together with an ASRS-ultra II (4 mm) electrolytic suppressor. The column and detector cell temperatures were kept at 30°C and 35°C, respectively. Quantification was made by using the external standard method. Single liquid standards (1 g L^{-1}; Fluka, Sigma-Aldrich, St. Louis, MO, USA) were used for inorganic ions and solid pure standards were used for alkylamines and carboxylic acids (pure grade > 99.5%; Chemie GmbH, Sigma Aldrich).

For elemental characterization, the aerosol-loaded filters were digested by a microwave oven (Milestone, Ethos ONE) according to the current legislation of the European Community in the field of air quality monitoring (UNI 14902:2005). The digestion mixture was composed of sub-boiling HNO_3 and ultra-pure H_2O_2 (Sigma-Aldrich, St. Louis, MO, USA). The resulting solutions were filtered and diluted to 15 ml with H_2O MilliQ. All the elements were determined by a magnetic sector inductively coupled plasma mass spectrometer (SF-ICP-MS) Element 2 by Thermo Scientific (Bremen, Germany).

For all chemical species measured, the detection limit (DL) was calculated by analysing the blank field filters, that are filters which were not used in the sampling but handled, extracted and analysed in the same way as the samples. DL values were computed as the mean signal of all analysed blank field filters plus three times the standard deviation. Concentrations of different chemical compounds lower than DL were replaced by half of the detection limit.

2.4 GAS-PARTICLE PARTITIONING MODELS

The two mechanisms that describe the partitioning of a SOC are adsorption on the aerosol surface and absorption into the organic matter [76]; there have been many discussions to explain whether absorption, adsorption or a combination of the two mechanisms is prevalent [82].

Gas particle partitioning can be explained by various empirical and theoretical models based on single- or polyparameter linear free energy relationships (spLFER, ppLFER). SpLFER models relate the partitioning constant to one of its chemical-physical properties, for example the subcooled liquid vapour pressure (pL^0) or the octanol-air partition coefficient, while the ppLFER models correlate the distribution constant to more than one property, considering all the significant molecular interactions between solute and sorbent [83].

The first models developed and conventionally used for the partitioning (Junge-Pankow Model) considered the adsorption only, assuming that the chemical compounds adsorbed to the active sites on the surface of the particles. An alternative model (Koa Model) was subsequently proposed which, assuming that the aerosol is coated with an organic film, considered the absorption of the chemical compounds in this organic phase relevant and used the Koa coefficient to describe the partitioning [75]. Given the importance of both adsorption and absorption processes, the dual model was subsequently proposed, describing the transition from the gaseous phase of semi-volatile organic compounds to atmospheric particulate matter (and vice versa) as the sum of two processes: absorption into the organic matter of atmospheric particulate matter and adsorption on elemental carbon of PM. This model has already been applied to polycyclic aromatic hydrocarbons by various authors (eg, Lohmann and Lammel, 2004) [27] but there is a lack of information about the validity of the model for other classes of compounds such as alkanes. In addition, the model is often criticized in literature because it tends to underestimate the partitioning of SOCs absorbed into the particulate matter. This is probably due to the fact that the model does not take into account other processes that may be important, such as adsorption on mineral surfaces and salts. A widely used approach nowadays to describe absorption is represented by the linear free energy relationships (ppLFER) model which is currently the most accurate method for describing phase equilibrium distribution. It is a multiple linear regression model that uses several descriptors as independent variables and can be used to estimate the distribution coefficients of a large number of compounds[84].

The gas-particle partitioning of a compound can be described through the distribution coefficient Kp:

$$Kp \text{ (m3µg-1)} = ((Cip / TSP)) / Cig \qquad \text{(eq. 1.1)}$$

where Cip and Cig are the concentration of the compound in the particulate and in the gaseous phase respectively and TSP is the concentration of the total suspended particulate[20,27]. The phase partitioning may also be described by the fraction θ of a compound in the particulate phase:

$$\theta = Cip / (Cip + Cig) \qquad \text{(eq. 1.2)}$$

where Cip is the concentration of the compound in the particulate phase (ng μg^{-1} of particles) and Cig is the concentration in the gaseous phase (ng m^{-3} of air).

Several models have been proposed to predict the partitioning of a semi-volatile compound between the particulate phase and the gaseous phase.

Originally suggested by Junge and subsequently revised by Pankow, the Junge-Pankow model is the most common model used to estimate the adsorption of a semi-volatile organic compound. If adsorption to active sites on the surface of the particles is the dominant process in the partitioning, then:

$$\theta = CjS / (CjS + pL°) \qquad \text{(eq. 1.3)}$$

The model relates the adsorbed fraction on the particles, θ, to the vapour pressure, $pL°$ (Pa), to the surface area of particles S (cm^2 of aerosol cm^{-3} of air) and to a constant Cj which depends on the molecular weight of the substance and the condensation heat.

Usually a value of Cj = 17.2 Pa is used, although it has been suggested that it may vary depending on the class of compound[75]. For individual analytes, Cj can be determined using measured θ and S, as well as temperature-corrected $pL°$ through Eq. 1.4,

$$Cj = \theta\, pL° / S (1- \theta) \qquad \text{(eq. 1.4)}$$

For the parameter S, values of 1.1×10^{-5} values for the urban atmosphere and 1.1×10^{-7} for rural sites were used.

The $pL°$ values at 298 K were obtained from the literature[85,86,87] and corrected for changes in the average ambient temperature during each sampling event.

Experimental θ can be converted to Kp (m^3air g^{-1} PM) using Eq. 1.*5*

$$Kp = \theta / C_{PM} (1- \theta) \qquad \text{(eq.1.5)}$$

where C_{PM} is PM concentration in air (g m^{-3}).

The partitioning coefficient Kp is often related with the sub-cooled liquid saturation vapour pressure (pL°):

$$\log Kp = m \log pL° + b \quad \text{(eq. 1.6)}$$

where m and b are the slope and the intercept, respectively. For equilibrium partitioning m is expected to have a value of near -1.

A good linearity with a slope near -1 is a necessary in a proof that gas/particle partitioning sorption is governed by physical adsorption, but such an observation does not exclude other sorption mechanism such as absorption into a liquid organic film coating the particles. With this assumption, Pankow[88] proposed an absorptive mechanism for partitioning of SOCs, based on their vapour pressure. This mechanism was later described by Finizio et al.[82] who suggested using the octanol-air partitioning coefficient KOA. For this model, KP was calculated using Eq 1.7.

$$Kp\ (abs) = 10^{-12} \left(\frac{fOM}{\rho oct}\ x\ \frac{\gamma octMWoct}{\gamma OMMWOM}\right) x\ Koa \quad \text{(eq. 1.7)}$$

where fOM is the fraction of organic matter (OM) in the particulate matter, ρOCT (0.82 kg L^{-1}) is the density of octanol, γOCT and γOM are activity coefficients of the target compound in octanol and organic matter, respectively, MWoct e MWOM are molecular mass of octanol (130 g mol^{-1}) and organic matter, respectively.

If octanol perfectly simulates the organic matter in PM, it can be assumed that γOCT/ γOM and MOCT/MOM =1[75]. A mean value of 500 g mol^{-1} for MOM was later suggested by Götz et al. [91], which results in MOCT/MOM of 0.26.

Eq. 1.7 can be simplified as follows:

$$Kp\ (abs) = 10^{-12}\ x\ KOA\ x\ fOMx\ 0.32 \quad \text{(eq. 1.8)}$$

For model calculations, experimentally determined KOA values were obtained from Beyer et al.[90] and Odabasi et al. [87] and corrected for changes in ambient temperature in each sampling event.

The choice of using pL° or KOA depends on whether the compound “feels” more like being dissolved in itself (pL°) or in octanol-like organic matter (KOA) [91].

It has been noted that eq. 1.8 under-predicts Kp values for PAHs by 10 to 50 times[75,76]. This could be due to the fact that absorption into OM alone is not sufficient in accounting for the PAHs sorption to particles but adsorption onto the soot fraction of atmospheric aerosol may be an important mechanism affecting the partitioning.

Given the importance of both processes, Dachs and Eisenreich[76] suggested the use of a dual model to simultaneously take into account the absorption in the organic matter of the TSP and the adsorption on soot.

This model can be formulated as Eq. 1.9

$$Kp\ (abs + ads) = 10^{-12}\left[\left(\frac{fOM}{\rho OCT}\ x \frac{\gamma OCTMWOCT}{\gamma OMMWOM}\right) KOA + \left(fEC\ x\ \frac{aEC}{asoot}\right) KSA\right] \qquad \text{(eq.1.9)}$$

where fEC (unitless) is the fraction of elemental carbon (EC) in PM, aEC and asoot (m^2 g^{-1}) are specific surface area of EC and soot, respectively, and KSA (L kg^{-1}) is soot-air partitioning coefficient. The latter was calculated using a thermodynamic estimation model suggested by van Noort [92]:

$$\log KSA = -0.85 \log pL0 + 8.94 - \log (998/asoot) \qquad \text{(eq.1.10)}$$

Assuming that EC accounts for the majority of soot, then aEC/a soot=1 [76]

The dual model uses octanol as a surrogate of OM in the absorptive partitioning and EC as a surrogate for soot in the adsorption process.

Considering the aforementioned assumption, eq. 1.9 becomes:

$$Kp\ (abs+ ads) = 10^{-12}\ x\ KOA\ x\ fOMx\ 0.32 + KSA\ x\ f\text{EC} \qquad \text{(eq.1.11)}$$

This model is often criticised for underestimating Kp, probably because of a lack of description of other partitioning processes such as adsorption on the mineral surfaces or on the air-water interface [73]. Even the choice of values for the parameters in equation 1.11 is important and may be in part responsible for the deviation from the experimental values. Moreover, octanol and soot may not perfectly simulate the effect of organic matter and elemental carbon.

Models based on more than 2 parameters (called poly-parameter linear free energy relationships), should be better in predicting the partitioning of SOCs.

The linear free energy relationships (ppLFER) model is increasingly used in literature to describe the distribution of organic compounds in different environments and to predict the distribution coefficients. It always refers to equilibrium partitioning; both absorption and adsorption processes to any type of materials are considered. The ppLFER model takes into account the molecular interactions between the compound (sorbate) and the sorbent phase.

The most used ppLFERs models are the linear solvation energy relationship developed by Abraham[93] for condensed phase-condensed phase (eq. 1.12) and condensed phase-

air systems (eq.1.13). Later Goss [94] combined the two equations to form a single ppLFER eq (eq. 1.14) which, in many cases, can be applied to both systems

$$\text{Log } Kp = eE + sS + aA + bB + vV + c \qquad \text{(eq.1.12)}$$

$$\text{Log } Kp = eE + sS + aA + bB + lL + c \qquad \text{(eq.1.13)}$$

$$\text{Log } Kp = sS + aA + bB + vV + lL + c \qquad \text{(eq.1.14)}$$

Kp is a logarithmic partition coefficient. The capital letters E, S, A, B, L, and V are solute descriptors for excess molar refraction (which describes interactions between solute's π- and solvent's n-electron pairs), polarizability/ dipolarity, solute H-bond acidity, solute H-bond basicity, logarithm of solute hexadecane-air partitioning coefficient (unitless), and McGowan molar volume (cm^3 mol^{-1})/100, respectively [84]. The corresponding small letters are known as system parameters, which reflect matrix-specific solute-independent contribution to Kp.

Each term quantitatively describes the energetic contribution of one type of intermolecular interaction to log K. aA represents the energetic contribution of H-bonding interactions between H- donating solute and H-accepting solvent, and bB describes the opposite relationship. vV in eq 12 and lL in eq 13 describe cavity formation and dispersion interactions, eE is an additional term to account for dispersion interactions, and sS describes interactions related to surface polarity of the molecule [84]. It should be noted that the system parameters do not give account of the absolute properties of the two phases but describe the "differences" between the two phases at a given temperature, because it is the difference that matters for partitioning. Arp et al.[74] categorized their samples collected in Europe based on the major component of PM, identified through scanning electron microscopy. Therefore, they developed a ppLFER equation for aerosols from urban and nonurban areas in Europe which is a good model since it represents the generic sorption properties of continental PM.

Two mechanisms are considered in the model: adsorption onto to elemental carbon (EC) and soluble salts and absorption into the organic matter. For the latter two scenarios are considered: partitioning into a single organic phase and partitioning into various OM fractions distributed across one or more organic phases. For each phase, an appropriate PPLFER equation is used and Kp is calculated by summing the individual partitioning constants. For the dual-phase ppLFER, absorption into OM, as well as adsorption onto soot are assumed.

Conventionally, octanol has been used as a surrogate for the organic matter. Nevertheless, it shows low water solubility and dipolarity/polarizability if compared to some constituent of the water soluble organic matter. In order to choose a better surrogate to represent Water Soluble Organic Matter (WSOM), Shapoury et al.[83] considered the following criteria: having water solubility and molecular mass close to those found for major WSOM constituents, the substance dipolarity (denoted by Abraham S descriptor), and availability of methods for determining solute-specific enthalpies of phase-transfer. Based on the three criteria mentioned above, the authors allocated DMSO-air to phase 'A' because it has both the highest water solubility and Abraham "S" descriptor.

The adsorption contribution can be approximated by carbonaceous material such as diesel soot, which is considered the most significant type of EC in polluted areas. During combustion of fuels, small graphite-like carbon particles can be formed due to incomplete combustion. These EC can agglomerate in larger particles while organic vapors adsorb on it. It can be assumed that EC accounts for most of soot carbon and that the atmospheric elemental carbon is comparable in its adsorptive properties to diesel soot. Soot is a mixture of EC and OM but represents an EC- dominated aerosol type. For this reason, system parameters for diesel soot [95] were used to simulate the adsorption process.

For multi-phase ppLFER, the model differentiates between various organic and inorganic phases of the particulate matter (PM).

As for the absorption contribution, it is assumed that OM to consist of two phases: (A) low or high molecular mass water-soluble and organic-soluble organic matter (WSOSOM) - eg. Humic-like substances, diterpenoid acids, aromatic poly-carboxylic acids, aliphatic dicarboxylic acids, n-alkenoic acids, n-alkanoic acids and (B) high molecular organic polymers (OPs)[83]. In addition, low or high molecular mass molecules that tend to be insoluble in water (WI), such as aliphatic and polycyclic aromatic hydrocarbons, contribute to OM but it has been shown that this fraction could contribute ≤5% of OM in urban aerosols.

The mass fraction for the phases 'A' and 'B' was estimated using the data reported by Rogge et al. [28] for Rubidoux, 75 kilometers off Los Angeles that assigned to phase A 60% of OM and 40% to phase 'B'. These estimated fractions were subsequently corrected for the OM fraction in PM (fOM) which was determined from the organic carbon concentration using the conversion factors of 1.6 and 2.1 for urban and non-urban sites respectively [96].

As already explained for the dual-phase ppLFER, DMSO-air was chosen to represent phase A of the organic matter.

Phase B represents organic polymers originated from natural sources (e.g. cellulose) as well as condensation and polymerization of gaseous organics in the atmosphere. This polymer originates from plant debris and is made of D-glucose units. As a result, cellulose could potentially form hydrogen bonds with solutes which undergo such type of interaction, particularly via the surface chains. To simulate nonspecific and specific molecular interactions for polymeric OM, a ppLFER model for Polyurethane-air was assigned to OM phase B.

In addition to absorption into OM, adsorption to elemental carbon (EC) and inorganic surfaces must be considered. For this reason, regarding the adsorption contribution, it has been chosen to use system parameters for diesel soot [95], ammonium sulfate, and ammonium chloride[97]. As reported in Shapoury et al. [83], the soot specific surface area was set to 18.21 $m^2 g^{-1}$ – i.e. the geometric mean of surface areas for traffic, wood, coal, and diesel soot (i.e., 59.4, 3.6, 8.2, and 62.7 $m^2 g^{-1}$).

Relative humidity does not have substantial effect on adsorption of organic vapors to diesel soot [95] but has some effects on adsorption to ammonium sulfate and ammonium chloride [97]; therefore, relative humidity at the sampling sites was taken into consideration when choosing the system parameters for salt surfaces. When the mass mixing ratios of marine salts in PM are expected to be high, the ppLFER model for ammonium chloride can be replaced by the model for sodium chloride [83].

Adsorption on mineral dust was not considered since Arp et al.[74] noted that out of several samples with different sources, a mineral-rich sample with Sahara origin demonstrated the lowest partitioning constants for nonpolar organic compounds.

All partitioning constants were corrected for the effect of near-ground temperature, the units normalized, and then individual partitioning coefficients were summed to obtain total Kp.

CHAPTER 3. PARTICULATE MATTER IN THE CITY OF MILAN

The Lombardy Region is a very critical area for air pollution, because of its geographic conformation and the weather-climatic conditions. During winter, PM concentrations are higher because of the inversion layer that tends to remain low, limiting the circulation of the air, promoting mist and smog formation and concentrating pollutants in the atmospheric layer closest to the ground.

Traffic is considered the main source of pollution in urban areas [9], so the competent authorities have to order traffic block or identify restricted traffic areas to reduce this phenomenon. To discourage the use of pollutant private lines, reduce traffic and pollution and raise resources for investment in public transport, the city of Milan, starting from January 2012, established a system of paid access to the central area of the city called AREA C.

To study this phenomenon, a sampling campaign was conducted during 2013 in 3 seasonal periods at a traffic site (January, July and October). In October, the sampling was simultaneously performed at the traffic site and in limited traffic site in the city center within the low emission zone (LEZ).

The chemical characterization of the aerosol was performed: Organic and Elemental Carbon (OC and EC, by thermal-optical transmittance), water-soluble inorganic ions, carboxylic acid and alkylamines (by ionic chromatography), Polycyclic Aromatic Hydrocarbons (PAHs) and C20 to C32 n-alkanes (ALKs) by gas chromatography-mass spectrometry; elements (by a magnetic sector inductively coupled plasma mass spectrometer).

An overview of the TSP concentrations and of the chemical composition will be presented and an in-depth analysis of the PAHs and n-alkanes concentrations will follow. The choice of sampling TSP rather than PM10, PM2.5 or even the finest fraction, derives from the fact that this was an exploratory study, made to understand if there were any differences inside and outside the LEZ.

The main features of gas/particle partition of the two chemical classes will be described. An attempt to apply some of the best available models will also be made to evaluate the relative importance of adsorption on soot and absorption into the organic matter.

3.1 TSP CONCENTRATIONS

The filters were weighed three times before and after sampling to determine the mass of TSP deposited on the filter (see Chapter 2, Par.1.1). The detection limit was calculated (DL winter/summer= 1.5 μg m^{-3}, DL autumn= 0.9 μg m^{-3}). The resulting values were corrected for the contribution of blank filters. The obtained mass was then divided to the volume of air sampled to obtain the concentration of TSP (μg m^{-3}).

TSP concentrations measured at TR site in winter (WI), summer (SU) and autumn (AU) are presented in Fig.3.1.

TSP concentrations were 2 times higher in winter (131 ± 49 μg m^{-3}) compared to summer and autumn when similar TSP concentrations of 48 ± 7 μg m^{-3} (SU) and 57 ± 19 μg m^{-3} (AU) were measured at the TR site. Within the LEZ in AU the concentrations were similar to the TR site (52 ± 19 μg m^{-3}) with a R^2= 0.75 between the two sites (Fig. 3.2). This data indicates that there aren't significant differences in TSP concentration between the two sites, despite the different impact of the traffic source. This result is in accordance with other studies on the effectiveness of the ECOPASS measure, now replaced by AREA C[51,98] which highlighted that there is no reduction in concentrations of PM10, PM2,5 and PM1 in the atmosphere within the ECOPASS area compared to the outside area. Data indicates that small-scale emission reduction measures (such as a local reduction of traffic) do not involve measurable improvements in local PM levels, but inter-regional interventions are needed.

By comparing the obtained data with the weather conditions measured by ARPA Lombardy it can be noticed that the lower TSP concentrations occurred during atmospheric precipitation, which are the main mechanism of PM removal.

By comparing TSP measures with data derived from ARPA stations for PM10 (the fraction of particles < 10 mm d_{ae}, also known "PM respirable fraction"), it possible to calculate that PM10 was the major fraction (75 ± 5%) of TSP samples in all seasons and at both sites in Milan.

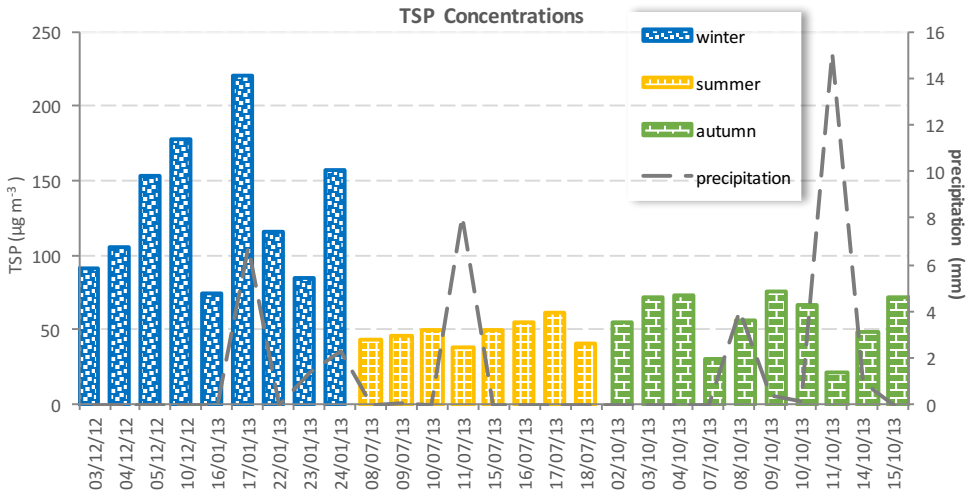

Figure 3.1 . TSP concentrations (µg m-3) in winter, summer and autumn 2013 and precipitations (mm)

The higher concentrations recorded in winter may be due to the sources of PM and the weather conditions: the mixing layer is lower during winter, limiting the vertical mixing of air masses and concentrating the pollutants close to the ground. On the contrary, during summer, the sunshine and the consequent convection favour the dilution of air pollutants. Moreover, an important source of PM emission that is the heating of offices and homes, is missing during summer.

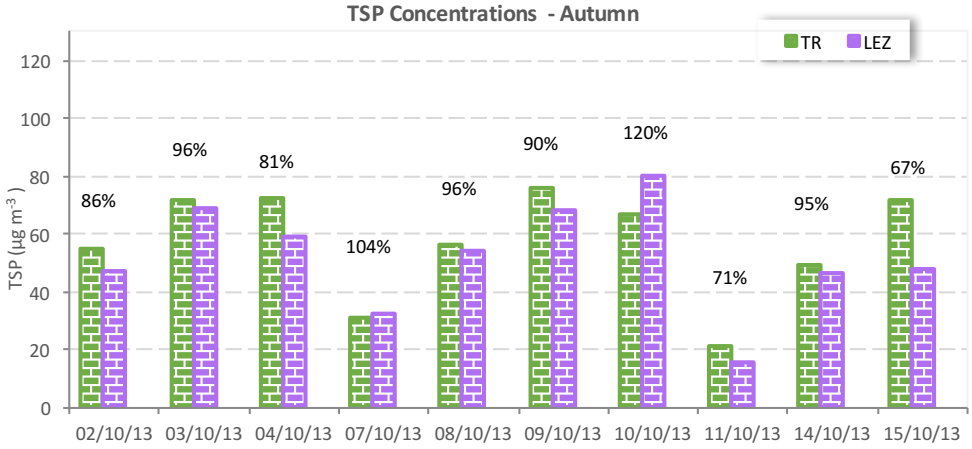

Figure 3.2 TSP concentrations (µg m-3) in autumn at a traffic site (TR) site and within the Low Emission Zone (LEZ). The numbers are the ratio LEZ/TR %

3.2 CHEMICAL COMPOSITION

The major chemical components of PM (Table 3.1) were OC (also converted to OM, organic matter, as 1.6 x OC[96]), EC, SO_4^{2-}, NO_3^-, NH_4^+ and mineral dust (estimated by measurements of elements including Al, Ca, Mg, Fe, K[99]). These single chemical components accounted on average 26% (OM), 4.1% (EC), 6.8% (SO_4^{2-}), 16.6%(NO_3^-), 6% (NH_4^+) and 15% (mineral dust) of TSP, summing up to ≅75% of particle mass. The chemical composition analysed for TSP in Milan is consistent with that of the PM10 fraction in Milan[9], as well as that reported by Putaud et al.[99] for other urban sites across Southern Europe (contributions to PM10 mass: OM = 26%; EC= 6%; SO_4^{2-} =12%; NO_3^- = 9%; mineral dust = 21%).

The average concentration of carboxylic acids, which are typically attributed to secondary sources, at the TR site was at a maximum in SU (∑CAs = 0.96 ± 0.29 μg m^{-3}). This was quite high if compared with other summer campaigns in Milan in the years 2006-2009, when the average concentration of ∑CAs was 0.47 ± 0.07 μg m^{-3} for PM10 samples [9]. This could indicate an important contribution of secondary organics in the PM samples during this summer 2013 campaign.

In the present study has been measured for the first time in Milan the concentrations of alkylamines, of which has been found at low but detectable concentrations DMA^+ (0.04 μg m^{-3} in SU; 0.09-0.10 μg m^{-3} in W and late-SU) and TEA^+ (0.36-0.42 μg m^{-3} in late-SU). Despite the very important role that these alkylamines are supposed to play in aerosol chemistry and secondary formation, there are still very few data about their concentrations in PM ambient samples [100].

The concentrations of primary trace organic compounds, PAHs and n-alkanes, will be discussed in the next paragraphs.

Table 3.1 Average values and standard deviation of carbonaceous fraction (OC, EC and total carbon, TC), elements, inorganic ions, carboxylic acids, alky amines, some meteorological parameters and gas pollutants separately for the different seasons (winter (W), su

				Traffic (TR) site			LEZ site
				Winter - WI (n=5)	Summer - SU (n=7)	Autumn - AU (n=10)	Autumn - AU (n=10)
				Mean SD	Mean SD	Mean SD	Mean SD
Meteo Data[a]		Global Rad	W m^{-2}	54 ±25	247 ± 41	158 ± 82	158 ± 82
		T	°C	4.2 ± 1.3	25.7 ± 0.8	15.9 ± 1.3	15.9 ± 1.3
		RH	%	78.4 ± 8	54 ± 3.6	69.9 ± 16	69.9 ± 16
Gas pollutants[a]		NOx	µg m^{-3}	160.8± 44	53 ± 05.3	112.5 ± 35.1	112.5 ± 35.1
		O_3	µg m^{-3}	8.4 ± 6	85 ± 10.4	25.2 ± 15.1	25.2 ± 15.1
TSP chemical	Carbonaceous	OC		26.5 ± 17.5	7.5 ± 0.8	9.0± 3.2	7.4 ± 1.9
composition	fraction (µg m^{-3})	EC		6.2 ± 2.9	1.5 ± 0.4	2.6 ± 1.1	1.6 ± 0.6
		TC		32.8 ± 20.3	9.0 ± 0.9	11.6 ± 4.2	9.0 ± 2.4
	Element (µg m^{-3})	Al		0.7 ± 0.4	0.3 ± 0.1	0.4± 0.2	0.4± 0.3
		Ca		3.4 ± 1.8	1.2 ± 0.3	1.9 ± 0.4	1.9 ± 0.5
		V		0.0037 ± 0.0016	0.0017 ± 0.0004	0.0017 ± 0.0008	0.0014 ± 0.0007
		Mn		0.053 ± 0.023	0.016 ± 0.002	0.022 ± 0.007	0.016 ± 0.006
		Fe		4.2 ± 2.0	0.9 ± 0.1	1.1 ± 0.6	0.7 ± 0.3
		Co		0.0017 ± 0.0008	0.0004 ± 0.0001	0.0007 ± 0.0008	0.0006 ± 0.0003
		Ni		0.0080 ± 0.0033	0.0018 ± 0.0004	0.0105 ± 0.0076	0.0119 ± 0.0084
		Cu		0.161 ± 0.075	0.032 ± 0.009	0.047± 0.027	0.026 ± 0.010
		Zn		0.229 ± 0.129	0.049 ± 0.013	0.064 ± 0.026	0.039 ± 0.009
		As		0.0021 ± 0.0012	0.0009 ± 0.0002	0.0012 ± 0.0005	0.0010 ± 0.0004
		Cd		0.0037 ± 0.0023	0.0006 ± 0.0003	0.0007 ± 0.0004	0.0006 ± 0.0003
		Ba		0.078 ± 0.041	0.016 ± 0.005	0.025 ± 0.014	0.016 ± 0.007
		Ce		0.0021 ± 0.0009	0.0008 ± 0.0001	0.0007 ± 0.0003	0.0006 ± 0.0003
		Nd		0.0006 ± 0.0004	0.0002 ± 0.0000	0.0002 ± 0.0001	0.0002 ± 0.0002
		Gd		0.00047 ± 0.00022	0.00014 ± 0.00004	0.00008 ± 0.00005	0.00007 ± 0.00002
		Pb		0.143 ± 0.081	0.022 ± 0.023	0.016 ± 0.011	0.010 ± 0.005
		Mo		0.009 ± 0.004	0.002 ± 0.001	0.001 ± 0.001	0.001 ± 0.001
		∑ elements		9.019 ± 4.344	2.574 ± 0.299	2.977 ± 1.465	2.350 ± 1.4518
	Inorganic ions (µg m^{-3})	F-		0.08 ± 0.04	0.02 ± 0.01	0.02 ± 0.02	0.02 ± 0.03
		Cl-		3.7 ± 3.4	0.1 ± 0.0	0.7 ± 0.8	0.6 ± 0.8
		NO3-		16.5 ± 6.6	5.7 ± 2.2	10.9 ± 6.6	10.2 ± 6.5
		SO4=		4.0 ± 1.5	3.5 ± 0.3	4.2 ± 2.6	4.5 ± 2.6
		NH4+		3.9 ± 1.4	2.7 ± 0.4	4.2 ± 2.9	4.0 ± 3.0
		K+		5.56 ± 2.41	0.27 ± 0.05	0.71 ± 0.74	0.62± 0.63
		Ca++		2.6 ±1.2	1.6 ± 0.3	1.6 ± 0.7	1.5 ± 0.5
		∑ ions		38.8 ± 12.5	12.5 ± 4.4	23.3 ± 12.2	23.1 ± 12.2
	Carboxylic acids (Cas) (µg m^{-3})	**∑ CAs**		1.32 ± 0.53	0.96 ± 0.29	0.75 ± 0.18	0.73 ± 0.21
	Alkylamines (µg m^{-3})	DMA+		0.10 ± 0.03	0.04 ± 0.00	0.09 ± 0.02	0.10 ± 0.01
		TEA+		<0.32	<0.32	0.36 ± 0.02	0.342 ± 0.10

a= Data obtained from the Lombardy Regional Agency for Environmental Protection (ARPA), which monitors the air quality of Milan at various stations inside and outside LEZ.
The data has been taken from four ARPA stations: "Verziere" and "Senato" stations for the LEZ site; "Marche" and "Senato" for the TR site.

3.2.1 PAHs

PAHs Concentrations. To take into account filter and PUF plug processing and transport, the detection limit (DL) was estimated. For the particulate phase, DL was estimated by blanks field filters: three combined with the winter and summer sampling at MI (n=1 in winter and n=2 in summer) and four combined with the autumn sampling (n=2 at LEZ site and n=2 at TR site). The gaseous phase detection limits were estimated by blank field PUF plugs: three combined with the winter and summer sampling at MI (n=1 in winter and n=2 in summer). For the autumn campaign the blank PUF plugs collected during the winter and summer campaign were used.

Considering the very similar contamination between the blanks of winter and summer, the three samples were used together to calculate a unique detection limit for the winter-summer campaign.

All the blank field filters and the blank PUF plugs were processed and analysed as the real samples. Their concentrations were used to calculate the detection limit (DL) for the PAHs as in the eq. 3.1:

$$DL=\mu B +3*\sigma B \qquad \text{(eq. 3.1)}$$

where µB and σB were the average concentration and standard deviation of the blank field filter (ng/filter), respectively.

The mean values got by the blank field filter and PUF plugs were subtracted to the valid sample data.

The recovery factors were always applied: the concentrations were corrected for the deuterated PAHs recoveries.

Table 3.2 PAHs average concentrations in the blank field filters and DL (ng/filter)

Winter- Summer									
	NAPH	**ACTY**	**ACT**	**FLN**	**PHE**	**ANT**	**FLNT**	**PYR**	**BaA**
Average	1.1	0.0	0.0	0.1	0.4	0.0	0.2	0.1	0.1
DL	2.1	0.0	0.0	0.2	0.6	0.0	0.8	0.5	0.5
	CPcdP	**CHR**	**BbF**	**BkF**	**BeP**	**BaP**	**DBahA**	**I123cdP**	**BghiP**
Average	0.0	0.0	0.0	0.2	0.1	0.1	0.0	0.2	0.2
DL	0.0	0.7	0.0	0.7	0.5	0.3	0.0	1.0	1.2
Autumn									
	NAPH	**ACTY**	**ACT**	**FLN**	**PHE**	**ANT**	**FLNT**	**PYR**	**BaA**
Average	0.2	nd	1.5	0.8	4.1	0.3	0.8	0.7	nd
DL	0.2	0.0	1.7	1.2	5.8	0.7	1.1	1.1	0.0
	CPcdP	**CHR**	**BbF**	**BkF**	**BeP**	**BaP**	**DBahA**	**I123cdP**	**BghiP**
Average	nd	0.0	0.0	nd	nd	nd	nd	nd	nd
DL	0.0	1.1	0.0	0.0	0.0	0.0	0.0	0.0	0.0

nd= not detected , DL= detection limit

Table 3.3 PAHs average concentrations in the blank PUF plugs and DL (ng/plug)

	NAPH	ACTY	ACT	FLN	PHE	ANT	FLNT	PYR	BaA
Average	19.6	0.3	8.2	7.5	28.4	1.4	8.5	10.8	0.6
DL	33.6	0.3	14.2	11.2	43.7	2.1	17.2	15.4	2.0
	CPcdP	**CHR**	**BbF**	**BkF**	**BeP**	**BaP**	**DBahA**	**I123cdP**	**BghiP**
Average	0.0	0.4	0.5	0.0	0.3	0.0	0.0	0.0	0.0
DL	0.0	0.7	0.7	0.0	0.4	0.0	0.0	0.0	0.0

nd= not detected , DL= detection limit

The PAHs were measured for all the samples collected during winter, summer (at TR site) and autumn (at TR and LEZ site). Their concentrations are summarized in Tab. 3.4.

As for the particulate phase, 9 samples were collected in winter, 8 samples in summer and 20 samples in autumn (n=10 at TR site; n=10 at LEZ site). For the gaseous phase 9 samples were collected in winter, 8 samples in summer and 7 samples in autumn (n=3 at TR site; n=4 at LEZ site).

Table 3.4 PAHs concentrations in the particulate and in the gaseous phase

		TR winter (n=9)		TR summer (n=8)		TR autumn (n=10)		LEZ autumn (n=10)	
		Average	St.Dev.	Average	St.Dev.	Average	St.Dev.	Average	St.Dev.
Conc (ng m-3)	particulate	74.92	22.54	0.86	0.76	3.50	2.38	2.38	1.26
% in TSP		0.0625	0.0234	0.0019	0.0017	0.0064	0.0035	0.0052	0.0029
		TR winter (n=9)		TR summer (n=8)		TR autumn (n=3)		LEZ autumn (n=4)	
		Average	St.Dev.	Average	St.Dev.	Average	St.Dev.	Average	St.Dev.
Conc (ng m^{-3})	gaseous	83.25	61.46	14.57	5.70	3.99	1.47	3.44	0.85

n = number of samples; PAHs = NAPH, ACTY, ACT, FLN, PHE, ANT, FLNT, PYR, BaA, CPcdP, CHR, BbF, BkF, BeP, BaP, DBahP, I123cdP, BghiP

The PAHs concentrations (ng m^{-3}) in winter and summer show markedly different values. As for the particulate phase, they were similar to previous measurements in Milan in the years 2006-2009 [9].

The total (particulate + gaseous) concentrations were 158.17±66.86 ng m^{-3} (MIN: 61.02 ng m^{-3}, MAX: 271.21 ng m^{-3}) during winter and 15.48±6.40 ng m^{-3} (MIN: 9.72 ng m^{-3}, MAX: 28.39 ng m^{-3}) in summer. In autumn, at both sites the concentrations were slightly higher than those found in summer for the particulate phase but lower for the gaseous phase. In all the seasons, the total PAHs were more concentrated in the gaseous than particulate phase. These values are in the same order of magnitude with other studies undertaken in other Italian cities [101, 102, 103].

Comparing the two sites during autumn, there is a good correlation (R^2 PM phase= 0.86; R^2 gas phase= 0.99) with respect to the concentration of PAHs. The PAHs concentrations were lower within the LEZ both for the particulate and the gaseous phase: a reduction of 32% for PAHs in the particulate phase and of 14% in the gaseous phase was found within LEZ. As for particulate phase the maximum PAHs concentrations (TR= 9.68 ng m^{-3}; LEZ= 5.16 ng m^{-3}) were recorded during the last day of sampling (15/10/2013). This increase in concentrations may be due to the addition of an emission source: heating. Following the regulations on heating systems (DPR 412/93) from 15th of October to 15th of April it is permitted to turn on the heat for 14 hours a day.

The gaseous PAHs showed a preference for a small number of compounds (PHE, FLN, FLNT, PYR, ACTY) highly concentrated in air. On the contrary, the particulate PAHs were low concentrated, but a wider range of compounds were detected in the particulate matter (Fig. 3.3 and 3.4).

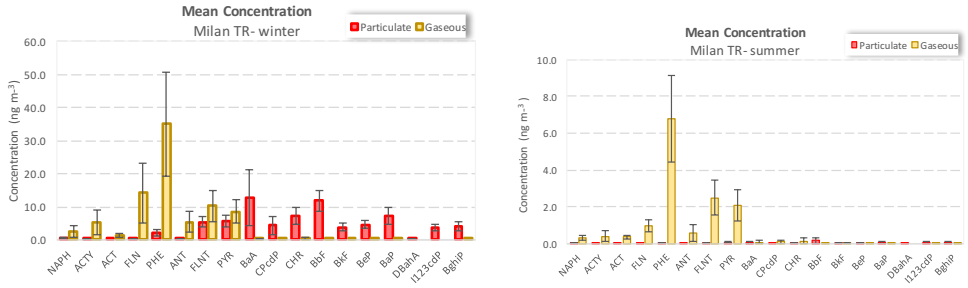

Figure 3.3 PAH concentrations (ng m-3) in the particulate and gaseous phases during winter and summer 2013 (crossbars: standard deviation of the average).

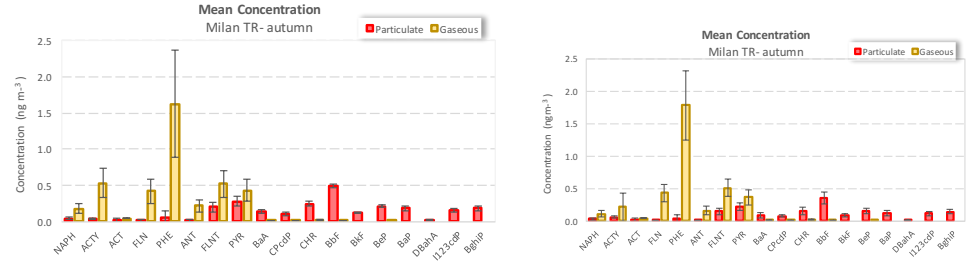

Figure 3.4 PAH concentrations (ng m-3) in the particulate and gaseous phases during autumn 2013 at TR and LEZ site (crossbars: standard deviation).

Benzo(a)Pyrene is the only PAH regulated under EU Directives (limit: 1 ng m^{-3}) and is often used as a marker of the exposure to PAHs considered carcinogenic to humans. The average annual value at TR site was 2.4 ng m^{-3}. All exceedances were observed during the cold period (mean value in WI=6.8±2.5 ng m^{-3}). This result is in accordance with other studies[104].

It was present only in the particulate phase, while in the gaseous phase BaP wasn't detected. In summer and autumn the concentrations were always below the legal limit (SU= 0.1±0.1 ng m^{-3} AU at TR site=0.2±0.0 ng m^{-3}). The autumn concentrations are similar to those found in Munich by Schauer et al.[105] during October 2002 (BaP at a high-traffic site = 0.17 ± 0.03 ng m^{-3}). The concentrations recorded in autumn within the LEZ were lower than those found outside (AU at LEZ site = 0.1±0.0 ng m^{-3}).

PAHs Distribution Pattern. The PAH distribution pattern was calculated as the ratio of the concentration of a single PAH to the concentration of the total PAHs (∑18 PAHs; Fig. 3.5)

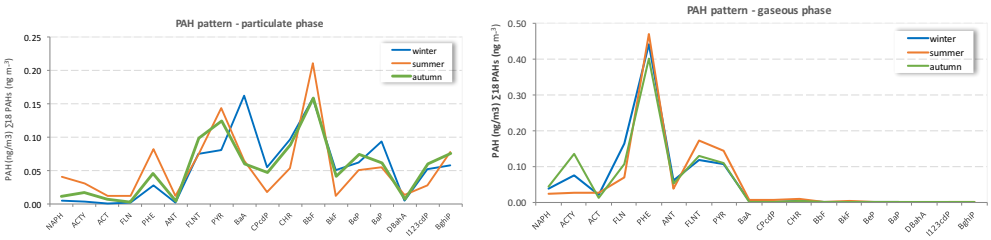

Figure 3.5 PAH distribution pattern in the particulate and gaseous phases during winter, summer and autumn

In the particulate phase the predominant PAH was BbF in all three seasons (WI: 16%; SU: 18%; AU: 16%). During winter after BbF the most abundant PAHs were BaA (16%), CHR (10%) and BaP (9%) while in summer and autumn they were PYR (SU=12%; AU=13%), and BghiP (SU = 9% and AU=8%).

PAHs are present in atmospheric PM, and they derive from various combustion processes, traffic being an important source in urban areas [106]. There are many sources of PAHs in vehicle exhaust, including unburned fuel, lubricating oil and pyrosynthesis. As reported in Perrone et al.[107], in gasoline vehicles, five ring PAHs (BbF, BjF, BeP, BaP, dBahA) plus six ring PAHs (BghiP) accounted for about 55% of total PAHs while in diesel vehicles four ring PAHs (PYR, BaA, CHR) were dominant (85%).

The results obtained in the sampling campaign show that the contribution to the emission of PAHs is given by both types of vehicles (gasoline and diesel) with a slight prevalence of gasoline vehicles, demonstrated by the abundance of BghiP.

In the gaseous phase at TR site PHE was the most abundant compound (WI: 42%; SU: 47%; AU: 40%) followed by FLNT (WI: 13%; SU: 17%; AU: 13%) and PYR (WI: 10%; SU: 14%; AU: 11%). Moreover, the gaseous PAHs were only that lighter than BaA. This is consistent with other studies[108, 109, 110, 111].

The distribution pattern in autumn was the same at both site (Fig. 3.6): the most abundant PAHs in the particulate phase were BbF (TR= 16%; LEZ= 17%), PYR (TR= 13%; LEZ= 12%) FLNT (TR an LEZ= 10%) and BghiP (TR= 8%; LEZ= 9%) while in the gaseous phase the predominant PAH was PHE (TR= 40%; LEZ= 48%).

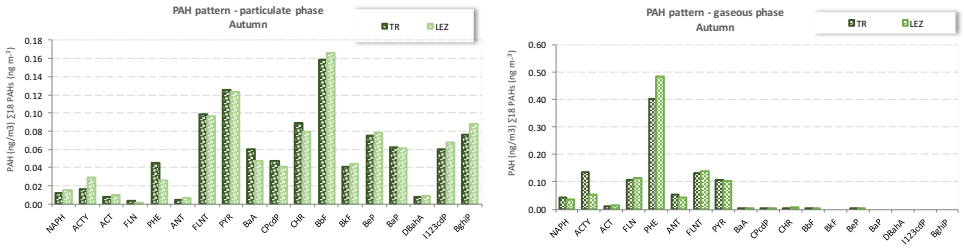

Figure 3.6 PAH distribution pattern in the particulate and gaseous phases during autumn at TR and LEZ site

PAHs Partitioning. The particulate to total (particulate + gaseous) concentration ratio of each PAH for the summer season is shown in Fig. 3.7.

The analyzed PAHs can be divided in three groups in function of the phase partitioning:

- *volatile PAHs: 2-3 aromatic rings,* lighter than FLNT (≤20% in the gaseous phase).
- *semi-volatile PAHs:* 3-4 aromatic rings (FLNT and PYR; 20-80% in the particulate phase);
- *not-volatile* PAHs: 5-6 aromatic rings, with a molecular weight higher than PYR (≥ 80% in the particulate phase)

The phase distribution was in agreement with the volatility characteristics of the compounds.

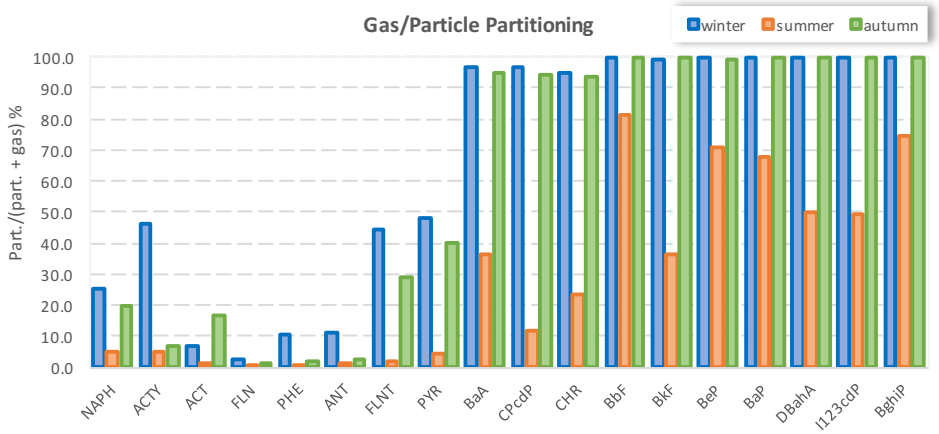

Figure 3.7 Gas/particle partition of the PAHs during winter, summer and autumn 2013 at TR site (crossbars: standard deviation of the average).

The gas/particle partitioning recorded in winter and in autumn were similar. The samples of the two seasons didn't show significant differences. A slightly different trend was found for the summer samples probably because of the changing of the meteorological conditions (like temperature and snow precipitation) which can affect the partitioning process.

As for the autumn sample (Fig. 3.8), the partitioning trends outside (TR) and within (LEZ) the Low Emission Zone were similar, with slight variations for some non-volatile PAHs (ACTY, ACT, ANT).

This result probably indicates that traffic restriction measures do not intervene in modifying the partitioning of semi-volatile compounds. However, in this study, only 7 samples were considered, therefore a longer sampling campaign would be needed.

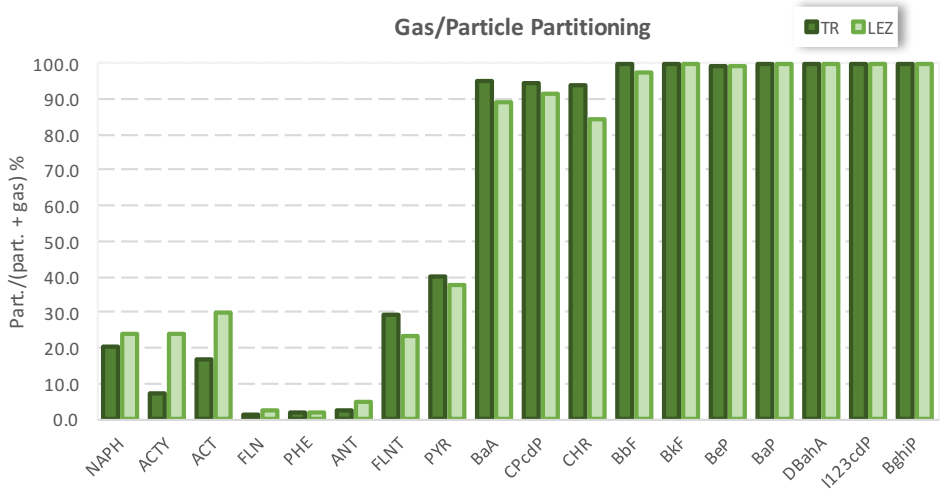

Figure 3.8 Gas/particle partition of the PAHs during autumn 2013 at TR and LEZ site (crossbars: standard deviation of the average).

Kp coefficient. The gas/particle partitioning coefficient, Kp, was calculated for all the samples as explained in eq. 1.1 (Tab. 3.5).

Table 3.5 Experimental log Kp

log Kp(m^{-3} µg)	winter (n=9)		summer (n=8)		autumn (n=7)	
	Average	St.Dev.	Average	St.Dev.	Average	St.Dev.
FLN	-3.94	0.50	-3.79	0.21	-2.83	0.00
PHE	-3.19	0.46	-3.80	0.25	-2.78	0.16
ANT	-3.28	0.66	-3.52	0.14	-2.65	0.08
FLNT	-2.18	0.62	-3.27	0.19	-2.17	0.16
PYR	-2.10	0.58	-3.05	0.18	-1.89	0.14
BaA	-0.29	0.58	-1.82	0.27	-0.60	0.24
CHR	-0.52	0.58	-2.01	0.30	-0.76	0.35

The mean log Kp values were well correlated between the seasons. As expected, the correlation was a bit lower between the winter and the summer samples (R^2 = 0.95) but became a bit higher between the winter and the autumn samples (R^2 = 0.97) and even better between summer and autumn samples (R^2 = 0.99). Except for fluorene and phenanthrene, the experimentally calculated log Kp became slightly more negative in summer, meaning that the same PAH tended to partition more in the gaseous phase during summer.

The temperature corrected Log pL^0 was calculated for all the samples (Tab. 3.6).

Table 3.6 Temperature corrected log pL0 (Pa)

log pL^0 (Pa)	winter (n=9)		summer (n=8)		autumn (n=7)	
	Average	St.Dev.	Average	St.Dev.	Average	St.Dev.
FLN	-0.97	0.07	-0.04	0.05	-0.51	0.15
PHE	-1.92	0.08	-0.84	0.06	-1.39	0.17
ANT	-1.96	0.08	-0.88	0.06	-1.43	0.17
FLNT	-3.23	0.09	-1.97	0.07	-2.60	0.20
PYR	-3.46	0.10	-2.15	0.08	-2.81	0.20
BaA	-4.88	0.11	-3.43	0.09	-4.16	0.23
CHR	-5.10	0.11	-3.57	0.09	-4.34	0.24

The relationship between the mean log Kp for the PAHs and temperature corrected log pL° is represented in Fig. 3.9.

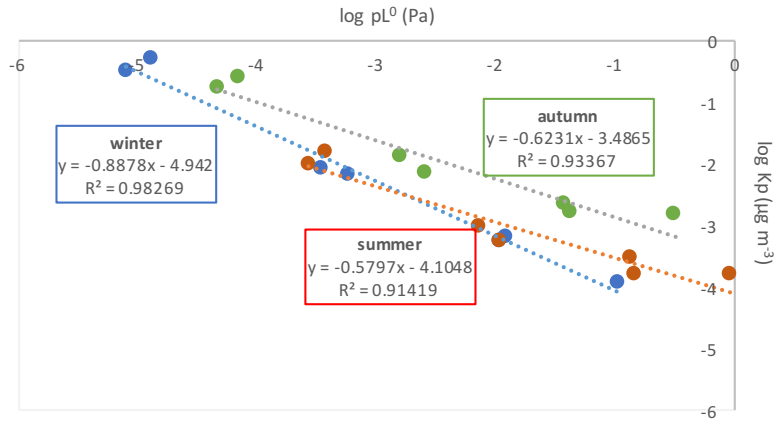

Figure 3.9 Temperature corrected log pL0 vs experimental log Kp linear regression for the PAHs (FLN, PHE, ANT, FLNT, PYR, BaA, CHR).

A strong correlation for log Kp vs log pL° were found (R^2: 0.93-0.99 in winter, 0.51-0.93 in summer and 0.91-0.99 at SC in autumn). The slopes were always negative and with variable values (winter: -0.79 to -0.98; SC summer: -0.35 to - 0.65; SC autumn: -0.54 to -1.07). The negative slope indicates a decreasing association of the PAHs with the particulate phase as vapor pressure increases. At equilibrium, the slope should be close to -1[88]. For the samples, the mean slopes ranged between -0.5 and -0.9, suggesting that

the non-equilibrium conditions might have prevailed especially during summer or may result from the presence of not-exchangeable compounds in the particles[20,112]. Negative slopes and higher than -1 were found in literature[113,114].

The phase partitioning may also be described by the fraction θ of a compound in the particulate phase. The experimental adsorbed fraction on the particles, θ, was calculated and then compared to the predicted θ calculated using the temperature corrected Log pL^0 (eq. 1.3). Value of Cj = 17.2 Pa and of S=1.1 x 10^{-5} were used.

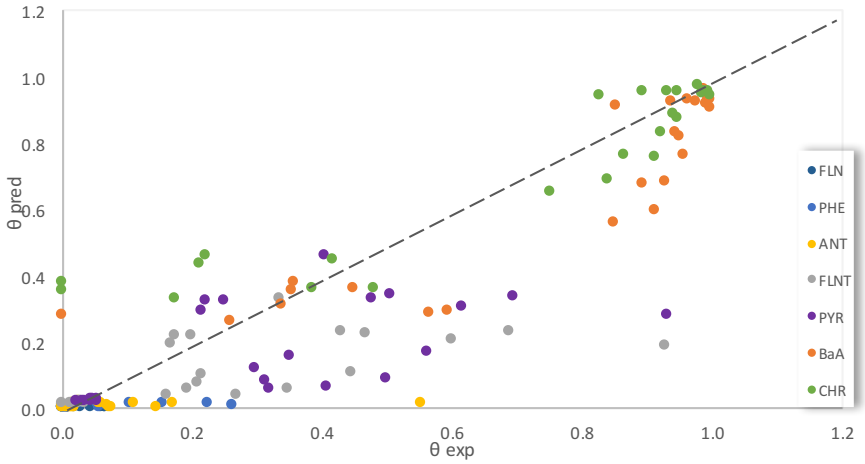

Figure 3.10 Predicted versus experimental ϑ for Milan (n = 24), Junge-Pankow model

A great variability between the samples, mainly due to differences between the seasons led to a large scatter plot, as reported in Fig. 3.10. In particular, summer samples showed the worst correlation as shown in Fig.3.11.

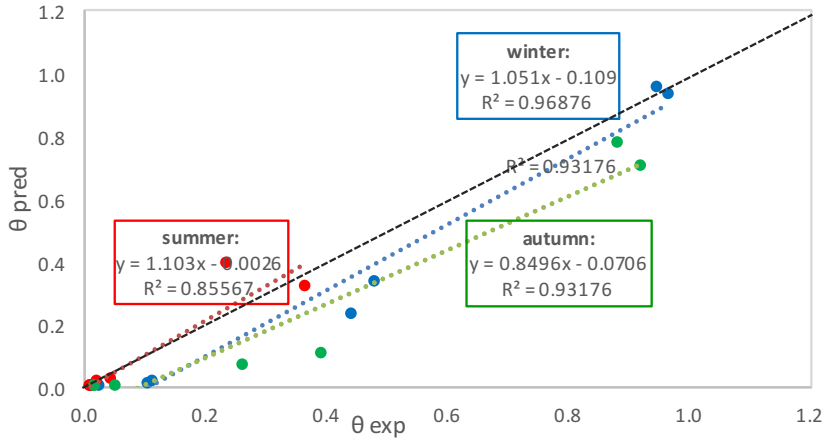

Figure 3.11 Mean predicted versus experimental ϑ for the PAHs (FLN, PHE, ANT, FLNT, PYR, BaA, CHR).

The results show that the Junge-Pankow underestimate the partitioning. Lammel[20] suggested that adopting a value of Cj = 17.2 Pa would under-predict θ of semi-volatile PAHs. The model was found to be inadequate to predict the partitioning, indicating that another process, like absorption in OM, could be significant for the phase partitioning.

The experimental log Kp was also correlated against the octanol-air partitioning coefficient (Fig. 3.12). The temperature corrected log K_{OA} were calculated from tabulated values at 25°C found in literature (Tab. 3.7).

Table 3.7 Temperature corrected and literature data for log Koa

log Koa	winter (n=9)		summer (n=8)		autumn (n=7)		
	Average	St.Dev.	Average	St.Dev.	Average	St.Dev.	**logKoa(25°C)**
FLN	7.54	0.06	6.72	0.05	7.13	0.13	6.9
PHE	8.43	0.07	7.48	0.06	7.96	0.15	7.68
ANT	8.47	0.07	7.51	0.06	8.00	0.15	7.71
FLNT	9.65	0.08	8.52	0.07	9.09	0.18	8.76
PYR	9.58	0.08	8.51	0.06	9.05	0.17	8.73
BaA	11.36	0.10	9.99	0.08	10.68	0.21	10.28
CHR	11.38	0.10	10.01	0.08	10.70	0.21	10.3

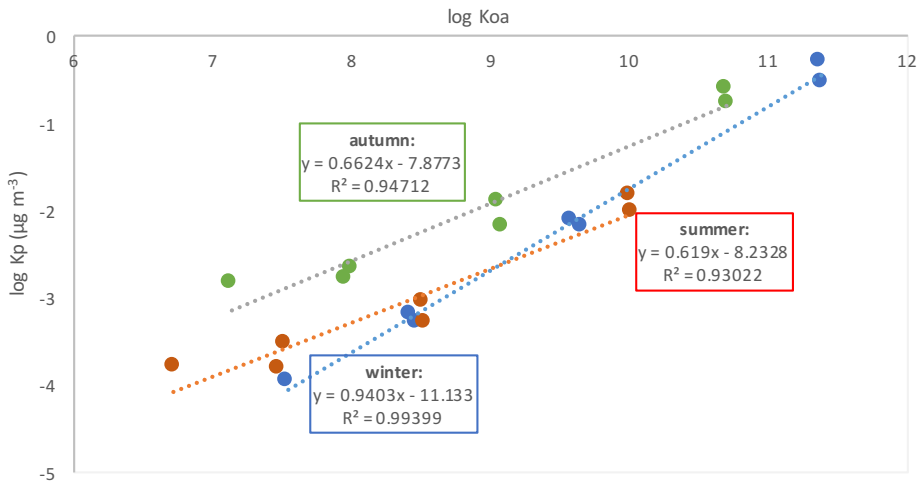

Figure 3.12 Temperature corrected log Koa vs experimental log Kp linear regression for the PAHs (FLN, PHE, ANT, FLNT, PYR, BaA, CHR).

A very good correlation was found for the log Kp vs log Koa regression (R^2: 0.96-1.00 in winter, 0.50-0.94 in summer and 0.92-0.98 at SC in autumn). For the equilibrium partition, the slope is expected to have a value near +1. The measured values were between 0.83 to 1.05 in winter, 0.42 to 0.69 in summer and 0.58 to 1.03 in autumn therefore it seems that the equilibrium was not reached, especially in summer.

The good regressions suggested that the semi-volatile PAHs “feel” equally being dissolved in themselves or in octanol-like organic matter[91].

The predicted log Kp was calculated using the temperature corrected log Kp (eq.1.8). The Koa absorption model can be used to predict values of Kp from knowledge of only Koa and the organic fraction of the aerosol, fOM. The conversion from organic carbon to organic matter was made assuming that the organic matter fraction(fOM) is 1.6 times the organic carbon fraction (fOC). The results obtained by linear regression of measured versus predicted Kp values are shown in Fig 3.13 and the differences between the season are shown in fig 3.14.

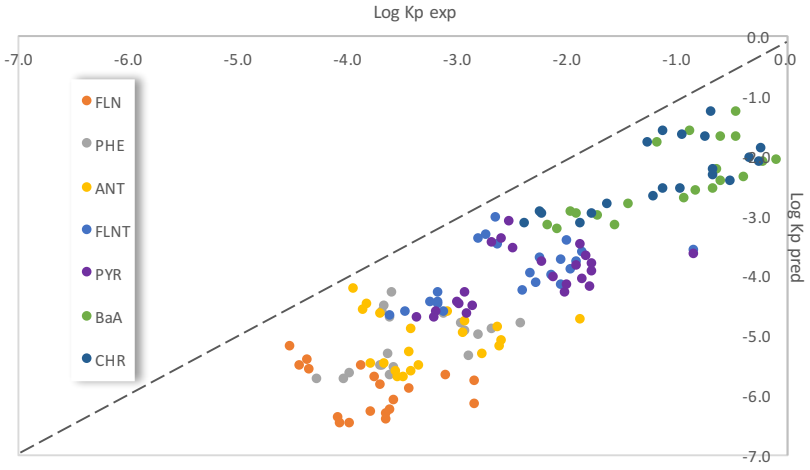

Figure 3.13 Predicted versus experimental ϑ for Milan (n = 24), Koa model

For the analyzed samples, the model always underestimated the partitioning for PAHs, as noted also in previous studies[75,77,87]. This could potentially be related to the underestimation of the term γOCT/γOM or possibly due to the high affinity of PAHs to soot particles, a parameter that is not accounted for in that model [83].

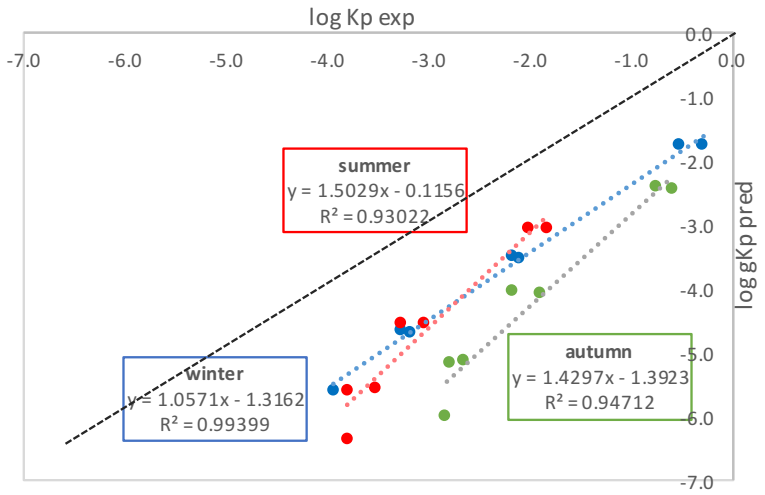

Figure 3.14 Mean predicted versus experimental log kp for the PAHs (FLN, PHE, ANT, FLNT, PYR, BaA, CHR).

An attempt to predict the gas/particle partitioning coefficient Kp applying the dual model described in Lohmann and Lammel [27] (eq. 1.11) was made.

The corrected log Kp were than compared with that predicted Kp (Fig. 3.15)

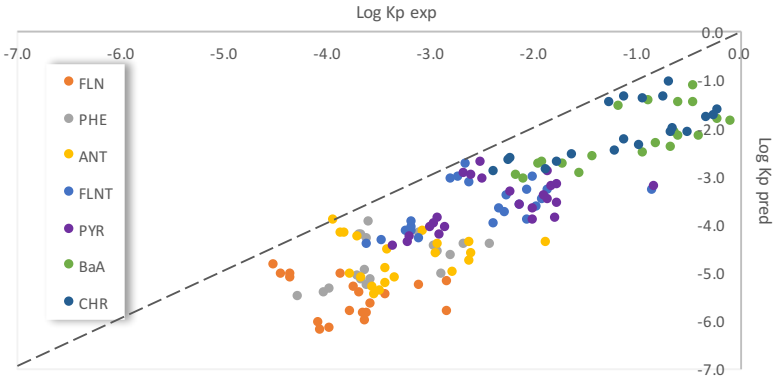

Figure 3.15 Predicted versus experimental Kp for Milan (n = 24), Dual model

To get the predicted log Kp, Koa and Ksa values were calculated. For the winter samples collected in December, for which chemical analysis to determine organic and elemental

carbon were not performed, average values of EC and OM obtained for the other samples were used (OC: 12.5 µg m^{-3}; EC: 2.9 µg m^{-3}).

For all the three seasons, a good correlation was found between the measured and the predicted log Kp ($R^2 \geq 0.93$) as shown in Fig 3.16. The results showed that the dual model under-predicted the PAHs partitioning: the measured particulate fraction was higher than the predicted one.

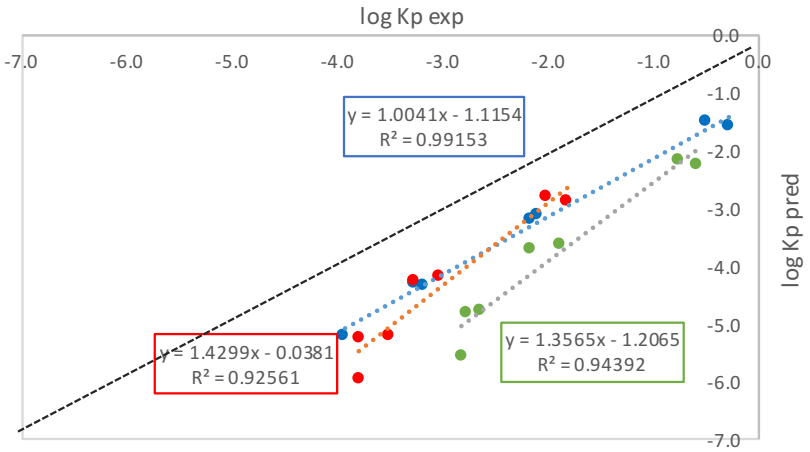

Figure 3.16 Mean predicted versus experimental log kp for the PAHs (FLN, PHE, ANT, FLNT, PYR, BaA, CHR

As suggested by Lohmann and Lammel[27] all the measured log Kp should be reported to 298 K using eq.3.2 in order to ensure the comparability between sample collected under various atmospheric conditions:

$$\log Kp\ (298K) = \log Kp\ (T) + [\log pL\ (T) - \log pL\ (298K)] \qquad \text{(eq 3.2)}$$

Applying the temperature correction, the prediction was better, especially for the winter samples (Fig. 3.17): the plot got closer to the 1-1 line.

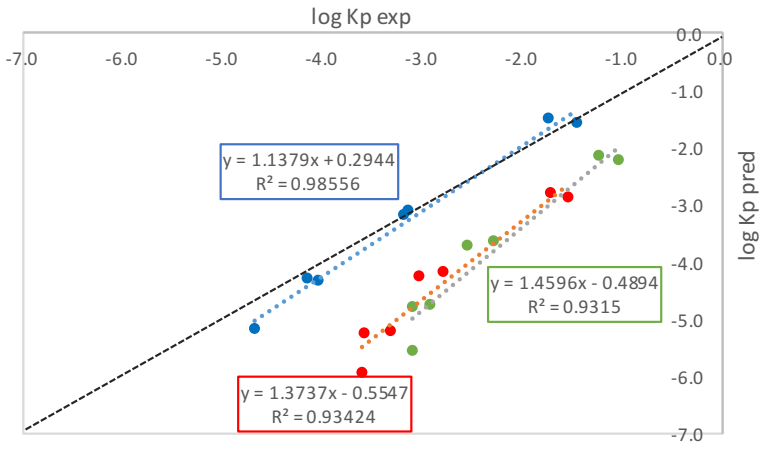

Figure 3.17 Mean predicted versus experimental temperature corrected log kp for the PAHs (FLN, PHE, ANT, FLNT, PYR, BaA, CHR

The model hereinbefore used, showed a systematic underestimation of the partitioning of the semi-volatile PAHs. The gas-particle partitioning was studied using a PPLFERs model, considering two mechanisms for PAHs partitioning: absorption into OM and adsorption onto soot.

The system parameters for diesel soot [95] and for DMSO[115] were used for adsorption and absorption contribution respectively. The solute descriptors for the considered PAHs were taken from the literature [116, 117] (Tab.3.8).

The partitioning constants related to absorption and adsorption processes calculated using eq 1.14, were corrected for the effect of near- ground temperature at the site using the solute-specific enthalpies of phase transfer, which were calculated for the corresponding ppLFER systems[118,119]. Total Kp was determined by summing the individual partitioning coefficients after normalizing the units.

Table 3.8 System parameters and Solute descriptors for PPLFER model

System parameters

	e	s	a	b	v	l	c
EC[a]	-	-	2.70	2.45	-	1.09	-8.47
DMSO[b]	-0.22	2.90	5.04	0.00		0.72	-0.56

Solute Descriptors

	E	S	A	B	V	L
FLN[c]	1.59	1.06	0.00	0.25	1.357	6.922
PHE[c]	2.06	1.29	0.00	0.26	1.454	7.632
ANT[c]	2.29	1.34	0.00	0.28	1.454	7.568
FLNT[c]	2.38	1.55	0.00	0.24	1.585	8.827
PYR[c]	2.81	1.71	0.00	0.28	1.585	8.833
BaA[d]	2.74	1.68	0.00	0.37	1.823	10.124
CHR[c]	3.03	1.73	0.00	0.33	1.823	10.334

a= Roth, et al 2005; b= Abraham et al., 2010; c=Sprunger et al 2007;d=Ariyasena et al.2014 .

Fig. 3.18 shows predictions made following the PPLFER method. A can be seen, the majority of the data points were predicted within 1 order of magnitude accuracy, with the exception of fluorene and anthracene

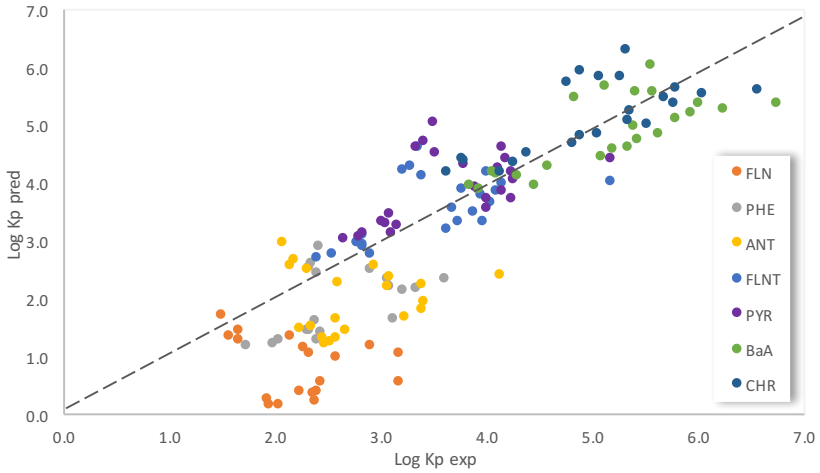

Figure 3.18 Predicted versus experimental Kp for Milan (n = 24), PPLFER model

A strong correlation for the experimental vs the predicted log Kp were found (R^2: 0.86-0.97 in winter, 0.51-0.87 in summer and 0.83-0.97 in autumn), as shown in Fig 3.19

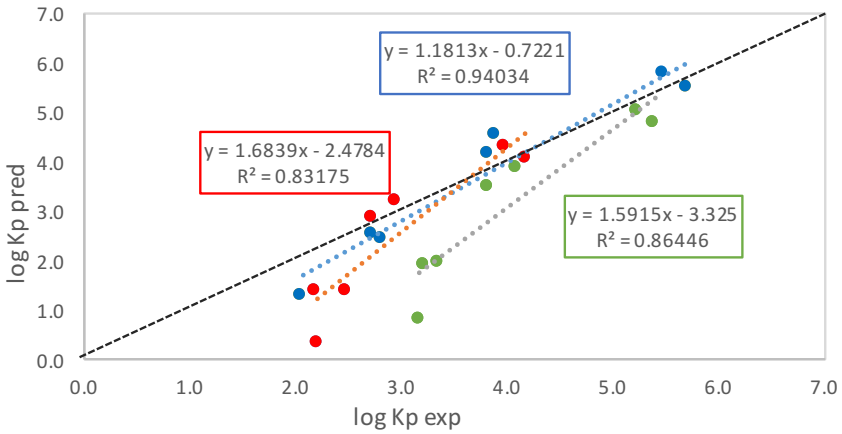

Figure 3.19 Mean predicted versus experimental log kp for the PAHs (FLN, PHE, ANT, FLNT, PYR, BaA, CHR

These results suggest that the ppLFER model predicts accurately the gas-particle partitioning of PAHs without showing season variability related to PM composition and sources. In the light of these results, a comparison between the two sampling sites in autumn was made.

Experimental and predicted log Kp for TR site and LEZ site, presented in Table 3.9, didn't show any inter-site variability (R^2:0-99-1.00)

Table 3.9 Predicted and Experimental log Kp for autumn samples

	pred log Kp ($m^3 g^{-1}$)		exp log Kp (m3 g-1)	
	TR	LEZ	TR	LEZ
FLN	0.71	0.76	3.17	3.17
PHE	1.75	1.80	3.11	3.33
ANT	1.80	1.85	3.32	3.39
FLNT	3.28	3.34	3.84	3.83
PYR	3.64	3.70	4.13	4.09
BaA	4.56	4.62	5.29	5.48
CHR	4.80	4.86	5.22	5.25

The gas-particle partitioning was lastly studied using a multi-phase ppLFERs model that considers absorption into OM and adsorption onto soot and soluble salts.

For adsorption contribution, the system parameters for diesel soot [95], Al and Fe oxides, ammonium sulphates and ammonium chloride [97] were used. For absorption, 2 OM

phases were considered and DMSO and polyurethane were chosen as surrogates (Tab. 3.10)

Table 3.10 System parameters for PPLFER model

System parameters for adsorption contribution

	e	s	a	b	v	l	c
EC[a]	-	-	2.70	2.45	-	1.09	-8.47
Al_2O_3[b]	-	-	3.38	5.54	-	0.68	-8.47
Fe_2O_3[c]	-	-	3.27	4.25	-	0.77	-8.47
$(NH)_4^2SO_4$[d]	-	-	2.13	5.34	-	0.88	-8.47
$(NH)_4Cl$[d]	-	-	2.28	4.72	-	0.92	-8.47

System parameters for absorption contribution

	e	s	a	b	v	l	c
DMSO[e]	-0.223	2.903	5.036	0		0.719	-0.556
PU-ETHER[f]	0	1.63	3.39	0	0.27	0.71	-3.02

a= Roth, et al 2005; b= Goss et al 2002; c= Goss etc al 2004; d= Goss et al 2003; e= Abraham et al., 2010; f=Schneider and Goss 200

Total predicted Kp, determined by summing the individual partitioning coefficients was compared to the experimental Kp (Fig. 3.20)

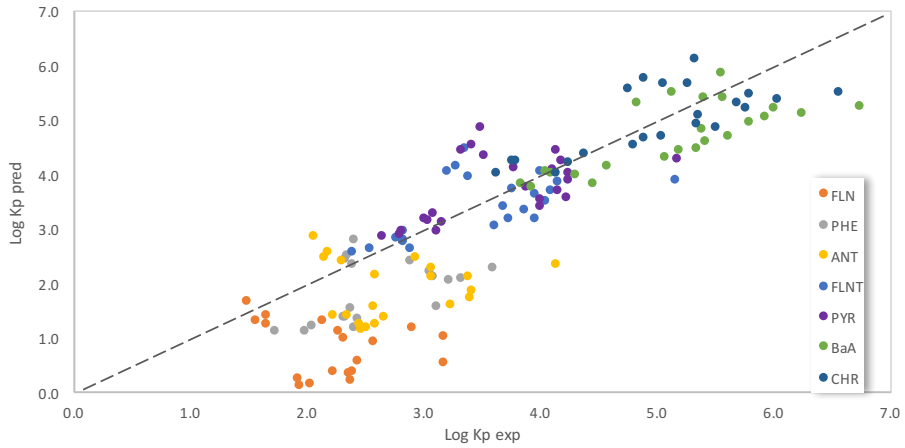

Figure 3.20 Predicted versus experimental Kp for Milan (n = 24), PPLFER model

The use of the multiphase approach didn't improve the prediction of the PAHs partitioning.

Fig. 3.21 show the mean values for sorption capacities related to adsorption and absorption processes considered in this study. Evidently, absorption was the main partitioning process dominated by the contribution of OSWSOM. Partitioning onto soot dominated the adsorption process among the considered phases considered, while adsorption onto soluble salts (<0.01% of the total KP) may be neglected.

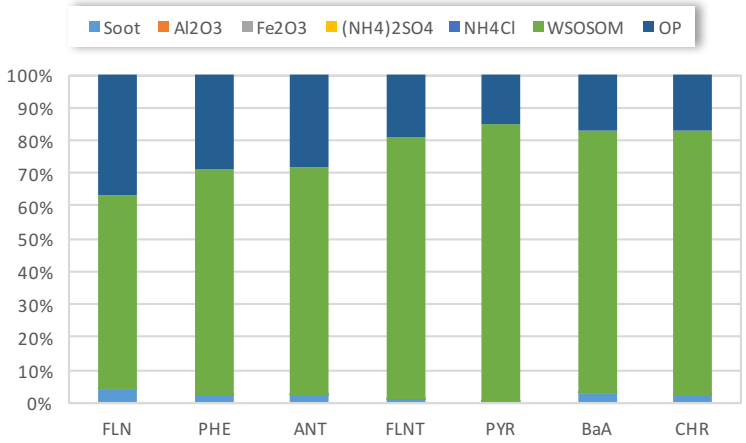

Figure 3.21 Contributions of individual phases to Kp determined using multi-phase ppLFER. OSWSOM: both organic soluble and water soluble organic matter; OP: organic polymers.

3.2.2 N-ALKANES

Alkanes Concentrations. As for PAHs, the blank field filters and the blank PUF plugs were processed and analysed as the real samples. Their concentrations were used to calculate the detection limit (DL) for the alkanes (eq. 3.1) both for the particulate and the gaseous phase (Tab 3.11, 3.12). Only the data higher than detection limit were considered valid. The mean values got by the blank field filter and PUF plugs were subtracted to the valid data.

The recovery factors were always applied: the concentrations were corrected for the deuterated Alkanes recoveries.

Table 3.11 Alkanes average concentrations in the blank field filters and DL (ng/filter)

Winter- Summer								
	C18	**C19**	**C20**	**C21**	**C22**	**C23**	**C24**	**C25**
Average	0.018	0.137	0.017	0.059	0.015	0.012	0.064	0.027
DL	0.025	0.155	0.020	0.070	0.017	0.014	0.078	0.049
	C26	**C27**	**C28**	**C29**	**C30**	**C31**	**C32**	
Average	0.047	0.048	0.095	0.068	0.130	0.044	0.022	
DL	0.074	0.092	0.127	0.123	0.153	0.080	0.034	
Autumn								
	C18	**C19**	**C20**	**C21**	**C22**	**C23**	**C24**	**C25**
Average	0.104	0.093	0.053	0.010	0.044	0.006	0.038	0.025
DL	0.033	0.027	0.038	0.037	0.031	0.021	0.017	
	C26	**C27**	**C28**	**C29**	**C30**	**C31**	**C32**	
Average	0.033	0.027	0.038	0.037	0.031	0.021	0.017	
DL	0.041	0.048	0.060	0.061	0.048	0.037	0.028	

nd= not detected , DL= detection limit

Table 3.12 Alkanes average concentrations in the blank field PUF plugs and DL (ng/plug)

	C18	**C19**	**C20**	**C21**	**C22**	**C23**	**C24**	**C25**
Average	0.10	0.58	0.63	2.62	5.19	9.06	9.40	2.89
DL	0.12	1.06	1.08	4.61	8.81	14.82	14.27	3.94
	C26	**C27**	**C28**	**C29**	**C30**	**C31**	**C32**	
Average	1.28	1.15	1.24	1.14	0.85	0.96	0.47	
DL	1.70	1.67	2.45	1.57	1.26	1.40	0.63	

nd= not detected , DL= detection limit

The n-alkanes with 18 to 32 carbon atoms were measured for all the particulate and gaseous phase samples collected during winter, summer (at TR site) and autumn (at TR and LEZ site). Their concentrations are summarized in Tab. 3.13.

As for the particulate phase 9 samples were collected in winter, 8 samples in summer and 18 samples in autumn (n=10 at TR site; n=10 at LEZ site). For the gaseous phase 9 samples were collected in winter, 8 samples in summer and 7 samples in autumn (n=3

at TR site; n=4 at LEZ site). Only the n-alkanes with more than 19 carbon atoms will be considered in the following discussion.

Table 3.13 ALKs concentrations in the particulate and in the gaseous phase

		TR winter (n=9)		TR summer (n=8)		TR autumn (n=3)		LEZ autumn (n=4)	
		Average	St.Dev.	Average	St.Dev.	Average	St.Dev.	Average	St.Dev.
particulate	Conc (ng m-3)	299.43	170.30	43.37	5.33	50.48	14.88	55.32	46.79
	CPI	1.36	0.36	1.71	0.42	1.42	0.30	1.38	0.25
% in TSP		0.22	0.08	0.09	0.02	0.10	0.05	0.13	0.13
		Average	St.Dev.	Average	St.Dev.	Average	St.Dev.	Average	St.Dev.
gaseous	Conc (ng m^{-3})	126.88	19.72	95.21	4.46	111.72	21.46	147.74	80.06
	CPI	0.99	0.14	0.95	0.02	1.02	0.07	1.00	0.08

n = number of samples; PAHs = C18,C19,C20,C21,C22,C23,C24,C25,C26,C27,C28,C29,C30,C31,C32

The alkanes concentrations (ng m^{-3}) in winter and summer showed markedly different values.

The total (particulate + gaseous) average concentrations were 426.31±176.43 ng m^{-3} (MIN: 221.56 ng m^{-3}, MAX: 741.69 ng m^{-3}) during winter and 138.58±7.32 ng m^{-3} (MIN: 126.65 ng m^{-3}, MAX: 151.19 ng m^{-3}) in summer. In autumn, the n-alkanes concentrations were similar to those found in summer for the particulate phase but higher for the gaseous phase.

Comparing the two sites during autumn, excluding the first day of sampling which showed extremely high concentration for alkanes in the particulate phase, the results showed a reduction of 15% within the LEZ for the particulate phase (TR= 49.05±15.04 ng m^{-3}; LEZ= 41.71±19.50 ng m^{-3}); for the gaseous phase the concentrations were higher at LEZ site (reduction at TR =32%). Slightly higher concentrations were reported in literature[36,103, 110,111.]

As shown in Fig. 3.22 and 3.23, the n-alkanes lower than n-C24 were more concentrated in the gaseous phase; the opposite was true for the n-alkanes higher than n-C24. This trend was correlated to the volatility of the compounds. In fact, the lower molecular weight alkanes generally are more volatile and have a greater gaseous phase concentration. On the contrary, the higher molecular weight compounds are less volatile and have greater association with the particulate phase. The same was reported by Mandalakis et al.[113] and Bi et al.[111].

The winter samples had a different behavior. In fact, even alkanes lower than n-C24 were more concentrated in the particulate phase.

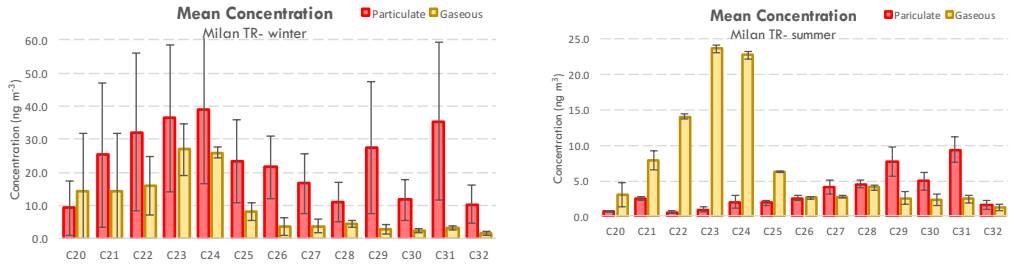

Figure 3.22 Alkanes concentrations (ng m-3) in the particulate and gaseous phases during winter and summer 2013 (crossbars: standard deviation of the average).

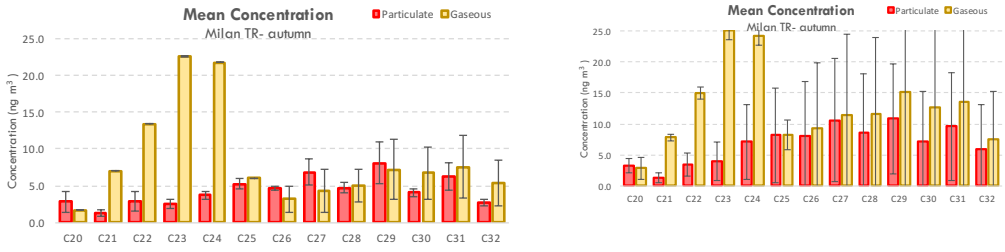

Figure 3.23 Alkanes concentrations (ng m-3) in the particulate and gaseous phases during autumn 2013 at TR and LEZ site (crossbars: standard deviation of the average).

Alkane Distribution Pattern. The n-alkanes carbon distribution pattern was calculated as the ratio of the concentration of a single n-alkane to the concentration of the total n-alkanes (n-C20 to n-C32). In Fig3.24., the mean distribution pattern for the two phases is reported.

The distribution pattern of particulate n-alkanes is usually linked to the specific sources and it is generally due to a combination of two different patterns: 1) the anthropogenic n-alkanes (e.g., emitted by vehicular exhausts and lubricant residues), identified as the n-alkanes with < 26 carbon atoms; 2) the natural n-alkanes (e.g., epicuticular waxes), identified as the n-alkanes with > 25 carbon atoms and an odd carbon number preference. A combination of the two could be identified in the overall pattern of the Lombardy Region.

During winter, it is possible to see the Gaussian distribution centered around n-C24, which is the most abundant alkane (13%) followed by C31 (13%), C23 (12%) and C22 (10%). During summer and autumn, the typical Gaussian distribution in the particulate phase was hidden by the important presence of the odd n-alkanes > 26 carbon atoms. In summer, the most abundant alkanes were C31 (22%), C29 (18%) C30 (12%) and in autumn C29(15%), C27 and C31 (12%), C25 (10%). It seemed that the anthropogenic source contributed more to the particulate n-alkane emissions in winter, while the natural source was stronger in summer.

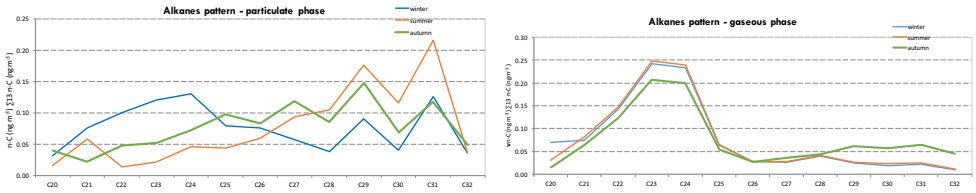

Figure 3.24 Alks distribution pattern in the particulate and gaseous phases during winter, summer and autumn

For the gaseous phase, the carbon distribution pattern showed a Gaussian distribution centered around C23-C24 (C23: WI=22%, SU=25%, AU=21%; C24: WI=21%, SU=24%, AU=20%). In all the seasons, the maximum contribution was by the alkanes from C20 to C24.

The alkanes distribution patter was the same at the traffic site and within the low emission zone during autumn, as shown in Fig.3.25, meaning that the same type of sources is present in the two different sites.

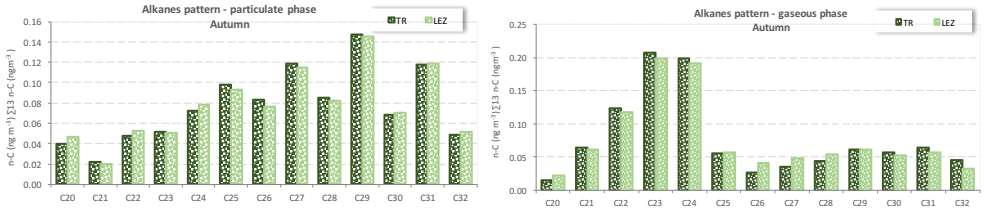

Figure 3.25 Alks distribution pattern in the particulate and gaseous phases during autumn at TR and LEZ site

Since n-alkanes are source-specific[21,32,33] (i.e. their carbon distribution pattern is related to the sources), it is possible to discriminate the contribution of different sources by means of the Carbon Preference Index (CPI) which is got by the odd to even n-alkane ratio.

In Fig. 3.26 the CPI values for the winter, summer and autumn samples is reported.

The mean CPI was 1.36 in winter, 1.71 in summer and 1.41 in autumn suggesting a mixed source for the particulate n-alkanes. In the gaseous phase, it was 0.99 in winter, 0.95 in summer and 1.02 in autumn suggesting a mixed source both for the particulate and the gaseous n-alkanes, with a prevalence of anthropogenic source (CPI ~ 1 means source of anthropic origin).

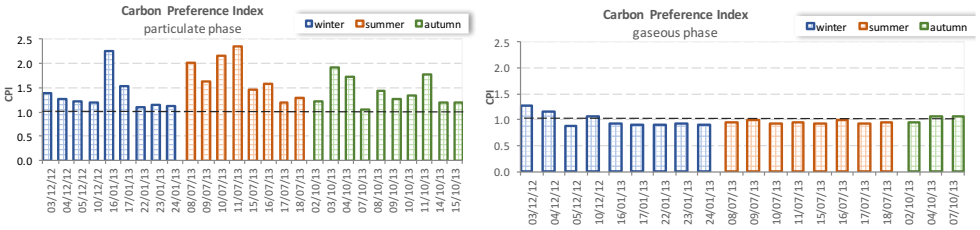

Figure 3.26Carbon distribution pattern for winter, summer and autumn samples in the particulate and gaseous phase.

A good correlation (R^2=0,77) was found for the CPI calculated at the two different sites. Average values of 1.35 and 1.00 was calculated at LEZ for the particulate and gaseous phase respectively. This result proves the presence of the same type of sources at the two sites (Fig .3.27)

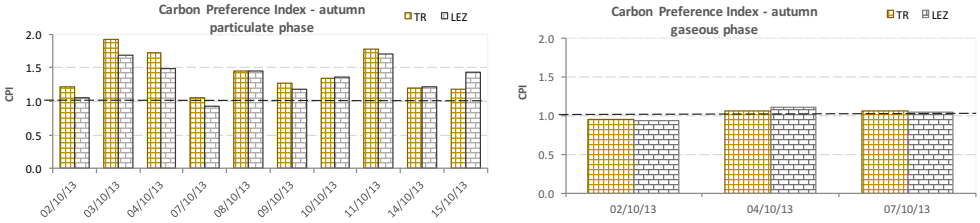

Figure 3.27 Carbon distribution pattern for autumn samples at TR and LEZ site in the particulate and gaseous phase.

Alkanes Partitioning. The particulate to total (particulate + gaseous) concentration ratio of each n-alkane for the summer season is shown in Fig.3.28

Three groups could be identified in function of the partitioning between the gaseous and particulate phases:

- *volatile* n-alkanes: compounds lighter than n-C23(≤20% in the particulate phase).
- *semi-volatile* n-alkanes: n-C23 to n-C25 (20-80% in the particulate phase)

- *not-volatile* n-alkanes: compounds with a molecular weight higher than n-C25 (≥ 80% in the particulate phase)

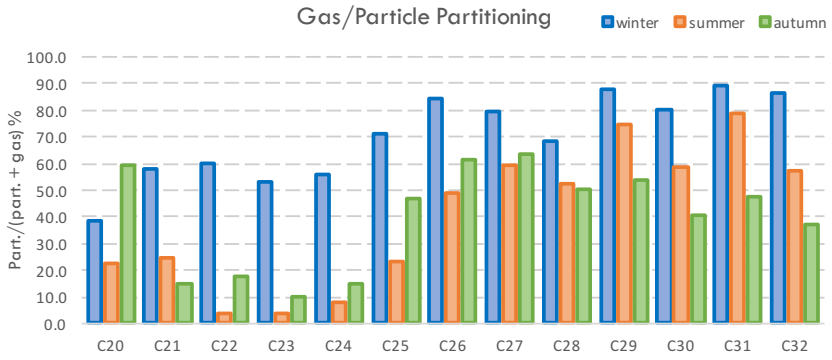

Figure 3.28 Gas/particle partition of the ALKs during winter, summer and autumn 2013 at TR site (crossbars: standard deviation of the average).

As for the winter samples, the trend was similar to what is expected, while in summer and autumn the phase distribution wasn't in perfect agreement with the volatility characteristics of the compounds.

This could be due to the higher temperature recorded in summer (28-32°C) and autumn (13-16°C) compared to winter (2-8°C) which may have favored the volatilization of the compounds. During autumn, a similar trend was found at the two sites (Fig. 3.29)

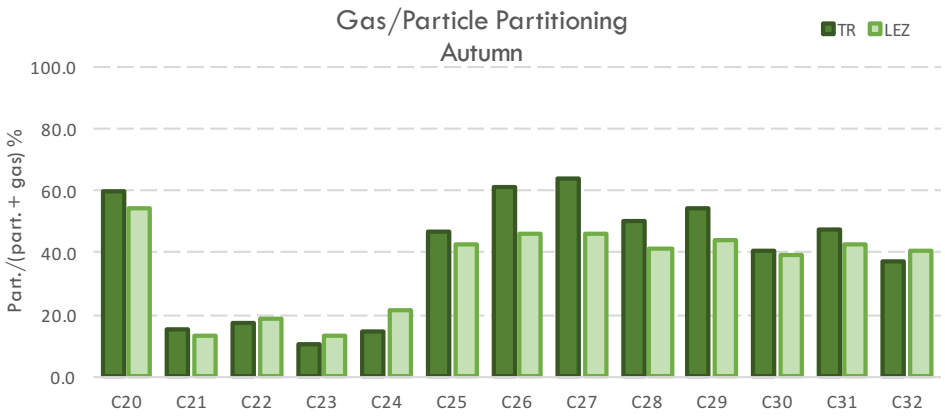

Figure 3.29 . Gas/particle partition of the ALKs during autumn 2013 at TR and LEZ site (crossbars: standard deviation of the average).

Kp coefficient. The gas/particle partitioning coefficient, Kp, was calculated for the summer samples as explained in eq. 1.1. (Tab.3.14)

Table 3.14 Experimental log Kp

log Kp(m^{-3} µg)	winter (n=9)		summer (n=8)		autumn (n=7)	
	Average	St.Dev.	Average	St.Dev.	Average	St.Dev.
C22	-1.90	0.24	-3.07	0.13	-2.42	0.22
C23	-2.04	0.22	-3.11	0.16	-2.68	0.29
C24	-1.98	0.19	-2.76	0.19	-2.46	0.31
C25	-1.67	0.13	-2.21	0.10	-1.85	0.34
C26	-1.33	0.21	-1.69	0.05	-1.65	0.56
C27	-1.46	0.23	-1.52	0.15	-1.61	0.52

The mean log Kp values were well correlated between the seasons. As expected, the correlation was lower between the winter and the summer samples (R^2 = 0.90) but became a bit higher between the winter and the autumn samples (R^2 = 0.93) and between summer and autumn samples (R^2 = 0.94).

The temperature corrected Log pL^0 was calculated for all the samples (Tab. 3.15).

Table 3.15 Temperature corrected log pL0 (Pa)

log pL^0 (Pa)	winter (n=9)		summer (n=8)		autumn (n=7)	
	Average	St.Dev.	Average	St.Dev.	Average	St.Dev.
C22	-2.23	0.12	-3.93	0.10	-3.08	0.26
C23	-1.01	0.12	-2.78	0.10	-1.89	0.27
C24	-1.52	0.13	-3.36	0.11	-2.43	0.29
C25	-1.89	0.14	-3.81	0.11	-2.84	0.30
C26	-2.31	0.14	-4.30	0.12	-3.31	0.31
C27	-2.46	0.14	-4.51	0.12	-3.48	0.32

The relationship between the mean log Kp for the n-alkanes from C22 to C27 and temperature corrected log pL° is represented in Fig. 3.30.

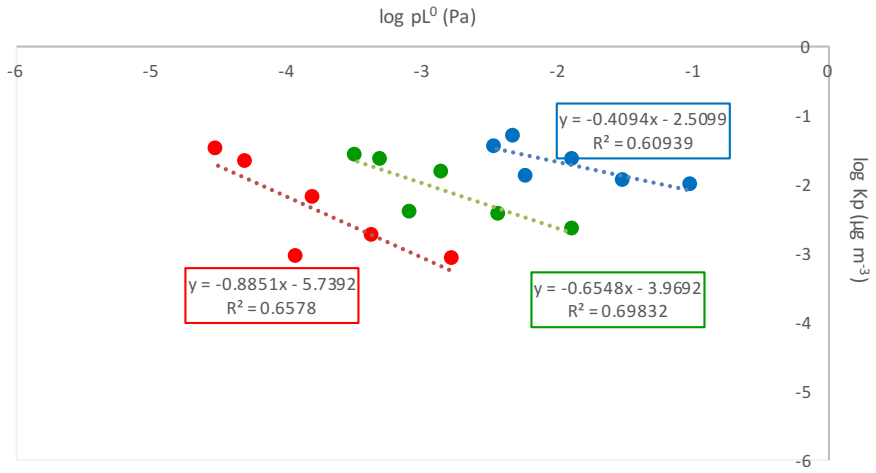

Figure 3.30 Experimental Kp vs log for the ALKs (C22 C23, C24, C25, C26, C27).

The correlation for log Kp vs log pL° was weak: in winter, the coefficient of determination (R^2) was between 0.47 and 0.70, in summer between 0.54 and 0.72 and in autumn between 0.26 and 0.80. The negative slope of the regression indicates a decreasing association of a compound with the particulate phase as vapor pressure increases. At equilibrium, the slope for either adsorption or absorption should be close to -1 [88]. The measure data measured suggested that the gas/particle partition wasn't at equilibrium.

The phase partitioning may also be described by the fraction θ of a compound in the particulate phase. The experimental adsorbed fraction on the particles, θ, was

calculated and then compared to the predicted θ calculated using the temperature corrected log pL^0. Value of Cj = 17.2 Pa and of S=1.1 x 10^{-5} were used.

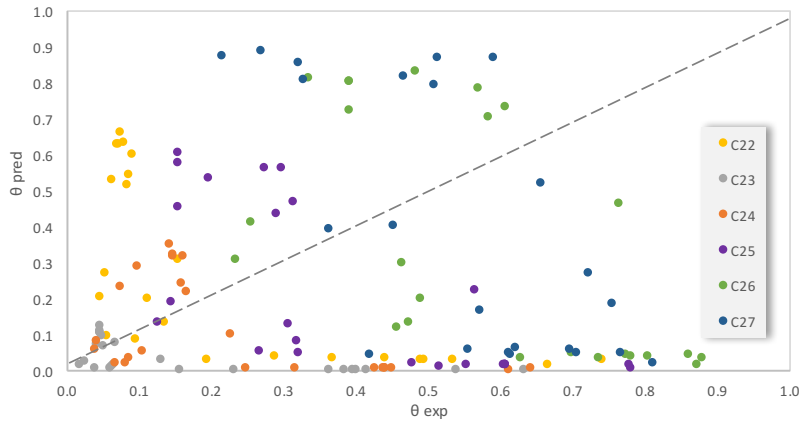

Figure 3.31 Predicted versus experimental ϑ for Milan (n = 24), Junge-Pankow model

A great variability between the samples, mainly due to differences between the seasons led to a large scatter plot, as reported in Fig. 3.31. In particular, winter samples showed the worst correlation as shown in Fig.3.32.

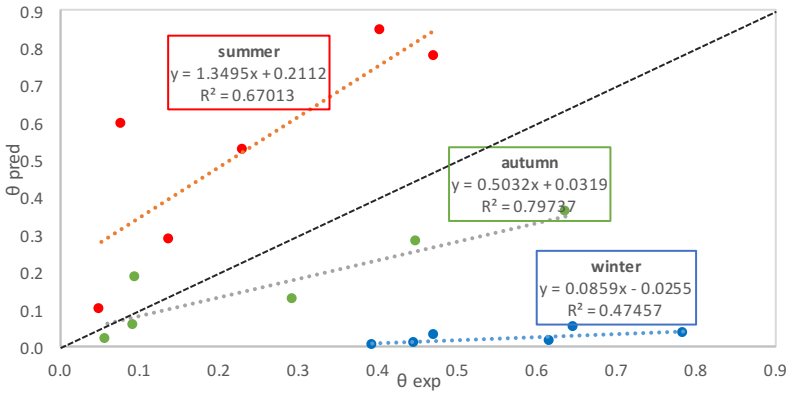

Figure 3.32 Mean predicted versus experimental ϑ for the ALKs (C22 C23, C24, C25, C26, C27).

The results show that the Junge-Pankow underestimated the partitioning for winter and autumn samples, whereas it over-predicted the partitioning for summer samples. As for PAHs, the model was found to be inadequate to predict the partitioning, indicating that another process, could be significant for the phase partitioning.

The experimental log Kp was also correlated against the octanol-air partitioning coefficient (Fig. 18). The temperature corrected log K_{OA} were calculated from tabulated values at 25°C found in literature (Tab. 3.16).

Table 3.16 Temperature corrected and literature data for log Koa

log Koa	winter (n=9)		summer (n=8)		autumn (n=7)		
	Average	St.Dev.	Average	St.Dev.	Average	St.Dev.	**logKoa(25°C)**
C22	8.68	0.12	6.99	0.10	7.84	0.26	7.34
C23	9.11	0.12	7.34	0.10	8.23	0.27	7.70
C24	9.53	0.13	7.69	0.11	8.61	0.29	8.07
C25	9.96	0.14	8.04	0.11	9.00	0.30	8.44
C26	10.39	0.14	8.39	0.12	9.39	0.31	8.81
C27	10.80	0.14	8.75	0.12	9.78	0.32	9.17

An extremely better correlation for the log Kp vs log Koa regression (R^2: 0.50-0.85 in winter, 0.87-0.97 in summer and 0.66-0.91 at SC in autumn) compared to that for Log Kp vs pL^0

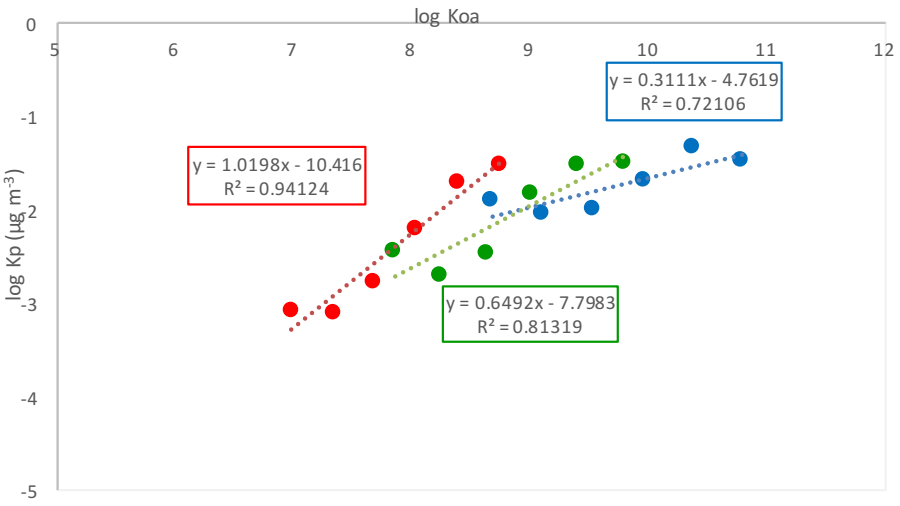

Figure 3.33 Experimental Kp vs log Koa for the ALKs (C22 C23, C24, C25, C26, C27).

For the equilibrium partition, the slope is expected to have a value of near +1. The measured values ranged from 1.43 to 2.50 in winter, 0.81 to 1.02 in summer and 1.03 to 1.50.

The quite good regression for log Kp vs Koa, compared to the bad regressions for Kp vs pL^0, suggested that the semi-volatile Alks "feel" being dissolved or in octanol-like organic matter more than in themselves [91].

The predicted log Kp was calculated using the temperature corrected log Koa. The Koa absorption model can be used to predict values of Kp from knowledge of only Koa and the organic fraction of the aerosol, fOM. For the conversion from organic carbon to organic matter was made assuming that the organic matter fraction (fOM) is 1.6 times the organic carbon fraction (fOC). The results obtained by linear regression of measured versus predicted Kp values are shown in Fig 19. and the differences between the season are shown in fig 3.34.

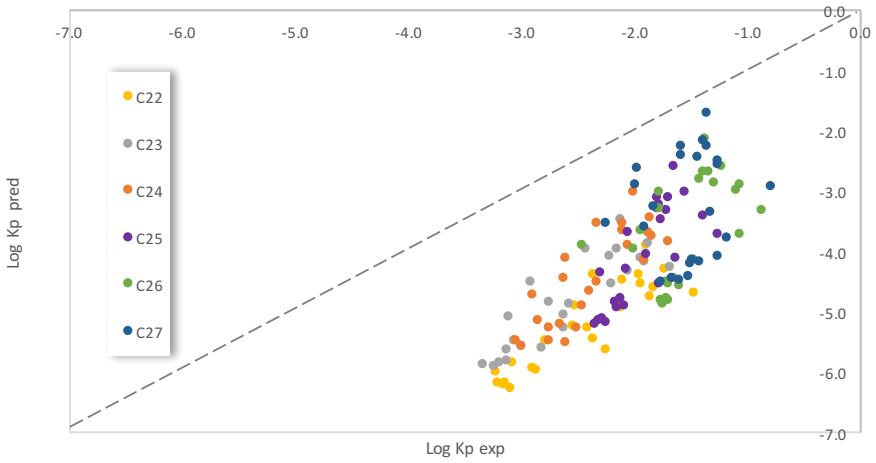

Figure 3.34 Predicted versus experimental Kp for Milan (n = 24), Koa model

Exactly like for PAHs, the model always underestimated the partitioning for n-alkanes.

Despite a better correlation compared to the Junge- Pankow model, the Koa model always underestimated the partitioning for considered alkanes, for the samples collected in all the three seasons (Fig. 3.35).

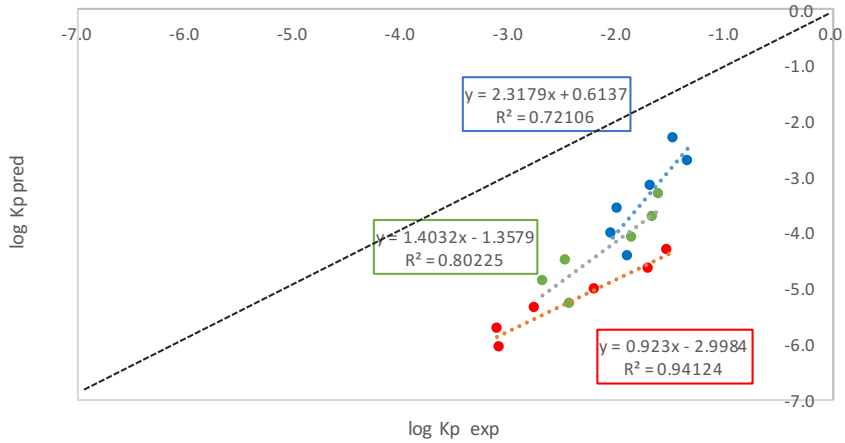

Figure 3.35 Mean predicted versus experimental Kp for the ALKs (C22 C23, C24, C25, C26, C27)

An attempt to predict the gas/particle partitioning coefficient Kp applying the dual model described in Lohmann and Lammel[27] was made. The corrected log Kp were than compared with that predicted Kp (Fig. 3.36)

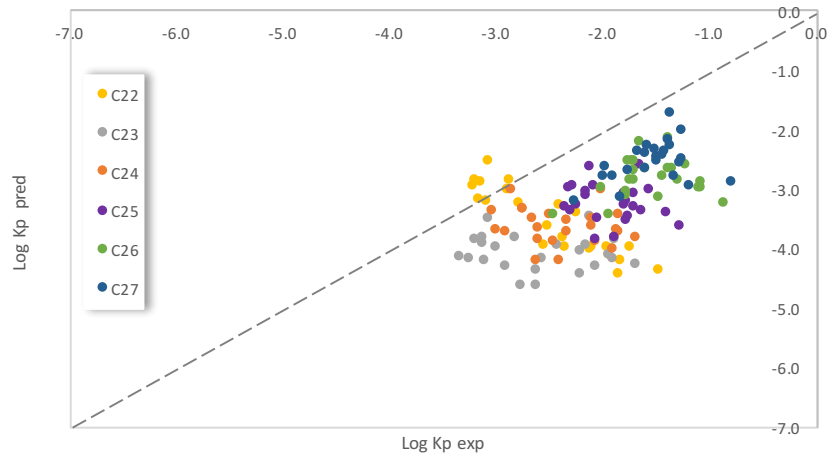

Figure 3.36 Predicted versus experimental Kp for Milan (n = 24), Dual model

To get the predicted log Kp, Koa and Ksa values were calculated. For the winter samples collected in December, for which chemical analysis to determine organic and elemental

carbon were not performed, average values of EC and OM obtained for the other samples were used (OC: 12.5 µg m^{-3}; EC: 2.9 µg m^{-3}).

A good correlation was found between the measured and the predicted log Kp for the summer samples, while a quite bad correlation was found for summer and winter as shown in Fig 3.37.

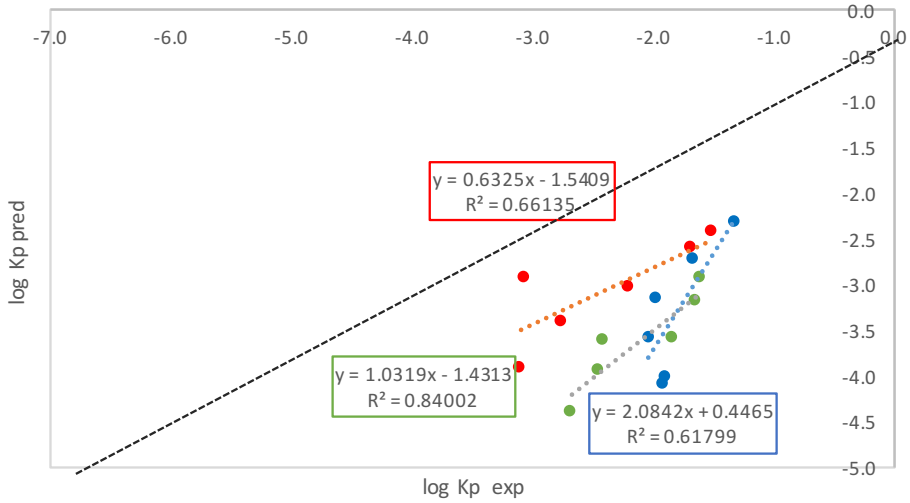

Figure 3.37 Mean predicted versus experimental Kp for the ALKs (C22 C23, C24, C25, C26, C27).

A slightly better correlation was found for winter samples normalizing the experimental Kp at 298K (as recommended by Lohmann and Lammel[27]) as reported in Fig. 3.38

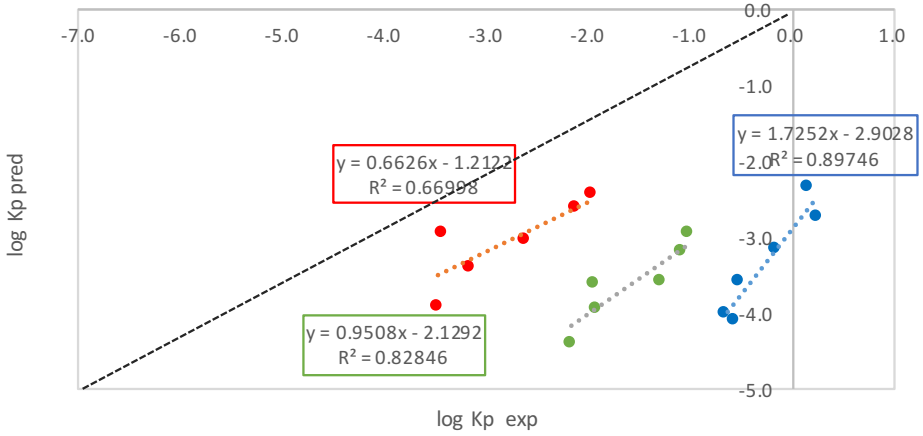

Figure 3.38 Mean predicted versus experimental Kp for the ALKs (C22 C23, C24, C25, C26, C27).

Nevertheless, the results showed that the dual model under-predicted the alkanes partitioning.

The model hereinbefore used, showed a systematic underestimation of the partitioning of the semi-volatile alkanes.

The gas-particle partitioning was studied using a PPLFERs model, considering two mechanisms for the partitioning: absorption into OM and adsorption onto soot.

The system parameters for diesel soot [95] and for DMSO[115] were used for adsorption and absorption contribution respectively. The solute descriptor for the considered alkanes were taken from the literature[120,121] (Tab. 3.16).

Table 3.17 System parameters for PPLFER model

System parameters

	e	s	a	b	v	l	c
EC[a]	-	-	2.70	2.45	-	1.09	-8.47
DMSO[b]	-0.22	2.90	5.04	0.00		0.72	-0.56

Solute Descriptors

	E	S	A	B	V	L
C22[c]	0.00	0.00	0.00	0.00	3.208	10.740
C23[d]	0.00	0.00	0.00	0.00	3.349	11.252
C24[c]	0.00	0.00	0.00	0.00	3.490	11.758
C25[c]	0.00	0.00	0.00	0.00	3.631	12.264
C26[c]	0.00	0.00	0.00	0.00	3.772	12.770
C27[c]	-	-	-	-	3.913	13.244

a= Roth, et al 2005; b= Abraham et al., 2010; c=Sprunger et al 2010;d=Abraham et al.2010 .

The partitioning constants related to absorption and adsorption processes calculated using eq 14, were corrected for the effect of near- ground temperature at the site using the solute-specific enthalpies of phase transfer, which were calculated for the corresponding ppLFER systems[118.119]. Total Kp was determined by summing the individual partitioning coefficients after normalizing the units.

Fig. 3.39 shows predictions made following the PPLFER method. A can be seen, the majority of the data points were predicted within 1 order of magnitude accuracy, with the exception of C21 (which was always under-predicted) and C27 (which was for most samples over predicted).

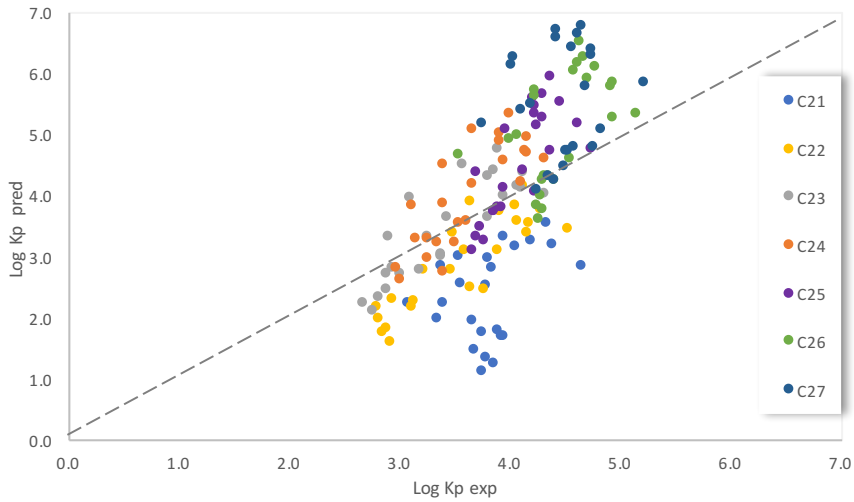

Figure 3.39 Predicted versus experimental Kp for Milan (n = 24), Dual phase ppLFER model

A strong correlation for the experimental vs the predicted log Kp were found (R^2: 0.50-0.86 in winter, 0.87-0.97 in summer and 0.66-0.91 in autumn) as shown in Fig 3.40

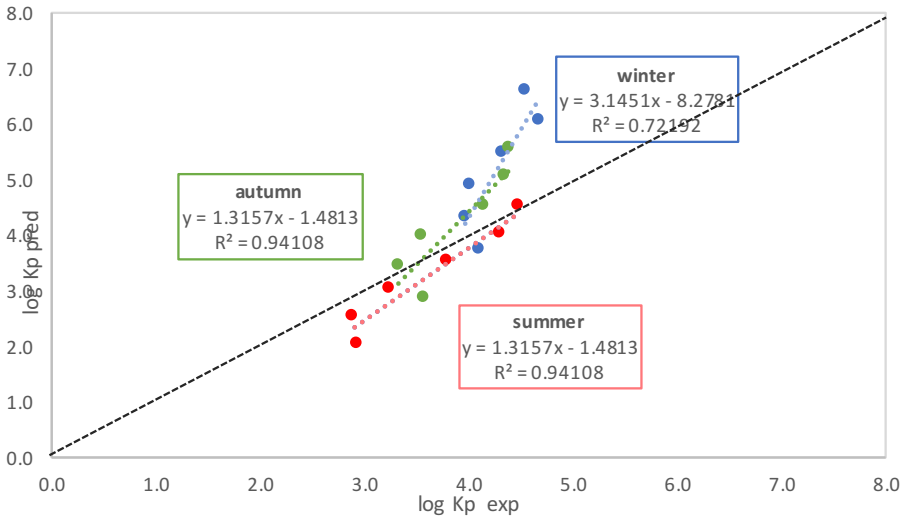

Figure 3.40 Mean predicted versus experimental Kp for the ALKs (C22 C23, C24, C25, C26, C27).

These results suggest that the ppLFER model predicted accurately the gas-particle partitioning of alkanes without showing season variability related to PM compositions and sources. In the light of these results, a comparison between the two sampling sites in autumn was made.

Experimental and predicted log Kp for TR site and LEZ site, presented in Table 3.17, didn't show any inter-site variability (R^2:0-99-1.00)

Table 3.18 Predicted and experimental Kp for autumn samples at TR and LEZ site

	pred log Kp(m^{-3} g^{-1})		exp log Kp(m^{-3} g^{-1})	
	TR	LEZ	TR	LEZ
C22	3.08	2.71	3.61	3.55
C23	3.64	3.25	3.38	3.27
C24	4.19	3.78	3.63	3.48
C25	4.75	4.32	4.27	4.06
C26	5.30	4.85	4.47	4.25
C27	5.82	5.35	4.47	4.34

The gas-particle partitioning was lastly studied using a multi-phase PPLFERs model that considers absorption into OM and adsorption onto soot and soluble salts.

For adsorption contribution, the system parameters for diesel soot[95], Al and Fe oxides, ammonium sulphates and ammonium chloride[97] were used. For absorption, 2 OM phases were considered and DMSO and polyurethane were chosen as surrogates (Tab. 3.10)

Total predicted Kp, determined by summing the individual partitioning coefficients was compared to the experimental Kp (Fig. 3.41)

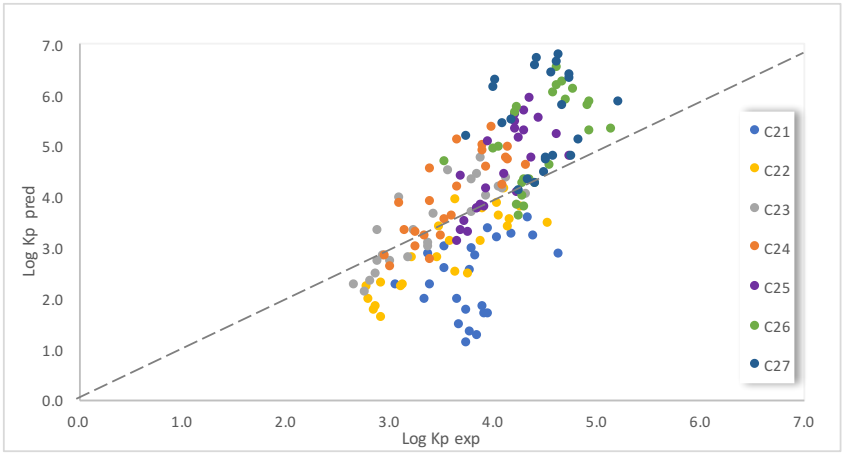

Figure 3.41 Predicted versus experimental Kp for Milan (n = 24), Multi-phase ppLFER model

The use of the multiphase approach didn't improve the prediction of the alkanes partitioning.

Fig. 3.42 shows the contribution of the adsorption and absorption processes considered in this study.

Evidently, adsorption on soot was the main partitioning process and the contribution was higher for the heavier alkanes. The contribution of high molecular mass organic polymers (OP) was the most important for the absorption and this contribution was inversely proportional to EC (i.e. the contribution decreases with increasing the molecular weight of the compound). Adsorption onto soluble salts may be neglected.

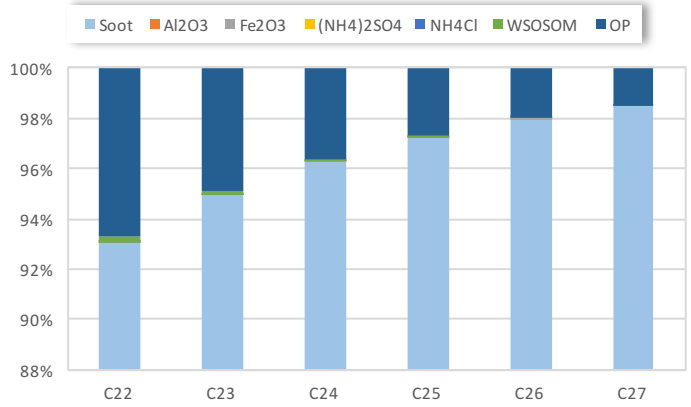

Figure 3.42 Contributions of individual phases to Kp determined using multi-phase ppLFER. OSWSOM: both organic soluble and water soluble organic matter; OP: organic polymers.

3.3 BLACK CARBON CONCENTRATIONS INSIDE AND OUTSIDE THE LOW EMISSION ZONE

Through the chemical analysis on the samples collected in Milan, a 36% decrease in the concentrations of the Elemental Carbon from the traffic site to the LEZ for EC (36%) was observed. Since EC is a product of the incomplete combustion and it is considered as a marker of the traffic source, such results demonstrate the impact of local traffic source on the elemental carbon concentrations. As explained in Chapter 1 (Par 1.2) EC is often also referred to as Black Carbon due to light absorbing properties.

As mentioned in Chapter 1, Black Carbon is emitted form a great variety of sources, mainly from incomplete combustion processes by engines and biomass burning.

The contribution of traffic and wood smoke can be measured through model based on light absorption measurements at ultraviolet (UV) to infrared wavelengths[121].

BC from wood burning has a greater absorption in the UV wavelength as compared to BC from fossil fuel[122]. The wavelength dependence of the aerosol absorption coefficients (β_{abs}) is proportional to $\lambda^{-\alpha}$, where λ is wavelength and α is the absorption exponent. Higher α values were observed in wood burning due to the strong absorption in the UV regime[122]. α from wood burning (α_{wb}) varies as a function of the combustion efficiency and is affected by the type of wood burning and the combustion regime. Several studies have reported consistent α value for fossil fuel (α_{ff}) and wood burning (α_{wb}) of about 1.1 and 2.0 respectively[123, 124, 125]. The total absorption at a wavelength is the sum of the absorption due to fossil fuels (BC_{ff}) and wood burning (BC_{wb})[122].

In the light of these findings, a pilot study on BC concentrations was conducted in Milan. The monitoring campaign took place in Milan at two sites: a site within the Campus of the University of Milano Bicocca (U9, Viale dell'Innovazione) and a limited traffic site in the city centre within the low emission zone (VN; Villa Necchi Campiglio, Via Mozart). The sampling campaign was conducted simultaneously outside and within the Low Emission Zone from March to October 2015 by means of two aethalomethers AE31 (Magee Scientific Co. Berkeley CA).

The mean values of the Black Carbon concentrations measured at U9 and VN during 2015 are reported in Fig. 3.43

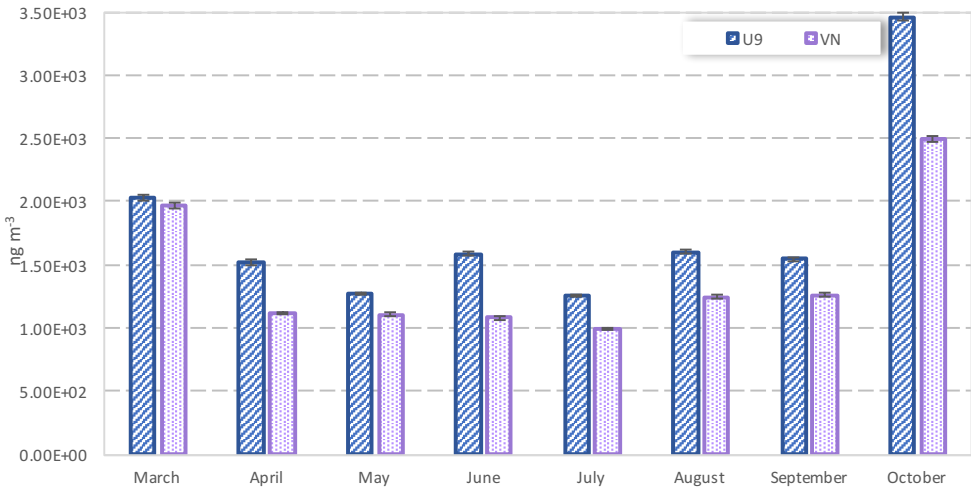

Figure 3.43 Average BC concentrations at U9 and VN (crossbars: standard deviation).

BC concentrations were always higher at U9 site than at VN: the average values during the whole sampling period were 1783±19 ng m^{-3} at U9 and 1408 ± 14 ng m^{-3} at VN, with an average reduction of 21% within the low emission zone. The efficacy of black carbon measurements as an indicator of the impact of traffic restrictions has been illustrated by other studies[51,126,127] which demonstrated the impact of traffic restrictions on air quality.

As expected, the concentrations were lower during spring and summer and higher during winter-time. The highest concentrations of BC were recorded at both sites in October (U9= 3462±34 ng m^{-3}; VN=2496±24 ng m^{-3}) and March (U9= 2016±24 ng m^{-3}; VN=1966±19 ng m^{-3}).

Only for U9 site the measurements continued up to December. Form Fig 4.44 it is possible to see a growing trend of the concentrations from October to December.

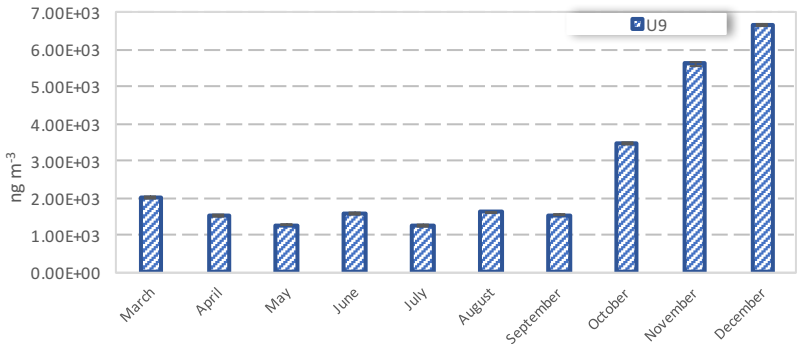

Figure 3.44 Average BC concentrations at U9 (crossbars: standard deviation).

This situation is typical of the Lombardy region and it is due to the different climatologic condition in winter and to a lowering of the inversion layer.

The contributions of fossil fuels combustion (eBC_ff) and of the biomass burning (eBC_bb) to the total concentrations of BC are presented in Fig. 3.45

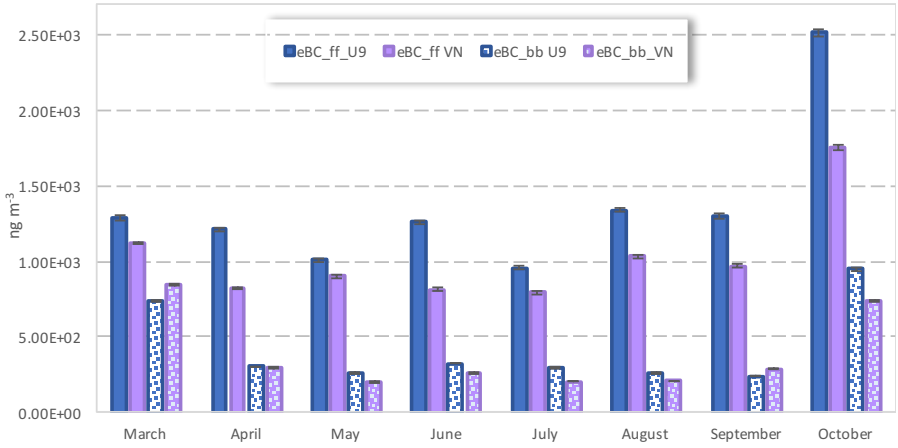

Figure 3.45 Average concentrations of eBC from fossil fuels (eBC_ff) and from biomass burning (eBC_bb) at U9 and VN

Biomass burning emissions are usually higher during winter time, when residential heating is turned on in the whole urban area, while during summer the contribute of Black Carbon emissions due to this source it is expected to be very low. In 2015 BC from wood burning followed this trend: the highest values were measured at both sites in October (U9= 948±10 ng m^{-3}; VN=740±9 ng m^{-3}) and March (U9= 737±9 ng m^{-3}; VN=844±9 ng m^{-3}). As expected from October to December at U9 the concentrations of eBC from biomass burning raised up to 2463 ±14 ng m^{-3}.

Traffic emissions are constant during the year. Differences can be registered during different months, but the variations are smaller than the biomass burning ones. From March to September BC concentrations from traffic were in the range of 958-1342 ng m^{-3} at U9 and 794-1122 ng m^{-3} at VN. An important increase was seen in October when the concentrations reached the highest values both at U9 (2514±10ng m^{-3}) and at VN (1756±16 ng m^{-3}).

BC from traffic showed always higher concentration compared to wood burning, meaning that the major part of BC in Milan comes from this source. The contribution from fossil fuels combustion, in fact, represents 73% of the total emission of BC. Moreover, it has to be noticed that, whereas the contribution from biomass burning was similar at the two sites (VN: -10%), BC from traffic was always higher at U9 (VN: -

25%). For this reason, such data can also be helpful to policy and decision makers in evaluating the benefits of local traffic reductions in urban areas.

The typical average daily trend (24h) of eBC from fossil fuels at the two site is represented in Fig. 3.46. Two peaks can be identified: the first around 7:00 am and the second, although less marked, around 9-11 pm. The causes of this behavior can be attributed to the traffic rush hour and the low boundary layer height, which occurs with the decrease of solar radiation.

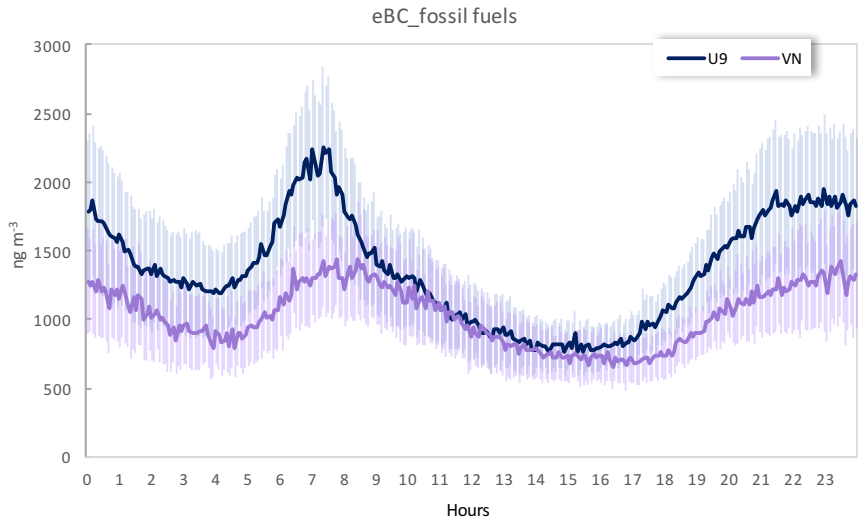

Figure 3.46 Typical daily trend of eBC from fossil fuels (ng m-3) at U9 and VN

As can be seen from Fig. 3.47 the trend was similar in the different months at both sites. The morning peak was higher than the second one for all the months except for July and August, especially at U9, when the concentrations were similar in the morning and in the evening. On the contrary, in October the second peak was much greater than first.

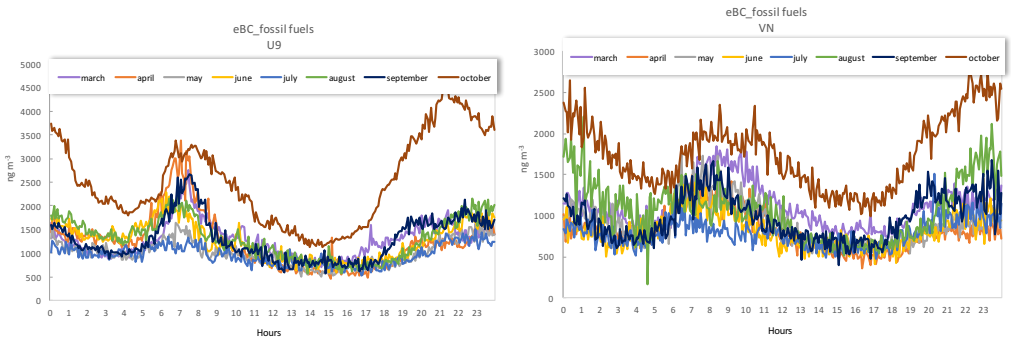

Figure 3.47 Typical trend (24h) of eBC from fossil fuels (ng m-3) at U9 and VN

Regarding the typical average daily trend (24h) of eBC from biomass burning (Fig. 3.48), there was a slight increase in the concentrations from 6 to 9 am and after 8 pm, which probably correspond with time of the activation of the heating systems.

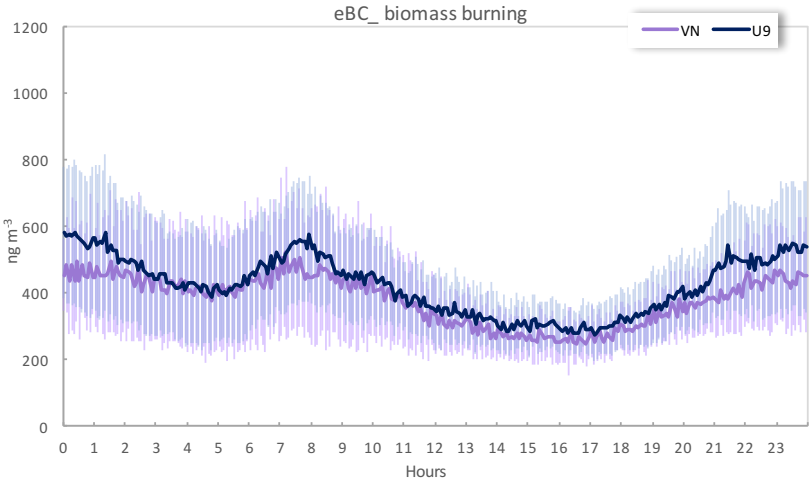

Figure 3.48 Typical daily trend of eBC from biomass burning (ng m-3) at U9 and VN

In fact, from Fig. 3.49, it is possible to notice that the trend described above was typical of the winter months (March and October) while during the other months the concentrations were the same all-day long.

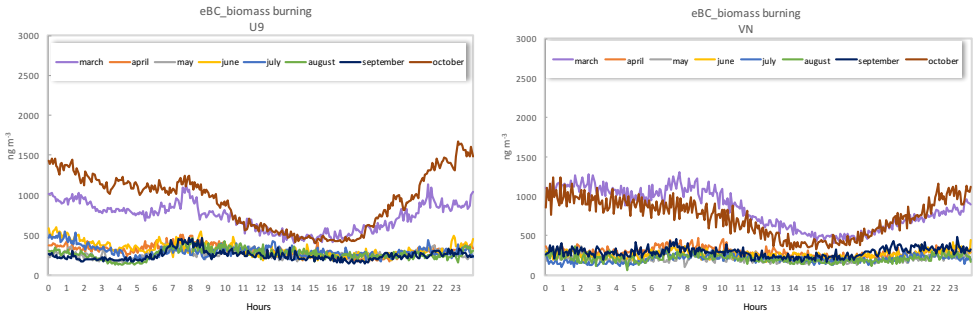

Figure 3.49 Typical trend (24h) of eBC from biomass burning (ng m-3) at U9 and VN

3.4 CONCLUSIONS

Two campaigns were performed to study the semi-volatile organic compounds in Milan: at a traffic site (TR) in winter and summer 2013 and simultaneously at traffic site and within the Low Emission Zone (LEZ) in autumn 2013. The samples of the particulate and gaseous phases of the air were collected simultaneously by a high-volume sampler equipped with quartz fiber filters and PUF plugs. All the samples were processed to determine the PAH and n-alkane concentrations. Moreover, a study on the concentrations of black carbon outside and inside the low emission zone of Milan was conducted from March to October 2015.

Seasonal differences in the atmospheric concentrations of PAHs, alkanes and BC were highlighted and a reduction of 32%, 15% and 21% was found within the LEZ for PAHs, alkanes and BC respectively, suggesting that traffic is an important source of this class of compounds.

For both the chemical classes, three groups were found in function of their phase partition:

- Volatile compounds, present for less than 20% in the particulate phase. The components of the group were and the PAHs lighter than FLNT and the n-alkanes lighter than n-C23.
- Semi-volatile compounds, present in the particulate phase for 20-80%. FLNT and PYR (for PAHs) and the n-alkanes from n-C23 to n-C25 are in this group.
- Not-volatile compounds, present for more than 80% in the particulate phase. The components of this group were the PAHs heavier than PYR and the n-alkanes with a molecular weight higher than n-C25

The phase partition of the two chemical classes was in agreement with the volatility characteristics of the compounds.

The log Kp coefficient was calculated and correlated against the log pL° (sub-cooled liquid vapor pressure) and log Koa (octanol-air partitioning coefficient). Strong correlations were found for both the regressions with the semi-volatile PAHs but not so strong with n-alkanes. The fraction θ of a compound in the particulate phase was calculated and compared to the θ predicted by the Junge-Pankow model.

The measured Kp was also compared with log Kp predicted by the Koa model, which take into account only the absorption process and later with the log Kp predicted by a dual model that took into account both the absorption in the organic aerosol and the adsorption onto the elemental carbon.

In general, a good correlation was found between the measured and the predicted log Kp for PAHs ($R^2 \geq 0.90$) and for alkanes ($R^2 \geq 0.80$) in winter and autumn but worse in summer ($R^2 = 0.65$). However, the regression lines didn't pass through the axis origin meaning that the models underestimate the partitioning and suggesting that other important factors should be added.

For this reason, the gas-partitioning was studied using a polyparameter linear free energy relationships (ppLFERs), that takes into account the molecular interactions between the compound (sorbate) and the sorbent phase. The dual-phase ppLFER considers adsorption onto to elemental carbon (EC) and absorption into the organic matter, whereas the multi-phase ppLFER considers adsorption onto to elemental carbon (EC) and soluble salts and absorption into various OM fractions. The model predicts very good the partitioning ($R^2 \geq 0.80$ for PAHs and ≥0.70 for alkanes). Absorption was the main partitioning process for PAHs, dominated by the contribution of OSWSOM while adsorption on soot and absorption into the high molecular mass organic polymers (OP) were the main partitioning process in the alkanes partitioning. For both the considered class of compounds, adsorption onto soluble salts (<0.01% of the total Kp) may be neglected.

CHAPTER 4. EMISSIONS FROM THE AIRPORT MILANO-MALPENSA

Airport emissions represent an intense, highly variable emission source whose impact on the population requires an accurate assessment. Most studies highlight knowledge gaps[128,129,130] which are a matter of concern as the literature indicates that aircraft emissions can significantly affect air quality near airports[131,132,133].

The project was part of a wider work on the environmental impact assessment of the airport, necessary for the fulfilment of the works envisaged by the new Masterplan concerning the extension of the existing cargo area. For this reason, the measurements carried out concerned, particularly, a set of atmospheric pollutants important from a regulatory point of view.

The study was conducted inside the airport at two sites with different emission sources in two different periods. Details on the sampling campaigns are reported in Chapter 2, Par 1.2. The concentrations and the dimensional distribution of the particulate matter (PM10 and PM2.5), the concentrations of Black Carbon and of gaseous pollutants such as NOx, ozone and volatile organic compounds have been determined. Moreover, micro-organic pollutants such as PAHs present in the PM were analysed. The data obtained were then compared with data collected from the Lombardy Regional Agency for Environmental Protection (ARPA) in the neighbouring cities (Fig. 4.1).

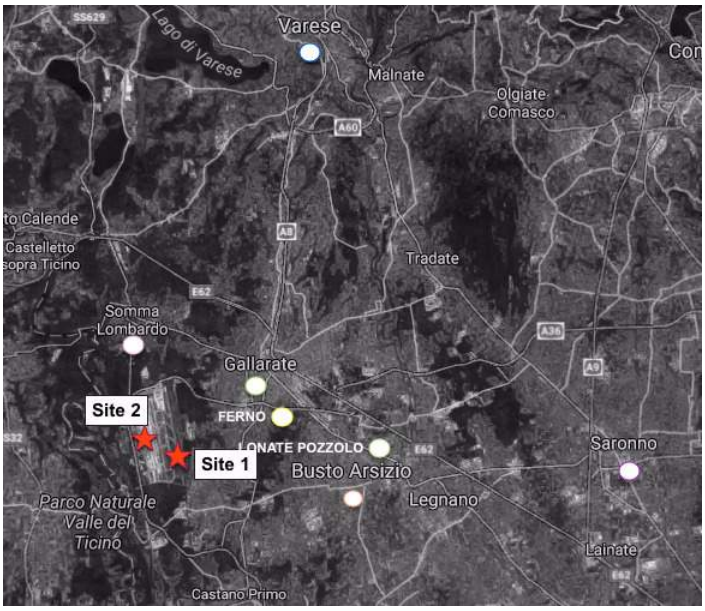

Figure 4.1 Localization of the monitoring stations considered in this study

4.1 PARTICULATE MATTER

Particulate Matter measurements were obtained by gravimetric (PM10, PM2.5) and optical (PM10. PM2.5 Pm1, N<250, N250-1000, N>1000) analysis.

The trend of the concentrations obtained through gravimetric system is shown in Fig.4.2 and 4.3.

The gravimetric measurements at site 1 showed average concentration of 37,5±19,4 µg m^{-3} and 30,5±16,6 µg m^{-3} for PM10 and PM2.5 respectively. At site 2 the concentrations of PM10 and PM2.5 were 43,5±33,7 µg m^{-3} and 34,45±27,32 µg m^{-3} respectively. Similar PM2.5 concentrations were found by Unal et al[132] at the Atlanta international Airport.

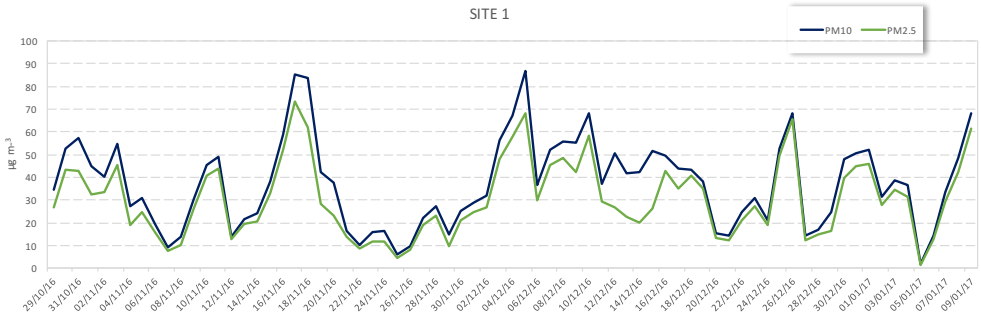

Figure 4.2 PM10 and PM2.5 concentrations (µg m-3) measured at Site 1

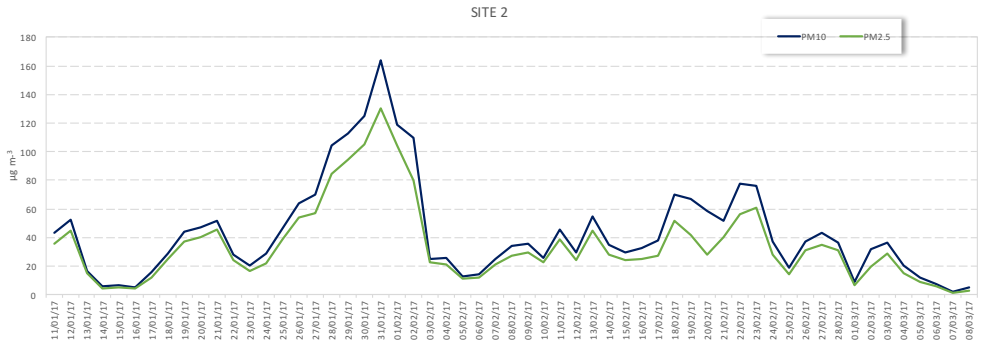

Figure 4.3 PM10 and PM2.5 concentrations (µg m-3) measured at Site 2

The measured PM10 concentrations got close to the annual limit of 40 µg m^{-3} imposed by the legislation; however, it is not possible to make a direct comparison between the values measured inside the airport and the annual limit since the campaign was conducted in a limited period of time and took place during the coldest months, when the situation is critical due to the lowering of the inversion layer. As mentioned in Chapter 1 (Par 1.3) for PM10 a daily limit at 50 µg m^{-3}, which should not be exceeded more than 35 days a year, was set. During the sampling campaign this limit was exceeded 20 times at site 1 and 17 times at site 2.

The trend of the PM10 and PM2.5 concentrations was compared to that from the ARPA stations in the bordering towns in order to verify local differences.

PM10 showed a variability modulated mainly by weather conditions. In fact, it is possible to observe a similar trend at all the considered sites (Fig. 4.4 and 4.5). Moreover, the concentrations at Malpensa during the first period of sampling (Site 1)

were lower than those at the other sites over the entire sampling period. During the second sampling campaign (Site 2) the concentrations at Malpensa were lower than or equal to the other stations except for Busto Arsizio which showed lower values.

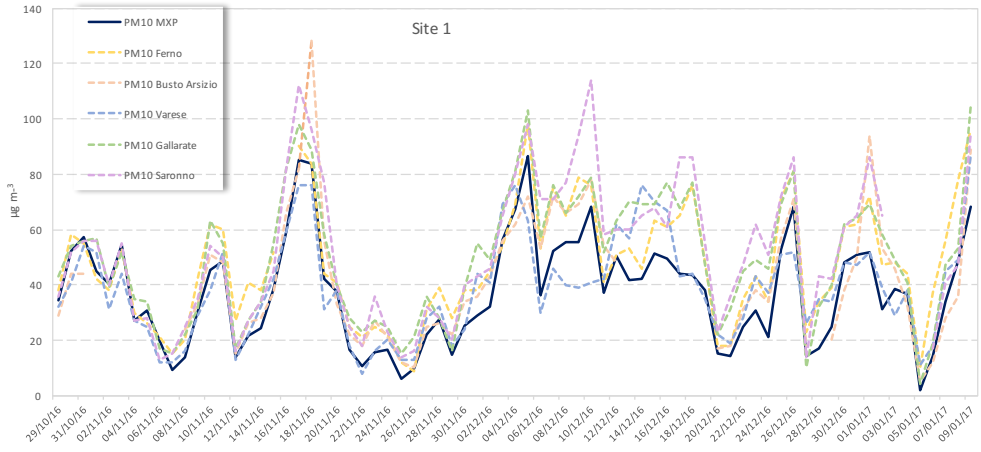

Figure 4.4 Trend of PM10 concentrations (µg m-3) measured in the Airport of Milano-Malpensa at Site 1 and the measurements from ARPA stations located in the neighboring cities

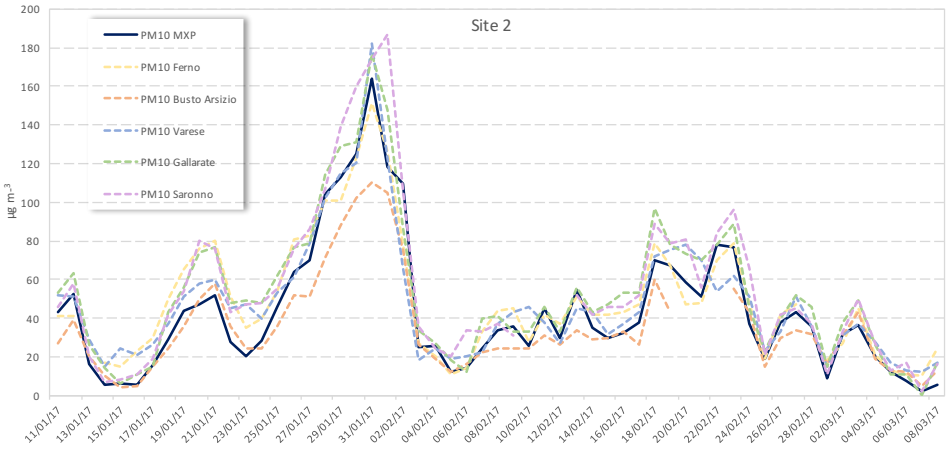

Figure 4.5 Trend of PM10 concentrations (µg m-3) measured in the Airport of Milano-Malpensa at Site 2 and the measurements from ARPA stations located in the neighboring cities

For PM2.5, the results were limited by the lack of measurements from the ARPA stations. Fig 4.6 and 4.7 show the comparison between PM2.5 measured inside the airport and those measured at Varese and Saronno.

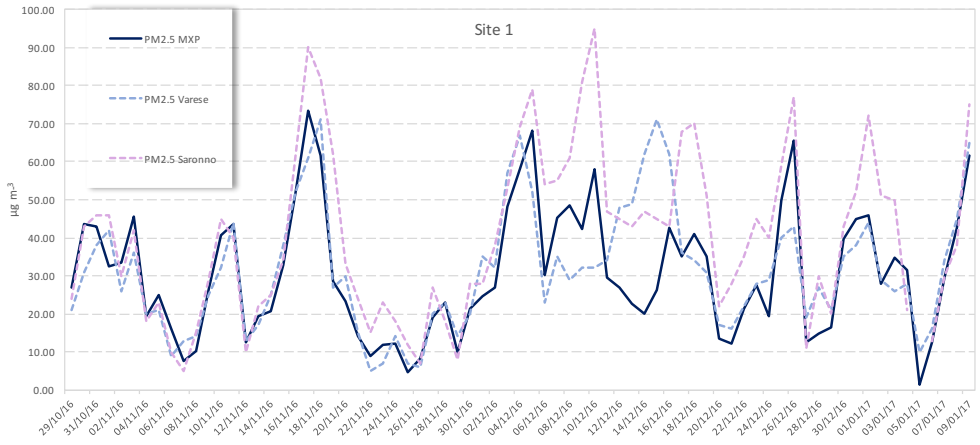

Figure 4.6 Trend of PM2.5 concentrations (µg m-3) measured in the Airport of Milano-Malpensa at Site 1 and the measurements from ARPA stations

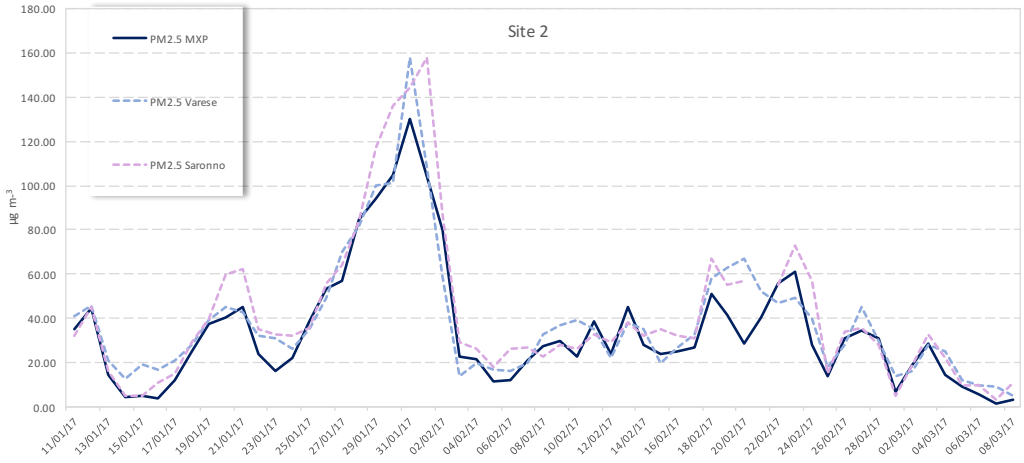

Figure 4.7 Trend of PM2.5 concentrations (µg m-3) measured in the Airport of Milano-Malpensa at Site21 and the measurements from ARPA stations

The trend was similar at the three sites with a good correlation between the concentrations (R^2=0.76) at Malpensa and Saronno ("blank" site, i.e. not-affected by the emissions from the airport). This means that PM2.5 concentrations inside the airport are mainly due to external factors.

PM10, PM2.5 and PM1 were analysed also by means of an Optical Particle Counter.

Although these values were not obtained by a certified method (gravimetric method), they have the advantage of describing the trend of mass concentrations at high

resolution. For this purpose, their validity was tested correlating the daily average value with that obtained by gravimetric measurements. The results, presented in Figure 4.8 (PM10: $R^2 = 0.9$; PM2.5; $R^2 = 0.93$) showed an excellent agreement.

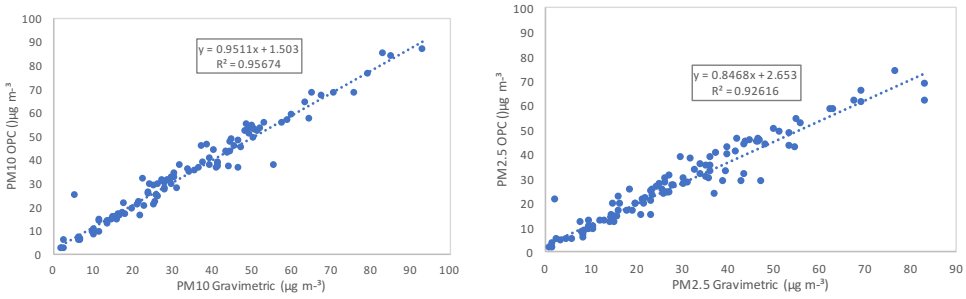

Figure 4.8 Correlation between average daily concentrations (24h) of PM10 (on the left) and PM2.5 (on the right) obtained by gravimetric measures (FAI Hydra Dual Channel) and by OPC (Grimm 107)

Through optical measurements realized by means of a CPC-OPC system it was possible to determine the trend of three dimensional macro-ranges of suspended particles: 4-250nm; 250-1000nm; >1000nm.

The typical average trends of the particles smaller than 250 nm (d <250, dominated by nanoparticles), the particles and with a diameter between 250 and 1000 nm and the particles larger than 1000 nm are shown in fig 4.9 and 4.10 for Site 1 and in Fig 4.11 and 4.12 for Site 2.

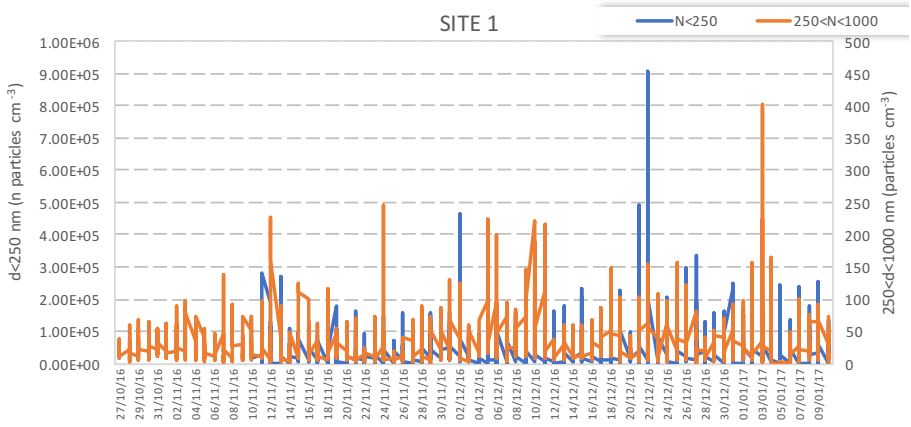

Figure 4.9 Trend of the concentrations of particles smaller than 250 nm (N250) and with a diameter between 250 and 1000 nm (250<N<1000) at Site 1

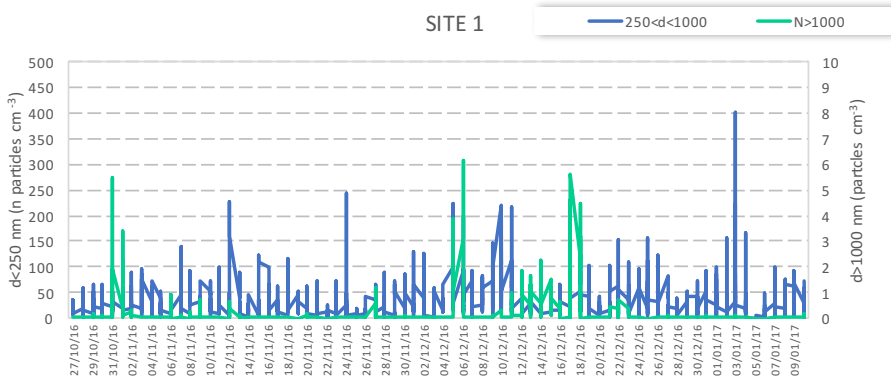

Figure 4.10 Trend of the concentrations of particles and with a diameter between 250 and 1000 nm(250<N<1000) and larger than 1000 nm (N>1000) at Site 1

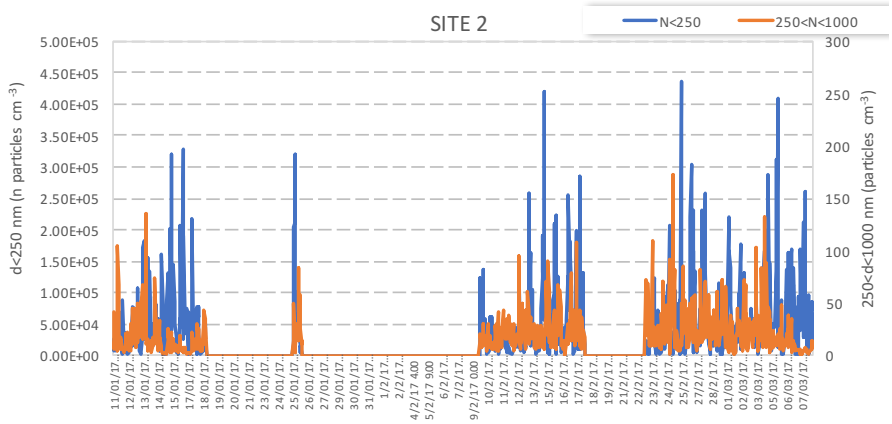

Figure 4.11 Trend of the concentrations of particles smaller than 250 nm (N250) and with a diameter between 250 and 1000 nm (250<N<1000) at Site 2

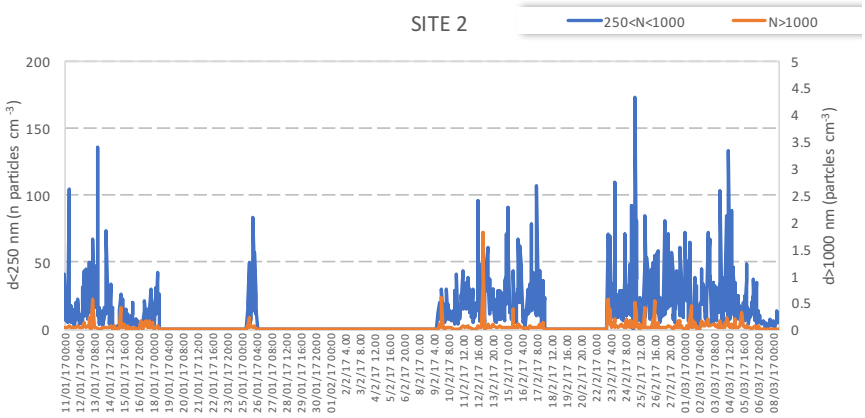

Figure 4.12 Trend of the concentrations of particles and with a diameter between 250 and 1000 nm(250<N<1000) and larger than 1000 nm (N>1000) at Site 2

The most important airport activity at site 1 is due to movement of aircraft during take-off and landing phases. The Airport activity shows a first peak at 7:30 am, followed by one at 11-11: 30 am and an evening peak at 7.00 pm. A corresponding increase in the concentration of the finest particles below 250 nm (N <250, dominated by nanoparticles) was measured by tandem CPC-OPC (Figure 4.13). In particular, concentrations of N <250 increased suddenly by 5.8 ± 3.4 times with the onset of air traffic between 6:30-7:30 am LST ($1.1*105 \pm 5.3*10^4$ particles cm^{-3}) compared to 0:00-6:30 am LST ($1.8*10^4 \pm 5.7*10^3$ particles cm^{-3}) and a rapid decrease during night after 11 pm ($5.0*10^4 \pm 1.0*10^4$ particles cm^{-3}) with the reduction of the airport activity compared to 7-11 pm LST ($1.0*10^5 \pm 2.4*10^4$ particles cm^{-3}).

A similar result is reported by Westerdahl et al.[134], where periodic peaks in the range of 20,000– 400,000 particles cm^{-3} observed in a location downwind the Los Angeles international Airport appeared to reflect emissions of individual aircraft takeoffs and landings.

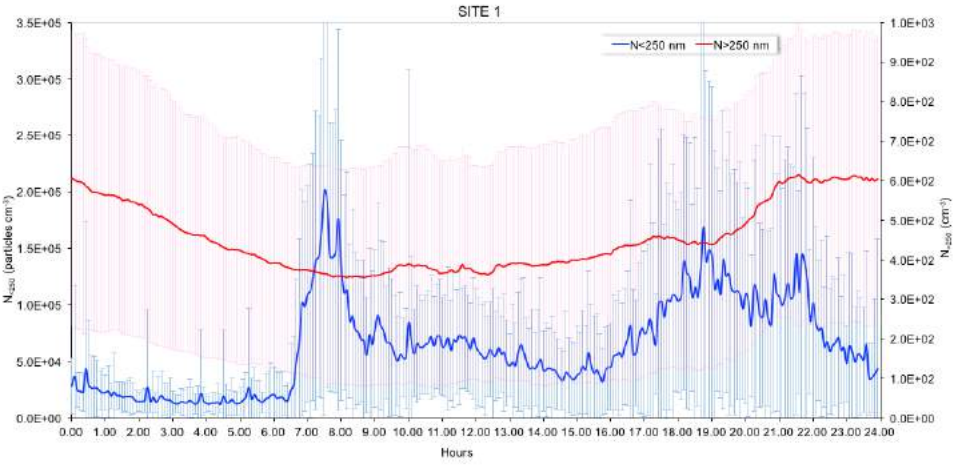

Figure 4.13 . Comparison between the trend of the concentrations of particles and with a diameter between 250 and 1000 nm(250<N<1000) and larger than 250 nm (N>250) at Site

The most important activity at site 2 (Terminal 1) is due to the movement of aircraft during the phases of taxing and the vehicles. Airport activity shows a first peak at 7:30 am, followed by one at 11:30 am and the last one at 8 pm. As for Site 1, a corresponding increase in the concentrations of the ultrafine particles (N <250) was measured (Figure 4.14). The concentrations of N <250 increased by 3.4 ± 2.0 times considering the 6: 00-7: 30 am LST ($7.1*10^4 \pm 2.6*10^4$ particles cm^{-3}) compared to the period from 0: 00-6: 00 LST ($2.1*10^4 \pm 9.7*10^3$ cm^{-3}). After 7:30 am, the concentrations of N <250 remained high and in line with the airport activity.

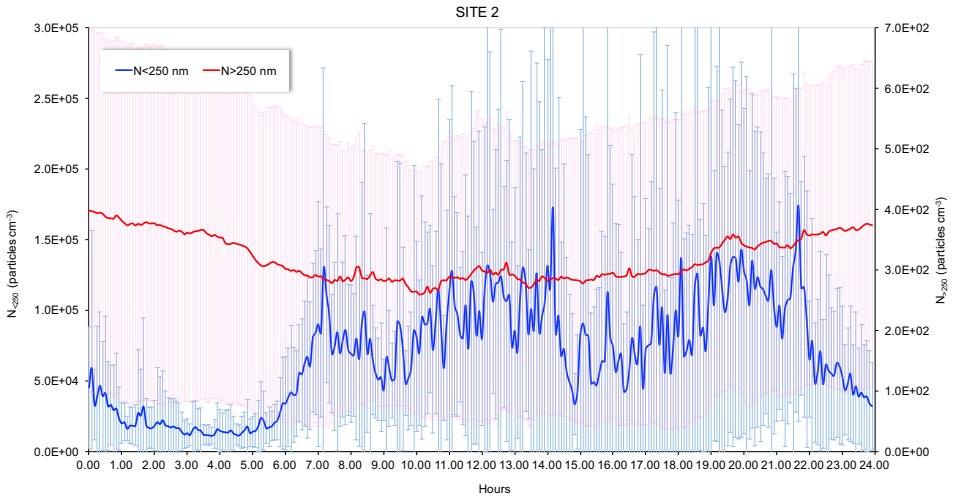

Figure 4.14 Comparison between the trend of the concentrations of particles and with a diameter between 250 and 1000 nm(250<N<1000) and larger than 250 nm (N>250) at Site 2

This correspondence between airport activity and the numerical concentration of the finest fraction of atmospheric particulate matter (both for Site 1 and Site 2) shows the local effect of airport emissions. However, it is necessary to consider that the ultrafine fraction is characterized by: 1) low residence time in the atmosphere due to rapid diffusion and coagulation with pre-existing particles in the atmosphere and 2) a negligible contribution to the mass of atmospheric particulate matter[2,135].

This behaviour results in a negligible contribution of airport emissions to PM10 and PM2.5 mass concentration in the atmosphere. In fact, the observed increase of the ultrafine particles did not correspond to the trend of the numerical concentrations of the particles in the accumulation mode and in the coarse fraction (N> 250) which showed a trend mostly modulated by the atmospheric thermodynamic conditions. Moreover, the typical increase in concentrations observed for the ultrafine fraction directly emitted by airport activities was not observed for the bigger particles. Fig.4.15 ad 4.16 shows the trend of PM10 concentration the estimated by OPC which exhibits a trend influenced predominantly by atmospheric mixing and not by in situ aerodynamic emissions.

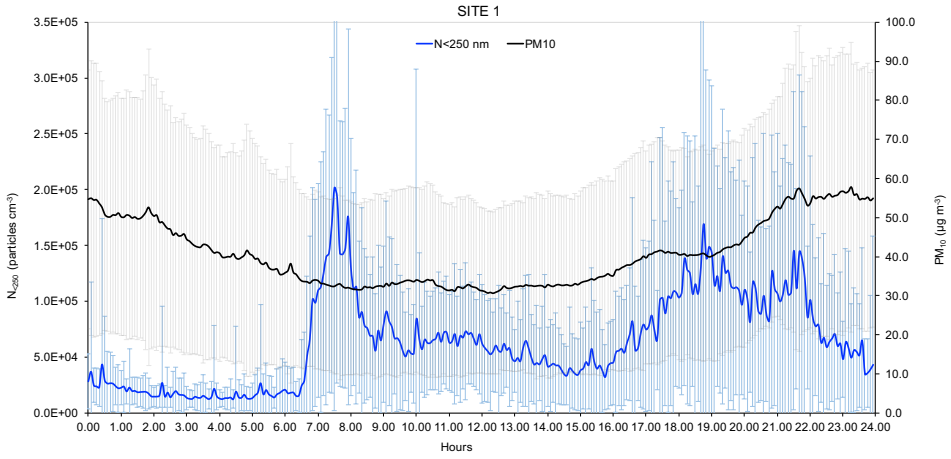

Figure 4.15 Comparison between the trend of the concentrations of particles smaller than 250 (N<250) and PM10 (measured by OPC) at Site1

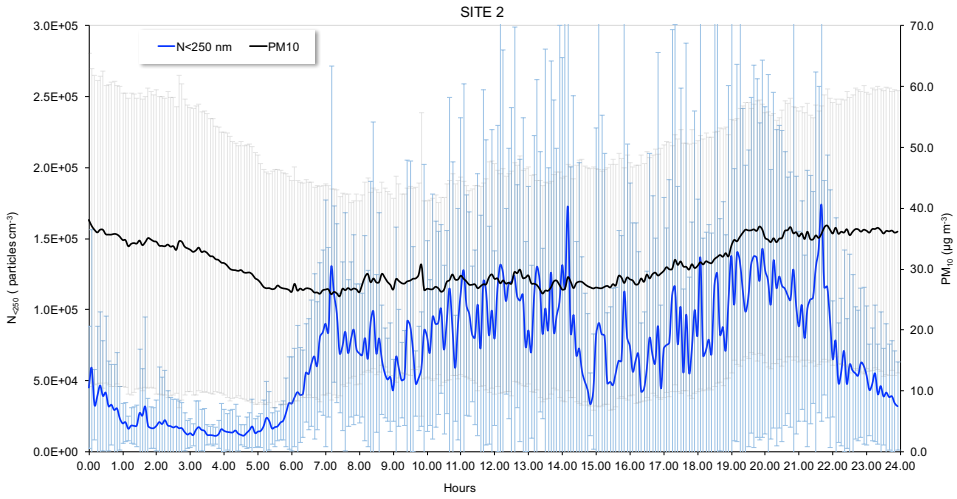

Figure 4.16 Comparison between the trend of the concentrations of particles smaller than 250 (N<250) and PM10 (measured by OPC) at Site2

The typical daily trend of PM1 and PM2.5 are in accordance with that of PM10, as shown in Fig. 4.17 and 4.18, characterized by low variability within 24 hours, with slightly higher concentrations at night.

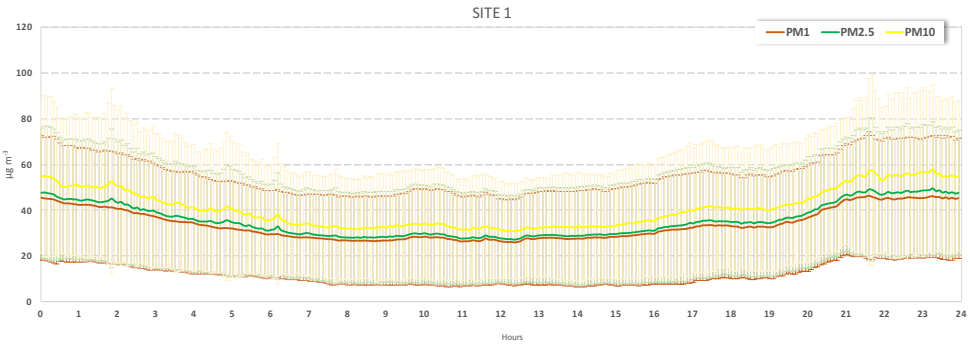

Figure 4.17 Typical daily trend (24h) of the concentrations of PM1, PM2.5 and PM10 at Site1

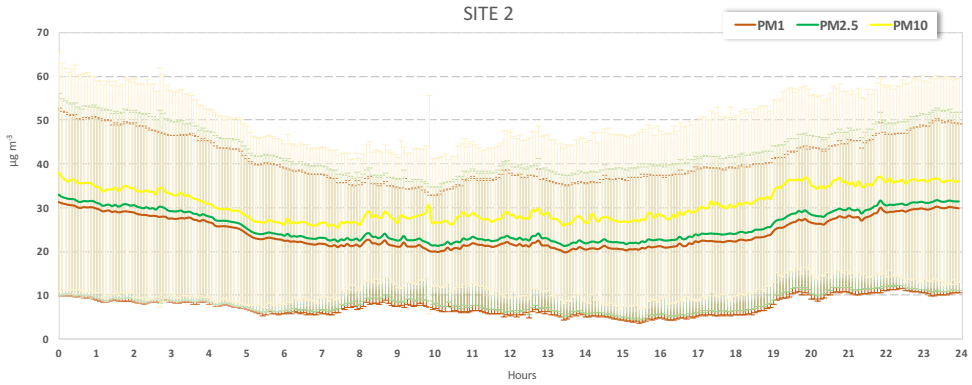

Figure 4.18 Typical daily trend (24h) of the concentrations of PM1, PM2.5 and PM10 at Site2

4.2 BLACK CARBON

The concentrations of Black Carbon (BC) were measured by means of an aethalomether. The BC trend observed inside the Airport of Malpensa were compared with that measures from at the ARPA stations and is presented in Fig 4.19 for Site 1 and Fig. 4.20 for site 2. The average concentrations at Site 1 were 2.92±2.01 µg m^{-3}, lower than those measured by ARPA equal to 5.51±3.31 µg m^{-3}. During the second campaign, carried on at Site 2, the concentrations inside the airport were 3.07±1.99 µg m^{-3} while outside the airport (ARPA stations) were 4.81±3.10 µg m^{-3}

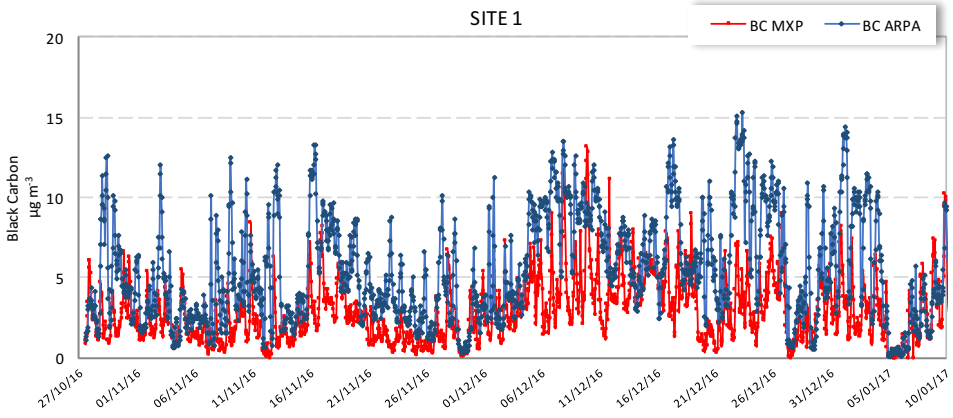

Figure 4.19 Comparison between BC trend at Site 1 and the measurement from ARPA stations

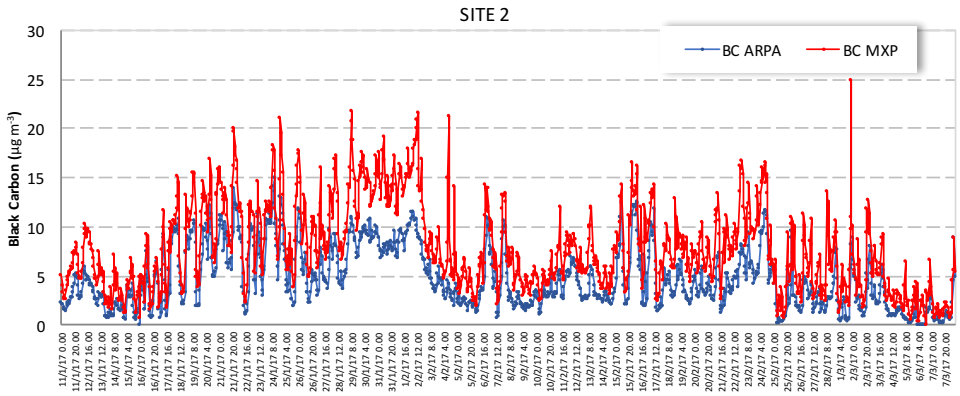

Figure 4.20 Comparison between BC trend at Site 2 and the measurement from ARPA stations

A study of the sources of BC was conducted in order to discriminate the contribution of fossil fuels combustion (eBC_ff) and of the biomass burning (eBC_bb; not present as a source within the airport) to the total concentrations of BC, using the method developed by Sandradewi[121]. eBC_ff trend between the runways (Fig. 4.21) appears to be related to the airport operations (landing and take- off) and to the trend of the finest fraction of atmospheric particulate matter (N <250; Fig.4.13), with an increase in the concentration from 6 am and a maximum around 8 pm (2.6 µg m^{-3}), while eBC_BB has the same pattern of PM10 (Fig. 4.15). Therefore, a localized source outside the airport shows, inside the airport, a trend influenced mainly by the atmospheric mixing just like the concentration of PM10, which appears to be more influenced by large-scale processes.

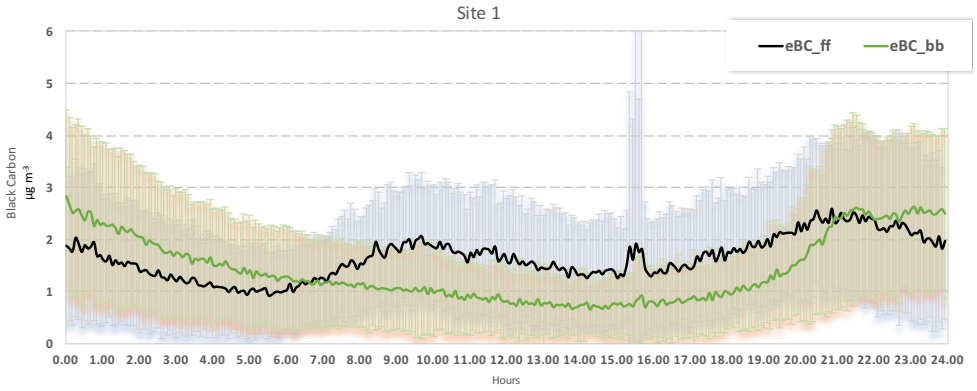

Figure 4.21 Average daily trend of eBC from fossil fuels (eBC_ff) and from biomass burning (eBC_bb) at Site 1

The combination of airport emissions and PM intrusion from external sources was investigated at Site 2 as well. In Fig. 4.22, the average daily trend of the eBC concentrations is reported in relation to its sources: combustion from fossil fuels (eBC_ff) and combustion of biomass (eBC_bb). Exactly like at Site 1, the eBC_ff trend is correlated to the airport operations and to the trend of the finest fraction of atmospheric particulate matter (N <250; Fig. 4.14). The eBC_bb, on the other hand, shows the same pattern of PM10 (Fig. 4.16), indicating that a source located outside the airport has, inside the airport, a trend that is influenced principally by atmospheric mixing.

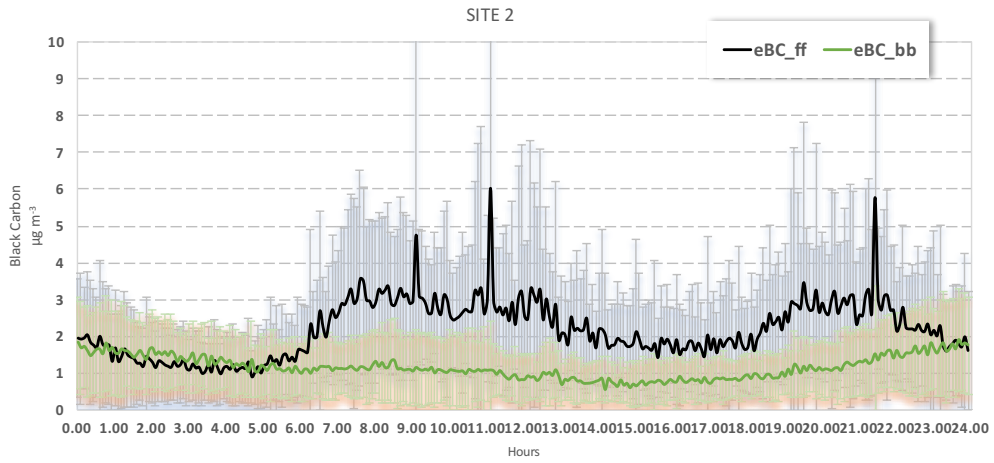

Figure 4.22 Average daily trend of eBC from fossil fuels (eBC_ff) and from biomass burning (eBC_bb) at Site 1

4.3 PAHs

PAHs Concentrations. The concentrations of 18 PAHs (from Naphtalene to Benzo(ghi)Perylene) present in the particulate matter were measured. Daily concentrations of PAHs in the PM10 fraction were analysed only for two weeks for each site while for PM2.5 weekly PAHs concentrations were determined for the entire sampling period. The average weekly PAHs concentrations in PM2.5 are reported in Fig.4.23

PAHs showed similar concentrations at the two sampling sites: the average values were 16.46 ±7.63 ng m^{-3} at Site 1 and 17.46 ± 9.09 ng m^{-3} at Site 2.

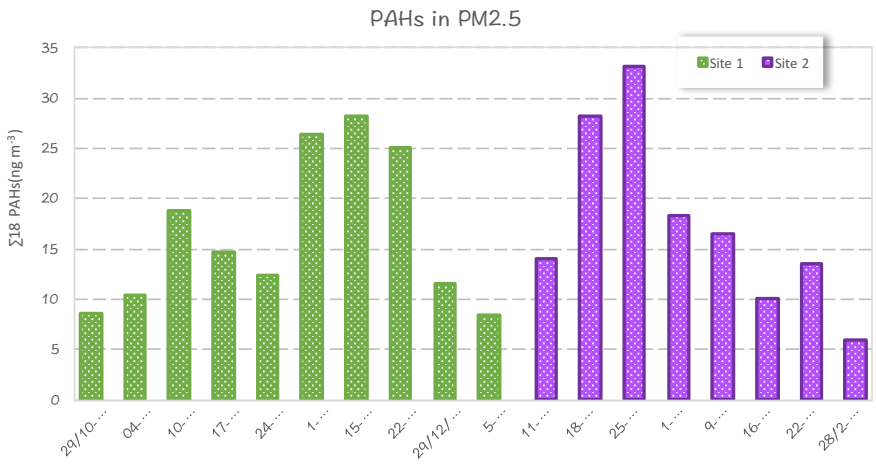

Figure 4.23 Weekly average PAHs concentrations (∑18 PAHS, ng m-3) in PM2.5 at Site 1 and Site 2

As for PM10, a significant decrease in PAHs concentrations was found in site 2. The average concentrations were 32.93 ± 15.77 ng m^{-3} at Site 1 and 13.21 ± 6.59 ng m^{-3} at Site 2. Observing the PAHs trend, it is possible to notice very low concentrations at Site 2 during the whole sampling period (Fig.4.24).

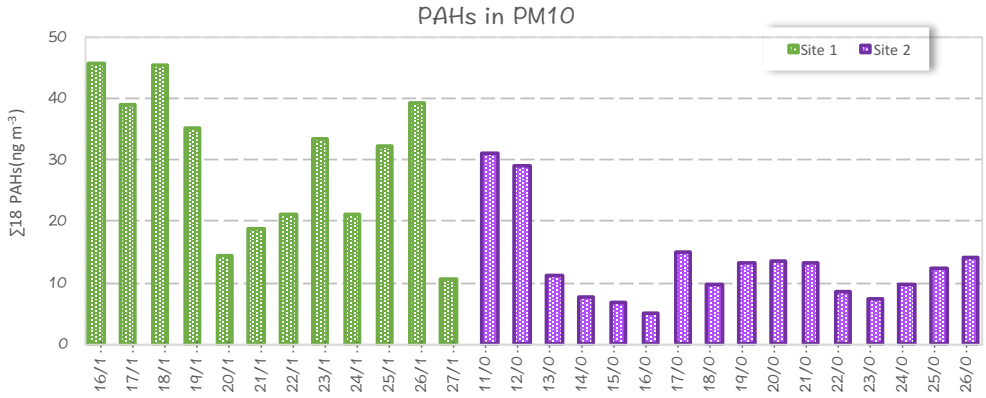

Figure 4.24 Weekly average PAHs concentrations (∑18 PAHS, ng m-3) in PM10 at Site 1 and Site 2

PAHs Distribution Pattern. The PAH distribution pattern was calculated as the ratio of the concentration of a single PAH to the concentration of the total PAHs (∑18 PAHs). As for PM2.5 the distribution pattern was the same for both sites (Fig. 4.25): the most abundant compounds were benzo(b)fluoranthene (24-23%) and benzo(a)pyrene (13-11%).

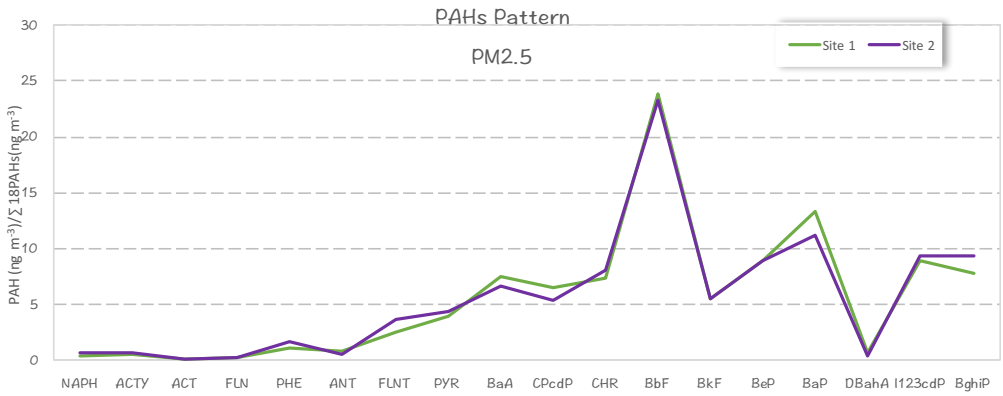

Figure 4.25 PAHs distribution pattern in PM2.5

In the PM10 samples, with reference to the 4-week sampling period, the predominant PAHs were the same as in PM2.5 (Fig.4.26): benzo(b)fluorantene (21-17%) and benzo (a) pyrene (12-10%) followed by chrisene, benzo(e)pyrene and benzo(ghi)perylene.

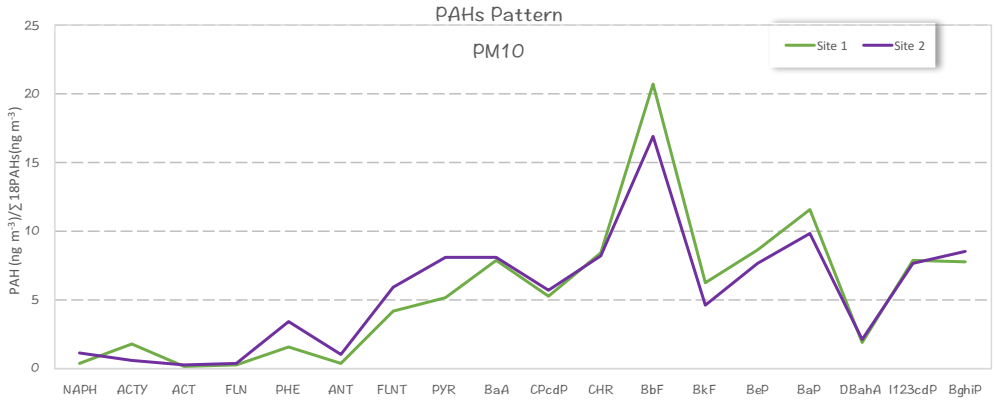

Figure 4.26 PAHs distribution pattern in PM10

***Figure 4.26**. PAHs distribution pattern in PM10*

Despite the small oscillations, the two sites were characterized by the same distribution pattern for both the PM fractions. Consequently, it can be declared that the detected PAHs probably came from the same type of emission source.

PAHs and BC. Since some compounds are not only emitted from aircrafts, the PAHs concentrations were compared to the trend of BC emitted from traffic and biomass burning.

The results showed a strong correlation (R^2= 0.75) between the concentrations of the 18 PAHs and the black carbon emitted by biomass combustion (Fig. 4.27). The linear function that relates the two compounds is clearly visible in Fig. 4.28.

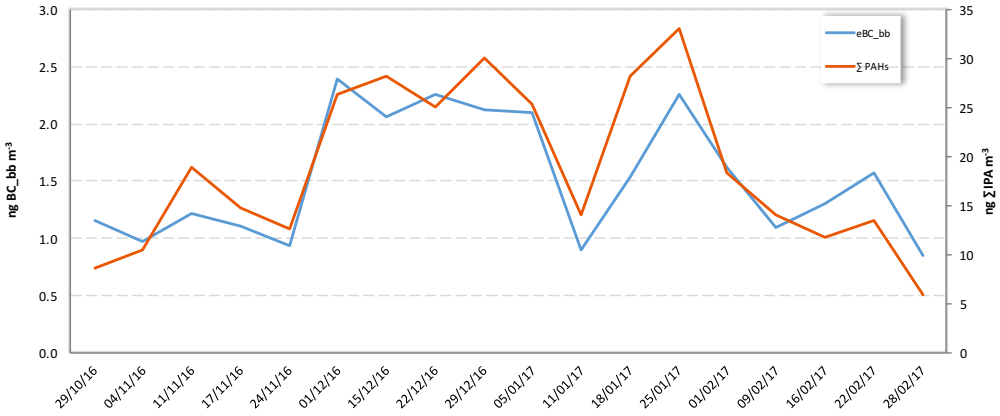

Figure 4.27 Concentration of BC from biomass burning (µg m-3) and of ∑18 PAHs in PM2.5 (ng m-3)

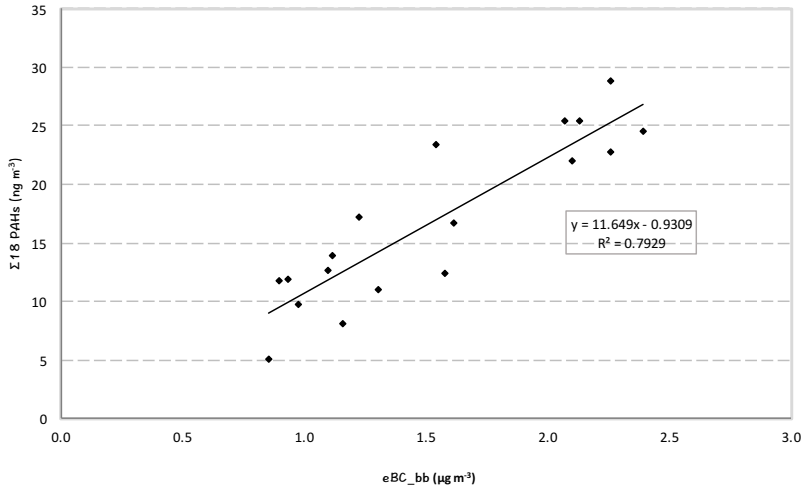

Figure 4.28 BC from biomass burning (µg m-3) vs of ∑18 PAHs in PM2.5 (ng m-3)

In contrast, no clear associations between the fraction of black carbon emitted from fossil fuels and PAHs concentrations were found. (Fig 4.29 and Fig.4.30). Therefore, the contribution of fossil fuels is not to be considered as one of the main sources of PAHs within the airport of Malpensa.

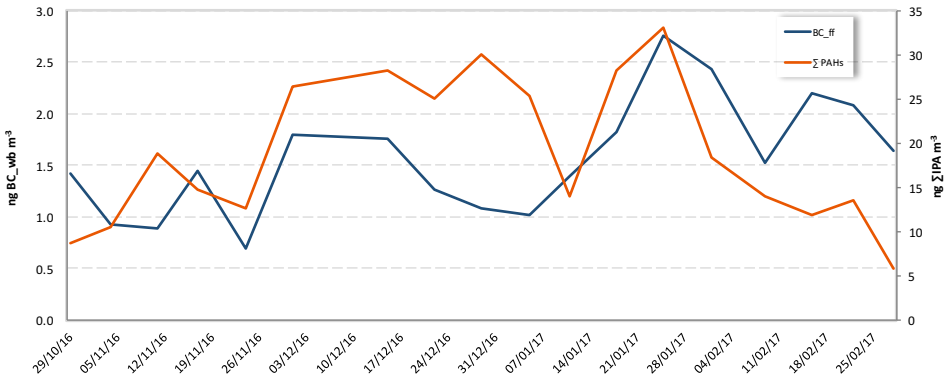

Figure 4.29 Concentration of BC from fossil fuels (µg m-3) and of ∑18 PAHs in PM2.5 (ng m-3)

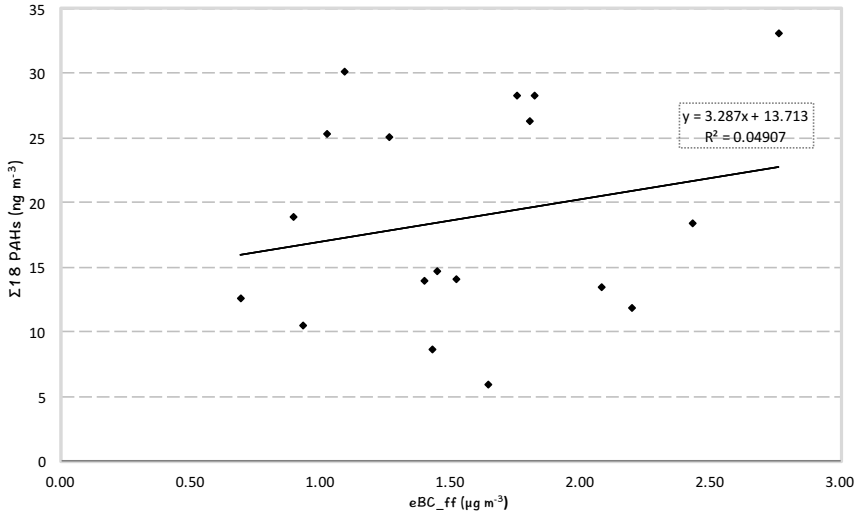

Figure 4.30 BC from fossil fuels (µg m-3) vs of ∑18 PAHs in PM2.5 (ng m-3)

Benzo(a)Pyrene. A focus on benzo(a)pyrene, which has been classified as carcinogenic for humans, is presented here.

As can be seen from Fig. 4.31, high concentrations of the compound were detected during the overall sampling period, with values above the limit (1 ng m^{-3}) imposed by the legislation. Average B(a)P values in PM2.5 of 2.15 ± 0.85 ng m^{-3} at Site 1 and 1.93 ± 0.93 ng m^{-3} at Site 2 were measures. However, since the legal limit is calculated on an

annual basis, the relevance of the data is not quantifiable since this study only refers to the autumn-winter period, which presents the most critical climatic weather conditions for PAHs emissions.

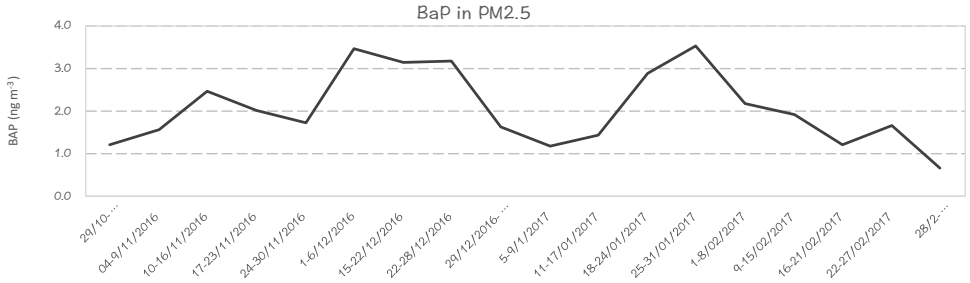

Figure 4.31 BaP concentrations (ng m-3) in PM2.5

Consistently with the trend observed for the sum of all PAHs, the differences between the two sites for B(a)P were emphasized in the PM10 fraction. The concentrations of B(a)P in PM10 were 3.53 ± 1.35 ng m^{-3} at Site 1 and 1.29 ± 0.62 ng m^{-3} at Site 2.

4.4 GASEOUS POLLUTANTS: NO_X AND O_3

4.4.1 NO, NO_2 AND NO_X

The trend of the concentrations of NO, NO_2 and NO_X (sum of NO and NO_2) found at Site 1 and Site 2 (high- temporal resolution measurements) are reported in Fig. 4.32 and 4.33.

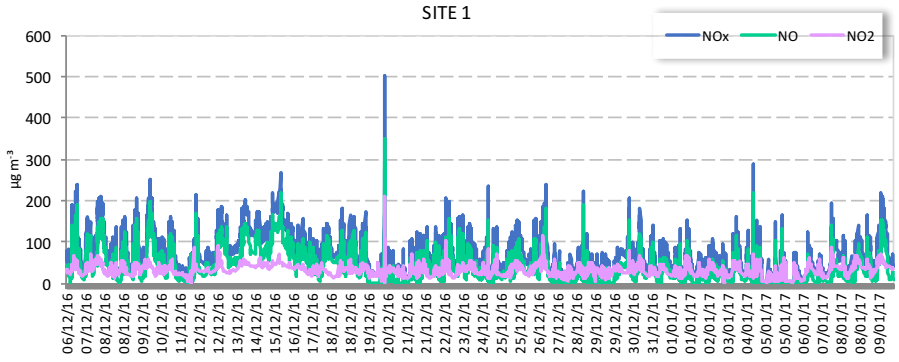

Figure 4.32 NO, NO2 and NOX concentrations (high temporal resolution-5 minutes) in Malpensa at Site 1

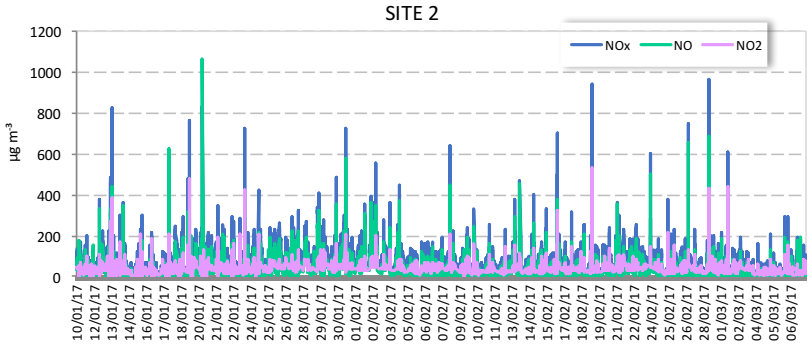

Figure 4.33 NO, NO2 and NOX concentrations (high temporal resolution-5 minutes) in Malpensa at Site 2

From the graphs, it is possible to see peaks of concentrations that are probably produced by the aircraft during the take-off phase.

Despite the peaks, the average concentrations of NO_2 (Fig. 4.34 and 4.35) were always lower than the annual limit imposed by the legislation (200 µg m^{-3} not to be exceeded more than 18 times over a year) and lower than the values measured from in the adjacent towns (ARPA stations).

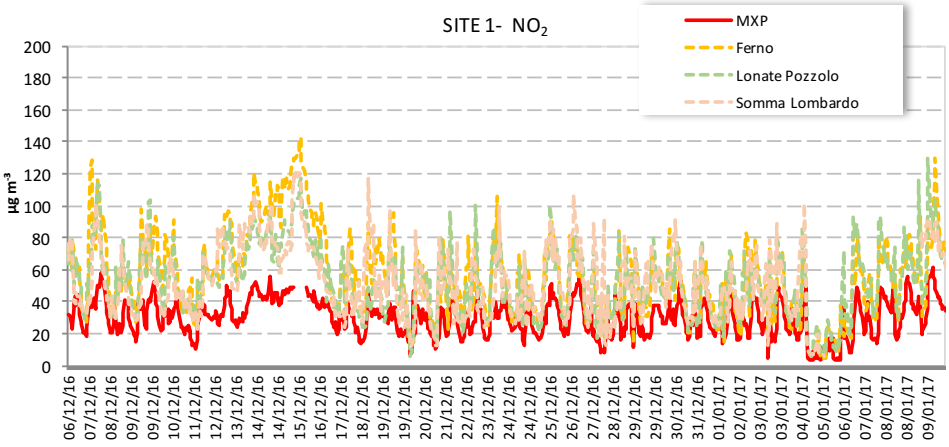

Figure 4.34 Hourly NO2 concentrations inside the airport at Site 1 (MXP) compared with those measured by the ARPA stations (Ferno, Lonate Pozzolo and Somma Lombardo)

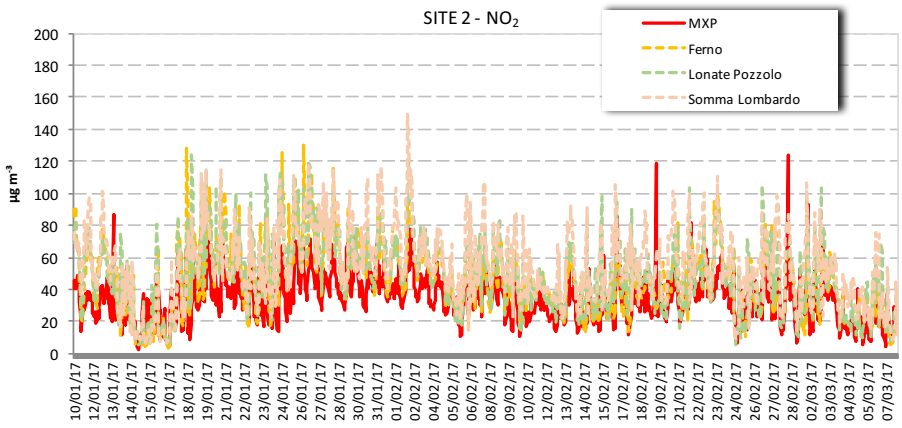

Figure 4.35 Hourly NO2 concentrations inside the airport at Site 2 (MXP) compared with those measured by the ARPA stations (Ferno, Lonate Pozzolo and Somma Lombardo)

The average daily concentrations of NO_X, NO, NO_2 in Malpensa are represented in Fig 4.36. NO_X ranged from a minimum of 10.5 µg m^{-3} to a maximum of 130.4 µg m^{-3} (NO: 2.3-86.6 µg m^{-3}; NO_2: 8.2-43.8 µg m^{-3}) at Site 1 and from 25.6 to 140.0 µg m^{-3} (NO: 7.2-91.6 µg m^{-3}; NO_2: 17.0-49.2 µg m^{-3}) at Site 2. Through the comparison with ARPA monitoring station (Fig. 4.37) it is possible to see that the NO_X concentrations inside the airport were lower than those measured in the adjacent area for the overall sampling period.

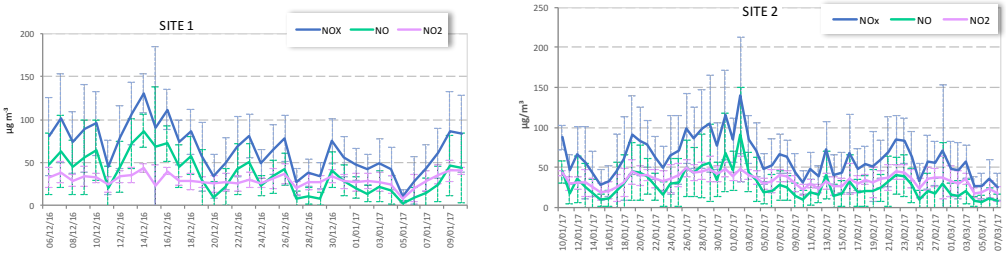

Figure 4.36 Daily NO_X, NO and NO_2 concentrations inside the airport at Site 1 and Site 2

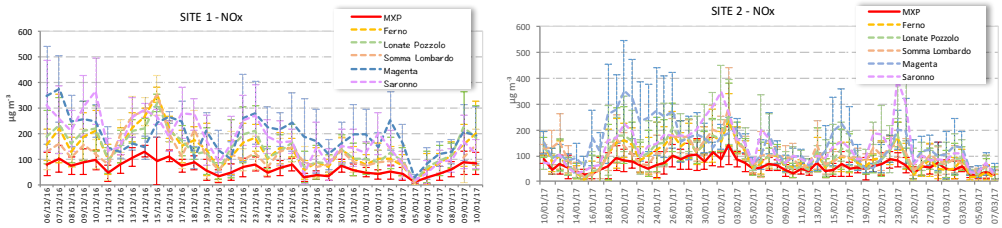

Figure 4.37 Daily NO_X concentrations inside the airport at Site 1 and Site 2 (MXP) compared with those measured by the ARPA stations (Ferno, Lonate Pozzolo and Somma Lombardo)

The time slots with the highest concentrations of pollutants were recorded in the morning from 8 to 11 am and in the evening from 8 to 11 pm, when the air traffic is intense (Fig. 4.38). The typical daily trend for NO_X is similar between the airport and the neighbouring sites, even though in the latter, the highest concentrations (especially for NO) were recorded from 8 am to 1 pm and from 5 to 8 pm which correspond to the rush hours of car traffic on the roads (Fig. 4.39).

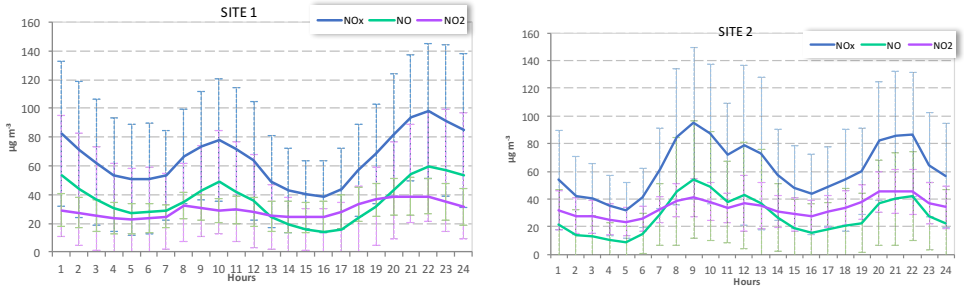

Figure 4.38 Typical trend of NOX, NO and NO2 concentrations during 24 hours inside the airport at Site 1 and Site 2

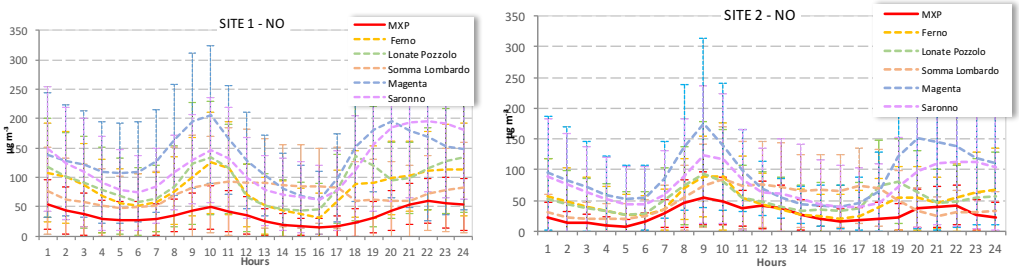

Figure 4.39 Typical trend of NO concentrations inside the airport at Site 1 and Site 2 (MXP) compared with those measured by the ARPA stations (Ferno, Lonate Pozzolo Somma Lombardo, Magenta and Saronno)

The comparison between the average concentrations found at Site 1 and Site 2 and those detected by the ARPA monitoring stations in the same period are presented in Fig.4.40.

The airport of Milano-Malpensa showed on average lower concentrations for NO_X, NO and NO_2 than the other sites. The average reduction inside Malpensa at Site 1 were: -52.4±78.35% (NO_X), -55.9±102.85% (NO), -47.5±53.78% (NO_2) compared to Ferno; -53.8± 80.46% (NO_X), -60±107.83% (NO), -42.94±50.18% (NO_2) compared to Lonate

Pozzolo and -50.1± 81.33% (NO_X), -54.84±108.94% (NO), -42.9±51.15 (NO_2) compared to Somma Lombardo.

The average reduction at Site 2 were: - 35.8±88.92% (NO_X), -43.2±134.89% (NO), -27.3±55.97(NO_2) compared to Ferno; -37.8±93.55% (NO_X), -45±141.68% (NO), -29.7±56.44% (NO_2) compared to Lonate Pozzolo and -39.4±87.28 (NO_X), -41.9±137.18% (NO), - 36.8±53.07 (NO_2) compared to Somma Lombardo.

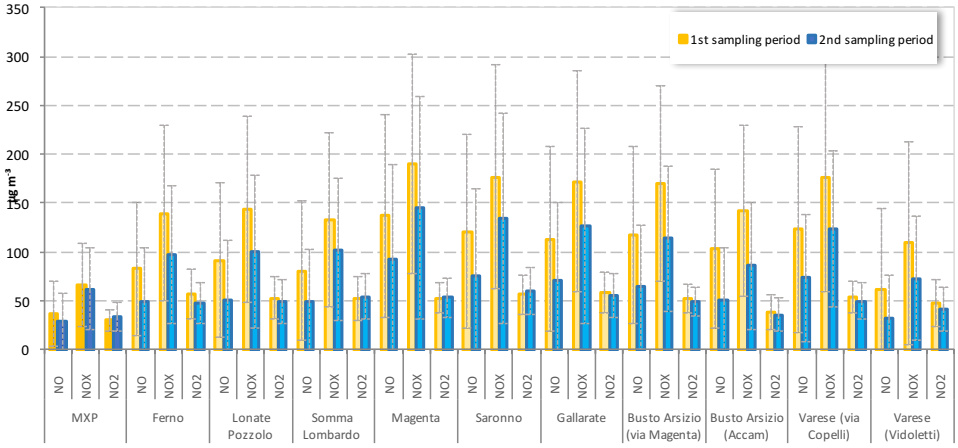

Figure 4.40 Average NOX, NO and NO2, concentrations (and standard deviations) inside the airport at Site 1 and Site 2 (MXP) compared with those measured by the ARPA stations

These data indicate that near the ARPA monitoring stations there are more intense and continuous emissions (e.g. traffic and heating systems) than those recorded inside the airport of Malpensa, thus contributing to generate higher NO_x emissions.

As for the atmospheric particulate matter, higher concentrations were found not only at sites that are potentially affected by the emissions from airport but also the "blank" sites (considered not affected by airport activities) showed higher values, meaning that impact of the airport emissions is not significant.

Finally, the difference in the concentrations of NO, NO_2 and NO_2 measured on Site 1 and Site 2 (higher on Site 1) is related to a generalized phenomenon, as the highest NO_x concentrations were measured at every station during the first period of sampling (December- January).

4.4.2 O_3

Ozone is a secondary pollutant and its behaviour is linked to the photochemical reactivity of its precursor (NO_X and VOC) in the atmosphere.

The average hourly concentrations of O_3 measured at Malpensa-airport and at the neighbouring towns (ARPA stations) are represented in Fig. 4.41 and 4.42.

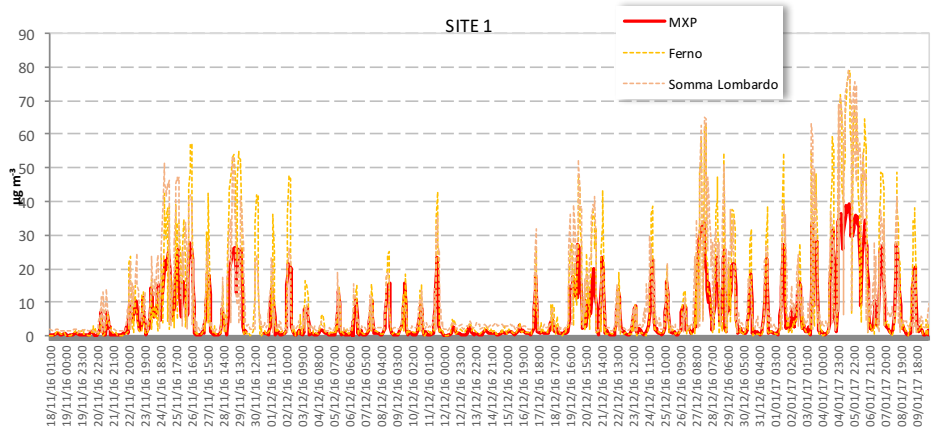

Figure 4.41 Average O_3, concentrations (and standard deviations) inside the airport at Site 1 and Site 2 (MXP) compared with those measured by the ARPA stations

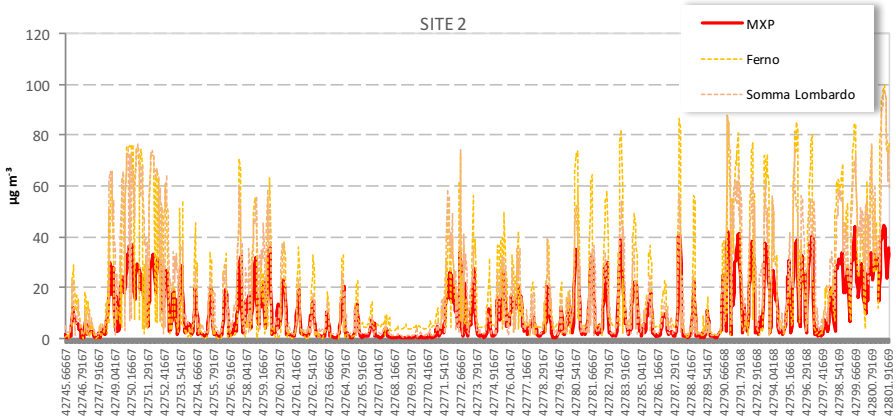

Figure 4.42 O3 concentrations (high temporal resolution-5 minutes) in Malpensa at Site 2

The O_3 concentrations were always lower at Malpensa than at the adjacent sites and they were lower than the values imposed by the legislations (hourly basis) of 180 µg m^{-3} (information threshold) and 240 µg m^{-3} (alert threshold).

Daily average concentration of 6.19±6.32 µg m^{-3} and 10.5±7.9 µg m^{-3} were recorded at Site 1 and site 2 respectively. The trend is reported in Fig.4.43 and 4.44 where the concentrations inside the airport are compared with the values from ARPA stations. It is possible to note that at Malpensa the concentrations were lower than the other sites during the overall sampling period.

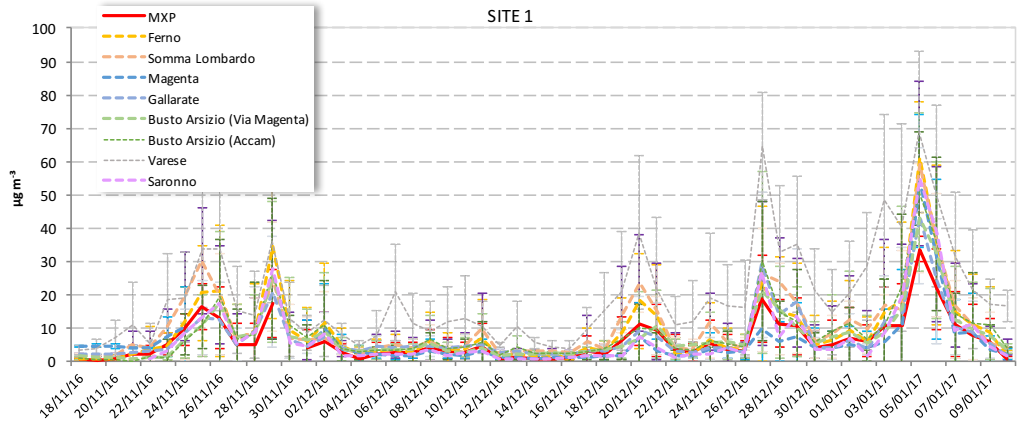

Figure 4.43 Daily O3 concentrations inside the airport at Site 1 (MXP) compared with those measured by the ARPA stations

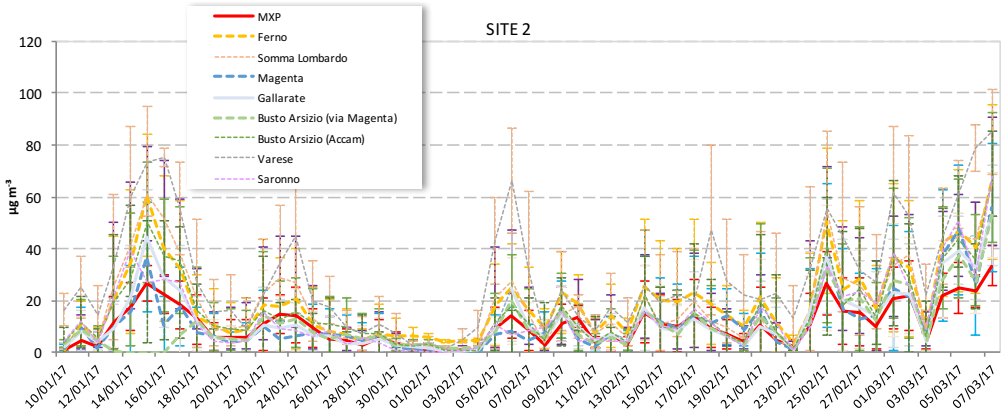

Figure 4.44 Daily O3 concentrations inside the airport at Site 2 (MXP) compared with those measured by the ARPA stations

The typical daily trend of O_3 was similar at both sites inside the airport with a maximum in the concentrations from 2 to 4 pm and a minimum during night time. O_3 trend seems unrelated to airport activities (Fig. 4.45)

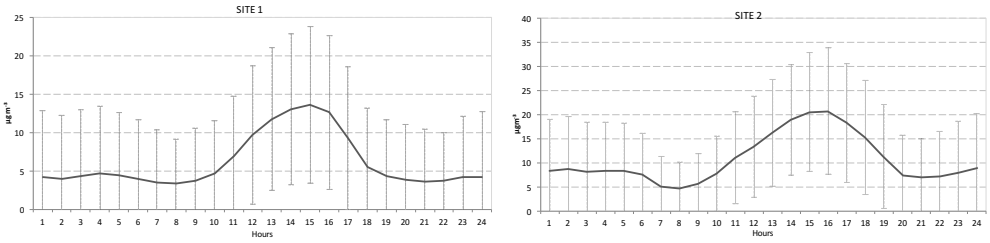

Figure 4.45 Typical trend of NO3, concentrations during 24 hours inside the airport at Site 1 and Site 2

The trend is similar at all the considered sites and is linked to the photochemical reactions that involve O_3 and it precursors. The concentrations at Malpensa were lower than those monitored by the ARPA station, with the sole exception of Magenta (Fig. 4.46 and 4.47).

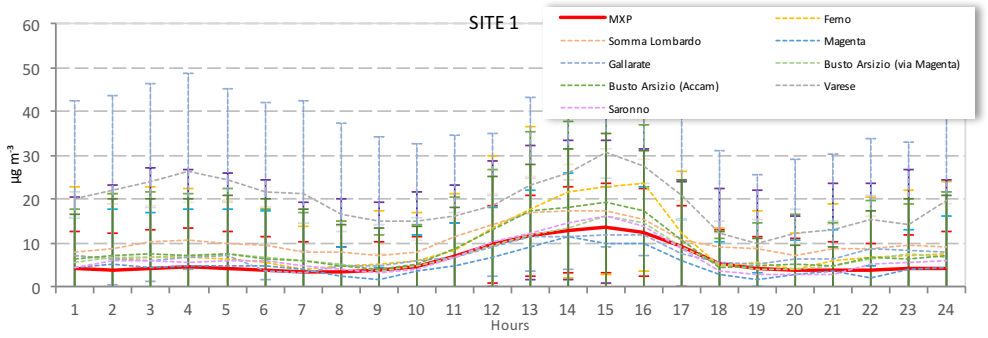

Figure 4.46 Typical trend of NO concentrations inside the airport at Site 1 (MXP) compared with those measured by the ARPA stations

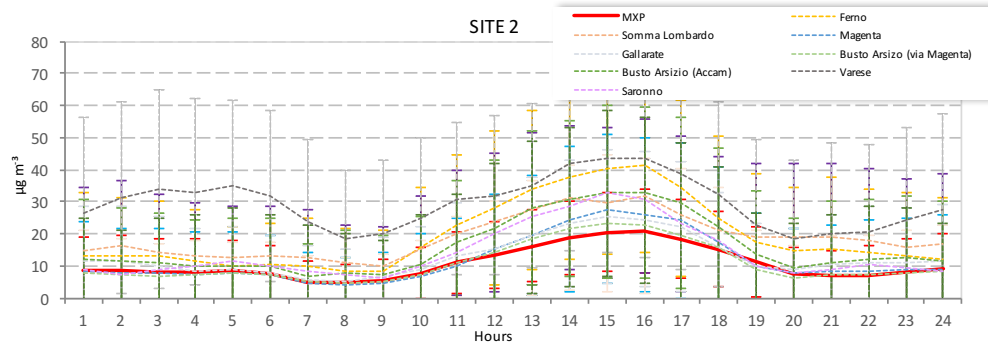

Figure 4.47 Typical trend of NO concentrations inside the airport at Site 2 (MXP) compared with those measured by the ARPA stations

The comparison between the average concentrations found at Site 1 and Site 2 and those detected by the ARPA monitoring stations in the same period are presented in Fig.4.48.

Just like NO_x the airport of Milano-Malpensa showed on average lower concentrations for O_3, than the other sites. The average O_3 concentration at Site 1 was 6.2 ± 8.7 µg m^{-3}, lower than that obtained by ARPA monitoring stations: 9.3 ± 15.6 µg m^{-3}, 10.6 ± 14.6 µg m^{-3}7.5 ± 14.2 µg m^{-3}, at Ferno, Somma Lombardo and Saronno respectively; the sole exception is represented by the city of Magenta where the average concentrations were 5.8 ± 11.3 µg m^{-3}.

With respect to Site 2, the mean concentration was 10.7 ± 11.1 µg m^{-3}, lower than that measured at Ferno, Somma Lombardo, Magenta and Saronno: 19.4 ± 23.0 µg m^{-3}, 18.8 ± 21.0 µg m^{-3}, 14.1 ± 20.4 µg $m^{-3}$and 11.9 ± 18.0 µg m^{-3}respectively.

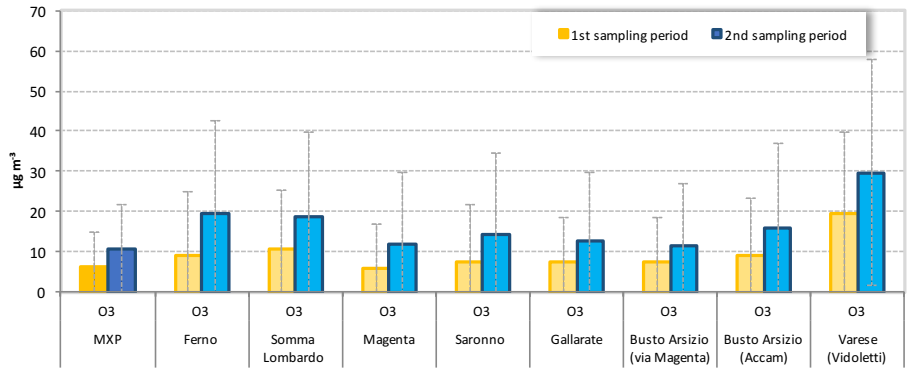

Figure 4.48 Average O3, concentrations (and standard deviations) inside the airport at Site 1 and Site 2 (MXP) compared with those measured by the ARPA stations

Again, the difference in the concentrations of O_3 measured on Site 1 and Site 2 (higher at Site 2) is related to a generalized phenomenon, as the highest O_3 concentrations were measured at every station during the second period of sampling (January-March).

During this months, in fact, the global incident radiation was 50% higher than the first period, favouring a shift of the photo-stationary equilibrium towards the production of NO_2 and therefore of O_3. As confirmed in the previous observation, Figure 4.49 shows the average value of the NO/NO_2 ratio measured inside and outside the airport sediment during both the sampling periods. It is possible to note that, in the second sampling period, the relative abundance of NO_2 was greater compared to the first period, thus promoting a higher O_3 formation.

The above data shows that, regarding ozone atmospheric pollution, there are no significant effects directly or indirectly linked to airport activities.

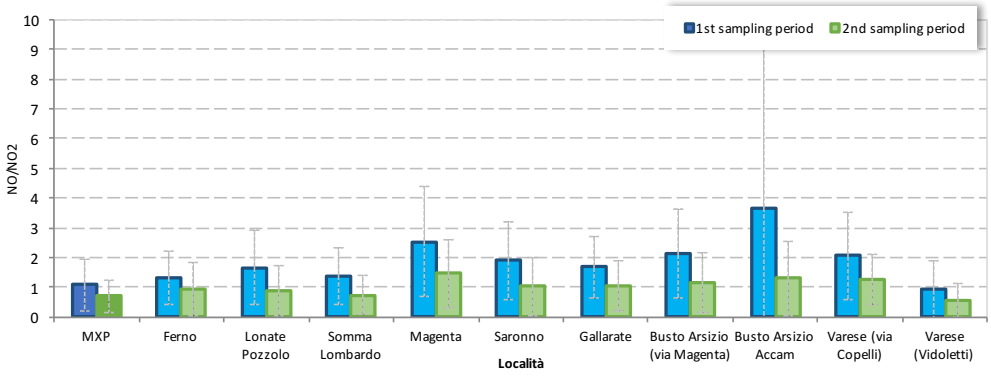

Figure 4.49 Average NO/NO2, ratio (and standard deviations) inside the airport at Site 1 and Site 2 (MXP) and outside.

4.5 VOC

The concentrations of different VOCs resulted to be quite variable. Fig.4.50 shows daily average concentrations of the investigated compounds at Site 1 and at Site 2.

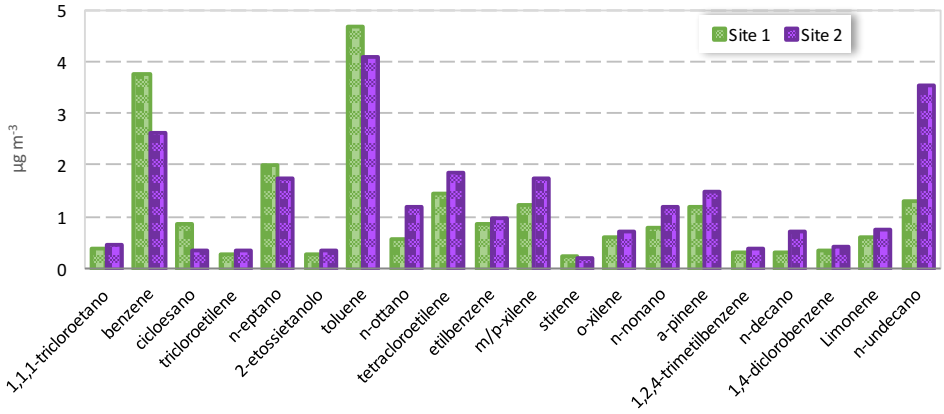

Figure 4.50 Average VOC concentrations inside the airport at Site 1 and Site 2

In general, no substantial differences between the two sites were found. An overview on the concentrations of BTEX is presented below.

Toluene was the predominant compound at both sites with slightly higher concentrations between the runways (4.7 ± 2.2 µg m^{-3}) than at Terminal 1 (4.1 ± 1.6 µg m^{-3}). An analogous result was found in a study by Beyersdorf et al.[136] that confirm that the formation of aromatic compounds (e.g., toluene) can occur at the higher power

settings (higher temperatures), while in the taxiing phases when the engines operate at low fuel efficiency, an increase in the concentrations of alkenes and alkynes can be seen.

Another important compound is Benzene which was, after toluene, the most abundant compound. The average concentrations of benzene were 3.6 ± 2.2 μg m^{-3} at Site 1 higher than those measure by the ARPA station located in Somma Lombardo where the average value was 2.9 ± 1.1 μg m^{-3}.

During the second sampling period, the concentrations found inside and outside the airport were almost identical (2.7 ± 1.1 μg m^{-3} at Site 2 and 2.7 ± 1.0 μg m^{-3} at Somma Lombardo).

Since the sampling campaign was carried out during the winter (the worst-case due to scarce atmospheric dispersion)[137], the observed values didn't show level of criticality given that they remained lower than the annual limit of 5 μg m^{-3}.

The comparison between the values measured inside the airport and by the ARPA stations was done also for Toluene, Xylene (orto, meta e para) e Etilbenzene. The concentrations of m-p-Xylene (Site 1:1.2±0.4 μg m^{-3}; Site 2 1.7±0.6 μg m^{-3}), o-Xylene (Site 1: 0.6±0.1 μg m^{-3}; Site 2: 0.7±0.3 μg m^{-3}) and Etilbenzene (Site 1: 0.9±0.3 μg m^{-3}; Site 2: 1.0±0.3 μg m^{-3}) are in agreement with the historical values measured by ARPA during a campaign carried on in 2011-2012[138].

VOCs are important compounds for the formation of O_3 as they are among the major competitors in the oxidation of NO to give NO_2. Therefore, high concentrations of VOCs lead to high NO_2 concentration without tropospheric ozone consumption. As shown in Fig. during the second sampling campaign, O_3 concentrations were higher than during the first period, while the ratio NO/NO_2 decreased (Fig.4.49). The increase in NO_2 concentrations during the second period is related to an increase in VOCs emissions. Inside the airport of Malpensa, concentrations of VOCs of 22.1 ± 14.8 μg m^{-3} for Site 1 and 25.1 ± 15.3 μg m^{-3} for site 2 were detected. The main contribution to NO oxidation is not attributable to BTEX (Site 1: 10,3 ± 5,3 μg m^{-3}; Site 2: 9,1 ± 3,8 μg m^{-3}) but to the other VOCs, such as alkanes or alkenes (Site 1: 11.8 ± 9.5 μg m^{-3}; Site 2: 16.0 ± 11.5 μg m^{-3}).

Fig. 4.51 shows that while BTEX have a greater presence at Site 1 since they are emitted by airplanes principally, the other VOCS are more abundant at Site 2 as they represent the background pollution of the surrounding areas.

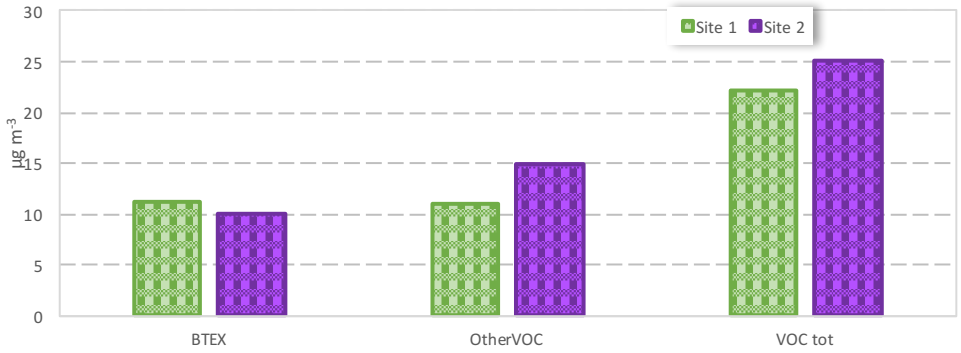

Figure 4.51 Average concentrations of VOC inside the airport at Site 1 and Site 2. The contribution of BTEX and of the other VOC is highlighted.

4.6 CONCLUSIONS

In the present chapter, the measurements on the concentrations of pollutants inside the airport were presented. The monitoring, carried on over a four-month period on two different sites within the airport, allowed to define concentrations of PM, BC, PAHs, NO_X, O_3 and VOC.

The analysis allowed to observe that the airport activity could influence the numerical concentrations of the ultrafine fraction of the particulate matter (N<250 nm) and the concentrations of Black Carbon. On the contrary, the trend of the larger particles in the accumulation mode and the coarse fraction of PM were not related to the airport activities but were mostly influenced by the atmospheric mixing and large-scale phenomena. The concentrations of atmospheric particulate matter resulted to be mainly modulated by conditions (humidity, wind direction and wind speed, temperature and precipitation) with significant local variations.

High PAHs atmospheric concentrations were measured inside the airport, but the concentration observed inside the airport were of a similar order of magnitude to those reported for the urban area of Milan [9]. The homogeneity of the distribution patterns in the two different country sites indicates that the analysed PAHs originate mainly from the same type of source. In particular, there was a strong correlation between the analysed PAHs and the fraction of black carbon due to biomass combustion, a phenomenon related to domestic heating and, consequently, widely seen in the coldest months of the year.

The measurements did not reveal a critical situation with regard to the concentrations of gaseous pollutants such as NO_X and O_3. The results showed that the concentrations were such as not to endanger the environment or to compromise the human health. The concentration of both the pollutants never exceeded the limits imposed by the legislation for health protection. The differences detected between the two sampling periods were related to wider phenomena: during the second sampling period (January to March) the global incident radiation was 50% higher than the first period, favouring the conversion of NO in NO_2 and the subsequent production of O_3. Moreover, the higher presence of Volatile Organic Compounds during the second sampling campaign, led to the formation of NO_2 and therefore O_3. The higher amount of VOCs found at Site 2 were not related to the presence of BTEX, an important group of VOCs principally emitted by vehicle exhaust gases, but to the carbonyl compounds (alkenes and alkanes), which are the precursors for the formation of NO_2 and O_3.

Finally, the comparison between the concentrations observed inside the airport and the measurement obtained from the ARPA stations in the area adjacent to the airport allowed to verify that the concentrations of the various pollutants at Malpensa Airport were lower than those in the surrounding area. Airport emission are, in fact, limited in space and time whereas in the urban centres the emission, even if lower, are continuous during the day, favouring an accumulation of the pollutants.

CHAPTER 5. PARTICULATE MATTER IN THE ARCTIC

The Arctic Region is a very critical area for global climate changes and for transport, deposition and accumulation processes of airborne pollutants. Since the 1980s, there has been increasing evidence that remote and pristine environment of the Arctic has been contaminated by anthropogenic contaminants. As most of these chemicals are not used or emitted in the Arctic region, they must have been transported over great distances from their sources

To study this process, a summer campaigns (20 June – 12 August 2011) were organized on board the oceanographic OCEANIA ship. Oceanographic activity was coupled with the study of the atmospheric Total Suspended Particles (TSP). Aerosol samples were collected during the cruise in the Artic Glacial Sea, from Tromsø (Norway) to Svalbard Islands, along longitudinal and latitudinal transects.

The chemical characterization of the aerosol was performed: Organic and Elemental Carbon (OC and EC, by thermal-optical transmittance), 9 water-soluble inorganic ions (IONs, by ionic chromatography), trace organic compounds (18 Polycyclic Aromatic Hydrocarbons, PAHs, and C20 to C32 n-alkanes, ALKs, by gas chromatography-mass spectrometry; 5 short aliphatic ammines, AMMs, and 5 mono- and dicarboxylic acids, MDCs, by ionic chromatography).

An overview of the TSP concentrations and of the chemical composition will be presented and an in-depth analysis of the PAHs and n-alkanes concentrations will follow.

The main features of gas/particle partition of the two chemical classes will be described. An attempt to apply some of the best available models will also be made to evaluate the relative importance of adsorption on soot and absorption into the organic matter.

5.1 TSP CONCENTRATIONS

The filters were weighed three times before and after sampling to determine the mass of TSP deposited on the filter (see Chapter 2, Par.1.1). The detection limit was calculated as the average of blank filters plus three times the standard deviation (DL = 1.2 µg m^{-3}, DL autumn= 0.9 µg m^{-3}). The resulting values were corrected for the contribution of blank filters. The obtained mass was then divided to the volume of air sampled to obtain the concentration of TSP (µg m^{-3}).

The average TSP concentration in summer 2011 was 5.2± 4.9 µg m^{-3} (Fig 5.1) with values up to 22.0 µg m^{-3}.

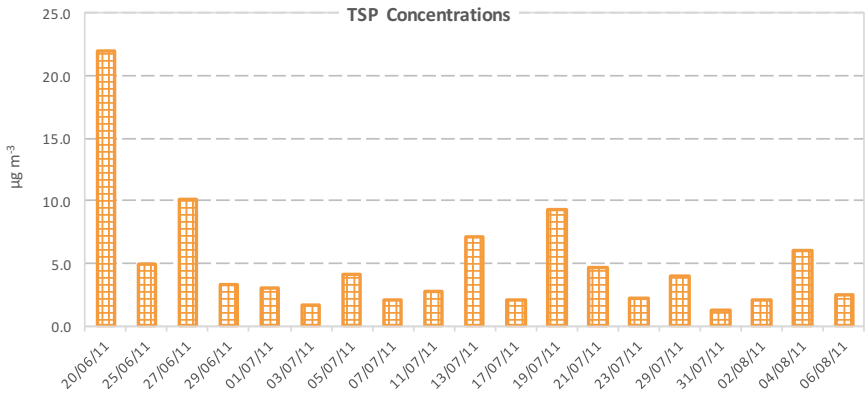

Figure 5.1 TSP concentrations (µg m-3) in summer 2011

The highest TSP concentrations were measured on the 20th June, when the ship departed from the port of Sopot (Poland) to start the cruise to the Svalbard; the concentrations showed a decreasing trend (with the only exception the 27th-28th June) until the July 3rd-4th, when the ship reaches the southern part of the Svalbard. From 5th to 22th July, the ship followed a route near the western coast of the Svalbard Islands: the peaks of concentrations observed on the 13th and 19th July were measured when the ship approached the coast.

5.2 CHEMICAL COMPOSITION

The major chemical components of PM (Table 5.1) were OC (also converted to OM, organic matter, as 2.1 x OC^{98}), EC, SO_4^{2-}, Cl^-, Na^+. These single chemical components accounted on average 26% (OM), 7.4% (EC), 10.6% (SO_4^{2-}), 32.6%(Cl^-), 15.9% (Na^+) of TSP, summing up to >90% of particle mass.

The average concentration of the total carbon was similar to the level measured over the Arctic ocean during late summer (av: 1.06 µg m^{-3})[141] but higher than that for spring aerosols collected at Alert (av: 0.32 µg m^{-3})[142] and also higher than those reported in the continental Arctic aerosols from Alert (av: 0.08 µg m^{-3})[141]. The higher total carbon concentrations in the marine aerosols from the Arctic Ocean suggest that the marine aerosols are influenced by the sea-to air emissions of marine organic matter.

The average concentration of sea salt aerosol was 4.1±2.2 µg m^{-3}, corresponding to about 70% of the total detected species. These data are in the middle between the sea

salt aerosol concentration measured over Southern Ocean (5.9±5.6 μg m^{-3}) and coastal East Antarctica (2.6±2.3 μg m^{-3}) [142]. Almost all the Cl^- and Mg^{2+} derived from sea salt aerosol.

The concentrations of primary trace organic compounds, PAHs and n-alkanes, will be discussed in the next paragraphs.

Table 5.1 Average values and standard deviation of carbonaceous fraction (OC, EC and total carbon, TC), inorganic ions, carboxylic acids and alkyamines

			(n=19)
			Mean SD
TSP chemical composition	Carbonaceous fraction (μg m^{-3})	OC	0.91 ± 0.15
		EC	0.54 ± 0.03
		TC	1.03± 0.35
	Inorganic ions (μg m^{-3})	Cl-	2.28 ± 1.33
		NO3-	0.12 ± 0.08
		SO4=	0.78± 0.38
		NH4+	0.05± 0.06
		Na+	1.17± 0.57
		Mg++	0.13± 0.08
		K+	0.04 ± 0.02
		Ca++	0.17 ± 0.07
		∑ ions	5.19 ± 2.36
	Carboxylic acids (Cas) (μg m^{-3})	**∑ CAs**	0.04 ± 0.03
	Alkylamines (μg m^{-3})	DMA+	<0.03
		TEA+	<0.01

5.2.1 PAHs

PAHs Concentrations. To take into account filter and PUF plug processing and transport, the detection limit (DL) was estimated. For the particulate phase, DL was estimated by blanks field filters while the gaseous phase detection limits were estimated by blank field PUF plugs. The mean values got by the blank field filter and PUF plugs were subtracted to the valid sample data. The recovery factors were always applied: the concentrations were corrected for the deuterated PAHs recoveries.

The PAHs were measured for 19 samples. Their concentrations summarized in Tab 5.2.

Table 5.2 PAHs concentrations in the particulate and in the gaseous phase

		summer 2011 (n=19)	
		Average	St.Dev.
Conc (pg m-3)	particulate	21.32	11.61
% in TSP		0.0007	0.0008
Conc (pg m^{-3})	gaseous	447.23	242.54

n = number of samples; PAHs = NAPH, ACTY, ACT, FLN, PHE, ANT, FLNT, PYR, BaA, CPcdP, CHR, BbF, BkF, BeP, BaP, DBahP, I123cdP, BghiP

The total (particulate + gaseous) concentrations were 447.5±254.1 pg m^{-3}. The PAHs concentrations (ng m^{-3}) in the particulate and in the gaseous phase show markedly different values.

The ∑PAH vapor phase concentrations ranged from 5 to 50 pg m^{-3}. Higher concentrations were found in other studies (Ny Alesund[143]: 0.6-2.0 ng m^{-3}; Mediterranean Sea[144]: 0.5-2.6 ng m^{-3}; Canadian Arctic[145]: 38-392 pg m^3).

The ∑PAHs vapor phase concentrations, much higher than the particulate phase, ranged from 163 to 1136 pg m^{-3} and were similar to or slightly higher than those measured in the Canadian Arctic from 1993 to 2000 [145] (113 to 516 pg m^{-3}).

The gas phase PAHs dominated in the total PAHs but not all compounds were dominant. On the contrary, the particulate PAHs were low concentrated and showed a preference for the semi-volatile PAHs (PHE, FLNT, PYR) (Fig. 5.2).

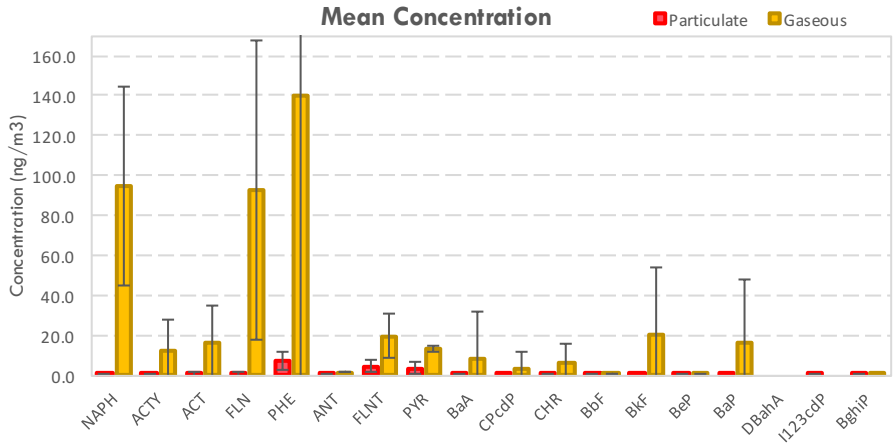

Figure 5.2 PAH concentrations (ng m-3) in the particulate and gaseous phases during winter and summer 2013 (crossbars: standard deviation of the average).

PAHs Distribution Pattern. The PAH distribution pattern was calculated as the ratio of the concentration of a single PAH to the concentration of the total PAHs (∑18 PAHs; Fig. 5.3)

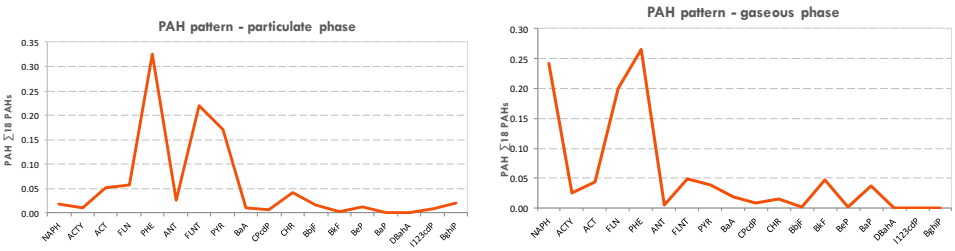

Figure 5.3 PAH distribution pattern in the particulate and gaseous phases

The most abundant PAHs in the particulate phase were the five semi-volatile PAHs, that together accounted for 80% of all the PAHs: on average phenantrene was 33% of all PAHs, fluoranthene 22%, pyrene 17%, fluorene 6%. Among the not-volatile PAHs, chrysene was the most concentrated (4%). All the other PAHs had average concentration lower than 1 pg m^{-3}.

In the gaseous phase PHE was the most abundant compound (27%) followed by NAPH (24%) and FLN (20%). This is consistent with other studies[108, 109, 110, 111].

PAHs Partitioning. The particulate to total (particulate + gaseous) concentration ratio of each PAH for the summer season is shown in Fig. 5.4.

The analyzed PAHs can be divided in three groups in function of the phase partition:

- *volatile PAHs: 2-3 aromatic rings,* lighter than FLNT (≤20% in the gaseous phase).
- *semi-volatile PAHs:* 3-4 aromatic rings (FLNT and PYR; 20-80% in the particulate phase);
- *not-volatile* PAHs: 5-6 aromatic rings, with a molecular weight higher than PYR (≥ 80% in the particulate phase)

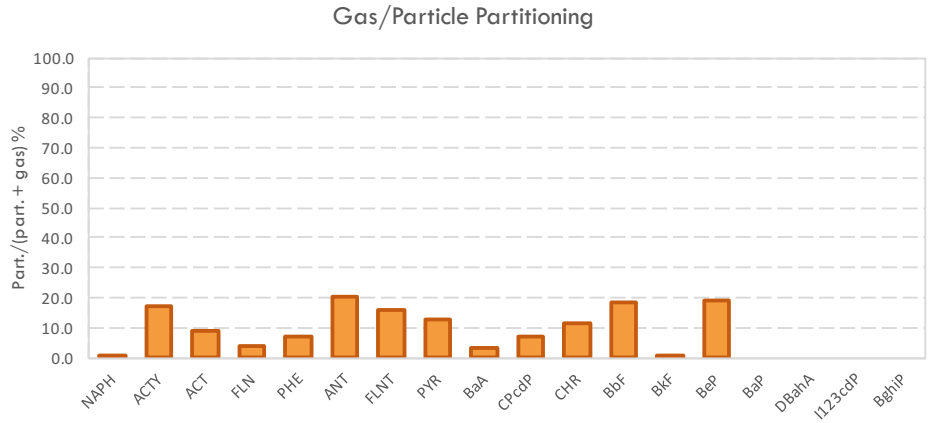

Figure 5.4 Gas/particle partition of the PAHs during winter, summer and autumn 2013 at TR site (crossbars: standard deviation of the average).

Since the gas phase dominated, the contribution of gaseous PAHs to ∑PAHs was around 80%.

Kp coefficient. The gas/particle partitioning coefficient, Kp, was calculated for all the samples as explained in eq. 1.1 (Tab. 3.5).

Table 5.3 Experimental log Kp, temperature corrected log pL0, temperature corrected and literature data for log Koa

	log Kp(m^{-3} μg^{-1})		log pL^0 (Pa)		log Koa		
	Average	St.Dev.	Average	St.Dev.	Average	St.Dev.	**logKoa(25°C)**
FLN	-2.36	0.59	-0.95	0.06	7.16	0.40	6.90
PHE	-1.80	0.64	-1.89	0.07	7.99	0.47	7.68
ANT	-1.36	0.70	-1.94	0.07	8.03	0.47	7.71
FLNT	-1.28	0.49	-3.20	0.08	9.13	0.55	8.76
PYR	-1.28	0.52	-3.43	0.09	9.09	0.53	8.73
BaA	-1.99	0.86	-4.85	0.09	10.74	0.67	10.28
CHR	-1.31	0.59	-5.06	0.10	10.75	0.67	10.30

The temperature corrected Log pL^0 was calculated for all the samples (Tab. 5.3).

The relationship between the mean log Kp for the PAHs and temperature corrected log pL° is represented in Fig. 3.9.

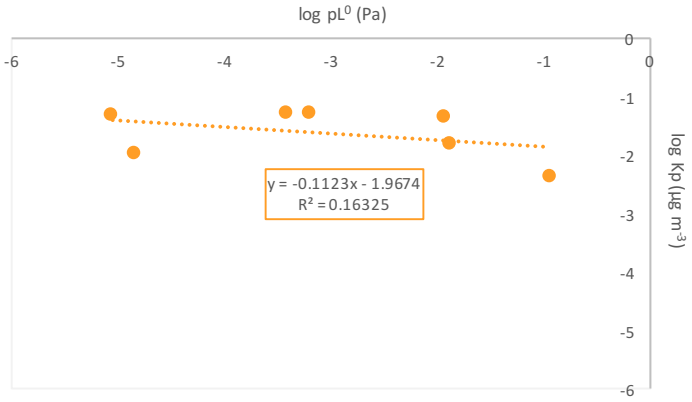

Figure 5.5 Temperature corrected log pL0 vs experimental log Kp linear regression for the PAHs (FLN, PHE, ANT, FLNT, PYR, BaA, CHR).

A weak correlation for log Kp vs log pL° was found (R^2: 0.00-0.84). In theory, the slope should be equal to -1 at equilibrium[88]. However, the slopes obtained in this study showed a deviation from the theoretical value of -1. The slopes were negative in the majority of the cases, with variable values (-0.81 to 0.40). The results suggest that non-equilibrium conditions might have prevailed.

The phase partitioning may also be described by the fraction θ of a compound in the particulate phase. The experimental adsorbed fraction on the particles, θ, was calculated and then compared to the predicted θ calculated using the temperature corrected Log pL^0 (eq. 1.3). Value of Cj = 17.2 Pa and of S=1.1 x 10^{-7} were used.

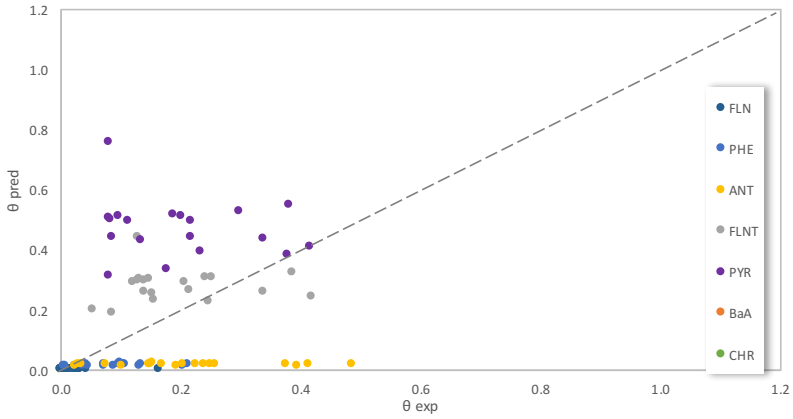

Figure 5.6 Predicted versus experimental ϑ (n = 19), Junge-Pankow model

A great variability between the samples led to a large scatter plot, as reported in Fig. 5.6. and a bad correlation (Fig.5.7).

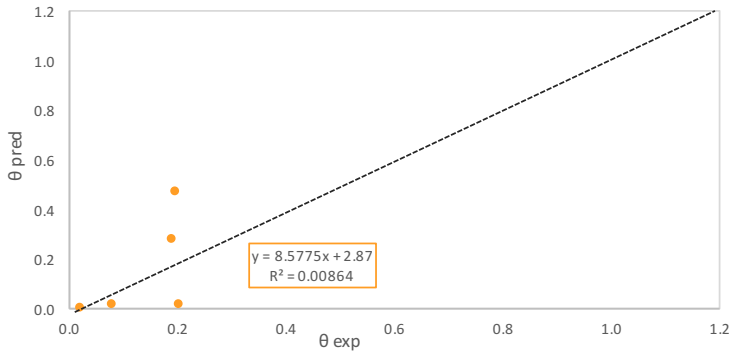

Figure 5.7 Mean predicted versus experimental ϑ for the PAHs (FLN, PHE, ANT, FLNT, PYR, BaA, CHR).

The experimental log Kp was also correlated against the octanol-air partitioning coefficient (Fig. 5.8). The temperature corrected log K_{OA} were calculated from tabulated values at 25°C found in literature (Tab. 5.3).

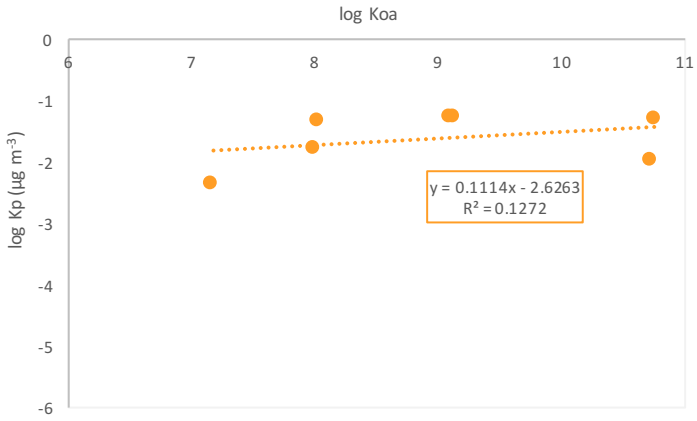

Figure 5.8 Temperature corrected log Koa vs experimental log Kp linear regression for the PAHs (FLN, PHE, ANT, FLNT, PYR, BaA, CHR).

A bad correlation was found for the log Kp vs log Koa regression (R^2: 0.00-0.86). For the equilibrium partition, the slope is expected to have a value near +1. The measured values were between -0.45 to 1.15 therefore it seems that the equilibrium was not reached.

The predicted log Kp was calculated using the temperature corrected log Kp. The Koa absorption model can be used to predict values of Kp from knowledge of only Koa and the organic fraction of the aerosol, fOM. For the conversion from organic carbon to organic matter was made assuming that the organic matter fraction(fOM) is 2.1 times the organic carbon fraction (fOC)[97]. The results obtained by linear regression of measured versus predicted Kp values are shown in Fig 5.9.

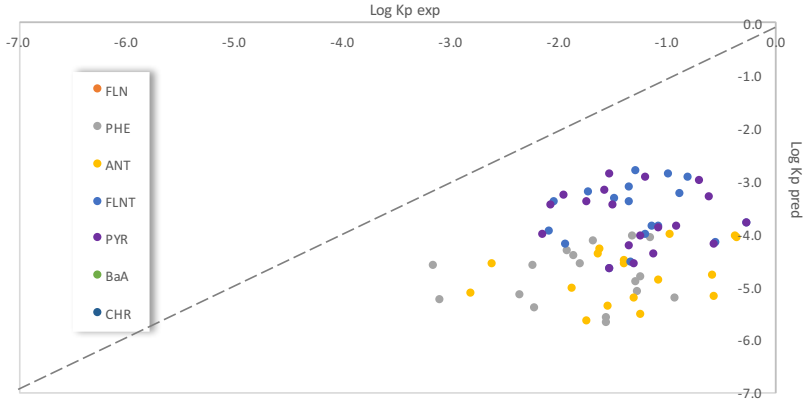

Figure 5.9 Predicted versus experimental log Kp (n = 19), Koa model

For the analyzed samples, the model always underestimated the partitioning for PAHs, as noted also in previous studies[75,77,87]. This could potentially be related to the underestimation of the term γOCT/γOM or possibly due to the high affinity of PAHs to soot particles, a parameter that is not accounted for in that model [83].

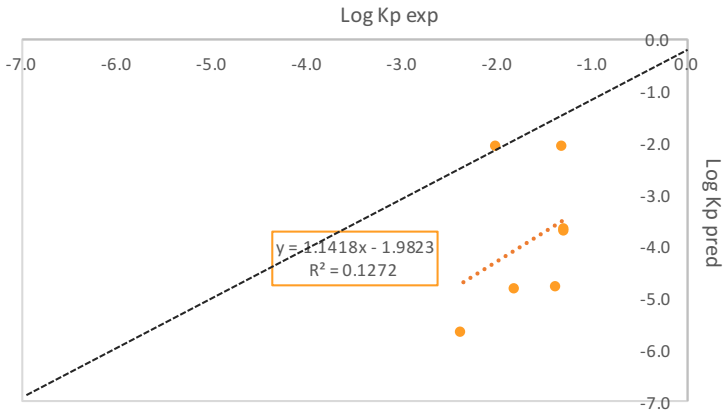

Figure 5.10 Mean predicted versus experimental log kp for the PAHs (FLN, PHE, ANT, FLNT, PYR, BaA, CHR).

An attempt to predict the gas/particle partitioning coefficient Kp applying the dual model described in Lohmann and Lammel [27] was made.

The corrected log Kp were than compared with that predicted Kp (Fig. 5.11)

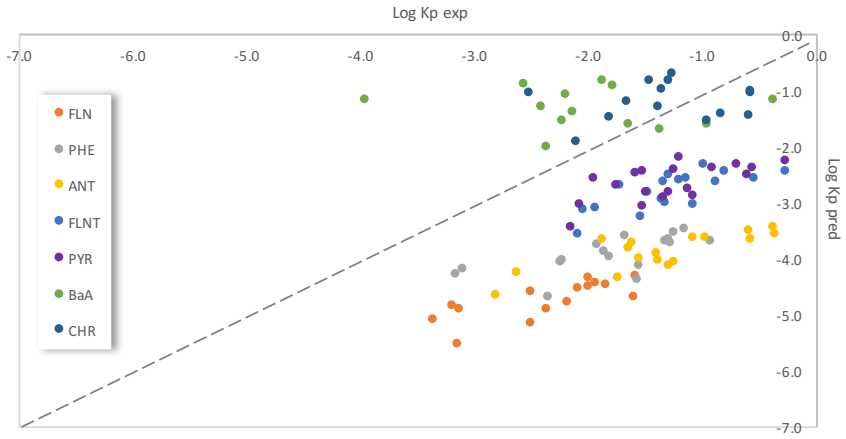

Figure 5.11 Predicted versus experimental Kp (n = 19), Dual model

To get the predicted log Kp, log Koa and Ksa values were calculated.

Again, a weak correlation was found between the measured and the predicted log Kp as shown in Fig 5.12. The results showed that the dual model under-predicted the partitioning of most PAHs.

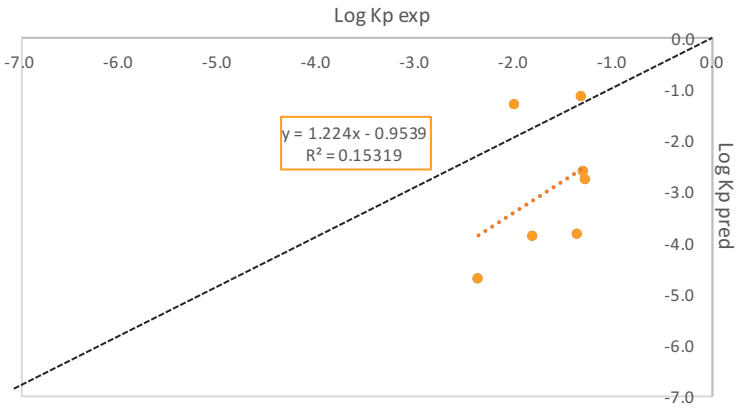

Figure 5.12 Mean predicted versus experimental log kp for the PAHs (FLN, PHE, ANT, FLNT, PYR, BaA, CHR

As suggested by Lohmann and Lammel [27] all the measured log Kp should be reported to 298 K using eq 3.2, in order to ensure the comparability between sample. Applying the temperature correction, the prediction improved significantly (R^2: 0.97) and the plot got closer to the 1-1 line (Fig. 5.13)

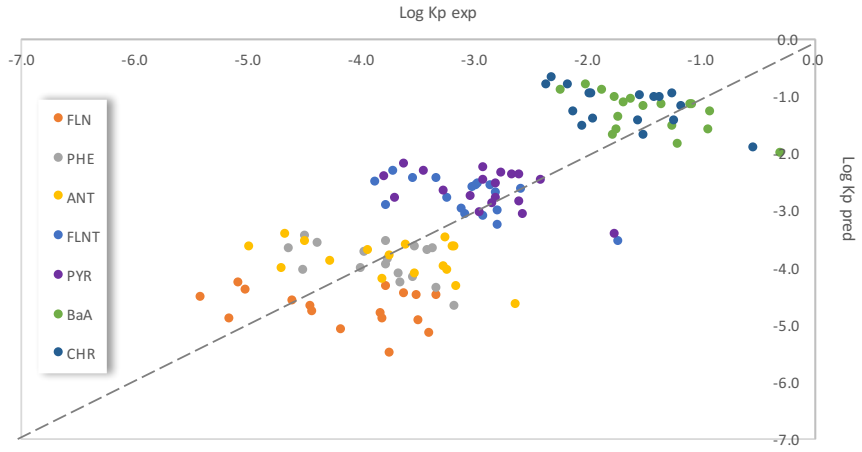

Figure 5.13 Predicted versus experimental temperature corrected log kp for the PAHs (FLN, PHE, ANT, FLNT, PYR, BaA, CHR

The gas-particle partitioning was studied using a PPLFERs model, considering two mechanisms for PAHs partitioning: absorption into OM and adsorption onto soot.

The system parameters for diesel soot [95] and for DMSO [115] were used for adsorption and absorption contribution respectively. The solute descriptors for the considered PAHs were taken from the literature [116, 117] (Tab.3.8). The partitioning constants related to absorption and adsorption processes, were corrected for the effect of near- ground temperature at the site using the solute-specific enthalpies of phase transfer, which were calculated for the corresponding ppLFER systems[118,119]. Total Kp was determined by summing the individual partitioning coefficients after normalizing the units.

Fig. 5.14 shows predictions made following the PPLFER method. A can be seen, the majority of the data points were predicted within 1 order of magnitude accuracy, with the exception of fluorene, anthracene and in most cases benzo(a)anthracene.

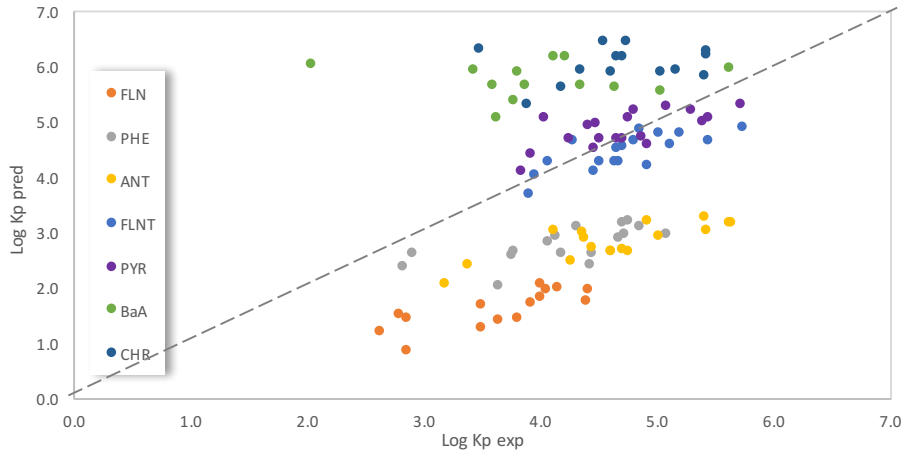

Figure 5.14 Predicted versus experimental Kp (n = 19), dual-phase ppLFER model

Due to high differences between the samples, in general the correlation wasn't so good, as shown in Fig 5.15 (R^2 FLN:0.60; R^2 ANT:0.65; R^2 FLNT:0.57).

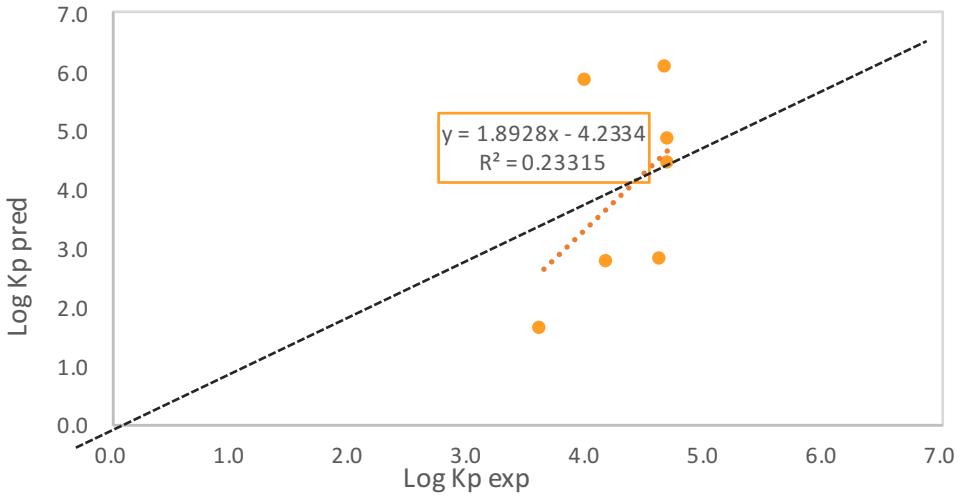

Figure 5.15 Mean predicted versus experimental log kp for the PAHs (FLN, PHE, ANT, FLNT, PYR, BaA, CHR)

These results suggest that the ppLFER model predicted quite accurately the gas-particle partitioning of PAHs

The gas-particle partitioning was lastly studied using a multi-phase PPLFERs model that considers absorption into OM and adsorption onto soot and soluble salts.

For adsorption contribution, the system parameters for diesel soot [95], Al and Fe oxides, ammonium sulphates and ammonium chloride [97] were used. For absorption, 2 OM phases were considered and DMSO and polyurethane were chosen as surrogates (Tab. 3.10).

Total predicted Kp, determined by summing the individual partitioning coefficients, was compared to the experimental Kp (Fig. 5.16)

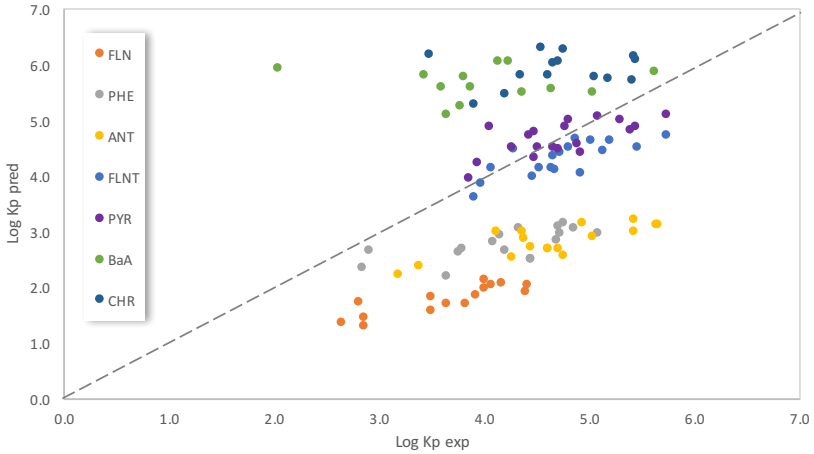

Figure 5.16 Predicted versus experimental Kp (n = 19), multi-phase ppLFER model

The use of the multiphase approach didn't improve the prediction of the PAHs partitioning.

Fig. 5.17 shows the mean values for sorption capacities related to adsorption and absorption processes considered in this study. Evidently, absorption was the main partitioning process dominated by the contribution of OSWSOM. Partitioning onto soot dominated the adsorption process among the considered phases considered, but contrary to what said for Milan, adsorption onto soluble salts has to be considered.

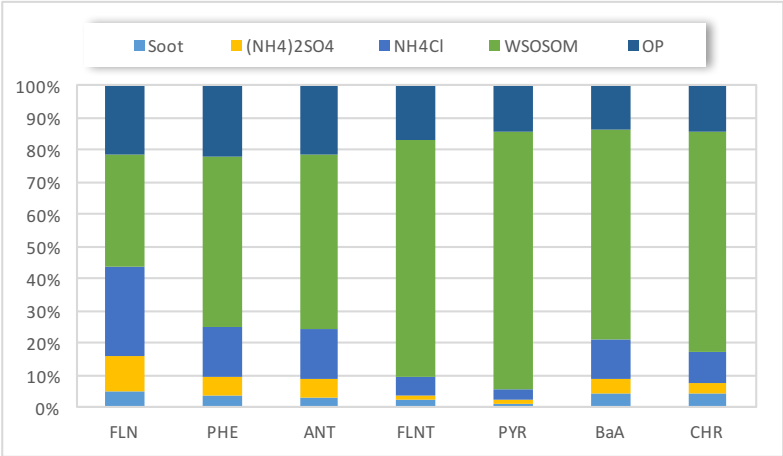

Figure 5.17 Contributions of individual phases to Kp determined using multi-phase ppLFER. OSWSOM: both organic soluble and water soluble organic matter; OP: organic polymers.

5.2.2 ALKANES

Alkanes Concentrations. As for PAHs, the blank field filters and the blank PUF plugs were processed and analysed as the real samples. Their concentrations were used to calculate the detection limit (DL) for the alkanes (eq. 3.1) both for the particulate and the gaseous phase. Only the data higher than the detection limit were considered valid. The mean values get by the blank field filter and PUF plugs were subtracted to the valid sample data.

The recovery factors were always applied: the concentrations were corrected for the deuterated Alkanes recoveries.

The alkanes were measured for 19 samples. Their concentrations summarized in Tab.5.4.

Table 5.4 ALKs concentrations in the particulate and in the gaseous phase

		summer 2011 (n=19)	
		Average	St.Dev.
Conc (ng m-3)	particulate	1.63	0.74
% in TSP		0.00006	0.00004
Conc (ng m^{-3})	gaseous	30.65	48.38

n = number of samples; ALKs = C20 to C32

The total (particulate + gaseous) concentration was on average 32.3±49.1 ng m^{-3}. The alkanes concentrations (ng m^{-3}) in the particulate and in the gaseous phase showed markedly different values.

The ∑ALKs particulate phase concentrations ranged from 0.5 to 3.2 ng m^{-3}. Similar values were measured by Fu over the Arctic Ocean[146] (0.14-4.5 ng m^{-3}) while higher concentrations were measured at Svalbard Islands[143] (19-97 ng m^{-3}). The ∑Alks vapor phase concentrations, much higher than the particulate phase, ranged from 1.4 to 191.8 ng m^{-3}

As shown in Fig. 5.18, the gas phase n-alkanes dominated, characterized by the concurrence of an n-alkane distribution with no carbon-number preference.

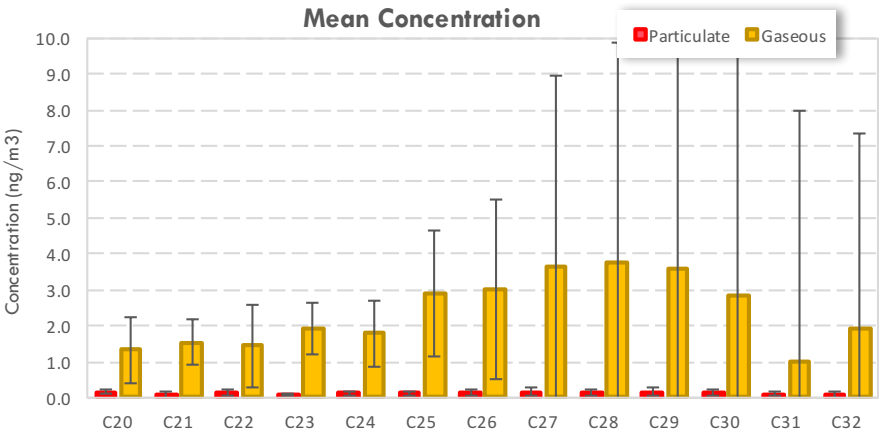

Figure 5.18 Alkanes concentrations (ng m-3) in the particulate and gaseous phases during winter and summer 2013 (crossbars: standard deviation of the average).

Alkane Distribution Pattern. The n-alkane carbon distribution pattern was calculated as the ratio of the concentration of a single n-alkane to the concentration of the total n-alkanes (n-C20 to n-C32). In Fig 5.19, the mean distribution pattern for the two phases is reported.

The most abundant alkanes were those with 24-32 carbon atoms (8-9% each), along with C20(11%) and C22(9%).

For the gaseous phase, the predominant alkane was C29 (10%); the other alkanes (except C31 and C24) contributed for the 8-9% each.

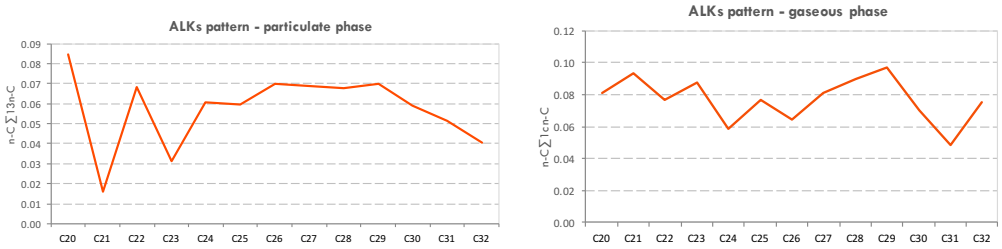

Figure 5.19 Alks distribution pattern in the particulate and gaseous phases

Since n-alkanes are source-specific[21,32,33] (i.e. their carbon distribution pattern is related to the sources) it is possible to discriminate the contribution of different sources by

means of the Carbon Preference Index (CPI) which is got by the odd to even n-alkane ratio.

In Fig. 5.20 the CPI values are reported. The carbon preference index highlighted the absence of any odd/even predominance: it was on average 0.7 and 1.4 in the particulate and in the gas phase respectively. Only three samples for the PM phase had a CPI higher than 1.10, with values up to only 1.28. As for the gas phase, only one sample behaved differently, reaching a CPI value higher than 7.

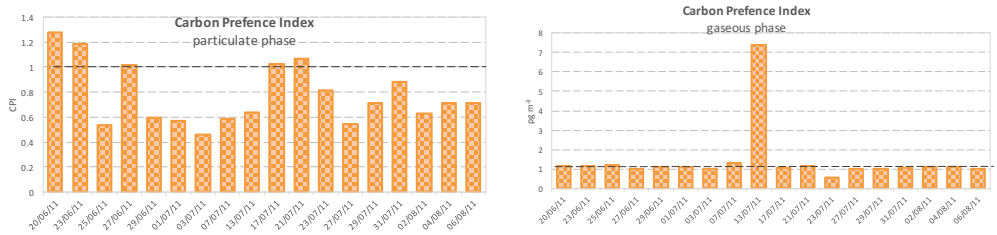

Figure 5.20 Carbon distribution pattern for winter, summer and autumn samples in the particulate and gaseous phase.

Alkanes Partitioning. The particulate to total (particulate + gaseous) concentration ratio of each Alkane for the summer season is shown in Fig. 5.21.

Three groups could be identified in function of the partition between the gaseous and particulate phases:

- *volatile* n-alkanes: compounds lighter than n-C23 (≤20% in the particulate phase).
- *semi-volatile* n-alkanes: n-C23 to n-C25 (20-80% in the particulate phase)
- *not-volatile* n-alkanes: compounds with a molecular weight higher than n-C25 (≥ 80% in the particulate phase)

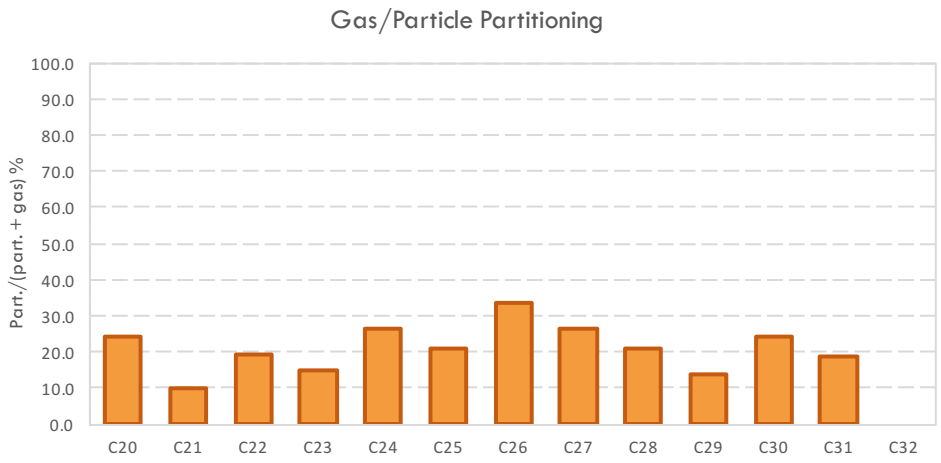

Figure 5.21 Gas/particle partition of the ALKs during winter, summer and autumn 2013 at TR site (crossbars: standard deviation of the average).

Since the gas phase dominated, the contribution of gaseous alkanes to ∑ALKs was around 70%.

Kp coefficient. The gas/particle partitioning coefficient, Kp, was calculated for the summer samples (Tab.5.5)

Table 5.5 Experimental log Kp, temperature corrected log pL0, Temperature corrected and literature data for log Koa

	log Kp(m^{-3} μg^{-1})		log pL^0 (Pa)		log Koa		
	Average	St.Dev.	Average	St.Dev.	Average	St.Dev.	**logKoa(25°C)**
C22	-1.54	0.61	-2.28	0.11	19.88	0.25	7.34
C23	-1.90	0.78	-1.06	0.11	20.86	0.26	7.70
C24	-1.44	0.77	-1.57	0.12	21.83	0.28	8.07
C25	-1.62	0.77	-1.94	0.12	22.81	0.29	8.44
C26	-1.28	1.14	-2.37	0.13	23.79	0.30	8.81
C27	-1.64	0.73	-2.52	0.13	24.73	0.31	9.17

The temperature corrected Log pL^0 was calculated for all the samples (Tab. 5.5).

The relationship between the mean log Kp for the n-alkanes from C22 to C27 and temperature corrected log pL° is represented in Fig. 5.22.

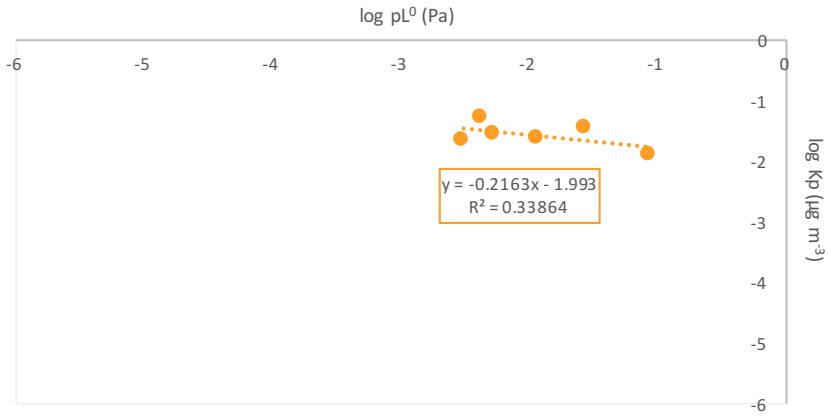

Figure 5.22 Experimental Kp vs log for the ALKs(C22 C23, C24, C25, C26, C27).

The correlation for log Kp vs log pL° was weak: the determination coefficient (R^2) was between 0 and 0.70. At equilibrium, the slope for either adsorption or absorption should be close to -1 [88]. The measured data (between -0.92 and -0.13) suggested that the gas/particle partition wasn't at equilibrium.

The phase partitioning may also be described by the fraction θ of a compound in the particulate phase. The experimental adsorbed fraction on the particles, θ, was calculated and then compared to the predicted θ calculated using the temperature corrected Log pL^0. Value of Cj = 17.2 Pa and of S=1.1 x 10^{-7} were used.

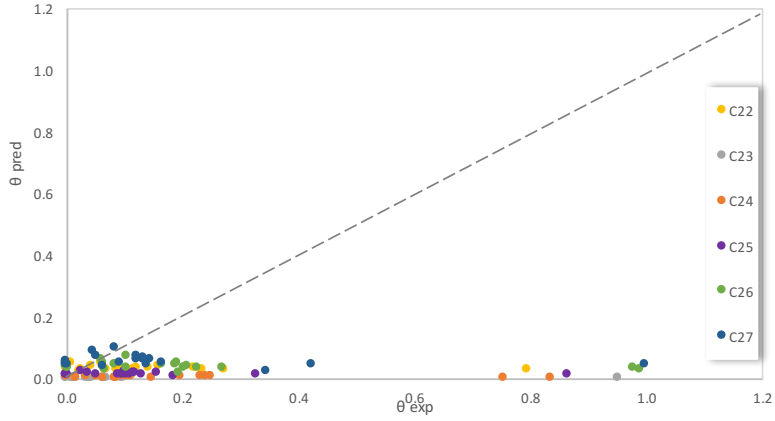

Figure 5.23 Predicted versus experimental ϑ (n = 19), Junge-Pankow model

A great variability between the samples led to a large scatter plot, as reported in Fig. 5.24. showing a bad correlation as shown in Fig.5.25.

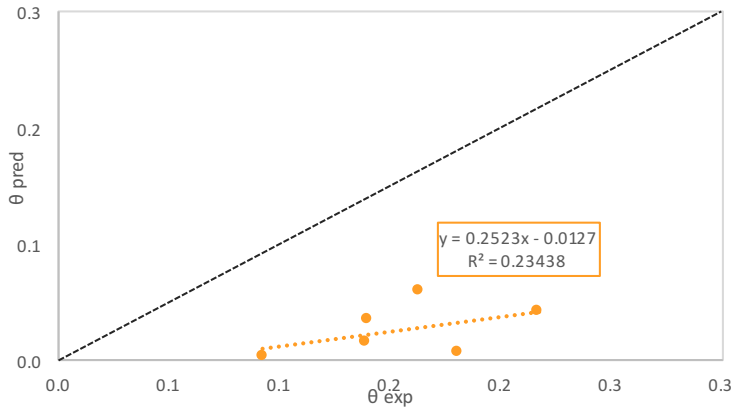

Figure 5.24 Mean predicted versus experimental ϑ for the ALKs (C22 C23, C24, C25, C26, C27).

The results show that the Junge-Pankow underestimated the partitioning. The model is, therefore, inadequate to predict the partitioning, indicating that another process, could be significant for the phase partitioning.

The experimental log Kp was also correlated against the octanol-air partitioning coefficient (Fig. 5.26). The temperature corrected log Koa were calculated from tabulated values at 25°C found in literature (Tab. 5.5).

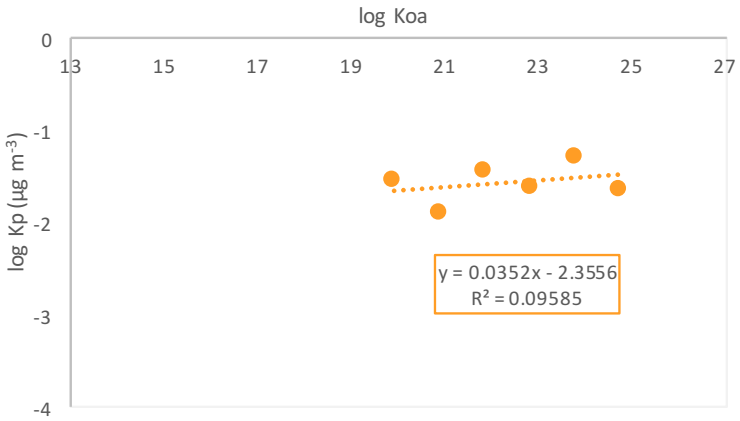

Figure 5.25 Experimental Kp vs log Koa for the ALKs(C22 C23, C24, C25, C26, C27).

The correlation correlation for the log Kp vs log Koa regression didn't improve, actually got worse compared to that for log Kp vs log pL^0.

For the equilibrium partition, the slope is expected to have a value of near +1. The measured values ranged from -0.25 to 0.31.

The predicted log Kp was calculated using the temperature corrected log Koa (eq.8). For the conversion from organic carbon to organic matter was made assuming that the organic matter fraction (fOM) is 2.1 times the organic carbon fraction (fOC). The results obtained by linear regression of measured versus predicted Kp values are shown in Fig. 5.27.

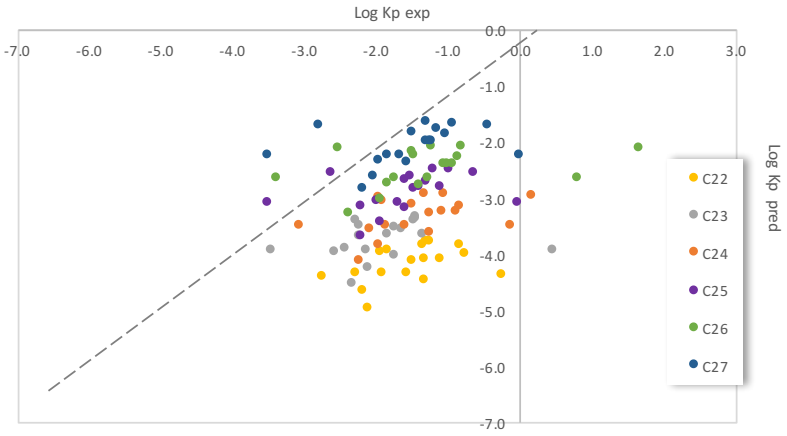

Figure 5.26 Predicted versus experimental Kp (n = 19), Koa model

Despite a slightly better correlation compared to the Junge-Pankow model, the Koa model always underestimated the partitioning for the considered alkanes (5.28).

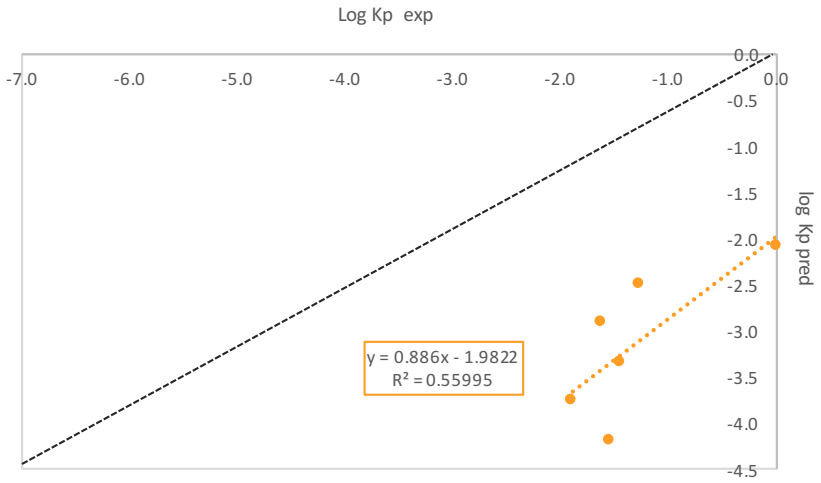

Figure 5.27 Mean predicted versus experimental Kp for the ALKs (C22 C23, C24, C25, C26, C27

An attempt to predict the gas/particle partitioning coefficient Kp applying the dual model described in Lohmann and Lammel[27] was made. The corrected log Kp was than compared with the predicted Kp (Fig. 5.29)

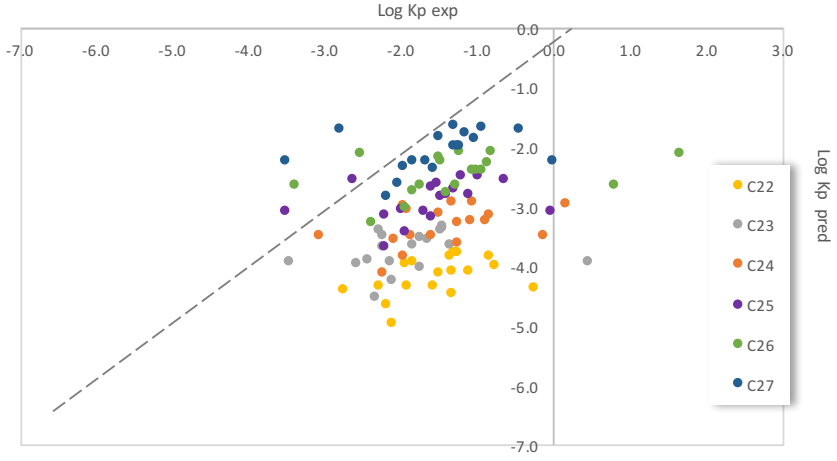

Figure 5.28 Predicted versus experimental Kp (n = 19), Dual model

To get the predicted log Kp, Koa and Ksa values were calculated.

A weak correlation was found between the measured and the predicted log Kp as shown in Fig 5.30.

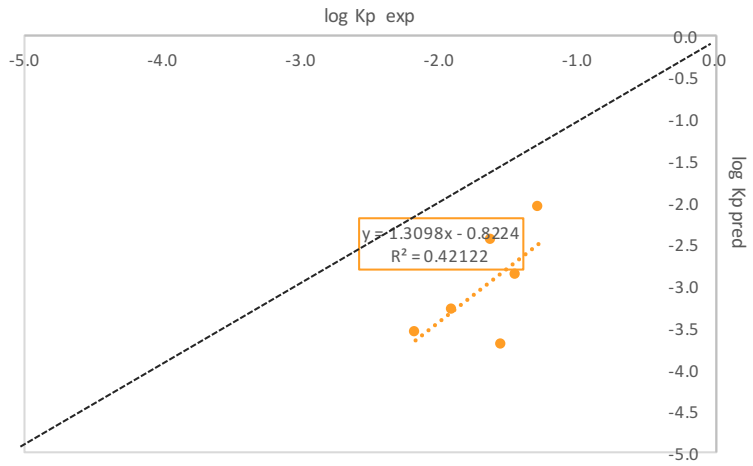

Figure 5.29 Mean predicted versus experimental Kp for the ALKs (C22 C23, C24, C25, C26, C27).

No big differences were found normalizing the experimental Kp at 298K (as recommended by Lohmann and Lammel[27]) as reported in Fig. 5.31

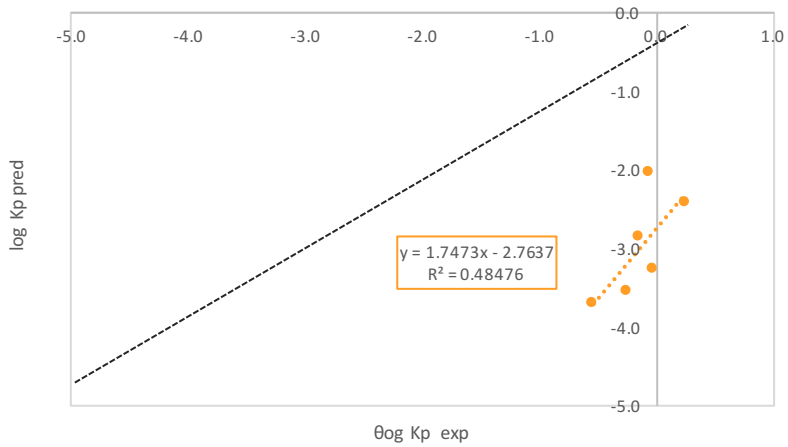

Figure 5.30 Mean predicted versus experimental Kp for the ALKs (C22 C23, C24, C25, C26, C27).

The results showed that also the dual model tended to under-predict the alkanes partitioning.

The gas-particle partitioning was studied using a PPLFERs model, considering two mechanisms for the partitioning: absorption into OM and adsorption onto soot.

The system parameters for diesel soot [95] and for DMSO[115] were used for adsorption and absorption contribution respectively. The solute descriptors for the considered alkanes were taken from the literature[120,121] (Tab. 3.16).

The partitioning constants related to absorption and adsorption processes were corrected for the effect of near- ground temperature at the site using the solute-specific enthalpies of phase transfer, which were calculated for the corresponding ppLFER systems[118.119]. Total Kp was determined by summing the individual partitioning coefficients after normalizing the units.

Fig. 5.32 shows predictions made following the PPLFER method. A can be seen, the majority of the data points were predicted within 1 order of magnitude accuracy, with the exception of C26 and C27, which were for most samples over predicted.

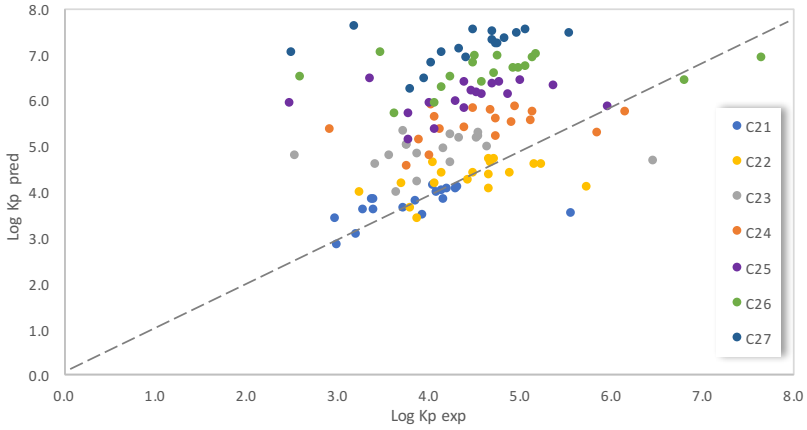

Figure 5.31 Predicted versus experimental Kp (n = 19), Dual phase ppLFER model

Despite the good prediction, a not so strong correlation for the experimental vs the predicted log Kp was found as shown in Fig 5.33, due to the high variability between the samples.

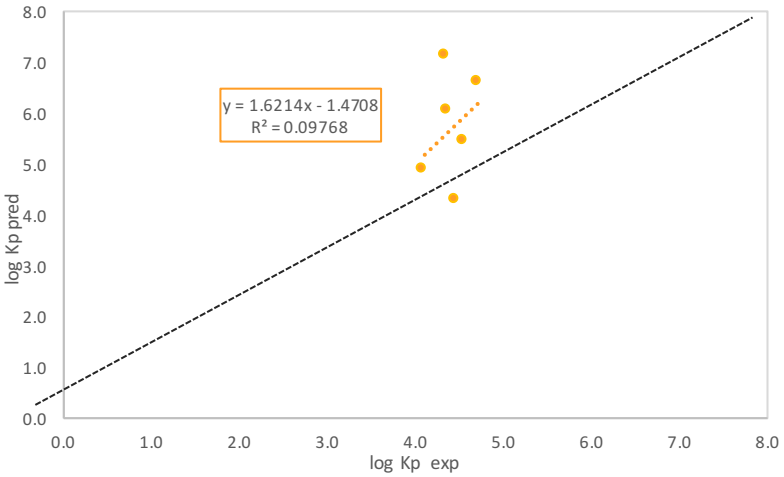

Figure 5.32 Mean predicted versus experimental Kp for the ALKs (C22 C23, C24, C25, C26, C27).

The gas-particle partitioning was lastly studied using a multi-phase PPLFERs model that considers absorption into OM and adsorption onto soot and soluble salts

For adsorption contribution, the system parameters for diesel soot[95], Al and Fe oxides, ammonium sulphates and ammonium chloride[97] were used. For absorption, 2 OM phases were considered and DMSO and polyurethane were chosen as surrogates (Tab. 3.10)

Total predicted Kp, determined by summing the individual partitioning coefficients, was compared to the experimental Kp (Fig. 5.34)

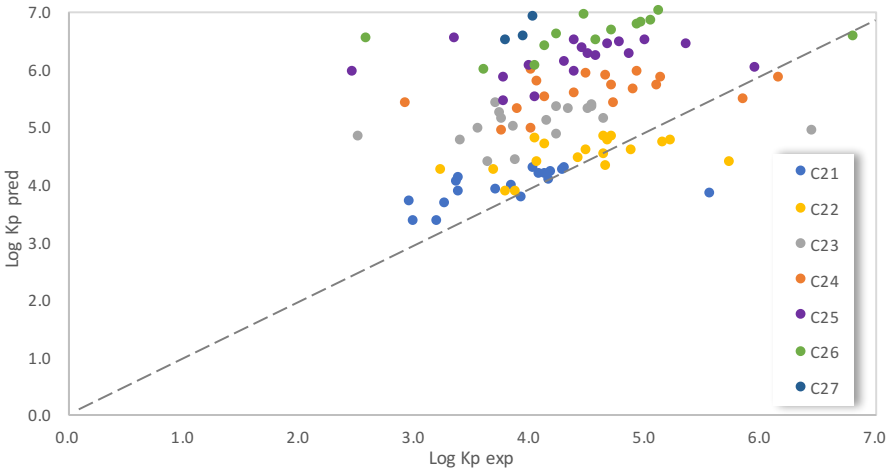

Figure 5.33 Predicted versus experimental Kp (n = 19), Multi-phase ppLFER model

The use of the multiphase approach didn't improve the prediction of the alkanes partitioning. Fig. 5.34 show the mean values for sorption capacities related to adsorption and absorption processes considered in this study.

Evidently, adsorption on soot was the main partitioning process and the contribution was higher for the heavier alkanes. Adsorption onto soluble salts even if on a small scale, contributes to the partitioning. The contribution of water soluble organic soluble organic matter (WSOSOM) was the most important for the absorption and this contribution was inversely proportional to EC (i.e. the contribution decreases with increasing the molecular weight of the compound).

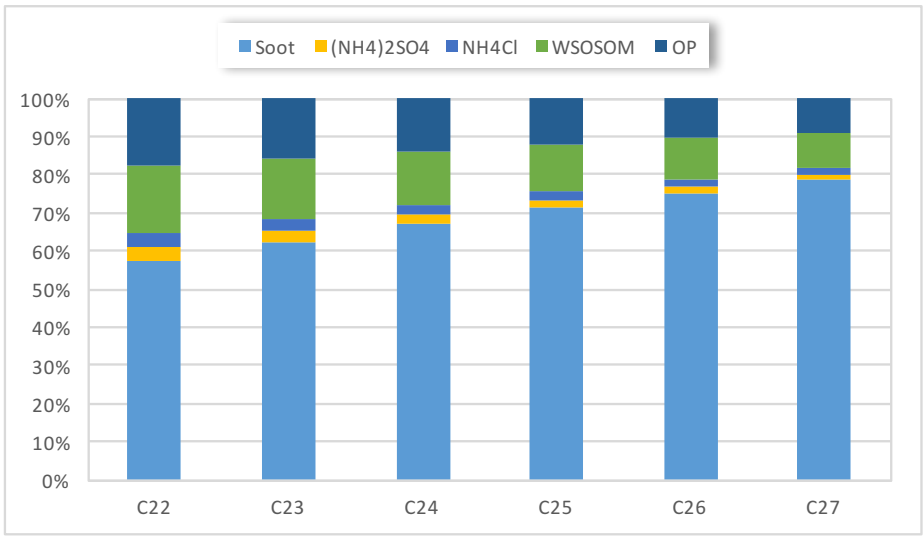

Figure 5.34 Contributions of individual phases to Kp determined using multi-phase ppLFER. OSWSOM: both organic soluble and water soluble organic matter; OP: organic polymers.

5.3 CONCLUSIONS

A sampling campaign was performed in summer 2011 on board of the OCEANIA ship, to study the semi-volatile organic compounds in the Arctic. The samples of the particulate and gaseous phases of the air were collected simultaneously by a high-volume sampler equipped with quartz fiber filters and PUF plugs. All the samples were processed to determine the PAH and n-alkane concentrations.

The results showed that, even in a remote site such as the Arctic Sea, organic pollutants of anthropic origin such as PAHs and n-alkanes are present. These may be emitted in part from local sources and partly from medium latitudes[72, 147].

For both the chemical classes, three groups were found in function of their phase partition:

- Volatile compounds, present for less than 20% in the particulate phase. The components of the group were and the PAHs lighter than FLNT and the n-alkanes lighter than n-C23.
- Semi-volatile compounds, present in the particulate phase for 20-80%. FLNT and PYR (for PAHs) and the n-alkanes from n-C23 to n-C25 are in this group.
- Not-volatile compounds, present for more than 80% in the particulate phase. The components of this group were the PAHs heavier than PYR and the n-alkanes with a molecular weight higher than n-C25

The gaseous phase prevailed for both the chemical classes.

The log Kp coefficient was calculated and correlated against the log pL° (sub-cooled liquid vapor pressure) and log Koa (octanol-air partitioning coefficient). Not so strong correlations were found for both the regressions. The fraction θ of a compound in the particulate phase was calculated and compared to the θ predicted by the Junge-Pankow model.

The measured Kp was also compared with log Kp predicted by the Koa model, which take into account only the absorption process and later with the log Kp predicted by a dual model that took into account both the absorption in the organic aerosol and the adsorption onto the elemental carbon.

In general, a bad correlation was found between the measured and the predicted log Kp for PAHs ($R^2 < 0.30$) and for alkanes ($R^2 < 0.20$) The regression lines didn't pass through the axis origin for all the compounds, meaning that the models underestimate the partitioning and suggesting that other important factors should be added.

For this reason, the gas-partitioning was studied using a polyparameter linear free energy relationships (ppLFERs), that takes into account the molecular interactions between the compound (sorbate) and the sorbent phase. The dual-phase ppLFER considers adsorption onto to elemental carbon (EC) and absorption into the organic matter, whereas the multi-phase ppLFER considers adsorption onto to elemental carbon (EC) and soluble salts and absorption into various OM fractions. The model predicts well the partitioning. Absorption was the main partitioning process for PAHs, dominated by the contribution of OSWSOM while adsorption on soot was the main partitioning process in the alkanes partitioning. Conversely to what found for the urban atmosphere of Milan, for both the considered class of compounds, adsorption onto soluble salts cannot be neglected, since it contributes, even if on a small scale, to the partitioning process.

CHAPTER 6. CARCINOGENIC RISK ASSESSMENT

Atmospheric PAHs are of particular interest since they are of major concern in all environmental compartments due to their mutagenic and carcinogenic properties[148,149,150]. The most common carcinogenic effect of PAHs on human cells is DNA damage through the formation of adducts in many organs, including liver, kidney, lungs, etc.[151,152].

Several toxicological studies in animals [World Health Organization–International Programme on Chemical Safety (WHO– IPCS) 1998] and occupational studies in humans[153] demonstrated also an excess risk of lung cancer associated with PAHs inhalation. Individual PAHs are likely to induce cancer through different mechanisms; for this reason, risk estimation for PAHs exposures is complex.

For many years research on atmospheric PAHs has mainly focused on the PAHs that have health implications and thus on quantitative analysis of 16 PAHs prioritized by the United States Environmental Protection Agency (EPA). In general, the carcinogenic properties of PAHs increase with the number of aromatic rings. Benzo[*a*] pyrene (BaP) has been the most extensively studied PAH and is the usual marker for carcinogenic levels of PAHs in environmental studies. The other PAHs have been ranked according to cancer potency relative to BaP using toxic equivalence factors (TEFs).

The aim of the present study was to estimate the carcinogenic potency of the emitted PAHs and the lifetime lung cancer risk of PAH exposure by inhalation in people living in urban and near remote sites, including the impact of both gaseous and particulate phases.

6.1 TOXIC EQUIVALENCY FACTORS: BAP EQUIVALENCY

The evaluation of carcinogenic risk assessment induced by the inhalation of the mixture of PAHs was performed using toxic equivalent factors (TEFs) with benzo[a]pyrene (B[a]P) as the reference compound with conventional value of 1[154].
The benzo[a]pyrene (BaP) equivalent (BaP_{eq}) concentration of individual PAHs was calculated by multiplying their concentration by their RPF.

Equivalent atmospheric toxic concentrations (C_{EQ}), expressed in B[a]P equivalent concentrations (ng m^{-3}), were calculated by multiplying the concentration of the PAHs by their TEF using eq 6.1:

$$Ceq = \sum_{i=1}^{n} [PAH]i \ \ x\ TEFi \qquad \text{(eq. 6.1)}$$

TEF values used in this study[155] are shown in Table 6.1

Table 6.1 Toxic equivalent factors (TEF) used for the cancer risk assessment calculation.

	TEF
NAPH	0.001
ACTY	0.001
ACT	0.001
FLN	0.001
PHE	0.001
ANT	0.01
FLNT	0.001
PYR	0.001
BaA	0.1
CHR	0.01
BeP	0.002
BbF	0.1
BkF	0.1
BaP	1
I123cdP	0.1
DBahA	1
BghiP	0.01

6.2 LIFETIME LUNG CANCER RISK OF PAHS IN THE ATMOSPHERE

The inhalation cancer risk for the PAH mixture was estimated by multiplying the sum of the individual BaPeq concentrations by the unit risk (UR) of exposure to BaP (Eq. 6.2)

$$Cancer\ Risk = \ Ceq\ x\ UR\ (BaP) \qquad \text{(eq. 6.2)}$$

where UR is the Inhalation unit risk of exposure to BaP to BaP (specifically, "the calculated, theoretical upper limit possibility of contracting cancer when exposed to BaP at a concentration of one microgram per cubic meter of air for a 70-year lifetime").

A value of 1.1×10^{-6} per ng m^{-3} based on data for respiratory tract tumors from inhalation exposure in hamsters[156] was used in the inhalation cancer risk assessment for UR(BaP)

6.3 RESULTS

6.3.1 THE URBAN AREA OF MILAN

Table 6.2 shows the average BaP-eq values in the gas phase and in the particle phase in Milan, for the 17 target PAHs and the total PAHs, by sampling period.

Table 6.2 Average BaP-eq (ng/m3) for gas and particle phases in the Milan, during different sampling periods

	MILAN (Particle/gas phase)		
PAH	winter	summer	autumn
NAPH	4.8E-04 / 2.45E-03	2.6E-05 / 3.23E-04	3.6E-05 / 1.41E-04
ACTY	3.3E-04 / 5.35E-03	2.0E-05 / 4.27E-04	5.6E-05 / 3.34E-04
ACT	5.7E-05 / 1.18E-03	5.9E-06 / 3.81E-04	2.6E-05 / 4.58E-05
FLN	1.4E-04 / 1.42E-02	8.1E-06 / 9.84E-04	8.6E-06 / 4.05E-04
PHE	2.1E-03 / 3.51E-02	5.8E-05 / 6.78E-03	1.3E-04 / 1.65E-03
ANT	2.1E-03 / 5.37E-02	7.7E-05 / 6.07E-03	1.7E-04 / 1.77E-03
FLNT	5.3E-03 / 1.02E-02	6.1E-05 / 2.51E-03	2.8E-04 / 4.95E-04
PYR	5.8E-03 / 8.58E-03	9.6E-05 / 2.09E-03	3.5E-04 / 3.85E-04
BaA	1.3E+00 / 3.14E-02	6.4E-03 / 1.06E-02	1.6E-02 / 8.29E-04
CHR	7.3E-02 / 1.23E-03	5.0E-04 / 1.10E-03	2.3E-03 / 6.69E-05
BbF	2.4E-02 / 6.69E-04	3.6E-04 / 3.34E-04	9.3E-04 / 4.52E-05
BkF	3.8E-01 / 1.28E-03	2.2E-03 / 2.49E-03	1.3E-02 / 4.58E-04
BeP	4.7E-01 / 2.32E-03	4.9E-03 / 3.73E-03	2.3E-02 / 0.00E+00
BaP	7.2E+00 / 4.77E-03	5.3E-02 / 9.32E-03	2.0E-01 / 1.18E-03
DBahA	4.1E-02 / 4.08E-03	1.5E-03 / 1.37E-03	2.6E-03 / 0.00E+00
I123cdP	3.8E+00 / 0.00E+00	4.5E-02 / 0.00E+00	1.9E-01 / 0.00E+00
BghiP	4.2E-02 / 0.00E+00	8.0E-04 / 9.98E-06	2.5E-03 / 0.00E+00
Total PAHs (PM/gas)	13.29 / 0.18	0.12 / 0.05	0.45 / 0.01
Total PAHs (PM+gas)	13.47	0.16	##

As for the city of Milan, the mean equivalent toxic concentration was extremely higher in the "cold" period (13.47 ng m^{-3}) than in the "warm" period (0.16 ng m^{-3} in summer and 0.46 ng m^{-3} in autumn). Summer values were in agreement with the literature, but the results obtained for the winter season in Milan were absolutely higher [47,155]. The highest equivalent concentration in the PM phase value reached 20 ng m^{-3} during January. The contribution of the gas phase to the total BaP-eq values in this study was substantial only for summer, with values around 30%. This high contribution was due to the presence of some heavy PAHs in the gas phase with high TEFs. It is worth noting that BaP-eq values for the particle phase were higher than those for the gas phase

The annual mean equivalent concentration was ≈ 4.7 ng m^{-3}. This induces an excess of risk, considering an entire life exposure to the observed concentrations in 2013 and based on UR(BaP) value of 1.1×10^{-6} per ng m^{-3}, $\approx 1.5 \times 10^{-5}$ (1.5 additional cases per

100,000 people exposed). The winter season showed the highest estimated risk with values of 1.48×10^{-5}. In summer and autumn, the estimated risk was 1.80×10^{-7} and 5.03×10^{-7} respectively. Figure 6.1 shows the average lifetime lung cancer risk estimated for each PAH, by sampling period.

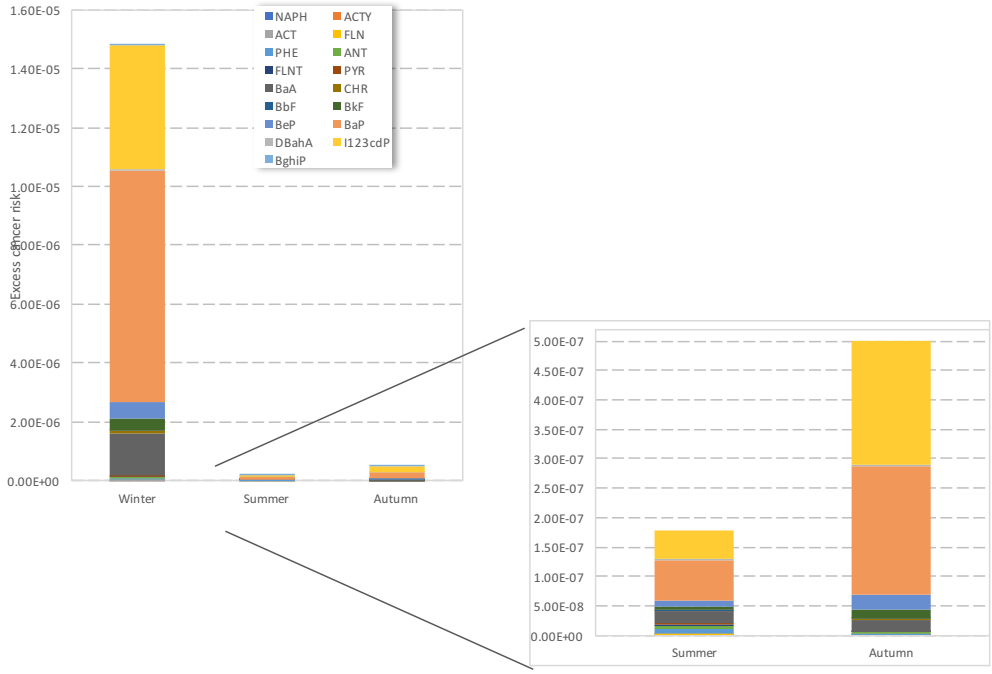

Figure 6.1 Average estimated lifetime lung cancer risk expressed as excess cancer risk per person exposed, by period and PAH

These results are consistent with other studies performed in China[157], but are slightly higher than observations made in France[155].

6.3.2 THE AIRPORT OF MILANO-MALPENSA

Table 6.3 shows the average BaP-eq values in the particle phase (PM10 and PM2.5) in the airport of Milano-Malpensa, for the 17 target PAHs and the total PAHs in two different sampling periods.

Table 6.3 Average BaP-eq (ng/m3) in PM10 and PM2.5 in the airport of Milano-Malpensa

	MILAN-MALPENSA (PM10 / PM2.5)	
PAH	SITE 1	SITE 2
NAPH	<DL / 5.9E-05	<DL / 8.1E-05
ACTY	0.00 / 8.2E-05	1.60E-04 / 1.1E-04
ACT	0.00 / 1.4E-05	6.38E-05 / 1.5E-05
FLN	0.00 / 3.3E-05	2.10E-05 / 4.3E-05
PHE	0.00 / 1.5E-04	4.60E-05 / 3.1E-04
ANT	0.01 / 1.2E-03	5.59E-03 / 9.2E-04
FLNT	0.00 / 4.8E-04	1.05E-04 / 7.2E-04
PYR	0.00 / 6.4E-04	8.81E-04 / 8.6E-04
BaA	0.17 / 1.3E-01	1.09E-01 / 1.3E-01
CHR	0.03 / 1.3E-02	1.06E-02 / 1.5E-02
BbF	0.01 / 7.8E-03	2.22E-03 / 7.9E-03
BkF	0.65 / 9.7E-02	2.20E-01 / 9.9E-02
BeP	0.20 / 1.5E-01	6.21E-02 / 1.5E-01
BaP	2.69 / 2.2E+00	9.79E-01 / 1.9E+00
DBahA	0.36 / 1.3E-02	1.28E-01 / 9.5E-03
I123cdP	0.54 / 1.5E+00	2.55E-01 / 1.6E+00
BghiP	0.02 / 1.3E-02	9.83E-03 / 1.5E-02
Total PAHs (PM10/PM2.5)	4.7 4.1	1.8 3.9

The mean equivalent toxic concentration for PM10 was slightly higher in the first sampling period (October-January 2016: 4.7 ng m^{-3}) than in the second period (January-March 2017:1.8 ng m^{-3}), while the values were comparable for PM2.5: 4.06 and 3.89 ng m^{-3} in the first and in the second period respectively.

The mean equivalent concentration for the investigated period was ≈ 6.5 ng m^{-3} for PM10 and 7.9 ng m^{-3} for PM2.5. This induces an excess of risk, based on UR(BaP) value of 1.1×10^{-6}, considering an entire life exposure to the observed concentrations of PM10 $\approx 7.11 \times 10^{-6}$ (7.1 additional cases per 1,000,000 people exposed). For PM2.5 the excess of risk of cancer was a little higher, $\approx 8.77 \times 10^{-6}$ (8.8 additional cases per 1,000,000 people exposed). Since PAHs are mainly present in the fine fraction, the difference between PM10 and PM2.5 is explained.
Figure 6.1 shows the average lifetime lung cancer risk estimated for each PAH, by sampling period.

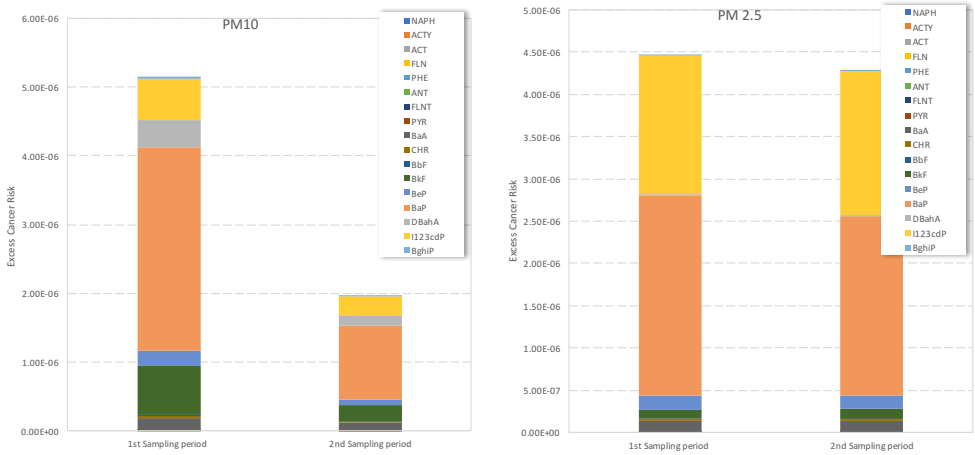

Figure 6.2 Average estimated lifetime lung cancer risk expressed as excess cancer risk per person exposed for PM10 and PM2.5 by sampling period and PAH.

6.3.3 REMOTE SITES: THE ARCTIC

Table 6.2 shows the average BaP-eq values in the gas phase and in the particle phase in Milan, for the 17 target PAHs and the total PAHs, by sampling period.

Table 6.4 Average BaP-eq (ng/m³) for gas and particle phases in the Arctic

	ARCTIC (Particle/gas phase)		
PAH	Summer		
NAPH	3.6E-07	/	9.5E-05
ACTY	2.4E-07	/	1.2E-05
ACT	1.0E-06	/	1.7E-05
FLN	1.2E-06	/	9.3E-05
PHE	7.1E-06	/	1.4E-04
ANT	5.8E-06	/	1.9E-05
FLNT	4.7E-06	/	2.0E-05
PYR	3.8E-06	/	1.4E-05
BaA	2.5E-05	/	8.2E-04
CHR	7.1E-06	/	1.2E-05
BbF	7.1E-07	/	6.9E-05
BkF	3.8E-06	/	2.0E-03
BeP	2.7E-05	/	4.0E-04
BaP	2.3E-05	/	1.6E-03
DBahA	0.0E+00	/	0.0E+00
I123cdP	2.0E-04	/	0.0E+00
BghiP	3.9E-06	/	0.0E+00
		/	
Total PAHs (PM/gas)	3.2E-04	/	5.4E-03
Total PAHs (PM+gas)		#####	

The mean equivalent toxic concentration in the arctic in summer (particulate + gaseous) was 0.00567 ng m^{-3}. The highest equivalent concentration value reached was 1,15 ng m^{-3} on 21st July. The contribution of the gas phase to the total BaP-eq values in this study was substantial. This high contribution was due to the presence of some heavy PAHs in the gas phase with high TEFs.
Figure 6.1 shows the average lifetime lung cancer risk estimated for each PAH, by sampling period.

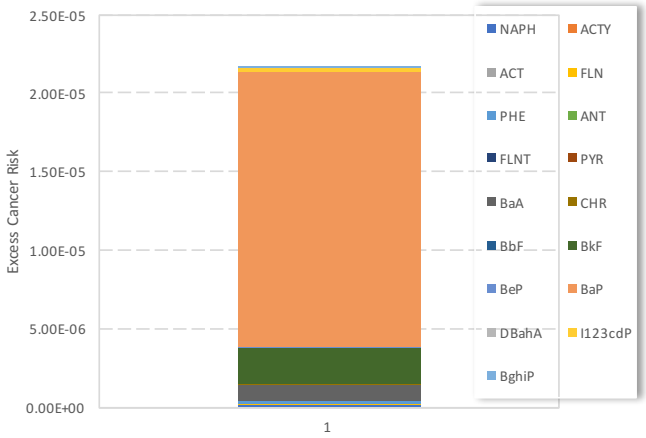

Figure 6.3 Average estimated lifetime lung cancer risk expressed as excess cancer risk by PAH.

The excess of risk and based on UR(BaP) value of 1.1×10^{-6} per ng m^{-3}, considering an entire life exposure to the observed concentrations in summer 2011, was $\approx 2.16 \times 10^{-5}$ (2 additional cases per 100,000 people exposed). This is an extremely high value for a remote site such as the Svalbard Islands.

6.4 CONCLUSIONS

People living in the urban area of Milan have a great inhalation cancer risk due to PAH exposure. Inhalation exposure from ambient air is inevitable for the entire population living in urban areas. The major PAH contributors to the total inhalation cancer risk were BaP, BaA, I123cdP, BeP, BkF, DahA at all the sites. However, their relative order varied season to season and site to site.

In order to decrease the inhalation cancer risk in the studied areas, the emissions of this PAHs would need to be reduced. Because these PAHs are bound to particulate

matter, this reduction could be achieved through general reductions in particulate matter emissions from combustion sources. Risk calculations showed that the contribution of the gas-phase PAHs to the total risk should be taken into account, especially during high-temperature periods.

This assessment of inhalation cancer risk has several uncertainties and limitations. First, the sampling sites used may not be representative of the entire urban areas evaluated. Second, the approach used assumes additive cancer risk. Different PAH isomers, in conjunction with other pollutants (including metals) may increase or decrease the toxicity of PAHs[157]. However, even with these uncertainties, the assessment gives a general evaluation of the inhalation cancer risk associated with PAH exposure in different sites.

The average estimated lifetime lung cancer risk was equal to the WHO and the U.S. EPA recommended values (10^{-5}) for Milan and for the Arctic region, but lower than the threshold value of 10^{-3} considered a definite risk according to criteria used in similar risk assessment studies[47]. Despite uncertainties associated with the sampling methodology and the calculations, these findings suggest that it would be prudent to take PAHs concentrations in both gas and particle phases into account in future health-risk legislation. The real risk values may otherwise be underestimated.

CHAPTER 7. CONCLUSIONS

During the last decades, a wide number of scientific studies about the chemical characterization of particulate matter and other atmospheric pollutants were published. The most important aspect related to air pollution is the health effect on the exposed population. Organic components of PM such as PAHs, have been shown to cause pathologies of the respiratory system and cardiovascular disease as well as to increase the risk of lung cancer [36].

This work intended to describe experimentally the distribution of two classes of semi-volatile compounds in different environments and different seasons and to implement a suitable phase distribution model that is valid in different environments.

This study provided a contribution on the knowledge of the concentration of this class of compound, in addition to n-alkanes, in different seasons and in sites with very different degree of anthropization, source types, climatic conditions and different temperatures.

A first sampling campaign was conducted in the city of Milan, located in the Lombardy Region, one of the most polluted areas in Italy. It is a critical area since its morphological and meteorological conditions, together with the high urbanization and industrialization, determine frequent high air pollution situations (mostly in winter). Samples collected during different seasons (winter, summer and autumn) showed big differences in the atmospheric concentrations of PM and of the investigated compounds. TSP concentrations were 2 times higher in winter (129 ± 60 μg m^{-3}) compared to summer and autumn when similar TSP concentrations of 50 ± 7 μg m^{-3} (summer) and 57 ± 19 μg m^{-3} (autumn) were measured. PAHs were 10 times more concentrated in winter (158 ± 67 ng m^{-3}) than in summer (15 ± 6 ng m^{-3}) and autumn (7 ± 3 ng m^{-3}) and also alkanes were 2-3 more concentrated in winter (426 ± 7 ng m^{-3}) compared to summer (139 ± 7 ng m^{-3}) and autumn (162 ± 36 ng m^{-3}).

The Authorities tried to mitigate this serious situation with different abatement strategies, but the air quality is only weakly improved. Nevertheless, the results from a sampling campaigns performed at 2 locations in Milan, with different traffic loads, showed a decrease in the concentrations, from a traffic site to the low emission zone, of EC (-36%) PAHs (-32%), n-alkanes (-15%) some elements (between -27% and -37% for Cu, Zn, Pb, Mo, Ba, Fe, Mn) and BC (-21%). Such result demonstrates the impact of

local traffic source on the concentrations of specific PM chemical components (EC, PAHs and elements) which are known for their adverse health effects on the exposed population. For this reason, such data can also be helpful to policy and decision makers in evaluating the benefits of local traffic reductions in urban areas.

High PM concentrations were also measured during a second sampling campaign conducted inside the airport of Milano-Malpensa with values ranging from 30 ± 16 and 37 ± 19 μg m^{-3} for PM10 and from 35 ± 27μg m^{-3} to 43± 3 μg m^{-3} for PM2.5. High PAHs atmospheric concentrations, similar to those reported in the literature for the urban area of Milan[9] were also measured in PM2.5 (17± 8 ng m^{-3}). These results underline the fact that PM trends in this area are more influenced by atmospheric mixing and by large-scale processes.

It is generally assumed that the high latitudes of both hemispheres are uncontaminated regions but in the last decades high concentrations of several pollutants were revealed in and around the Arctic. The Arctic is no longer a pristine environment, free of anthropogenic contaminants. As most of these chemicals are not used or emitted in the Arctic region, they must have been transported over great distances from their sources. The occurrence in these pristine environments has been explained by the process of global cold-trapping and fractionation, and long-range atmospheric transport has been identified as one of the main pathways for POPs to polar regions.

In order to study the differences between urban and remote sites and to better understand the pollution over the Arctic ocean, a sampling campaign was conducted during summer 2011 on board of the OCEANIA oceanographic ship from Tromsø (Norway) to the Svalbard Islands (Norway). TSP concentrations were, as expected, quite low (5.2± 4.9 μg m^{-3}) and so were PAHs (0.4 ± 0.2 ng m-3) and alkanes (32 ± 49 ng m^{-3}), with a high variability between the samples.

The description of the concentrations and the source emission profiles is not the only priority. In fact, once emitted, the compounds undergo evolution processes (e.g., condensation/evaporation, nucleation, reaction, deposition, etc.). an important aspect is the distribution of these semi-volatile organic compounds between the gas and the particulate phase that is arguably the most important parameter in describing their atmospheric behavior. Transport in the environment, bioavailability and bioaccumulation, toxic effects on organisms, transformation reactions strongly depend on the equilibrium partitioning of organic compounds. There remain several ambiguities in the literature regarding the dominating sorption mechanisms involved in gas/particle partitioning. The various mechanisms would depend on the presence of various aerosols components. The identification of the dominating sorption phases is

necessary to determine which aerosol properties determine the overall sorption capacity and to understand the possible transformation pathways. For instance, if contaminants adsorb to mineral surfaces they are likely still available for reaction with radicals and photolysis, whereas this is less likely to happen if they absorbed into the OM [74].

Many are the aspects of the atmospheric processes that need clarification. To this purpose, an in-depth study about the partition of PAHs and n-alkanes between the gaseous and particulate phases of the atmosphere was done.

The compounds of both the classes showed a phase partition in agreement with the volatility characteristics, while an effect of the temperature was recorded. A good correlation was found for both the regressions between the gas/particle partitioning coefficient and the sub-cooled liquid vapor pressure (pL°) or the octanol-air partitioning coefficient (Koa) for PAHs in Milan, but a different result was obtained for alkanes and for both the class of compound in the Arctic region.

The obtained experimental data were used for the implementation of partitioning models (eg. Junge-Pankow, Koa and Dual model), which have so far been applied almost exclusively to aromatic polycyclic hydrocarbons, while very few works concern other classes of compounds such as linear alkanes. This study was designed to verify their applicability to the class of semi-volatile alkanes. In general, both in Milan and in the Arctic, these models, which consider adsorption and/or absorption based on single parameter linear free energy relationships tended to underestimate the partitioning of PAHs and n-alkanes.

For this reason, the gas-partitioning was studied using a polyparameter linear free energy relationships (ppLFERs), that takes into account the molecular interactions between the compound (sorbate) and the sorbent phase. The results showed that this model predicts very good the partitioning for both the class of compound: at both sites (urban and remote) the absorption was the main partitioning process for PAHs, dominated by the contribution of water soluble organic soluble organic matter (OSWSOM) while adsorption on soot and absorption into the high molecular mass organic polymers (OP) were the main partitioning process in the alkanes partitioning.

The results underlined also that, whereas on both the considered class of compounds adsorption onto soluble salts (<0.01% of the total Kp) may be neglected in urban areas, it contributes, even if on a small scale, to the partitioning process in the Arctic region, due to the different composition of the aerosol.

Besides their behavior in the atmosphere and the mechanisms that steer the gas/particle partitioning, PAHs have been widely studied, primarily because of their potential carcinogenic and mutagenic properties. Inhalation is one of the main means of human exposure to polycyclic aromatic hydrocarbons (PAHs) because of their ubiquitous presence in the atmosphere[45]. However, most studies have considered only PAHs found in the particle phase and have omitted the contribution of the gas-phase PAHs to the risk.

The carcinogenic potency of the emitted PAHs and the lifetime lung cancer risk of PAH exposure by inhalation in people living in urban and near remote sites, was studied including the impact of both gaseous and particulate phases. The results showed that people living in the urban area of Milan have a great inhalation cancer risk due to PAH exposure exposed. Contrary to what can be imagined, also in a remote site such as the Svalbard Island, the equivalent toxic concentrations were extremely high. Risk calculations showed that the contribution of the gas-phase PAHs to the total risk should be taken into account. Even though the average estimated lifetime lung cancer risk didn't exceed the WHO and the U.S. EPA recommended values (10^{-5}), the emissions of this PAHs would need to be reduced in order to decrease the inhalation cancer risk in the studied areas.

The present work tries to give some important lacking data to improve the knowledge of complex atmospheric processes. The study of the partitioning models showed that the ppLFER model should be considered a better choice for describing sorption processes. Although limited by solute descriptor availability and by a still insufficient knowledge of the OM composition, the ppLFER model presented here showed promising results in predicting PAH gas-particle partitioning constants. Furthermore, it was tested on other relevant substance classes (such as Alkanes) with reasonably good predictions. In summary, the ppLFER approach for modeling gas-particle partitioning is conceptually satisfying and holds considerable potential in the prediction of the partitioning of the semi-volatile compounds present in different environments, without having to perform costly and time-consuming laboratory techniques.

CHAPTER 8. BIBLIOGRAPHY

1. Pope C.A., Burnett R.T., Thun M.J., Calle E.E., Krewski D., Ito K., Thurston G.D., 2002. *Lung cancer, cardiopulmonary mortality and long-term exposure to fine particulate air pollution.* Journal of the American Medical Association 287 (9), 1132–1141.
2. Seinfeld J.H., Pandis S.N., 2006. *Atmospheric Chemistry and Physics: from air pollution to climate change, II*; John Wiley & Sons Inc., Ed.; Wiley-Interscience.
3. Poschl, U., 2005. *Atmospheric Aerosols: Composition, Transformation, Climate and Health Effects*. Angew. Chemie-Int. Ed., 44 (46), 7520–7540.
4. Cubison M.J., Alfarra M., Rallan J., Bower K.N., Coe H., Mcfiggans G.B., Whitehead J.D., Williams P.I., Zhang Q., Jimenez J.L., Hopkins J., Lee J., 2006. *The characterization of pollution aerosol in a changing photochemical environment*. Atmos. Chem. Phys. Atmospheric Chemistry and Physics, 6, 5573-5588. 2006
5. Whitby K.T., 1978. *The physical characteristics of sulfur aerosols*. Atmospheric Environment, 12, 135-159
6. EPA, 2004. *Air quality criteria for particulate matter*. U.S. Environmental Protection Agency. Research T, NCriangle Park. EPA/600/P-99/002Af-bF
7. Wang X., Chancellor G., Evenstad J., Farnsworth, J.E., Hase A., Olson G.M., Sreenath A., Agarwal J.K., 2009 *A Novel Optical Instrument for Estimating Size Segregated Aerosol Mass Concentration in Real Time*. Aerosol Science and Technology 43(9) 939-950.
8. Lippman M., Chen L.C., 2009. *Health effects of concentrated ambient air particulate matter (CAPs) and its components*. Crit. Rev. Toxicol. 39 (10), 865-913.
9. Perrone M.G., Larsen B.R., Ferrero L., Sangiorgi G., De Gennaro G., Udisti R., Zangrando R., Gambaro A., Bolzacchini E., 2012. *Sources of high PM2.5 concentrations in Milan, Northern Italy: molecular marker data and CMB modelling.* Sci. Total Environ. 414, 343-355.
10. Gualtieri M., Franzetti A., Longhin E., Mantecca P., Bestetti G., Bolzacchini,E., Camatini M., 2011. *In vitro effects of microbiologically characterized Milan particulate matter*. Procedia Environmental Sciences, 4, 192–197.
11. Perrino C., Catrambone M., Dalla Torre S., Rantica E., Sargolini T., Canepari, S., 2014. *Seasonal variations in the chemical composition of particulate matter: a case study in the Po Valley. Part I: macro-components and mass closure.* Environmental Science and Pollution Research. Vol 21(6) 3999-4009.

12. Gualtieri M., Mantecca P., Corvaja V., Longhin E., Perrone M.G., Bolzacchini E,. Camatini M., 2009. *Winter fine particulate matter from Milan induces morphological and functional alterations in human pulmonary epithelial cells (A549).* Toxicology Letters 188, 52–62
13. Pant, P., Harrison R.M., 2012. *Critical Review of Receptor Modelling for Particulate Matter: A Case Study of India*. Atmospheric Environment, 49, 1–12.
14. Andreae M.O., Gelencser A., 2006. *Black Carbon or Brown Carbon? The Nature of Light-Absorbing Carbonaceous Aerosols.* Atmos. Chem. Phys., 6, 3131–3148.
15. Fuzzi S., Baltensperger U., Carslaw K., Decesari S., Denier Van der Gon H., Facchini M.C., Fowler D., Koren I., Langford B., Lohmann U. et al. 2015. *Particulate Matter, Air Quality and Climate: Lessons Learned and Future Needs*. Atmos. Chem. Phys., 15 (14), 8217–8299.
16. Kim K-H., Jahan S.A., Kabir E., Brown R.J.C., 2013. *A review of airborne polycyclic aromatic hydrocarbons (PAHs) and their human health effects*. Environment International 60, 71-80
17. Srogi K., 2007. *Monitoring of Environmental Exposure to Polycyclic Aromatic Hydrocarbons: A Review.* Environ. Chem. Lett. 5 (4), 169–195.
18. Perrone M.G., Gualtieri M., Ferrero L., Lo Porto C., Udisti R., Bolzacchini E., Camatini M., 2010. *Seasonal variations in chemical composition and in vitro biological effects of fine PM from Milan*. Chemosphere 78, 1368–1377
19. Keyte I.J., Harrison R.M., Lammel G, 2013. *Chemical reactivity and long-range transport potential of polycyclic aromatic hydrocarbons - a review*. Chem Soc Rev, 42, 9333-9391.
20. Lammel G., Klanova J., Ilic P., Kohoutek J., Gasic B., Kovacic I., Skrdlikova L., 2010. *Polycyclic aromatic hydrocarbons in air on small spatial and temporal scales – II. Mass size distributions and gas-particle partitioning*. Atmospheric environment 44, 5022-5027
21. Schauer J.J., Rogge W.F., Hildemann L.M., Mazurek M.A., Cass G.R., Simoneit B.R.T., 1996. *Source apportionment of airborne particulate matter using organic compounds as tracers*. Atmospheric Environment 30, 3837–3855.
22. Guo H., Lee S.C., Ho K.F., Wang X.M., Zou S.C., 2003. *Particle-associated polycyclic aromatic hydrocarbons in urban air of Hong Kong.* Atmospheric Environment 37, 5307–5317.
23. Ravindra K., Sokhi R., Van Grieken R., 2008a. *Atmospheric polycyclic aromatic hydrocarbons: source attribution, emission factors and regulation (review*). Atmospheric Environment 42, 2895–2921.

24. Ravindra K., Wauters E., Van Grieken R., 2008b. *Variation in particulate PAHs levels and their relation with the transboundary movement of the air masses*. Science of the Total Environment 396, 100– 110.
25. Pedersen D.U., Durant J.L., Taghizadeh K., Hemond H.F., Lafleur A.L., Cass G.R., 2005. *Human cell mutagens in respirable airborne particles from the Northeastern United States. 2.Quantification of mutagens and other organic compounds*. Environmental Science and Technology 39, 9547-9560.
26. Hannigan M.P., Cass G.R., Penman B.W., Crespi C.L., Lafleur A.L., Busby jr. W.F., Thilly W.G., Simoneit B.R.T., 1998. *Bioassay-Directed Chemical Analysis of Los Angeles airborne particulate matter using a human cell mutagenicity assay*. Environmental Science and Technology 32, 3502-3514.
27. Lohmann R., Lammel G., 2004. *Adsorptive and Absorptive Contributions to the Gas-Particle Partitioning of Polycyclic Aromatic Hydrocarbons: State of Knowledge and Recommended Parametrization for Modeling*. Environmental science & technology vol. 38, no. 14
28. Rogge W.F., Mazurek M.A., Hildemann L.M., Cass G.R., Simoneit B.R.T., 1993a. *Quantification of urban organic aerosols at molecular level: identification, abundance and seasonal variation*. Atmospheric Environment 27A, 1309–1330.
29. Rogge W.F., Mazurek M.A., Hildemann L.M., Cass G.R., Simoneit B.R.T., 1993b. *Sources of fine organic aerosol. 4.Particulate abrasion products from leaf surfaces of urban plants*. Environmental Science and Technology 27, 2700–2711.
30. Simoneit B.R.T., Eglinton G., 1977. *Organic matter of eolian dusts and its input to marine sediments*. In: Campos R., Goni J. (Eds.), Advances in Organic Geochemistry. ENADIMSA, Madrid, 415– 430.
31. Rogge W.F., Hildemann L.M., Mazurek M.A., Cass G.R., Simoneit B.R.T., 1993c. *Sources of fine organic aerosol. 2. Noncatalyst and catalyst-equipped automobiles and heavy-duty diesel trucks*. Environmental Science and Technology 27, 636–651.
32. Simoneit B.R.T., Sheng G., Chen X., Fu J., Zhang J., Xu Y., 1991. *Molecular marker study of extractable organic matter in aerosols from urban areas of China*. Atmospheric Environment 25A, 2111– 2129.
33. Zheng M., Cass G.R., Schauer J.J., Edgerton E.S., 2002. *Source apportionment of PM2.5 in the southern United States using solvent-extractable organic compounds as tracers*. Environmental Science and Technology 36, 2361–2371.
34. Simoneit B.R.T., 1984. *Organic matter of the troposphere III. Characterization and sources of petroleum and pyrogenic residues in aerosols over the Western United States*. Atmospheric Environment 18, 51–67.

35. Pietrogrande M.C., Mercuriali M., Perrone M.G., Ferrero L., Sangiorgi G., Bolzacchini E., 2010. *Distribution of n-Alkanes in the Northern Italy Aerosols: Data Handling of GC-MS Signals for Homologous Series Characterization.* Environmental Science and Technology, 44(11), 4232-4240.
36. IARC SCIENTIFIC PUBLICATION NO. 161, 2013. *Air pollution and cancer*
37. Sánchez-Pérez Y., Chirino Y.I., Osornio-Vargas A.R., Morales-Bárcenas R., Gutiérrez-Ruíz C., Vázquez-López I., García-Cuellar C.M., 2009. *DNA damage response of A549 cells treated with particulate matter (PM10) of urban air pollutants.* Cancer Letters 278, 192–200
38. Laden L., Neas L.M., Dockery D.W. and Schwartz J., 2000. *Association of Fine Particulate Matter from Different Sources with Daily Mortality in Six U.S. Cities*. Environmental Health Perspectives 108 (10), 941-947.
39. Samet J.M., Zeger S.L., Dominici F., Curriero F., Coursac I., Dockery D.W. et al 2000. *The National morbidity, Mortality and air pollution study. Part II: morbidity and mortality from air pollution in the United States.* Res.Rep. Health Eff. Inst, 94, 70.
40. Schwartz J., Neas L.M., 2000. *Fine particles are more strongly associated than coarse particles with acute respiratory health effects in schoolchildren*. Epidemiology, 11, 6-10.
41. Longhin E., Pezzolato E., Mantecca P., Gualteri M., Bolzacchini E., Camatini M., 2010. *Biological effects of Milan PM: The role of particle dimension and season of sampling*. Chemical engineering transactions, 22, 23-28.
42. Sioutas C., Delfino R.J. and Singh M., 2005. *Exposure Assessment for Atmospheric Ultrafine Particles (UFPs) and Implications in Epidemiologic Research*. Environmental Health Perspectives. 113 (8), 947-955.
43. Harrison R.M., Yin J., 2000. *Particulate matter in the atmosphere: which particle properties are important for its effects on health?* The science of the total environment 249, 85-101.
44. IARC 2010. *Some non-heterocyclic polycyclic aromatic hydrocarbons and some related exposures.* Monogr Eval Carcinog Risks Hum 92, 765–71.
45. Ramírez, N., Cuadras A., Rovira E., Marcé R.M, Borrull F., 2011. *Risk assessment related to atmospheric polycyclic aromatic hydrocarbons in gas and particle phases near industrial sites*. Environ Health Perspect. 119(8): 1110–1116.
46. Perrone M.G., Zhou J., Malandrino M., Sangiorgi G., Rizzi C., Ferrero L., Dommen J., Bolzacchini E., 2016 *PM chemical composition and oxidative potential of the soluble fraction of particles at two sites in the urban area of Milan, Northern Italy*. Atmospheric Environment 128, 104-113 .

47. Carbone C., Decesari, S., Mircea, M., Giulianelli, L., Finessi, E., Rinaldi, M., Fuzzi, S., Marinoni, A., Duchi, R., Perrino, C., Sargolini T., Varde M., Sprovieri F., Gobbi G.P., Angelini F. and Facchini M.C., 2010. *Size-resolved Aerosol Chemical Composition over the Italian Peninsula during Typical Summer and Winter Conditions*. Atmospheric Environment 44, 5269–5278.
48. Ferrero L., Cappelletti D., Moroni B., Sangiorgi G., Perrone M.G., Crocchianti S. and Bolzacchini, E., 2012. *Wintertime Aerosol Dynamics and Chemical Composition across the Mixing Layer over Basin Valleys*. Atmos. Environ. 56, 143–153
49. Rodriguez S., Van Dingenen R., Putaud J.P., Dell'Acqua A., Pey J., Querol X., Alastuey A., Chenery S., Ho K.F., Harrison R., Tardivo R., Scarnato B. and Gemelli, V., 2007. *A Study on the Relationship between Mass Concentration, Chemistry and Number Size Distribution of Urban Fine Aerosol in Milan, Barcelona and London*. Atmos. Chem. Phys. 7, 2217–2232.
50. Casati M., Rovelli G., D'Angelo L., Perrone M.G., Sangiorgi G., Bolzacchini E., Ferrero, L., 2015. *Experimental Measurements of Particulate Matter Deliquescence and Crystallization Relative Humidity: Application in Heritage Climatology.* Aerosol and Air Quality Research 15, 399–409.
51. Invernizzi G., Ruprecht A., Mazza R., De Marco C., Mocnik G., Sioutas C., Westerdahl D., 2011. *Measurement of black carbon concentration as an indicator of air quality benefits of traffic restriction policies within the ecopass zone in Milan, Italy*. Atmospheric Environment 45, 3522-3527
52. Ellison R.B., Greaves S.P., Hensher D.A., 2013. *Five years of London's low emission zone: Effects on vehicle fleet composition and air quality*. Transportation Research Part D 23, 25–33
53. Panteliadis P., Strak M., Hoek G., Weijers E., van der Zee S., Dijkema M., 2014. *Implementation of a low emission zone and evaluation of effects on air quality by long-term monitoring*. Atmospheric Environment 86, 113 -119
54. Rosenlund M., Berglind N., Pershagen G., Jarup L., Bluhm G., 2001. *Increased prevalence of hypertension in a population exposed to aircraft noise*. Occup Environ Med 58: 769– 773
55. Aydin Y., Kaltenbach M., 2007. *Noise perception, heart rate and blood pressure in relation to aircraft noise in the vicinity of the Frankfurt airport*. Clin Res Cardiol., 96(6),347-58.
56. Haralabidis A.S., Dimakopoulou K., Vigna-Taglianti F., Borgini MGP., Dudley M.L., Pershagen G., Bluhm G., Houthuijs D., Babisch W., Velonakis M., Katsouyanni K., 2008. *Acute effects of night-time noise exposure on blood pressure in populations living near airports.* Eur Heart J., 29(5), 658-64.

57. Matsui T., Uehara T., Miyakita T., Hitamatsu K., Osada Y., Yamamoto T., 2004. *The Okinawa study: effects of chronic aircraft noise on blood pressure and some other physiological indices*. J Sound Vib, 277:469-470.
58. Hardoy M.C., Carta M.G., Marci A.R., Carbone F., Cadeddu M., Kovess V., Dell'Osso L., Carpiniello B., 2005. *Exposure to aircraft noise and risk of psychiatric disorders: the Elmas survey--aircraft noise and psychiatric disorders*. Soc Psychiatry Psychiatr Epidemiol. 40(1):24-6.
59. Maschke C. 2011. Cardiovascular effects of environmental noise: Research in Germany. Noise Health, 13:205-11.
60. International Civil Aviation Organisation (ICAO), 2008. *Environmental Protection.* Annex 16 to the Convention on International Civil Aviation - volume II - Aircraft Engine Emissions. Montréal (Quebec), ICAO.
61. Hulskotter I., 2017. *Emissions of air pollutants from civil aviario in the Netherlands*. TNO report.
62. Yelvington, P. E., S. C. Herndon, J. Wormhoudt, J. T. Jayne, R. C., Miake-Lye, W. B. Knighton, and C. Wey. 2007. "Chemical Speciation of Hydrocarbon Emissions from a Commercial Aircraft Engine". Journal of Propulsion and Power 23(5), 912–8.
63. Cattani G, Di Menno di Bucchianico A, Gaeta A, Romano D, Fontana L, Iavicoli I., 2014. *Aeroporti e qualità dell'aria: una sintesi critica della letteratura scientifica*. Epidemiol Prev 38(3-4), 254-261
64. Di Menno di Bucchianico A, Cattani G, Gaeta A, Caricchia AM, Troiano F et al, 2014. *Inquinamento atmosferico in un'area urbana limitrofa all'aeroporto di Roma-Ciampino*. Epidemiol Prev 38(3-4): 244-253
65. Wood E.C., Herndon S.C., Timko M.T. et al., 2008*. Speciation and chemical evolution of nitrogen oxides in aircraft exhaust near airports*. Environ. Sci. Technol 42, 1884–1891
66. Herndon SC, Shorter JH, Zahniser MS et al., 2004. *NO and NO_2 emission ratios measured from inuse commercial aircraft during taxi and takeoff*. Environ Sci Technol 38: 6078-6084.
67. Barre L.A., 1986. *Arctic air pollution: an overview of current knowledge*. Atmospheric Environment 20 (1) 643-663.
68. Pacyna J.M., Vitols V. and Hanssen J.E.1984. *Size-differentiated composition of the arctic aerosol at Ny-Alesund, Spitsbergen*. Atmospheric Environment 18 (11), 2447-2459
69. Heidam N.Z., 1984. *The components of the Arctic aerosol*. Atmospheric Environment 18 (2) 329-343.

70. Rahn K.A., 1981. *The Mn/V ratio as a tracer of large-scale sources of pollution aerosol for the Arctic.* Atmospheric Environment 15 (8) 1457-1464.
71. Daisey J.M., McCaffrey. R.J. and. Gallagher R.A., 1981. *Polycyclic aromatic hydrocarbons and total extractable particulate organic matter in the Arctic Aerosol.* Atmospheric Environment 15 (8) 1353-1363,
72. Halsall C.J., Barrie L.A., Fellin P., Muir D.C.G, Billeck B.N., Lockhart L., Rovinsky F.Ya., Kononov E.Ya, Pastukhov B., 1997. *Spatial and Temporal Variation of Polycyclic Aromatic Hydrocarbons in the Arctic.* Atmosphere. Environ. Sci. Technol. 31, 3593-3599
73. Sangiorgi G., Ferrero L., Perrone M., Papa E., Bolzacchini E., 2014. *Semivolatile PAH and n-alkane gas/particle partitioning using the dual model: up-to-date coefficients and comparison with experimental data*. Environ Sci Pollur Res 21, 10163-10173
74. Arp H.P., Schwarzenbach R.P., Goss K.U., 2008. *Ambient gas/particle partitioning. 2: the influence of particle source and temperature on sorption to dry terrestrial aerosol*. Environ. Sci. Technol. 42, 5951-5957
75. Harner T. and Bidleman T.F., 1998. *Octanol-air partitioning coefficient for describing particle/gas partitioning of aromatic compounds in urban air.* Environ. Sci. Technol 32, 1494-1502
76. Dachs J. and Eisenrich S-J., 2000. *Adsorption onto aerosol soot carbon dominates gas-particle partitioning of polycyclic aromatic hydrocarbons.* Environ. Sci. Technol 34, 3690-3697
77. Petzold A., Ogren J.A., Fiebig M., Laj P., Li S.-M., Baltensperger U., Holzer-Popp T., Kinne S., Pappalardo G., Sugimoto N., Wehrli C., Wiedensohler A. and Zhang X.-Y., 2013. *Recommendations for reporting "black carbon" measurements*. Atmos. Chem. Phys., 13, 8365–8379
78. Eckhardt S., Hermansen O., Grythe H., Fiebig M., Stebel K., Cassiani M., Baecklund A. and Stohl A., 2013. *The influence of cruise ship emissions on air pollution in Svalbard –a harbinger of a more polluted Arctic?* Atmos. Chem. Phys., 13, 8401–8409,
79. Gilardoni S., Vignati E. and Wilson J., 2011. *Using measurements for evaluation of black carbon modeling*. Atmos. Chem. Phys., 11, 439–45
80. Gustafson KE, Dickhut RM (1997) *Distribution of polycyclic aromatic hydrocarbons in southern Chesapeake Bay surface water: Evaluation of three methods for determining freely dissolved water concentrations*. Environmental Toxicology and Chemistry 16, 452-461.

81. Birch, M.E., Cary, R.A., 1996. *Elemental carbon-based method for monitoring occupational exposures to particulate diesel exhaust.* Aerosol Sci. Technol. 25, 221-241.
82. Finizio A., Mackay D., Bidleman T. and Harner T., 1997. *Octanol-air partitioning coefficient as a predictor of partitioning of semi-volatile organic chemicals to aerosol*. Atmospheric environment 31 (15) 2289-2296
83. Shahpoury P., Lammel G., Albinet A., Sofuoglu A., Dumanoglu Y., Sofuoglu S.C., Wagner Z., Zdimal V.,2016. *Evaluation of a conceptual model for gas-particle partitioning of polycyclic aromatic hydrocarbons using polyparameter linear free energy relationships*. Environ. Sci Technol. 50, 12312- 12319.
84. Endo S. and Goss K-U., 2014. *Applications of polyparameter linear free energy relationships in environmental chemistry.* Environmental science & technology vol. 48, 12477-12491
85. Lei Y.D., Chankalal R., Chan A. and Wania F., 2002. *Supercooled liquid capor pressures of the polycyclic aromatic hydrocarbons*. J.Chem. Eng. Data 47, 801-806
86. Haftka J.J.H., Parson J.R., Govers H.A.J., 2006. *Supercooled liquid vapour pressures and related thermodynamic properties of polycyclic aromatic hydrocarbons determined by gas chromatography*. Journal of Chromatography A, 1135, 91-100.
87. Odabasi M., Cetin E., Sofuoglu A., 2006. *Determnation of octanol-air partition coefficients and supercooled liquid vapor pressures of PAHs as a function of temperature: Application to gas-particle partitioning in an urban atmosphere*. Atmospheric Environment 40, 6615-6625.
88. Pankow J.F., 1994. *An absorption model of gas/particle partitioning of organic compounds in the atmosphere*. Atmospheric Environment 28(2), 185-188.
89. Götz C.W., Scheringer M., MacLeod M., Roth C.M., Hungerbühler K., 2007. *Alternative approaches for modeling gas–particle partitioning of semivolatile organic chemicals: model development and compari- son.* Environ Sci Technol 41, 1272–1278
90. Beyer A., Wania F., Gouin T., Mackay D. Matthies M., 2002. *Selecting internally consistent physicochemical properties of organic compounds*. Environmental Toxicology and Chemistry 21 (5), 941–953.
91. Xiao H., Wania F., 2003. *Is vapor pressure or the octanol–air partition coefficient a better descriptor of the partitioning between gas phase and organic matter?* Atmos Environ 37, 2867–2878.
92. van Noort PCM., 2003. *A thermodynamics-based estimation model for adsorption of organic compounds by carbonaceous materials in environmental sorbents*. Environ Toxicol Chem 22,1179–1188.

93. Abraham, M. H., 1993. *Scales of solute hydrogen-bonding: their construction and application to physicochemical and biochemical processes*. Chem. Soc. Rev. 22 (2), 73−83.
94. Goss, K.-U., 2005. *Predicting the equilibrium partitioning of organic compounds using just one linear solvation energy relationship (LSER).* Fluid Phase Equilib. 233 (1), 19−22.
95. Roth C.M., Goss K-U. and Schwarzenbach R.P., 2005. *Sorption of a diverse set of organic vapors to diesel soot and road tunnel aerosols*. Environ. Sci Technol 39, 6632-6637.
96. Turpin B.J.; Lim H.J., 2001. *Species contributions to PM2.5 mass concentrations: Revisiting common assumptions for estimating organic mass*. Aerosol Sci. Technol. 35 (1), 602−610.
97. Goss K.-U. Buschmann J. Schwarzenbach R.P., 2003. *Determination of the surface sorption properties of talc, different salts, and clay minerals at various relative humidities using adsorption data of a diverse set of organic vapors*. Environ. Toxicol. Chem. 22 (11), 2667−2672.
98. Ruprecht A., Invernizzi G., 2009. *The effects of the traffic restriction fee (Ecopass) in the center of Milan on urban pollution with particulate matter: the results of a pilot study*. Epidemiol Prev; 33 (1-2): 21-26.
99. Putaud J.P., Van Dingenen R., Alastuey A., Bauer H., Birmili W., Cyrys J., et al., 2010. *A European aerosol phenomenology e 3: physical and chemical characteristics of particulate matter from 60 rural, urban, and kerbside sites across Europe*. Atmos. Environ. 44, 1308-1320.
100. Ge X., Wexler A.S., Clegg S., 2011. Atmospheric amines- Part I. A review. Atmos. Environ. 45, 524-546.
101. Caricchia A.M, Chiavarini S., Pezza M., 1999. *Polycyclic aromatic hydrocarbons in the urban atmospheric particulate matter in the city of Naples (Italy).* Atmospheric Environment 33, 3731-3738.
102. Amodio M., Caselli M., de Gennaro G., Tutino M., 2009. *Particulate PAHs in two urban areas of Southern Italy: Impact of the sources, meteorological and background conditions on air quality.* Environmental Research 109 812–820.
103. Cincinelli A., Del Bubba M., Martellini T., Gambaro A., Lepri L., 2007. *Gas-particle concentration and distribution of n-alkanes and polycyclic aromatic hydrocarbons in the atmosphere of Prato (Italy)*. Chemosphere 68, 472–478
104. Martellini T., Giannoni M., Lepri L., Katsoyiannis A., Cincinelli A., 2012. *One year intensive PM2.5 bound polycyclic aromatic hydrocarbons monitoring in the area of*

Tuscany, Italy. *Concentrations, source understanding and implications.* Environmental Pollution 164, 252-258.

105. Schauer C., Niessner R., Poschl U., 2003. *Polycyclic aromatic hydrocarbons in urban air particulate matter: decadal and seasonal trends, chemical degradation and sampling artifacts.* Environ. Sci. Technol 37, 2861-2868.
106. Zhang, Y.X., Tao, S., 2009. Global atmospheric emission inventory of polycyclic aromatic hydrocarbons (PAHs) for 2004. Atmos. Environ. 43, 812e819.
107. Perrone MG, Carbone C., Faedo D, Ferrero L., Maggioni A, Sangiorgi G., Bolzacchini E., 2014. Exhaust emissions of polycyclic aromatic hydrocarbons, n-alkanes and phenols from vehicles coming within different European classes. Atmospheric Environment 82, 391-400.
108. Tsapakis M., Stephanou E.G., 2005. *Occurrence of gaseous and particulate polycyclic aromatic hydrocarbons in the urban atmosphere: study of sources and ambient temperature effect on the gas/particle concentration and distribution*. Environmental Pollution 133, 147–156.
109. Delgado-Saborit J.M., Alam M.S., Pollitt J. G., Stark C., Harrison R.M., 2013*. Analysis of atmospheric concentrations of quinones and polycyclic aromatic hydrocarbons in vapor and particulate phases.* Atmospheric Environment 77, 974-982.
110. -Granadillo I.A., Alonso J.I.G., Sanz-Medel A., 2002. *Determination of n-alkanes and polycyclic aromatic hydrocarbons in atmospheric particulate and vapour phases in Oviedo, Spain, by GC-MS*. Journal of Environmental Monitoring 2, 218-222.
111. Bi X., Sheng G., Peng P., Chen Y., Zhang Z., Fu J., 2003. *Distribution of particulate- and vapour- phase n-alkanes and polycyclic aromatic hydrocarbons in urban atmosphere of Guangzhou, China*. Atmospheric Environment 37, 289-298.
112. Pankow J.F., Bidleman T.F., 1992. Interdependence of the slopes and intercepts from log–log correlations of measured gas-particle partitioning and vapour pressure - I. Theory and analysis of available data. Atmospheric Environment 26A (6), 1071–1080.
113. Mandalakis M., Tsapakis M., Tsoga A., Stephanou E.G., 2002. Gas-particle concentrations and distribution of aliphatic hydrocarbons, PAHs, PCBs and PCDD/Fs in the atmosphere of Athens (Greece). Atmospheric Environment 36, 4023-4035.
114. Galarneau E., Bidleman T.F., Blanchard P., 2006. Seasonality and interspecies differences in particle/gas partitioning of PAHs observed by the Integrated Atmospheric Deposition Network (IADN). Atmospheric Environment 40, 182-197.
115. Abraham M.H., Smith R.E., Luchtefeld R., Boorem A.J., Luo R., Acree W. Jr., 2010. Prediction of solubility of drugs and other compound in organic solvents. Journal of pharmaceutical sciences, 99, 1500-1515.

116. Sprunger, L., Proctor, A., Acree, W. E., Abraham, M. H. (2007) J. Chromatogr. A, 1175, 162-173.
117. Ariyasena, T. C., Poole, C. F. (2014) J. Chromatogr. A 1361, 240-254.
118. Kamprad, I., Goss, K.-U., 2007. Systematic investigation of the sorption properties of poly- urethane foams for organic vapors. Anal. Chem. 79, 4222–4227.
119. Goss, K.-U. 2004. The air/surface adsorption equilibrium of organic compounds under ambient conditions. Crit. Rev. Environ. Sci. Technol., 34 (4), 339−389.
120. Sprunger, L. M., Achi, S. S., Acree, W. E., Abraham, M. H. (2010) Fluid Phase Eq., 288, 139-144.
Abraham, M. H., Acree, W. E., Leo, A. J., Hoekman, D. (2009) New J. Chem., 33, 568-573.
121. Sandradewi J, Prévôt A, Weingartner E, Schmidhauser R, Gysel M, Baltensperger U (2008a) A study of wood burning and traffic aerosols in an Alpine valley using a multi-wavelength Aethalometer. Atmos Environ 42(1):101–112
122. Sandradewi J, Prevot AS, Szidat S, Perron N, Alfarra MR, Lanz VA, Weingartner E, Baltensperger U (2008b) Using aerosol light absorption measurements for the quantitative determination of wood burning and traffic emission contributions to particulate matter. Environ Sci Technol 42(9):3316–3323
123. Kirchstetter TW, Novakov T, Hobbs PV (2004) Evidence that the spectral dependence of light absorption by aerosols is affected by organic carbon. J Geophys Res Atmos.
124. Bond TC, Bergstrom RW (2006) Light absorption by carbonaceous particles: an investigative review. Aerosol Sci Technol 40(1):27–67.
125. Day DE, Hand JL, Carrico CM, Engling G, Malm WC (2006) Humidification factors from laboratory studies of fresh smoke from biomass fuels. J Geophys Res Atmos 111(D22).
126. Wang, X., Westerdahl, D., Chen, L., et al., 2008. Evaluating the air quality impacts of the 2008 Beijing Olympic Games: on-road emission factors and black carbon pro!les. Atmospheric Environment 43, 4535-4543.
127. Westerdahl, D., Wang, X., Pan, X., Zhang, K.M., 2009. Characterization of on-road vehicle emission factors and microenvironmental air quality in Beijing, China. Atmospheric Environment 43, 697-705.
128. Wood, E., Herndon, S., Miake-Lye, R.C., Nelson, D., Seeley, M., 2008a. Aircraft and Airport-Related Hazardous Air Pollutants: Research Needs and Analysis. ACRP Report 7. Transportation Research Board, Washington, D.C.
129. Lee, D.S., Pitari, G., Grewe, V., Gierens, K., Penner, J.E., Petzold, A., Prather, M.J., Schumann, U., Bais, A., Berntsen, T., Iachetti, D., Lim, L.L., Sausen, R., 2010.

Transport impacts on atmosphere and climate: aviation. Atmos. Environ. 44, 4678e4734.

130. Daley P.S. and Naugle D.F (1979) Measurement and Analysis of Airport Emissions, Journal of the Air Pollution Control Association, 29:2,113-116,
131. Mazaheri, M., Johnson, G.R., Morawska, L., 2009. Particle and gaseous emissions from commercial aircraft at each stage of the landing and takeoff cycle. Environ. Sci. Technol. 43, 441e446.
132. Unal, A., Hu, Y., Chang, M.E., Odman, M.T., Russell, A.G., 2005. Airport related emissions and impacts on air quality: application to the Atlanta International Airport. Atmos. Environ. 39, 5787e5798.
133. Carslaw, D.C., Ropkins, K., Laxen, D., Moorcroft, S., Marner, B., Williams, M.L., 2008. Near-field commercial aircraft contribution to nitrogen oxides by engine, aircraft type, and airline by individual plume sampling. Environ. Sci. Technol. 42, 1871e1876.
134. Westerdahl D., Fruin S.A., Fine P.L., Sioutas C., 2008. The Los Angeles International Airport as a source of ultrafine particles and other pollutants to nearby communities. Atmospheric Environment 42, 3143–3155
135. Costabile F., Birmili W., Klose S., Tuch T., Wehner B., Wiedensohler A., Franck U., Konig K., and Sonntag A., 2009. *Spatio-temporal variability and principal components of the particle number size distribution in an urban atmosphere.* Atmos. Chem. Phys., 9, 3163–3195.
136. Beyersdorf A, Thornhill KL, Winstead EL, Ziemba L, Blake D, Timko M, 2012. *Power-dependent speciation of volatile organic compounds in aircraft exhaust.* Atmospheric environment. 61: 275-282.
137. Ferrero, L., Riccio, A., Perrone, M. G., Sangiorgi, G., Ferrini, B. S., and Bolzacchini, E., 2011b. Mixing height determination by tethered balloon-based particle soundings and modeling simulations, Atmos. Res, 102, 145–156.
138. Colombi C., Gianelle V.,Lazzarin M. Progetto Malpensa 20 ottobre 2011 – 30 agosto 2012, ARPA Lombardia 2013,http://www2.arpalombardia.it/sites/qaria/_layouts/15/qaria/AttivitaProgetti.aspx?Page=AttProg-Archivio/AttProg_MALPENSA&title=Progetto%20Malpensa
139. Kawamura K, Ono K, Tachibana E, Charriére B, Sempéré R, 2012. Distributions of low molecular weight dicarboxylic acids, ketoacids and α-dicarbonyls in the marine aerosols collected over the Arctic Ocean during late summer. Biogeosciences 9:4725-4737
140. Narukawa, M., Kawamura, K., Li, S. M., and Bottenheim, J. W.: Stable carbon isotopic rations and ionic composition of the high Arctic aerosols: An increase in δ 13C values

from winter to spring, J. Geophys. Res.-Atmos., 113, D02312, doi:10.1029/2007JD008755, 2008.

141. Kawamura, K., Kasukabe, H., and Barrie, L. A., 2010. Secondary formation of water-soluble organic acids and α-dicarbonyls and their contributions to total carbon and water-soluble organic carbon: Photochemical aging of organic aerosols in the Arctic spring, J. Geophys. Res.-Atmos., 115, D21306.
142. Xu G., Gao Y., Lin Q., Li W., Chen L., 2013. Characteristics of water-soluble inorganic and organic ions in aerosols over the Southern Ocean and coastal East Antarctica during austral summer. Journal of Geophysical Research: Atmospheres 118:13,303-13,318
143. Cecinato A., Mabilia R., Marino F., 2000. Relevant organic components in ambient particulate matter collected at Svalbard Islands (Norway) . Atmospheric Environment 34 (2000) 5061}5066
144. Castro-Jiménez J, Berrojalbiz N., Wollgast J., Dachs J., 2012. Polycyclic aromatic hydrocarbons (PAHs) in the Mediterranean Sea: Atmospheric occurrence, deposition and decoupling with settling fluxes in the water column. Environmental Pollution 166, 40-47
145. Hung H., Blancharda T.P., Halsallb C.J., Bidlemanc T.F., Sternd G.A., Felline P., Muirf D.C.G., Barrieg L.A., Jantunena L.M., Helmd P.A., Maa J., Konoplev A. 2005. Temporal and spatial variabilities of atmospheric polychlorinated biphenyls (PCBs), organochlorine (OC) pesticides and polycyclic aromatic hydrocarbons (PAHs) in the Canadian Arctic: Results from a decade of monitoring. Science of the Total Environment 342, 119 – 144
146. Fu. P.Q., Kawamura K., Chen J., Charriere B., and R. Sempére R., 2013. Organic molecular composition of marine aerosols over the Arctic Ocean in summer: contributions of primary emission and secondary aerosol formation. Biogeosciences, 10, 653–667.
147. Masclet P., Hoyau V., Jaffrezo J.L. and Cachier H., 2000. Polycyclic aromatic hydrocarbon deposition on the ice sheet of Greenland. Part I. Superficial snow. Atmospheric Environment 34:3195–3207.
148. Samburova V., Connolly J., Gyawali M,. Yatavelli R L.N, Watts A C., Chakrabarty R K., Zielinska B., Moosmüller H., Khlystov A., 2016. Polycyclic aromatic hydrocarbons in biomass-burning emissions and their contribution to light absorption and aerosol toxicity. Science of the Total Environment 568, 391–401
149. IARC, 1983. Polynuclear aromatic compounds, part 1: chemical, environmental, and experimental data. Monographs on the Evaluation of the Carcinogenic Risk of Chemicals to Humans Vol. 32. International Agency for Research on Cancer, Lyon.

150. IARC, 1984. Polynuclear aromatic compounds, part 2: carbon blacks, mineral oils, and some nitroarenes. Monographs on the Evaluation of the Carcinogenic Risk of Chemicals to Humans Vol. 33. International Agency for Research on Cancer, Lyon.
151. Vineis, P., Husgafvel-Pursiainen, K., 2005. Air pollution and cancer: biomarker studies in human populations. Carcinogenesis 26, 1846–1855.
152. Xue, W.L., Warshawsky, D., 2005. Metabolic activation of polycyclic and heterocyclic aro- matic hydrocarbons and DNA damage: a review. Toxicol. Appl. Pharmacol. 206, 73–93.
153. Armstrong B, Hutchinson E, Unwin J, Fletcher T. 2004. *Lung cancer risk after exposure to polycyclic aromatic hydro- carbons: a review and meta-analysis*. Environ Health Perspect 112:970–978.
154. OEHHA, 2011. Chemical-specific Summaries of the Information Used to Derive Unit Risk and Cancer Potency Values. (Appendix B). http://www.oehha.ca.gov/air/hot_spots/ tsd052909.html.
155. Tomaz S., Shahpoury P., Jaffrezo J.-L, Lammel G., Perraudin E., Villenave E., Albinet A., 2016. *One-year study of polycyclic aromatic compounds at an urban site in Grenoble (France): Seasonal variations, gas/particle partitioning and cancer risk estimation*. Science of the Total Environment 565, 1071–1083.
156. Wang J., Chen S., Tian M., Zheng X., Gonzales L., Ohura T., Mai B. and Massey Simonich S.L., 2012. *Inhalation Cancer Risk Associated with Exposure to Complex Polycyclic Aromatic Hydrocarbon Mixtures in an Electronic Waste and Urban Area in South China*. Environ. Sci. Technol. 46, 9745−9752